Orbital forcing and its importance in understanding the warm Pliocene

Caroline Louise Prescott

Submitted in accordance with the requirements for a degree of Doctor of Philosophy

University of Leeds

School of Earth and Environment

November 2017

The candidate confirms that the work submitted is her own, except where work which has formed part of jointly authored publications has been included. The contribution of the candidate and the other authors to this work has been explicitly indicated below. The candidate confirms that appropriate credit has been given within the thesis where reference has been made to the work of others. The work within chapters 2, 3 and 4 of the thesis have appeared in publications as follows:

Prescott, C.L., Haywood, A.M., Dolan, A.M., Hunter, S.J., Pope, J.O. & Pickering, S.J. (2014). Assessing orbitally-forced interglacial climate variability during the mid-Pliocene Warm Period. *Earth and Planetary Science Letters*. The work from this publication forms chapter 2. The experimental design was planned by A.H. and C.P.. The experiments, processing, analysis and interpretation was completed by the candidate as well as the figures and written manuscript. The co-authors, A.H., A.D. and S.H. contributed specific expertise and with how to place the work into the broader scientific content. J.P. and S.P. gave technical help with the experiments.

Prescott C.L., Dolan A.M., Haywood A.M., Hunter S.J., Tindall J.C. (2018). Regional climate and vegetation response to orbital forcing within the mid-Pliocene Warm Period: a study using HadCM3. *Global and Planetary Change*. The work from this publication forms chapter 3. The experiment design and implementation, data analysis and presentation and the written manuscript was completed by the candidate. A.D. and A.H. advised on the experiment design and suggested improvements and advice on the manuscript. S.H. and J.T. provided technical support for the climate modelling and analysis of model output.

Prescott C.L., Dolan A.M., Haywood A.M., Hunter S.J., Tindall J.C.. Orbital forcing and the variability of the Indian monsoon during interglacials of the Pliocene. In preparation for submission to *Global and Planetary Change*. The work from this manuscript forms chapter 4. The work presented in this chapter including experiment design, data analysis and the written manuscript was completed by the candidate. A.H., and A.D. suggested improvements on the written manuscript and data presentation.

Two of the climate model simulations analysed in chapter 2 were used in **Haywood, A.M., Dolan, A.M., Pickering, S.J., Dowsett, H.J., McClymont, E.L., Prescott, C.L., Salzmann, U., Hill, D.J., Hunter, S.J., Lunt, D.J., Pope, J.O. & Valdes, P.J. (2013). On the identification of a Pliocene time slice for data-model comparison. *Philosophical transactions. Series A, Mathematical, physical, and engineering sciences.*** For this paper, the candidate ran the HadCM3 simulations that were presented.

The climate model simulations presented in chapter 2 were used in **De Boer, B., Haywood, A.M., Dolan, A.M., Hunter, S.J. & Prescott, C.L. (2017). The transient response of ice volume to orbital forcing during the warm Late Pliocene. *Geophysical Research Letters.*** The candidate contributed the HadCM3 experiments used to drive the ice sheet model simulations in this paper.

This copy has been supplied on the understanding that it is copyright material and that no quotation from the thesis may be published without proper acknowledgement.

Copyright © 2017 The University of Leeds and Caroline Prescott

The right of Caroline Prescott to be identified as Author of this work has been asserted by her in accordance with the Copyright, Designs and Patents Act 1988.

Acknowledgements

I acknowledge the European Research Council for the funding provided for this project and thank the members of the Earth System Science Institute (ESSI) and in particular, Palaeo@Leeds for the useful scientific discussions and feedback. There are also several people I would like to thank specifically:

My supervisors, Alan Haywood, Aisling Dolan and Stephen Hunter for their support and guidance throughout this process.

James Pope, Julia Tindall and Steven Pickering for the invaluable technical advice. In particular to James for his patience in answering my endless questions when I first started.

Rhian Rees-Owen and Edine Pape who deserve a special mention for making the past few years so much fun; also Rhian for giving me such useful feedback on parts of this thesis.

Ruza Ivanovic for keeping me caffeinated and being incredibly generous with both her time and practical advice.

Paul and Rachel Hodgson for their continued kindness as well as offering their home to use as my own in Leeds. Sue and Terry Prescott for letting me move in while writing up and especially to Terry for proof reading everything. And to Alex Feben for his understanding and patience throughout.

Abstract

The Pliocene is traditionally viewed as an epoch with a warm and stable climate. Data-Model comparisons for the mid-Pliocene (~3.3 – 3 Ma) have identified regions where models do not agree with geological proxies. Palaeoenvironmental syntheses used in these comparisons are time-averaged. It has been hypothesised that orbital cyclicity within the mid-Pliocene, not accounted for in previous model simulations or data syntheses, could contribute to data-model discord. Study of the Pleistocene (~11.7ka – 2.6 Ma) has established the importance of understanding climate variability and distinguishing the specific character of separate interglacial or glacial events. This thesis confirms such variability should be expected in the Pliocene. Using a climate model, two interglacials (MIS KM5c and K1) in the Pliocene are compared, and results demonstrate changes in the surface air temperatures (SATs) due to changes in orbital forcing can be substantial and differ between interglacials.

A further two interglacials (G17 and KM3) are investigated, and changes in regional vegetation patterns and the summer Indian monsoon in response to orbital forcing over the four interglacial events are analysed. A notable vegetation response is seen in the continental interiors of North America and Eurasia, where forests are replaced by grassland and shrubland, and is most widespread for interglacials with the strongest orbital forcing (most different from present day). The Indian monsoon is slightly stronger than pre-industrial in KM5c (an interglacial with near-modern orbit), driven by higher CO_2, and is significantly more intense in G17, K1 and KM3 than KM5c, due to orbital-driven increased seasonal SATs. Orbital forcing throughout Pliocene interglacials is found to have a significant effect on the simulation of regional climate, vegetation and the Indian monsoon system within the modelling framework used here. Time-averaged palaeoenvironmental synthesis therefore, cannot be expected to concur with climate model outputs using time specific orbital forcing.

Abbreviations

AGCM	Atmosphere General Circulation Model
AOGCM	Atmosphere-Ocean General Circulation Model
BASISM	British Antarctic Survey Ice Sheet Model
BIOME4	An offline mechanistic vegetation model
CAM3.1	Community Atmosphere Model version 3.1
CCSM3	Community Climate System Model version 3
CMIP	Coupled Model Intercomparison Project
DGVM	Dynamic Global Vegetation Model
DJF	December, January, February
DMC	Data-model comparison
EASM	East Asian Summer Monsoon
EAWM	East Asian Winter Monsoon
EIMR	Extended Indian Monsoon Rainfall
GCM	General Circulation Model
GISS	Goddard Institute for Space Studies
HadAM3	Hadley Centre Atmospheric Model version 3
HadCM3	Hadley Centre Coupled Model version 3
IAP	Institute of Atmospheric Physics
IPCC	Intergovernmental Panel on Climate Change
JJA	June, July, August
JJAS	June, July, August, September

LR04	Lisiecki and Raymo $\delta^{18}O$ Stack
MHI	Monsoon Hadley Index
MIS	Marine Isotope Stage
MMM	Multi-model mean
MOSES	Met Office Surface Exchange Scheme
mPWP	mid-Pliocene Warm Period
MSLP	Mean Sea Level Pressure
NCAR	National Center for Atmospheric Research
NH	Northern Hemisphere
PFT	Plant functional type
PlioMIP	Pliocene Model Intercomparison Project
PMIP	Palaeoclimate Modelling Intercomparison Project
PRISM	Pliocene Research, Interpretation and Synoptic Mapping
SAT	Surface air temperature
SH	Southern Hemisphere
SST	Sea surface temperatures
TRIFFID	Top-down Representation of Interactive Foliage and Flora Including Dynamics.

Contents

List of Figures

List of Tables

CHAPTER 1

INTRODUCTION

1.1 Scientific Background

1.1.1 Rationale

There is indisputable evidence of the warming of the climate system; atmosphere and ocean temperatures are rising, the amounts of snow and ice have diminished and sea level has risen (IPCC Synthesis Report, 2014). Numerical models of the Earth's system (climate models) have been developed to facilitate understanding of modern and future climate change. These climate models are at the forefront of research to understand the effect of greenhouse gas emissions (Flato et al., 2013). While these models are extremely complex, they only represent the existing state of knowledge and therefore need further validation and development. One model validation technique involves looking to Earth's history and assessing how well they reconstruct climates of the past. Geological proxies for key climate variables can provide quantitative information on climates of the past. If models can successfully reproduce large-scale climate changes that happened in the past, greater confidence can be placed in their projections of future climate change (Masson-Delmotte et al., 2013). The Earth system has been, and will continue to be, affected by external forcings such as changes in orbit, as well as internal forcings such as atmospheric composition. Palaeoclimate data and modelling can provide information on the Earth's response to the forcings and are specifically useful to facilitate understanding of feedbacks on time scales longer than a few centuries (Masson-Delmotte et al., 2013). One such time in Earth's history that could be used to aid understanding of future climate change is the Pliocene (Fig.1.1)

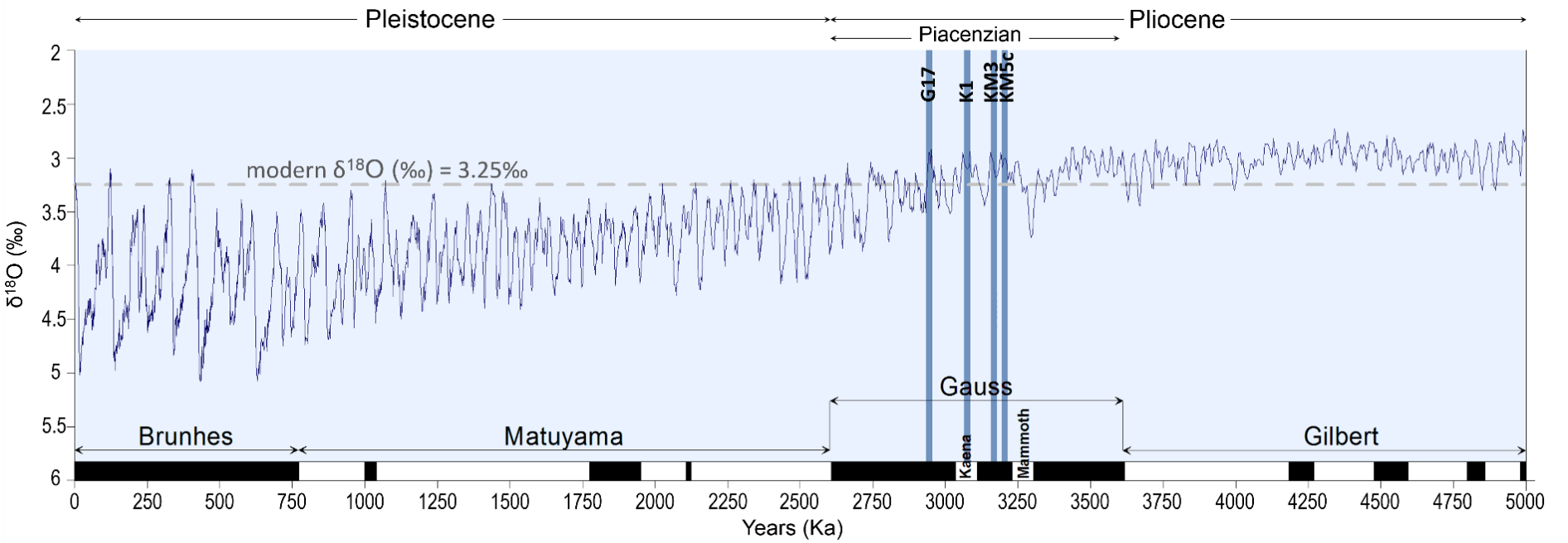

Figure 1.1 The Lisiecki & Raymo (LR04) benthic $\delta^{18}O$ stack and timescale over the last 5 million years (larger values representing cooler temperatures and/or increased ice volume). Geomagnetic reversal stratigraphy is shown above the x-axis. Epochs and Stage shown at the top. The interglacials targeted in this thesis (G17, K1, KM3 and KM5c) are shown by the vertical blue bars. Modified from Raymo et al. (2009)

1.1.2 The Pliocene epoch

The Cenozoic Era, spanning the past 65 million years is the most recent of the three Phanerozoic eras (Gradstein et al., 2005). The $\delta^{18}O$ records displays a number of episodes of global cooling and warming with relative ice sheet growth and decay (Zachos et al., 2001). These stepwise transitions were on top of a gradual long-term cooling climate, from the hot, ice-free greenhouse world of the Palaeocene (66 – 56 Ma) to the cooler climate of the Pleistocene characterised by the glacial/interglacial cycles (Zachos et al., 2001). Towards the end of the Cenozoic Era, was the Pliocene (5.33 to 2.59 Ma), the youngest of two epochs that make up the Neogene period (23.0 – 2.59 Ma) (Gradstein et al., 2005). The Pliocene is made up of two stages, the Zanclean (5.33 – 3.60 Ma) and the Piacenzian (3.60 – 2.59 Ma). The Pliocene epoch, while a time of global cooling compared to the previous, warmer Miocene epoch, is the last period of sustained warmth before the emergence of the large scale glaciations of the Pleistocene (Lisiecki & Raymo, 2005; Fedorov et al., 2013).

1.1.3 Mid Piacenzian (Pliocene) Warm Period

The middle part of the Piacenzian Stage of the Pliocene epoch (3.264 to 3.025 My ago), also referred to as the mid-Pliocene Warm Period (mPWP), is the most recent extended period of the past significantly warmer than today (Raymo et al., 1996; Jansen et al., 2007; Haywood et al., 2013a). It offers an opportunity to understand a warmer than present world, as well as to assess the predictive ability of numerical models (Haywood et al., 2016). The mPWP provides an accessible example of a world that is similar to what models estimate could be the Earth at the end of this century (Jansen et al., 2007). There are many similarities between the mPWP and the modern world, such as continental positions, oceanic circulation patterns and extant biota that facilitate comparison between the two (Dowsett et al., 2013a). Geological data indicate that sea surface temperatures were warmer, especially in the high latitudes (Dowsett et al., 2010), and climate model predictions have found global annual mean surface temperatures were 2.7 – 4.0 °C higher than the pre-industrial (Haywood et al., 2013b).

Carbon isotope data suggests carbon dioxide (CO_2) levels were ~380 ppmv during the mPWP, with the warmest intervals reaching 45 ppmv higher (Raymo et al., 1996). Figure 1.2 shows a recent summary of Pliocene CO_2 data. Kürschner et al. (1996) estimated that CO_2

fluctuated between 280 and 370 ppmv from the inverse relationship between pCO_2 and stomatal parameters on oak leaves. Isotopic analysis of alkenones (Pagani et al., 2010) has also confirmed the higher end of pCO_2 estimates of Raymo et al. (1996) and reconstructed CO_2 levels at peak temperatures were between 365 and 415 ppmv. Seki et al. (2010) demonstrated that alkenone and boron based pCO_2 estimates agree well when carried out on the same core material. This multi-proxy reconstruction indicated that pCO_2 was 50 – 120 ppmv higher in the Pliocene compared to pre-industrial (280 ppmv). Bartoli et al. (2011) also contributed to the previously published evidence that suggested pCO_2 was higher by 130 ppmv compared to pre-industrial.

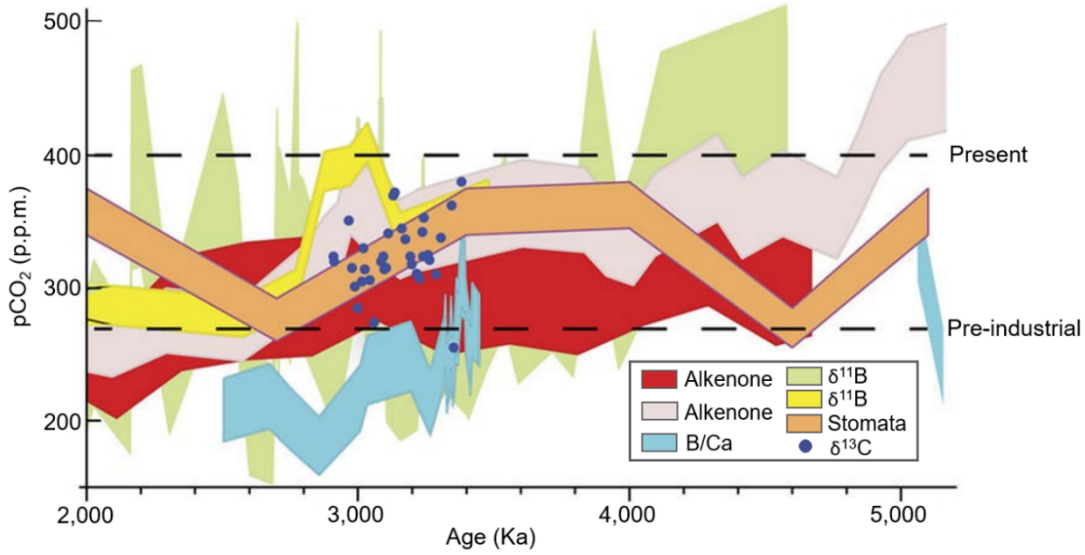

Figure 1.2 Estimates of Pliocene atmospheric CO_2 with pre-industrial and present (horizontal dashed line) for comparison. Modified from Fedorov et al., (2013). Records from: Kürschner et al., 1996; Raymo et al., 1996; Tripati et al., 2009; Pagani et al., 2010; Seki et al., 2010; Bartoli et al., 2011.

Alongside generally increased CO_2 levels, there is much evidence to suggest that mean sea level was changed during the Pliocene (Fig.1.3). Published estimates of peak sea level in the Pliocene have a wide range, though a ~25 m peak has been widely cited (Raymo et al., 2009). Dowsett and Cronin (1990) estimated a peak of 35 m +/- 18 m from uplift rates for the Orangeburg Scarp in North and South Carolina. Miller et al (2012) estimated peak sea level at 95% confidence was 22 +/- 10 m higher than modern. This estimate implies a loss of the equivalent of the Greenland and West Antarctic ice sheets as well as some loss from the East Antarctic ice sheet (Miller et al., 2012). Alongside the reduction of ice sheets, other processes that affect water volume include thermal expansion and variations in groundwater and lake

storages (Miller et al., 2005). The IPCC summarised with high confidence that global mean sea level during interglacials in the mPWP was higher than present, due to the deglaciation of the Greenland and West Antarctic ice sheets and areas of East Antarctic ice sheet, and that sea level was not higher than 20 m above present (Masson-Delmotte et al., 2013).

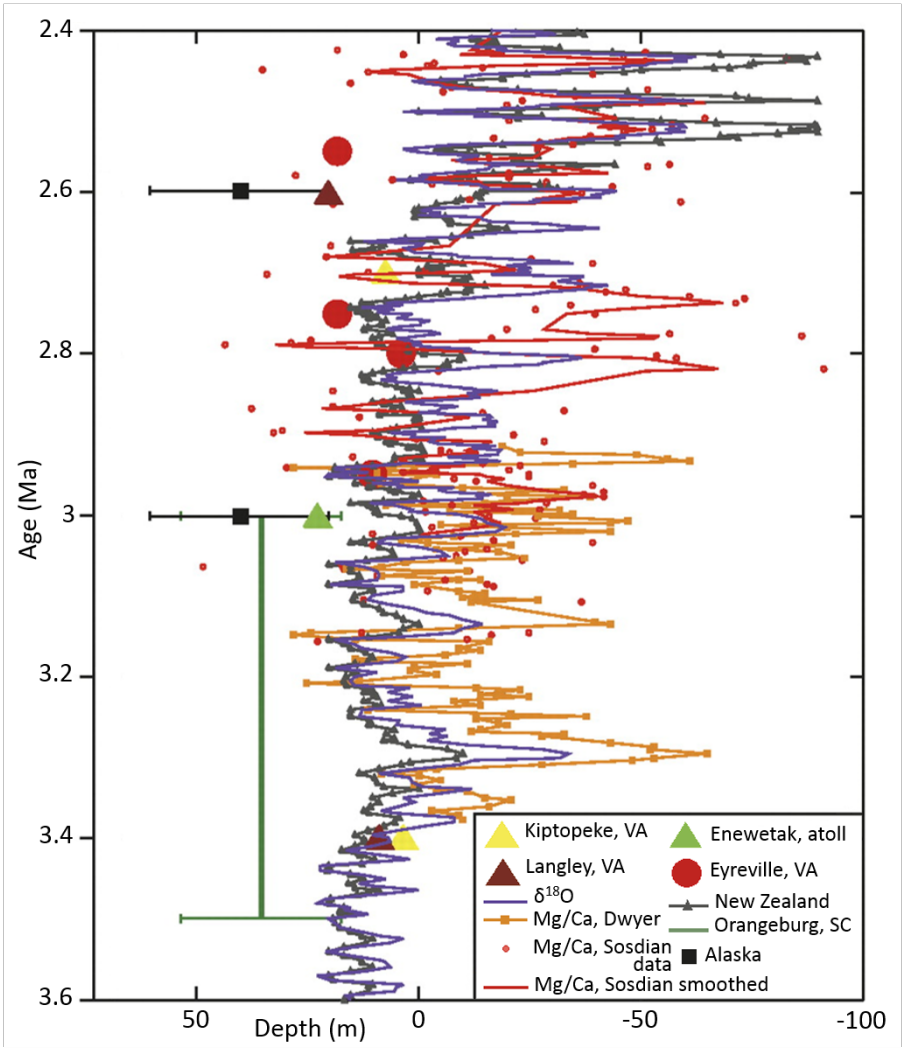

Figure 1.3 Comparison of late Pliocene sea-level estimates: $\delta^{18}O$ scaled to sea level using assumptions outlined in Miller et al. (2012) (see also Miller et al., 2005); Mg/Ca-based estimates (Sosdian & Rosenthal, 2009; Dwyer & Chandler, 2009); Enewetak Atoll (Pacific Ocean; Wardlaw & Quinn, 1991); Eyreville, Virginia (United States; Miller et al., 2012); Kiptopeke and Langley, Virginia (Hayden et al., 2008); New Zealand (Naish, 1997; Naish & Wilson, 2009; Miller et al., 2012); Orangeburg Scarp, South Carolina (Dowsett & Cronin, 1990); and Alaskan terraces (Brigham-Grette & Carter, 1992). Green error bars indicate error estimate for uplift for Orangeburg Scarp (Dowsett and Cronin, 1990). Modified from Miller et al. (2012).

The greatest differences between Pliocene vegetation and pre-industrial are in the high latitudes (Fig.1.4). In many areas taiga forest grew instead of polar tundra with the boundary of these biomes further north (Thompson & Fleming, 1996; Salzmann et al., 2008).

There is also a northward expansion of temperate forests in Eurasia and North America seen in the Pliocene compared to pre-industrial (Salzmann et al., 2008). The differences between pre-industrial and Pliocene vegetation in the mid latitudes are less apparent and largely indicate a wetter climate in the Pliocene (Thompson & Fleming, 1996). The vegetation of the Piacenzian stage in the Pliocene predominantly point towards a warmer and moister climate (Salzmann et al., 2008).

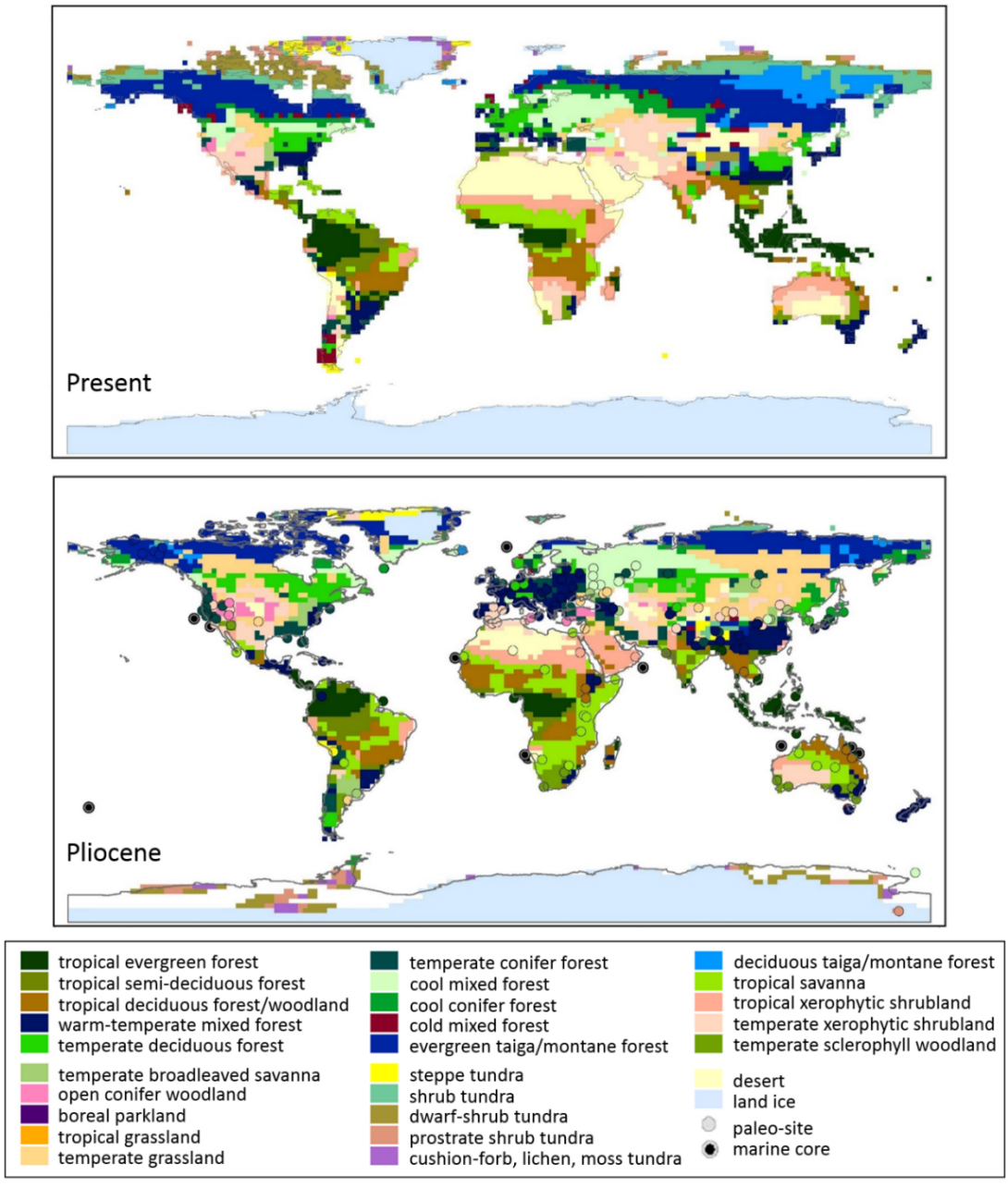

Figure 1.4 Global map of observed biomes (upper figure) and Late Pliocene data-model hybrid biome reconstruction (lower figure), based on 202 palaeobotanical sites and the output of a HadAM3/BIOME4 vegetation model (modified from Salzmann et al., 2008).

1.1.4 The PRISM project

A significant contribution to the current understanding of the mPWP is the Pliocene Research, Interpretation and Synoptic Mapping (PRISM) project which has been the focus of two decades of intensive investigations into all aspects of the mPWP climate system resulting in a series of palaeoenvironmental reconstructions: PRISM0, PRISM1, PRISM2 and PRISM3D (Dowsett et al., 2013a). The PRISM project was created with two primary goals: to identify causes and variability in mPWP climate and to create datasets that could be used as boundary conditions by climate modelling groups to investigate the mechanisms of climate change (Dowsett et al., 1999). The PRISM interval (between 3.264 and 3.025 Myr ago) precedes the first strong oxygen isotope excursions symbolising the shift to Pleistocene climate with enhanced ice volume in the Northern Hemisphere and increased variation between glacial and interglacials times (Dowsett et al., 2013b).

Originally, the PRISM reconstruction focussed on the sea surface temperatures, at first just for the North Atlantic (Dowsett & Poore 1991), before being developed into a Northern Hemisphere-wide reconstruction for PRISM0 (Dowsett et al., 1994). Applying a 'time slab' approach (Dowsett & Poore 1991) the PRISM project reconstructed conditions representing an average interglacial (warm period) throughout the mPWP (~300 kyrs), and found warming concentrated to the high latitudes, specifically through the North Atlantic with minimal change in sea surface temperatures (SSTs) in the tropics (Dowsett & Poore 1991; Dowsett et al. 1994; 1996). This discovery was hypothesised to be because of changes in meridional heat flux causing decreased sea ice and planetary albedo feedbacks driving an amplification of warming at the high latitudes (Dowsett et al., 1992). A global reconstruction was introduced in PRISM1 (Dowsett et al., 1996) and PRISM2 (Dowsett et al., 1999). The PRISM time slab of the marine reconstruction is 240,000 years wide and the vegetation reconstruction (Fig. 1.4) is for the whole Piacenzian Stage (1 million years wide) (Salzmann et al., 2008; Dowsett et al., 2009).

The PRISM3D reconstruction, has been developed to include new analytical techniques and data-model hybrid approaches (Dowsett et al., 2010). There are four main ways the PRISM3D reconstruction differs from earlier versions. PRISM3D used the vegetation model BIOME4 to produce a synthesis of vegetation information from the 202 site reconstruction and model output (Fig. 1.4; Salzmann et al., 2008). The PRISM3D Antarctic and Greenland

ice sheet reconstructions are similarly created from a data-model hybrid method using the British Antarctic Survey Ice Sheet Model (BASISM) driven by a GCM experiment using PRISM2 boundary conditions (Hill et al., 2007). The PRISM3D for the first time includes a three-dimensional reconstruction of the global ocean thermal regime (Dowsett et al., 2009) and makes use of geochemical SST proxies adding to the existing faunal and floral based proxies (Dowsett et al., 2010).

Faunal analysis was used as a SST proxy in PRISM2 and earlier reconstructions, whereas PRISM3D incorporates a multi-proxy approach (Dowsett et al., 2010). The majority of reconstructed PRISM3D SSTs, however, are still from microfossils of planktonic foraminifera (near-surface dwelling marine single-celled organisms with calcium carbonate shells) from Deep Sea Drilling Project (DSDP) and Ocean Drilling Program (ODP) cores (Dowsett et al., 2013b). Statistical methods have been employed by the PRISM group to translate Pliocene faunal census data into estimates of SSTs (Dowsett & Robinson, 1998). In PRISM3D, faunal estimates of SSTs were derived either by using a factor analytic transfer function (Dowsett, 1991) or a revised modern analogue technique (Dowsett & Robinson, 1998), with adjustments to take into account Pliocene age assemblages (Dowsett et al., 2012). In some areas, due to better preservation of siliceous microfossils than carbonate microfossils, diatoms and radiolarian were used for quantitative SST estimates (Dowsett et al., 2012).

Analysing foraminifera shell chemistry is another way of estimating palaeotemperatures. The shells are mainly made up of calcium, carbon and oxygen, but also contain a small amount of magnesium (Robinson, 2011). The magnesium replaces calcium in the shells at a rate closely tied to water temperature (Robinson, 2011). Magnesium/calcium palaeothermometry (Mg/Ca) is a method where the ratio of the increase in magnesium in fossilised foraminifera shells is quantitatively used to reconstruct SSTs as well as to estimate deep ocean temperatures in the PRISM3D reconstruction (Dowsett et al., 2010). An alternative method relies on alkenones, long-chained organic compounds produced by a few species of haptophyte algae that live in the near-surface ocean (Robinson et al., 2008). A relationship between relative abundances of alkenones and water temperature during growth has been demonstrated in laboratory cultures (Marlowe et al., 1984) and modern marine samples (Volkman et al., 1980), where the extent of unsaturation changes with growth temperature.

This relationship is defined by the $U^{K'}_{37}$ index (Brassell et al., 1986), where $U^{K'}_{37}$ stands for unsaturated ketones with 37 carbon atoms, and is used to calculate mean annual SST in the PRISM3D reconstruction (Dowsett et al., 2010).

The PRISM3D SST estimates obtained from faunal data used a warm peak averaging (WPA) methodology to derive the warm phase of climate from the PRISM interval at each location (Dowsett & Poore, 1991; Fig.1.5). This strategy minimised limitations associated with correlating peaks and troughs in temperature time series separated by large geographical distances and ages of sites could be confidently associated to the PRISM time slab (Dowsett, 2007). In this method, a warm peak is defined as a temperature warmer than the estimates surrounding it in a stratigraphic sequence. A quality standard is undertaken on the warm peaks, based on a test of the communality of the data. An acceptable communality cut off is set at 0.7 by the PRISM group, which means the factor model must explain a minimum of 84% of the variance in the data (Dowsett, 2007). The warm peaks were established and the estimates that comply to the communality cut off were averaged (Dowsett et al., 2009) and then combined with the other proxy techniques for estimating SSTs (Fig.1.5).

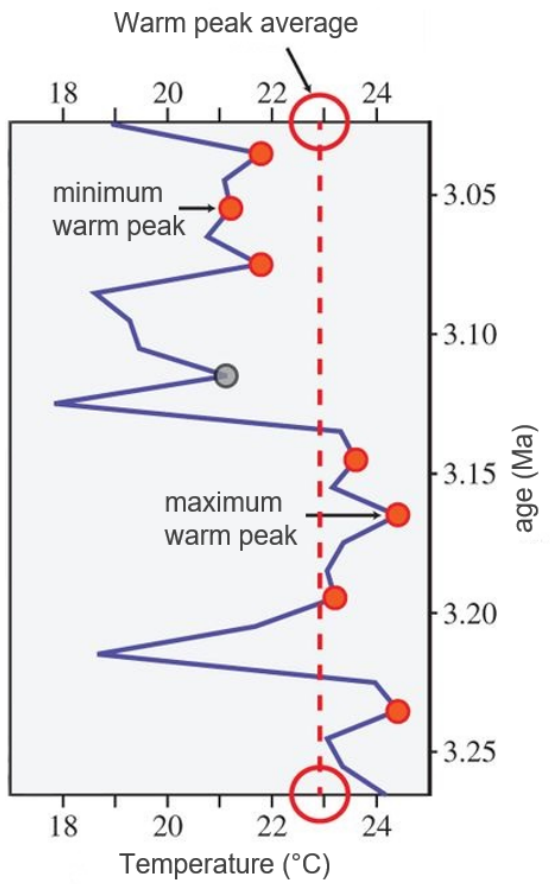

Figure 1.5 Schematic showing an example of the warm peak averaging (WPA) process adapted from Dowsett et al. (2013b). Warm peaks (red dots) in the PRISM time slab that do not fall below a predefined communality level (as with grey dot) are used to develop an 'average interglacial' SST. Maximum and minimum peaks are also designated and used as a 'climatological error bar' for the WPA estimate.

1.1.5 Modelling the Pliocene

In the first modelling study of the mPWP, Chandler et al. (1994) used the atmosphere only GISS GCM II (Goddard Institute for Space Studies General Circulation Model II) with PRISM0 SST, sea ice and vegetation boundary conditions. The version of the GISS GCM used had a resolution of 7° x 10°, CO_2 levels were fixed at 315 ppmv and a modern orbit was used. The simulation was limited to the Northern Hemisphere and resulted in 1.4 °C average warming compared to the GISS GCM current climate control simulation. There was little change of temperature at the tropics with amplification at high latitudes (Chandler et al., 1994).

The National Center for Atmospheric Research (NCAR) GENESIS climate model was then used again with PRISM0 boundary conditions; with CO_2 and orbit set at contemporaneous values (Sloan et al., 1996). GENESIS is an atmosphere only model with a resolution of 4.5° x 7.5°. There was a resulting 3.6 °C average global temperature increase from a present day simulation and increased precipitation (Sloan et al., 1996).

In a study to complement the above, Haywood et al. (2000) used the UK Met Office atmosphere only GCM (HadAM3) with the resolution of 2.5° x 3.75° initiated with PRISM2 boundary conditions. Compared to the present day control simulation, the model predicts an increase in the average warming of 1.9 °C with warming at its greatest in high latitudes and a reduced equator-to-pole temperature gradient of 6 °C (Haywood et al., 2000).

The above modelling studies have been restricted to using atmospheric GCMs with prescribed SSTs and are therefore unable to simulate feedbacks of the ocean on climate. Haywood & Valdes (2004) completed the first simulation of the mPWP with a fully coupled atmosphere-ocean model. HadCM3 (Hadley Centre Coupled Climate Model version 3) was used and coupled to the PRISM2 boundary conditions with a CO_2 concentration of 400 ppmv. When compared to the present day, the simulation results showed a 3.09 °C increase in global average surface temperature and the largest magnitude of warming at high latitudes with the equator-to-pole temperature gradient reduced by 9.04 °C (Haywood & Valdes, 2004).

Following Haywood & Valdes (2004), a considerable number of climate simulations were run for the mPWP with fully coupled atmosphere-ocean models (Jiang, 2005; Haywood & Valdes, 2006; Bonham et al., 2009), however, they incorporated only a few climate models (e.g. HadCM3, IAP AGCM; Institute of Atmospheric Physics). To explore uncertainty in the model predictions of the mPWP, a multi-model ensemble PlioMIP (Pliocene Model Intercomparison Project) was added as a part of PMIP (Palaeoclimate Modelling Intercomparison Project).

1.1.6 The PlioMIP project

All models in PlioMIP used boundary conditions from the PRISM3D palaeoenvironmental reconstruction (Haywood et al., 2010). This, combined with a set experiment design, provided a structure to enable more rigorous comparison between models. Two experiments were designed: one with atmosphere only models (AGCMs) and the second with coupled atmosphere-ocean climate models (AOGCMs). The multi-model mean (MMM) surface air temperature (SAT) with the atmosphere only AGCMs showed a minimal change from pre-industrial between 15° north and south of the equator with increasing temperature change moving into the high latitudes, particularly over Greenland and the Arctic Basin (Haywood et al., 2013b). The MMM results from the coupled AOGCMs simulated SAT warming of 1-2 °C over oceans and 1-6 °C over land in the tropics compared to pre-industrial, with mid to high latitudes showing a pattern of increasing SAT change from pre-industrial. The models largely agree in their predictions of tropical SAT change with larger variability in the high latitudes of both hemispheres. The range in global annual mean surface air temperature warming is 1.76 °C for the AOGCMs. This range illustrates how the models are responding differently to identical boundary conditions. All models simulate polar amplification of SAT when compared to pre-industrial although the magnitude is model dependent (Haywood et al., 2013b).

1.1.7 Data-model comparison

A terrestrial data-model comparison used 45 palaeobotanical sites to assess how the PlioMIP MMM simulated SATs (Salzmann et al., 2013: Fig.1.6). The comparison indicated that the models underestimated the SAT reconstructed by the terrestrial proxies in the mid to high latitudes of the Northern Hemisphere, this mismatch is notably high in Eurasia where

temperature differences reach 18 °C (Salzmann et al., 2013: Fig.1.6). These large temperature differences between the models and the proxy data are from sites that the authors assessed to be high or very high confidence (Salzmann et al., 2013). There is less data available for the low latitudes but the few temperature estimates available suggest the models overestimate temperatures in tropical regions (Salzmann et al., 2013: Fig.1.6).

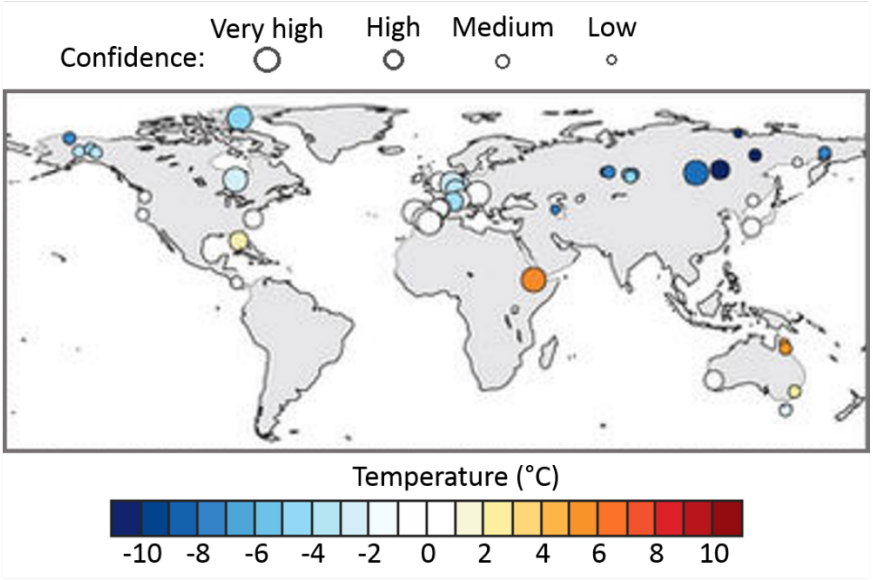

Figure 1.6 Difference between PlioMIP MMM SAT anomaly and proxy-based Pliocene SAT anomalies. Modified from Salzmann et al. (2013).

Annual SST results from the PlioMIP project were compared with the PRISM mean annual SST estimates at 100 locations in the PRISM3D marine reconstruction (Dowsett et al., 2013a: Fig.1.7). This study finds general agreement between the PlioMIP MMM and the PRISM3D reconstruction with a few significant differences. Whereas polar amplification of SSTs with maximum increase in the North Atlantic is one of the fundamental patterns seen in the PRISM dataset, this is not the case in the MMM results (Dowsett et al., 2013a). Individual models in the ensemble do simulate polar amplification but not to the magnitude seen in the PRISM3D reconstruction (section c in Fig.1.7). There is a large inter-model spread of results specifically in the North Atlantic, which may be due to the highly variable position of the Gulf stream and North Atlantic drift (Dowsett et al., 2013a). Warming is predicted at low latitudes in all simulations in the PlioMIP ensemble but only seen at PRISM3D sites that are associated with upwelling, whereas the rest of the sites reconstructed SSTs are indistinguishable from modern (Dowsett et al., 2013a: section a in Fig.1.7).

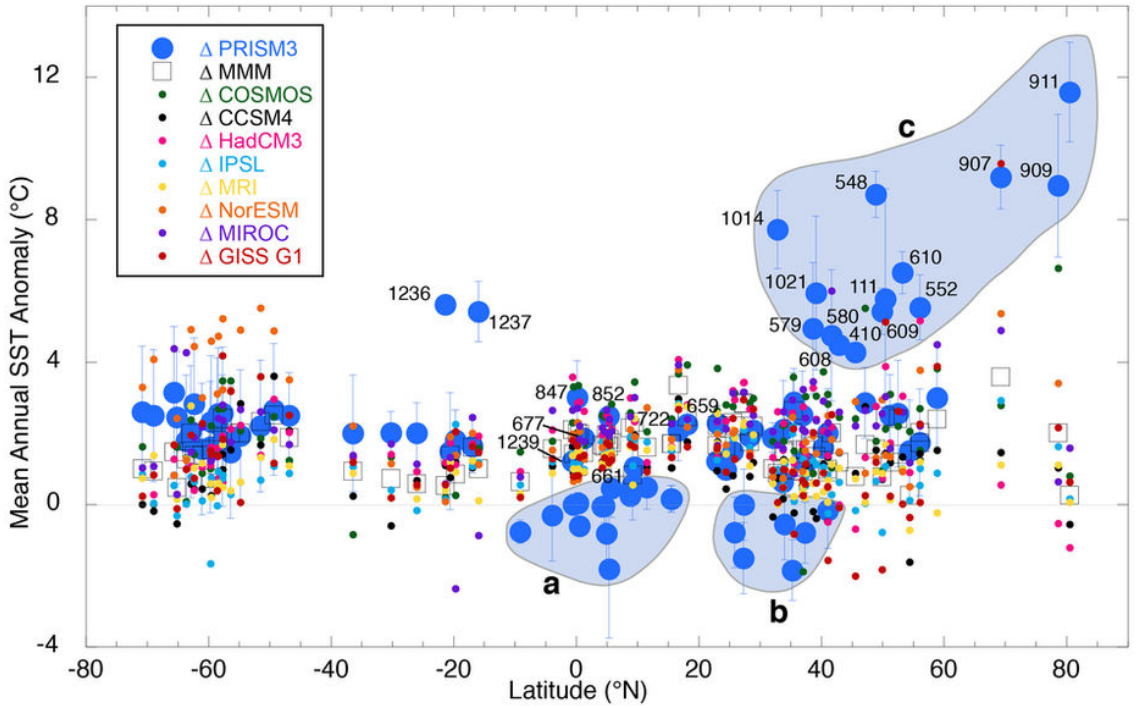

Figure 1.7 Scatter plot of MMM anomalies (squares) from PlioMIP and PRISM3 data anomalies (large blue circles) by latitude. Vertical bars on data anomalies represent the variability of warm climate phase within the time-slab at each locality. The small coloured circles represent individual model anomalies; model data from the location of the PRISM sites were used. Encircled areas are (a) PRISM low latitude sites outside of upwelling areas; (b) North Atlantic coastal sequences and Mediterranean sites; (c) large anomaly PRISM sites from the northern hemisphere and the numbers are some of the specific Ocean Drilling Program sites discussed in Dowsett et al. (2013a).

While Dowsett et al. (2013a) found discord between the models and data at low latitude sites (Fig.1.7), proxy reconstructions of tropical SST's in the mPWP is an ongoing area of research with known limitations. Warm water species of foraminifera (used in the PRISM3D reconstruction) are the most fragile and sustain dissolution preferentially which causes a cooler temperature estimate (Dowsett et al., 2012). Moreover, the alkenone based techniques used in the PRISM3D time slab are ineffective in the warm tropics as they do not record temperatures above 28 °C, due to the saturation of the $U^{K'}_{37}$ index at around this temperature (Robinson, 2011).

In addition, recent studies suggest pre-Pleistocene Mg/Ca based SST estimates are affected by changes in the Mg/Ca ratio of sea water (O'Brien et al., 2014; Evans et al., 2016). Looking at proxy comparisons of Mg/Ca and TEX^{H}_{86} at site 1143 in the southern South China Sea, O'Brien et al. (2014) found the previous SST estimates were too low and suggested this was

due to long term shifts in seawater chemistry. New SST estimates were 2-3 °C warmer than existing data which resolves the discrepancy between the previous SST reconstructions and PlioMIP (O'Brien et al., 2014). The Mg/Ca seawater record calculated in O'Brien et al. (2014) is based on data from only one site and therefore may be biased due to any site specific complications of the individual geochemical records (such as a shift in seasonality of a given proxy or a change in carbon dissolution intensity through time) (Evans et al., 2016). A more recent study by Evans et al. (2016) using multiple sites (four sites spanning last ~5 Ma), and therefore a more robust calculation of Mg/Ca seawater in the Pliocene, found that both surface and deep ocean Mg/Ca derived temperatures have been underestimated by 0.9 – 1.9 °C. Even this more conservative number goes some way to resolving the data-model differences in the tropical areas in the Pliocene and suggests that future data records that include this correction for seawater chemistry changes in the Pliocene may be a better match for the climate model simulated temperatures.

1.1.8 Limitations of time averaged PRISM reconstructions

At each site, the PRISM3D reconstruction represents an average warm climate signal that occurred during the time slab and should not be considered a reconstruction of environmental conditions that existed together at a discrete moment in time (Haywood et al., 2013a). While evidence suggests climate variability during the mPWP is smaller than for the past 2 million years, clear variations do occur on orbital time scales (Haywood et al., 2013a). There was a degree of variability within this interval based on the marine isotopic records and temperature time series analysed by the PRISM group that was not conveyed in the reconstructions (Dowsett et al., 2013b). Some of the significant mismatches between models and data seen in Salzmann et al. (2013) and Dowsett et al. (2013a) have been attributed to the fact that the climate models were run using one single (modern) orbital configuration. However, the proxy records represent multiple intervals of time through the mid-Pliocene with various orbital forcings (Haywood et al., 2013a). A climate model simulation uses one orbital forcing (based on one moment in time) and therefore the data and the models are not reproducing the same objective. This makes conclusions on model performance based on the data-model comparison between model simulations and the PRISM reconstruction difficult to separate from the intrinsic limitations of this time slab method (Haywood et al., 2013a). To progress with data-model comparisons in the mPWP, this orbital uncertainty needs to be taken into consideration.

1.1.9 Orbital forcing

The shape of the Earth's orbit and axis of rotation are perturbed by the gravitational interaction between other bodies in the solar system and are therefore slowly changing with time (Valdes & Glover, 1999). These fluctuations in the angle of tilt and Earth's orbit, relative to the sun, modify the seasonal and latitudinal distribution of incoming solar radiation reaching the Earth and have a controlling influence on climate (Jansen et al., 2007). A record of these orbitally-driven climate cycles can be observed in marine and terrestrial sequences (deMenocal, 2004; Tzedakis, 2005). There are three parameters controlling the shape of the Earth's orbit and the orientation of the axis of rotation: eccentricity, obliquity and precession (Fig.1.8).

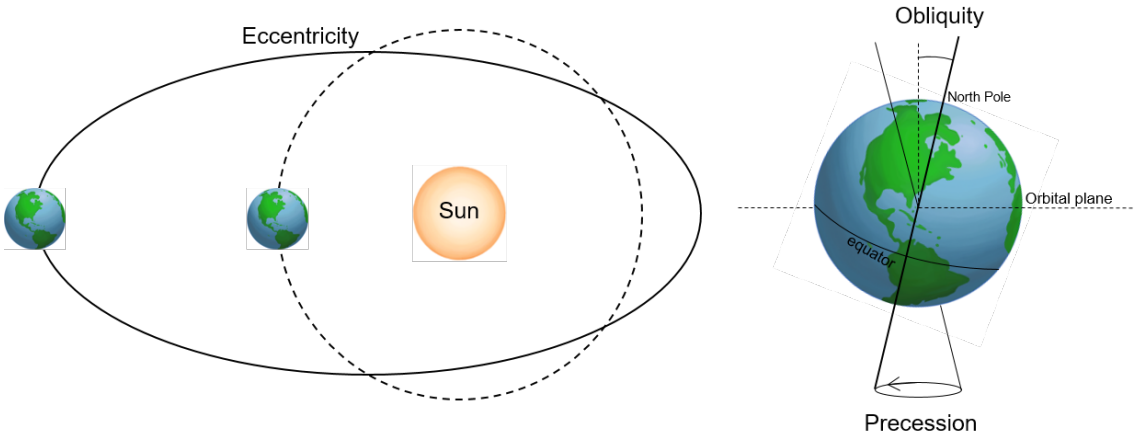

Figure 1.8 Orbital parameters. Figure showing eccentricity, obliquity and precession.

The Earth's orbit around the sun is an ellipse and the parameter eccentricity defines the shape of the orbit. The Earth's eccentricity varies between 0.000055 (nearly circular orbit) and 0.0679 (Laskar et al., 2011) at periodicities at 400 kyr and approximately 100 kyr (Jansen et al., 2007). The eccentricity is the only parameter that can change the total annual insolation (by a small amount) and modulates precession and seasonal contrast by altering the distance from the Earth and the Sun in different seasons (Berger & Loutre, 1994).

The Earth rotates around an axis that leans at an angle relative to the perpendicular of the orbital plane which varies over time at a periodicity of 38 to 43 kyr (Lisiecki & Raymo, 2007). The obliquity parameter is the angle of tilt, which moves from 22.1° to 24.5°, with a larger angle increasing seasonality (warmer summers and colder winters) (Huybers, 2006). The

effects of the obliquity parameter however, are not uniform throughout the Earth, with increased obliquity increasing the annual solar radiation at higher latitudes but decreasing at lower latitudes (Berger, 1988).

Precession refers to the change in the orientation of the Earth's rotational axis with periodicities of approximately 19 and 23 kyr, for example, if a hemisphere is pointed towards the sun at perihelion (point of Earth's orbit closest to the sun) that hemisphere will also be pointed away at aphelion (point of the orbit furthest from the sun) and the seasonal contrast will be greater (Berger & Loutre, 1991). In climate related studies, the climatic precession parameter is used, defined as $e\sin\omega$ (where e is the eccentricity and ω is the longitude of perihelion, which is the angle between the moving Northern Hemisphere spring equinox and the perihelion (Huybers & Aharonson, 2010)). The climatic precession defines where summer/winter occur with respect to the perihelion and aphelion from the Sun and plays an opposite role in each hemisphere, i.e. warm NH summer occurs with a cold SH winter (and vice versa). As eccentricity modulates precession, if the eccentricity is zero, there is no effect of precession on climate (as perihelion = aphelion). The climatic precession parameter along with obliquity acts to redistribute insolation along latitudes and seasons but has no effect on the annual insolation (Berger, 1988).

The above parameters cause changes in insolation and occur from both orbital (eccentricity) and rotational (obliquity and precession) changes in the Earth's astronomy. In this thesis however, the term 'orbital' is used to refer to any changes in the Earth's orbit or orientation that result in long term changes in the distribution of insolation.

1.1.10 Climate variability

The Pliocene has predominantly been treated as a stable average interglacial. While there is increased variability after the Pliocene/Pleistocene boundary in the LR04 stack, there is still variability throughout the Pliocene that needs to be understood. Palaeoclimate studies of the later Quaternary period (0 - 2.58 million years ago) have established the importance of understanding climate variability.

In a compilation of ice, marine and terrestrial palaeoclimate records from the last 800 kyrs, Lang & Wolff (2011) assessed climate patterns of glacial and interglacial strength. A wide range of interglacial and glacial behaviour was noted with a general pattern of increased strength over the last 450 kyrs than the preceding 350 kyrs. Tzedakis et al. (2009), also looking at the palaeoclimate records from the last 800 kyrs, discussed the large diversity among interglacials throughout this time with differences in intensity, duration and internal variability. It was also observed that both the intensity and duration of warmth of the interglacials in this time varied geographically.

Using the Community Climate System Model 3 (CCSM3), Herold et al. (2012) compared the simulated climate response to peak interglacial forcing for MIS 1, 5, 9, 11 and 19. This modelling study found the greatest variation between the interglacials occurred in sea ice margins and across the northern mid-latitudes, where large variations in insolation combined with sizable terrestrial areas lead to significant temperature differences between the interglacials (Herold et al., 2012).

While the fluctuations of temperature change in the Quaternary were significantly greater during glacial times than interglacials (Jouzel et al., 2007), the present interglacial (the Holocene ~11.5 ka BP to present) was interrupted by cold relapses (Wanner et al., 2015). A study of multiple globally distributed Holocene high-resolution proxy records identified six cooling events approximately at intervals of 2500 and 1500 years (Mayewski et al., 2004). These climate variations, although weaker in amplitude than is seen in the Pleistocene, were larger and more frequent than is commonly recognised (Mayewski et al., 2004). It was also demonstrated that not all sites responded synchronously or equally during these events (Mayewski et al., 2004). The discovery that Holocene climate change can be abrupt, even in the absence of the large unstable ice sheets that so dramatically affected Pleistocene climate, is further impetus for improving understanding of Pliocene climate variability.

Whilst the benthic oxygen isotope record implies a reduced feedback between orbital forcing and ice volume/bottom water temperatures in the Pliocene (compared to the Pleistocene), orbital forcing remained an important driver of regional surface temperature variability, as well as seasonality changes, throughout the Pliocene (Haywood et al., 2016). While it is important to study both glacials and interglacials to assess Pliocene climate variability, as

discussed in Dolan et al (2015) in the first modelling study targeting Marine Isotope Stage (MIS) M2 (the "Pliocene glacial"), there are significant challenges when simulating cooler events during the Pliocene. There are no explicit boundary conditions designed for use when simulating a Pliocene glacial climate due to a lack of evidence for the locations of ice masses during M2 (Dolan et al., 2015). Therefore, while it is imperative to also look at the cooler periods throughout the Pliocene to assess a complete picture of Pliocene climate variability, in this thesis the emphasis is on interglacial climate variability. Here, interglacials are defined as any isotope excursion which results in a more negative $\delta^{18}O$ than the Holocene average. Concentrating on these warmer periods within the Pliocene is a natural progression from the PlioMIP project that simulated an average warm Pliocene, as well as the original aims of the PRISM project of targeting the mPWP to understand a warmer world and the climate processes within.

1.2 Aims and Research Questions

Aim: To investigate interglacial climate variability during the mPWP and explore the importance of orbital climate variability in understanding mPWP climates and the ability of climate models to reproduce them.

This thesis is based on snapshot sensitivity experiments carried out with a fully coupled General Circulation Model (GCM) and can be addressed by a number of objectives which have been framed as research questions. Each of the results chapters 2, 3 and 4 explicitly addresses at least one of these research questions. The rest of this chapter explores the scientific background to each research question and some general information on methods used. A more detailed introduction, model description and methodology is found in each chapter. Each of the three results chapters has been written as research articles for publication in peer-reviewed journals. The preface before each chapter details the publication status of each paper as well as specifying the contributions of co-authors for these publications.

Research Questions		Chapter
RQ1	What is the predicted temperature variability around two interglacial events with different characteristics of orbital forcing in the mPWP and what are the implications for terrestrial and marine data-model comparison?	2
RQ2	To what degree does orbital forcing drive changes in surface climatological and land cover response between four interglacial events in the mPWP and how does the addition of vegetation feedbacks in a model alter this?	3
RQ3	How does orbital forcing influence a critical component of the climate system, the Indian monsoon, during mPWP interglacials?	4

Table 1.1 Research questions and the chapter in which they are addressed.

1.2.1 RQ1: What is the temperature variability around two interglacial events with different characteristics of orbital forcing in the mPWP and what are the implications for data-model comparison?

As discussed previously, data-model comparisons in the mPWP have indicated some areas of agreement between the climate model outputs and geological data temperature estimates, however, differences have been observed in the high latitudes. The reasons for these differences will be complex and difficult to assign to one particular element of either the proxy data or the climate models. An area to explore is the time averaged nature of the global palaeoenvironmental synthesis used in the DMC (Haywood et al., 2013a, 2016). The limitations in correlating one marine or land site to another over large geographical distances originally favoured the establishment of a time slab to which the ages of these sites could be more confidently ascribed (Dowsett and Poore 1991). The time slab for the PRISM3D global marine synthesis was ~240 kyr long (Dowsett et al., 2010) and the PRISM3D global vegetation reconstruction was constructed from information for the entire Piacenzian Stage of the Pliocene epoch (~1 million years) (Salzmann et al., 2008). In short, RQ1 is to investigate the hypothesis that a component of data-model inconsistencies is related to the time slab nature of the current PRISM palaeoenvironmental synthesises and the limited characterisation of Pliocene orbital variability in existing proxy data and climate model simulations.

This is explored by completing a series of orbital forcing sensitivity experiments using a fully coupled atmosphere-ocean GCM around two interglacial events, KM5c and K1, in the

mPWP to quantify the magnitude of orbitally-forced temperature changes across both interglacial events and how that variability around each interglacial differs. KM5c is characterised by a near modern orbital forcing within a period of low eccentricity and low precession, while MIS K1 occurred during one of the lightest benthic oxygen isotope excursions in the mPWP with stronger orbital forcing. A suite of 30 orbital sensitivity simulations centred on the two isotope excursions with different orbital forcing characteristics, MIS KM5c and K1 are analysed.

1.2.2 RQ2: To what degree does orbital forcing drive changes in surface climatological and land cover response between four interglacial events in the mPWP and how does the addition of vegetation feedbacks alter this?

Salzmann et al (2008) developed a compilation of middle Pliocene vegetation data from 202 marine and terrestrial sites and compared it with the output of BIOME4 forced by climatology from a HadAM3 (the atmosphere only version of the model used in this thesis) Pliocene simulation. The model simulation was initialised with PRISM2 boundary conditions and run with a modern orbit. They found the BIOME4 results compared favourably with the palaeodata. The vegetation data however was an incorporation of records from the whole Piacenzian Stage of the Pliocene (~1 million years). Most records within this reconstruction are not dated on orbital timescales, and could therefore represent interglacial or glacial conditions, and the model simulation run with a modern orbit did not include potential for orbital variability. While the PRISM3D vegetation synthesis is representative of the entire Piacenzian Stage, there are published vegetation records that suggest there were vegetation changes on orbital timescales (Leroy & Dupont, 1994; Willis et al., 1999; Gao et al. 2012; Tarasov et al., 2013). To date there have been no modelling studies exploring this potential vegetation changes to differences in orbital forcing in the Pliocene. To continue the aims of the PRISM and PlioMIP projects in investigating the warm Pliocene, four of the most prominent interglacials are chosen as targets for exploration. These four interglacials, MIS G17, K1, KM3 and KM5c are simulated with PRISM3D boundary conditions and orbital forcing relative to the peak of the interglacial (Table 1.2). The simulated vegetation distribution is compared to assess the impact of orbital forcing on the simulation of vegetation.

Interglacial event modelled (MIS)	Peak of Interglacial (Ma)	Eccentricity	Climatic Precession	Obliquity
G17	2.950	0.04	-0.01776	23.96
K1	3.060	0.05	-0.05086	23.01
KM3	3.155	0.05	-0.04350	23.76
KM5c	3.205	0.01	0.00605	23.47

Table 1.2 Four interglacial events discussed in chapters 3 and 4. The age corresponding to the peak of each interglacial simulated and the orbital parameters of that peak. Astronomical parameters derived from Laskar et al. (2004).

In four further simulations of the interglacials, as well as changing the orbit parameters in the model, a dynamic vegetation model is coupled to the GCM. The importance of vegetation within palaeoclimate modelling experiments, particularly the interaction between vegetation and climate is well documented (Ganopolski et al., 1998; Levis et al., 1999; Foley et al., 2000). The climate-vegetation feedback is an important interaction and results not including this may under or overestimate climatological changes. To fully answer RQ2, the four simulated interglacials MIS G17, K1, KM3 and KM5c are simulated with a dynamic vegetation model which enables the vegetation to interact with the climate simulated. To understand how the addition of dynamic vegetation can impact the modelled climate response to orbital forcing, as well as to further understand the changes seen in vegetation distribution, the annual and seasonal surface air temperature and precipitation changes are investigated in the four interglacials in addition to the changes in simulated vegetation.

1.2.3 RQ3: How does orbital forcing influence a critical component of the climate system, the Indian monsoon, during Pliocene interglacials?

When exploring climate variability in the past, it is important not only to investigate global climate changes but also dynamic systems such as monsoons. Monsoons are seasonal occurrences and are responsible for the majority of low latitude summer rainfall (Christensen

et al., 2013). The Asian monsoon alone influences the societal and economic activity for almost two thirds of the world's population and includes two main systems: the Indian monsoon and the East Asian monsoon. The link between orbital forcing and the world's monsoon systems has been extensively studied with a wide range of evidence from different environmental indicators displaying that how the Asian monsoon varies depends on insolation (Joussaume et al., 1999; Jansen et al., 2007; Braconnot et al., 2008). Additionally, geological proxy records suggest orbital forcing has affected the long-term evolution of the Asian monsoon (Wang et al., 2005; Clift & Plumb, 2008).

In general, efforts in climate modelling and proxy reconstructions during the Piacenzian Stage have focused on reconstructing an average East Asian Pliocene monsoon (Zheng et al., 2004; Jiang et al., 2008; Wan et al., 2010; Suarez et al., 2011; Su et al., 2013; Zhang et al., 2013, 2015). There has been relatively little attention dedicated to the Indian monsoon system in the proxy and climate modelling communities and no specific work dedicated to modelling monsoon variability in the Pliocene. To answer RQ3, the surface climatology over the Indian monsoon area is compared between for the four interglacials (MIS G17, K1, KM3 and KM5c) to explore how the Indian monsoon may have varied due to the changing orbital parameters through the Piacenzian Stage.

1.3 Research approach

The research questions outlined above are addressed based on an ensemble of snapshot simulations carried out with the UK Met Office Hadley Centre Coupled Climate Model version 3 (HadCM3). The reasons for using HadCM3 will subsequently be discussed and information on the experimental design will then be detailed.

1.3.1 HadCM3

To answer the research questions as robustly as possible, a relatively high resolution GCM is required (e.g. for looking at regional climate systems such as the Indian monsoon) where it is still practical to carry out long integrations of several hundred years on top of initial spin up to a near steady state. HadCM3 has been extensively used in palaeoclimate simulations due to its relatively fast running time allowing long simulations to be undertaken. HadCM3 is also the model of choice for UK Pliocene research and has been used in the PlioMIP project. HadCM3 was one of the major models used in the IPCC Third and Fourth Assessments and contributes to the Fifth Assessment. Of particular relevance to RQ3, of 18 models in the CMIP3 database tested, HadCM3 was found to be one of six to simulate the present-day cycle of the Indian monsoon reasonably well (Annamalai et al., 2007). The model is set up for simulating the Pliocene by inputting Pliocene specific boundary conditions; this experimental design has been employed for HadCM3 in several published studies (Bragg et al., 2012; Howell et al., 2016) and described by Haywood et al. (2011) in the PlioMIP project. The model boundary conditions used in this thesis were produced by the PRISM group and are briefly summarised in the following paragraphs.

1.3.2 Boundary conditions

The experiments in this thesis were run based on the PlioMIP experimental design with PRISM3D boundary conditions (Haywood et al., 2010).

1.3.2.1 Topography and ice sheets

The PRISM3D topographic reconstruction is based on the Pliocene palaeogeography of Markwick, (2007). Figure1.8 shows the topography which is largely similar to modern. There are a few significant differences however. The coastlines were created to reflect a 25 m sea-level rise and the Hudson Bay was filled in at low elevations (Sohl et al., 2009). The ice sheet estimates were produced using BASISM coupled offline to the atmosphere only HadAM3. The predicted reconstruction was substantially different from modern ice sheets over Antarctica and Greenland. The West Antarctic ice sheet is absent and much reduced over Greenland and East Antarctica (Fig. 1.8; Hill et al., 2007; Haywood et al., 2010).

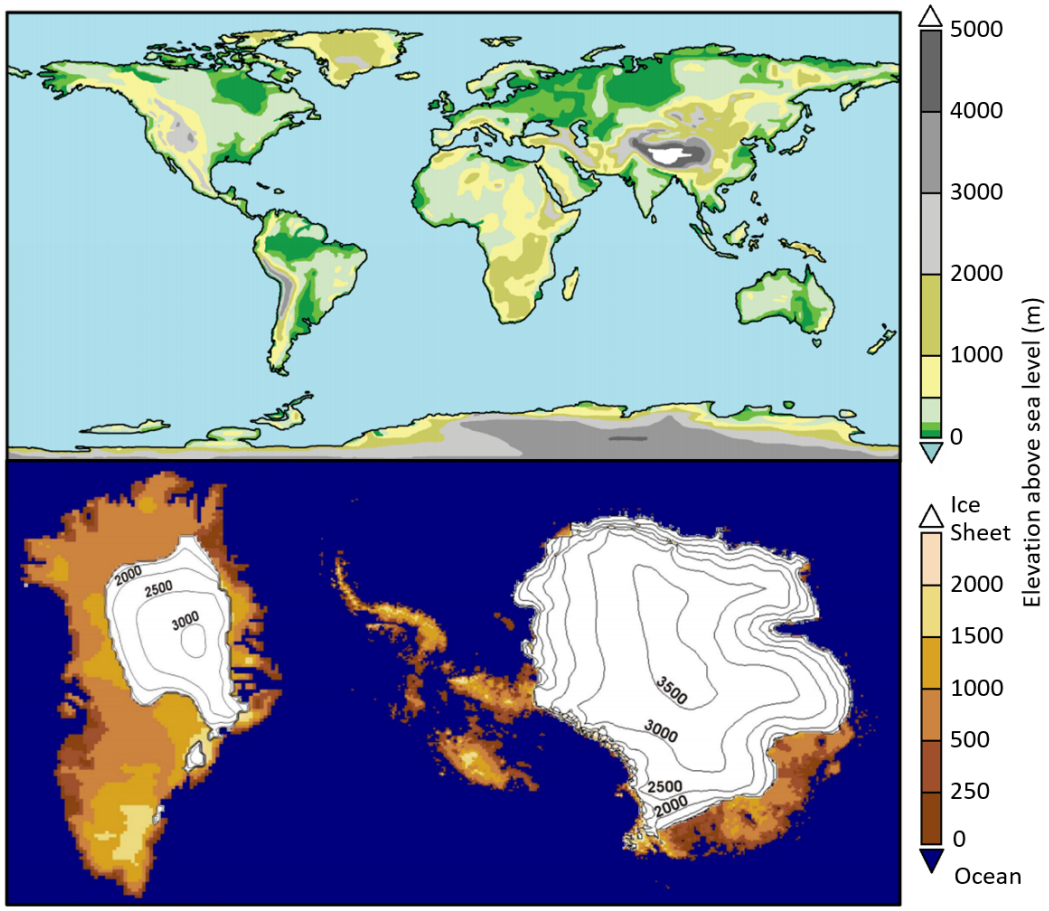

Figure 1.9 PRISM3D Topography reconstruction (top) from Sohl et al. (2009) and ice sheet reconstructions of Greenland (bottom-left) and Antarctica (bottom-right) modified from Haywood et al. (2010).

References

Annamalai, H., Hamilton, K. & Sperber, K.R. (2007). The South Asian Summer Monsoon and Its Relationship with ENSO in the IPCC AR4 Simulations. *Journal of Climate*. 20 (6). pp. 1071–1092.

Bartoli, G., Hönisch, B. & Zeebe, R.E. (2011). Atmospheric CO_2 decline during the Pliocene intensification of Northern Hemisphere glaciations. *Paleoceanography*. 26 (4).

Berger, A. (1988). Milankovitch Theory and climate. *Reviews of Geophysics*. 26 (4). pp. 624-657.

Berger, A. & Loutre, M.F. (1991). Insolation values for the climate of the last 10 million years. *Quaternary Science Reviews*. 10 (4). pp. 297–317.

Berger, A. & Loutre, M.F. (1994). Precession, Eccentricity, Obliquity, Insolation and Paleoclimates. In: Duplessy, J.C., Spyridakis, M.T. (eds) *Long-Term Climatic Variations*. NATO ASI Series (Series l: Global Environmental Change), Springer Berlin Heidelberg, 22. pp. 107–151.

Bonham, S.G., Haywood, A.M., Lunt, D.J., Collins, M. & Salzmann, U. (2009). El Nino-Southern Oscillation, Pliocene climate and equifinality. *Philosophical Transactions of the Royal Society A: Mathematical, Physical and Engineering Sciences*. 367 (1886). pp. 127–156.

Braconnot, P., Marzin, C., Grégoire, L., Mosquet, E. & Marti, O. (2008). Monsoon response to changes in Earth's orbital parameters: comparisons between simulations of the Eemian and of the Holocene. *Climate of the Past*. 4 (4). pp. 281–294.

Bragg, F.J., Lunt, D.J. & Haywood, A.M. (2012). Mid-Pliocene climate modelled using the UK Hadley Centre Model: PlioMIP Experiments 1 and 2. *Geoscientific Model Development Discussions*. 5 (2). pp. 837–871.

Brassell, S.C., Eglinton, G., Marlowe, I.T., Pflaumann, U. & Sarnthein, M. (1986). Molecular stratigraphy: a new tool for climatic assessment. *Nature*. 320 (6058). .pp. 129–133.

Brigham-Grette, J. & Carter, L.D. (1992). Pliocene marine transgressions of northern Alaska: circumarctic correlations and paleoclimatic interpretations. *Arctic*. 45 (1). pp. 74–89.

Chandler, M., Rind, D. & Thompson, R. (1994). Joint investigations of the middle Pliocene climate II: GISS GCM Northern Hemisphere results. *Global and Planetary Change*. 9 (3–4). pp. 197–219.

Christensen, J.H., Krishna Kumar, K., Aldrian, E., An, S.-I., Cavalcanti, I.F.A., de Castro, M., Dong, W., Goswami, P., Hall, A., Kanyanga, J.K., Kitoh, A., Kossin, J., Lau, N.-C., Renwick, J., Stephenson, D.B., Xie, S.-P. & Xhou, T. (2013). Climate Phenomena and their Relevance for Future Regional Climate Change. In: *Climate Change 2013; The Physical Science Basis. Contribution*

of Working Group I to the Fifth Assessment Report of the Intergovernmental Panel on Climate Change [Stocker, T.F., D. Qin, G.-K. Plattner, M. Tignor, S.K. Allen, J. Boschung, A. Nauels, Y. Xia, V. Bex and P.M. Midgley (eds.)]. Cambridge University Press, Cambridge, United Kingdom and New York, NY, USA.

Clift, P.D. & Plumb, R.A. (2008). *The Asian Monsoon, Causes History and Effects*. Cambridge University Press.

deMenocal, P.B. (2004). African climate change and faunal evolution during the Pliocene-Pleistocene. *Earth and Planetary Science Letters*. 220 (1–2). pp. 3–24.

Dolan, A.M., Haywood, A.M., Hunter, S.J., Tindall, J.C., Dowsett, H.J., Hill, D.J. & Pickering, S.J. (2015). Modelling the enigmatic Late Pliocene Glacial Event - Marine Isotope Stage M2. *Global and Planetary Change*. 128. pp. 47–60.

Dowsett, H.J. & Cronin, T.M. (1990). High eustatic sea level during the middle Pliocene: Evidence from the southeastern U.S. Atlantic Coastal Plain. *Geology*. 18 (5). pp. 435-438.

Dowsett, H.J. (1991). The Development of a Long-Range Foraminifer Transfer Function and Application to Late Pleistocene North Atlantic Climatic Extremes. *Paleoceanography*. 6 (2). pp. 259–273.

Dowsett, H.J. & Poore, R.Z. (1991). Pliocene sea surface temperatures of the north atlantic ocean at 3.0 Ma. *Quaternary Science Reviews*. 10 (2–3). pp. 189–204.

Dowsett, H.J., Cronin, T.M., Poore, R.Z., Thompson, R.S., Whatley, R.C. & Wood, A.M. (1992). Micropaleontological evidence for increased meridional heat transport in the north atlantic ocean during the pliocene. *Science (New York, N.Y.)*. 258 (5085). pp. 1133–5.

Dowsett, H., Thompson, R., Barron, J., Cronin, T., Fleming, F., Ishman, S., Poore, R., Willard, D. & Holtz, T. (1994). Joint investigations of the Middle Pliocene climate I: PRISM paleoenvironmental reconstructions. *Global and Planetary Change*. 9 (3–4). pp. 169–195.

Dowsett, H., Barron, J. & Poore, R. (1996). Middle Pliocene sea surface temperatures: a global reconstruction. *Marine Micropaleontology*. 27 (1–4). pp. 13–25.

Dowsett, H.J. & Robinson, M.M. (1998). Application of the modern analog technique (MAT) of sea surface temperature estimation to middle Pliocene North Pacific planktonic foraminifer assemblages. *Palaeontologia Electronica*. 1 (1). p.p. 22.

Dowsett, H.J., Barron, J.A., Poore, R.Z., Thompson, R.S., Cronin, T.M., Ishman, S.E. & Willard, D.A. (1999). Middle Pliocene paleoenvironmental reconstruction: PRISM 2. Open-File Report pp. 99-535. U.S. Dept. of the Interior.

Dowsett, H.J. (2007). The PRISM palaeoclimate reconstruction and Pliocene sea-surface temperature. In: M. Williams, A. M. Haywood, F. J. Gregory, & D. N. Schmidt (eds.) In: *Deep-time perspectives on climate change : marrying the signal from computer models and biological proxies*. London: Published for the Micropalaeontological Society by the Geological Society, p. 589.

Dowsett, H.J., Robinson, M.M. & Foley, K.M. (2009). Pliocene three-dimensional global ocean temperature reconstruction. *Climate of the Past*. 5 (4).pp. 769–783.

Dowsett, H., Robinson, M., Haywood, A.M., Salzmann, U., Hill, D., Sohl, L., Chandler, M., Williams, M., Foley, K. & Stoll, D. (2010). The PRISM3D paleoenvironmental reconstruction. *Stratigraphy*. 7 (2-3). pp. 123-139.

Dowsett, H.J., Robinson, M.M., Haywood, A.M., Hill, D.J., Dolan, A.M., Stoll, D.K., Chan, W.-L., Abe-Ouchi, A., Chandler, M.A., Rosenbloom, N.A., Otto-Bliesner, B.L., Bragg, F.J., Lunt, D.J., Foley, K.M. & Riesselman, C.R. (2012). Assessing confidence in Pliocene sea surface temperatures to evaluate predictive models. *Nature Climate Change*. 2 (5). pp. 365–371.

Dowsett, H.J., Foley, K.M., Stoll, D.K., Chandler, M.A., Sohl, L.E., Bentsen, M., Otto-Bliesner, B.L., Bragg, F.J., Chan, W.-L., Contoux, C., Dolan, A.M., Haywood, A.M., Jonas, J.A., Jost, A., Kamae, Y., Lohmann, G., Lunt, D.J., Nisancioglu, K.H., Abe-Ouchi, A., Ramstein, G., Riesselman, C.R., Robinson, M.M., Rosenbloom, N.A., Salzmann, U., Stepanek, C., Strother, S.L., Ueda, H., Yan, Q. & Zhang, Z. (2013a). Sea surface temperature of the mid-Piacenzian ocean: a data-model comparison. *Scientific reports*. 3. (2013).

Dowsett, H.J., Robinson, M.M., Stoll, D.K., Foley, K.M., Johnson, A.L.A., Williams, M. & Riesselman, C.R. (2013b). The PRISM (Pliocene palaeoclimate) reconstruction: time for a paradigm shift. *Philosophical transactions. Series A, Mathematical, physical, and engineering sciences*. 371 p. 20120524.

Dwyer, G.S. & Chandler, M.A. (2009). Mid-Pliocene sea level and continental ice volume based on coupled benthic Mg/Ca palaeotemperatures and oxygen isotopes. *Philosophical Transactions of the Royal Society A: Mathematical, Physical and Engineering Sciences*. [Online]. 367 (1886) .pp. 157–168.

Evans, D., Brierley, C., Raymo, M.E., Erez, J. & Müller, W. (2016). Planktic foraminifera shell chemistry response to seawater chemistry: Pliocene-Pleistocene seawater Mg/Ca, temperature and sea level change. *Earth and Planetary Science Letters*. 438. pp. 139–148.

Flato, G., Marotzke, J., Abiodun, B., Braconnot, P., Chou, S.C., Collins, W., Cox, P., Driouech, F., Emori, S., Eyring, V., Forest, C., Gleckler, P., Guilyardi, E., Jakob, C., Kattsov, V., Reason, C. & Rummukainen, M. (2013). Evaluation of Climate Models. In: T. F. Stocker, D. Qin, G.-K. Plattner, M. Tignor, S. K. Allen, J. Boschung, A. Nauels, Y. Xia, V. Bex, & P. M. Midgley (eds.). *Climate Change 2013 - The Physical Science Basis. Contribution of Working Group I to the Fifth Assessment of the Intergovernmental Panel on Climate Change*. Cambridge, United Kingdom and New York, NY,

USA: Cambridge University Press.

Foley, J.A., Levis, S., Costa, M.H., Cramer, W. & Pollard, D. (2000). Incorporating dynamic vegetation cover within global climate models. *Ecological Applications*. 10. pp. 1620-1632

Ganopolski, A., Kubatzki, C., Claussen, M., Brovkin, V. & Petoukhov, V. (1998). The influence of vegetation-atmosphere-ocean interaction on climate during the mid-holocene. *Science (New York, N.Y.)*. 280 (5371). pp. 1916–1919.

Gao, C., McAndrews, J.H., Wang, X., Menzies, J., Turton, C.L., Wood, B.D., Pei, J. & Kodors, C. (2012). Glaciation of North America in the James Bay Lowland, Canada, 3.5 Ma. *Geology*. 40 (11). pp. 975–978.

Hayden, T., Kominz, M., Powars, D.S., Edwards, L.E., Miller, K.G., Browning, J. V. & Kulpecz, A.A. (2008). Impact effects and regional tectonic insights: Backstripping the Chesapeake Bay impact structure. *Geology*. [Online]. 36 (4). pp. 327–330.

Haywood, A.M., Valdes, P.J. & Sellwood, B.W. (2000). Global scale palaeoclimate reconstruction of the middle Pliocene climate using the UKMO GCM: Initial results. *Global and Planetary Change*. 25 (3–4). pp. 239–256.

Haywood, A.M. & Valdes, P.J. (2004). Modelling Pliocene warmth: contribution of atmosphere, oceans and cryosphere. *Earth and Planetary Science Letters*. 218 (3–4). pp. 363–377.

Haywood, A.M. & Valdes, P.J. (2006). Vegetation cover in a warmer world simulated using a dynamic global vegetation model for the Mid-Pliocene. *Palaeogeography, Palaeoclimatology, Palaeoecology*. 237 (2–4). pp. 412–427.

Haywood, A.M., Dowsett, H.J., Otto-Bliesner, B., Chandler, M.A., Dolan, A.M., Hill, D.J., Lunt, D.J., Robinson, M.M., Rosenbloom, N., Salzmann, U. & Sohl, L.E. (2010). Pliocene Model Intercomparison Project (PlioMIP): experimental design and boundary conditions (Experiment 1). *Geoscientific Model Development*. [Online]. 3 (1). pp. 227–242.

Haywood, A.M., Dolan, A.M., Pickering, S.J., Dowsett, H.J., McClymont, E.L., Prescott, C.L., Salzmann, U., Hill, D.J., Hunter, S.J., Lunt, D.J., Pope, J.O. & Valdes, P.J. (2013a). On the identification of a Pliocene time slice for data-model comparison. *Philosophical transactions. Series A, Mathematical, physical, and engineering sciences*. 371 (2001). p.p. 20120515.

Haywood, A.M., Hill, D.J., Dolan, A.M., Otto-Bliesner, B.L., Bragg, F., Chan, W.-L., Chandler, M.A., Contoux, C., Dowsett, H.J., Jost, A., Kamae, Y., Lohmann, G., Lunt, D.J., Abe-Ouchi, A., Pickering, S.J., Ramstein, G., Rosenbloom, N.A., Salzmann, U., Sohl, L., Stepanek, C., Ueda, H., Yan, Q. & Zhang, Z. (2013b). Large-scale features of Pliocene climate: results from the Pliocene Model Intercomparison Project. *Climate of the Past*. [Online]. 9 (1). pp. 191–209.

Haywood, A.M., Dowsett, H.J. & Dolan, A.M. (2016). Integrating geological archives and climate

models for the mid-Pliocene warm period. *Nature Communications*. 7 p.p. 10646.

Herold, N., Yin, Q.Z., Karami, M.P. & Berger, A. (2012). Modelling the climatic diversity of the warm interglacials. *Quaternary Science Reviews*. 56. pp. 126–141.

Hill, D.J., Haywood, A.M., Hindmarsh, R.C.A. & Valdes, P.J. (2007). Characterizing ice sheets during the Pliocene: evidence from data and models. In: M. Williams, A. M. Haywood, F. J. Gregory, & D. N. Schmidt (eds.). *Deep-time perspectives on climate change: marrying the signal from computer models and biological proxies*. London: Geological Society of London, pp. 517–538.

Howell, F.W., Haywood, A.M., Dowsett, H.J. & Pickering, S.J. (2016). Sensitivity of Pliocene Arctic climate to orbital forcing, atmospheric CO 2 and sea ice albedo parameterisation. *Earth and Planetary Science Letters*. 441. pp. 133–142.

Huybers, P. (2006). Early Pleistocene Glacial Cycles and the Integrated Summer Insolation Forcing. *Science*. 313 (5786). p.pp. 508–511.

Huybers, P. & Aharonson, O. (2010). Orbital tuning, eccentricity, and the frequency modulation of climatic precession. *Paleoceanography*. 25 (4). p.p. PA4228

Jansen, E., Overpeck, J., Briffa, K.R., Duplessy, J.-C., Joos, F., Masson-Delmotte, V., Olago, D., Otto-Bliesner, B., Peltier, W.R., Rahmstorf, S., Ramesh, R., Raynaud, D., Rind, D., Solomina, O., Villalba, R. & Zhang, D. (2007). Palaeoclimate. In: S. Solomon, D. Qin, M. Manning, Z. Chen, M. Marquis, K. B. Averyt, M. Tignor, & H. L. Miller (eds.). *Climate Change 2007: The Physical Science Basis. Contribution of Working Group I to the Fourth Assessment Report of the Intergovernmental Panel on Climate Change*. Cambridge, United Kingdom and New York, NY, USA: Cambridge University Press.

Jiang, D. (2005). Modeling the middle Pliocene climate with a global atmospheric general circulation model. *Journal of Geophysical Research*. 110 (D14). p.p. D14107.

Jiang, D., Ding, Z., Drange, H. & Gao, Y. (2008). Sensitivity of East Asian climate to the progressive uplift and expansion of the Tibetan Plateau under the mid-Pliocene boundary conditions. *Advances in Atmospheric Sciences*. 25 (5). pp. 709–722.

Joussaume, S., Taylor, K.E., Braconnot, P., Mitchell, J.F.B., Kutzbach, J.E., Harrison, S.P., Prentice, I.C., Broccoli, A.J., Abe-Ouchi, A., Bartlein, P.J., Bonfils, C., Dong, B., Guiot, J., Herterich, K., Hewitt, C.D., Jolly, D., Kim, J.W., Kislov, A., Kitoh, A., Loutre, M.F., Masson, V., McAvaney, B., McFarlane, N., de Noblet, N., Peltier, W.R., Peterschmitt, J.Y., Pollard, D., Rind, D., Royer, J.F., Schlesinger, M.E., Syktus, J., Thompson, S., Valdes, P., Vettoretti, G., Webb, R.S. & Wyputta, U. (1999). Monsoon changes for 6000 years ago: Results of 18 simulations from the Paleoclimate Modeling Intercomparison Project (PMIP). *Geophysical Research Letters*. 26 (7). pp. 859–862.

Jouzel, J., Masson-Delmotte, V., Cattani, O., Dreyfus, G., Falourd, S., Hoffmann, G., Minster, B., Nouet, J., Barnola, J.M., Chappellaz, J., Fischer, H., Gallet, J.C., Johnsen, S., Leuenberger, M., Loulergue, L., Luethi, D., Oerter, H., Parrenin, F., Raisbeck, G., Raynaud, D., Schilt, A., Schwander, J., Selmo, E., Souchez, R., Spahni, R., Stauffer, B., Steffensen, J.P., Stenni, B., Stocker, T.F., Tison, J.L., Werner, M. & Wolff, E.W. (2007). Orbital and Millennial Antarctic Climate Variability over the Past 800,000 Years. *Science*. 317 (5839). pp. 793–796.

Kürschner, W.M., van der Burgh, J., Visscher, H. & Dilcher, D.L. (1996). Oak leaves as biosensors of late neogene and early pleistocene paleoatmospheric CO2 concentrations. *Marine Micropaleontology*. 27 (1–4). pp. 299–312.

Lang, N. & Wolff, E.W. (2011). Interglacial and glacial variability from the last 800 ka in marine, ice and terrestrial archives. *Climate of the Past*. 7 (2). pp. 361–380.

Laskar, J., Fienga, A., Gastineau, M. & Manche, H. (2011). La2010: A new orbital solution for the long term motion of the Earth. *Astronomy & Astrophysics*. 532. p.p. A89.

Leroy, S. & Dupont, L. (1994). Development of vegetation and continental aridity in northwestern Africa during the Late Pliocene: the pollen record of ODP site 658. *Palaeogeography, Palaeoclimatology, Palaeoecology*. 109 (2–4). pp. 295–316.

Levis, S., Foley, J.A. & Pollard, D. (1999). CO2, climate, and vegetation feedbacks at the Last Glacial Maximum. *Journal of Geophysical Research-Atmospheres*. [Online]. 104 (D24). pp. 31191–31198.

Lisiecki, L.E. & Raymo, M.E. (2007). Plio–Pleistocene climate evolution: trends and transitions in glacial cycle dynamics. *Quaternary Science Reviews*. 26. pp. 56–69.

Markwick, P.J. (2007). The palaeogeographic and palaeoclimatic significance of climate proxies for data-model comparisons. In: M. Williams, A. M. Haywood, J. Gregory, & D. Schmidt (eds.). *Deep-time perspectives on climate change : marrying the signal from computer models and biological proxies*. London: Micropaleontology Society, pp. 251–312.

Marlowe, I.T., Green, J.C., Neal, A.C., Brassell, S.C., Eglinton, G. & Course, P.A. (1984). Long Chain (n-C37-C39) alkenones in the Prymnesiophyceae. Distribution of alkenones and other lipids and their taxonomic significance. *British Phycological Journal*. 19 (3). pp. 203–216.

Masson-Delmotte, V., Schulz, M., Abe-Ouchi, A., Beer, J., Ganopolski, A., Gonzalez Rouco, J.F., Jansen, E., Lambeck, K., Luterbacher, J., Naish, T., Osborn, T., Otto-Bliesner, B., Quinn, T., Ramesh, R., Rojas, M., Shao, X. & Timmermann, A. (2013). Information from Paleoclimate Archives. In: T. F. Stocker, D. Qin, G.-K. Plattner, M. Tignor, S. K. Allen, J. Boschung, A. Nauels, Y. Xia, V. Bex, & P. M. Midgley (eds.). *Climate Change 2013 - The Physical Science Basis. Contribution of Working Group I to the Fifth Assessment of the Intergovernmental Panel on Climate Change*. Cambridge, United Kingdom and New York, NY, USA: Cambridge University Press.

Mayewski, P.A., Rohling, E.E., Stager, J.C., Karlén, W., Maasch, K.A., Meeker, L.D., Meyerson, E.A., Gasse, F., Van Kreveld, S., Holmgren, K., Lee-Thorp, J., Rosqvist, G., Rack, F., Staubwasser, M., Schneider, R.R. & Steig, E.J. (2004). Holocene climate variability. *Quaternary Research*. 62 (3). pp. 243-255.

Miller, K.G., Kominz, M.A., Browning, J. V., Wright, J.D., Mountain, G.S., Katz, M.E., Sugarman, P.J., Cramer, B.S., Christie-Blick, N. & Pekar, S.F. (2005). The Phanerozoic Record of Global Sea-Level Change. *Science*. 310 (5752). pp. 1293-1298.

Miller, K.G., Wright, J.D., Browning, J. V., Kulpecz, A., Kominz, M., Naish, T.R., Cramer, B.S., Rosenthal, Y., Peltier, W.R. & Sosdian, S. (2012). High tide of the warm Pliocene: Implications of global sea level for Antarctic deglaciation. *Geology*. 40 (5). pp. 407–410.

Naish, T. (1997). Constraints on the amplitude of late Pliocene eustatic sea-level fluctuations: New evidence from the New Zealand shallow-marine sediment record. *Geology*. [Online]. 25 (12). pp. 1139–1142.

Naish, T.R. & Wilson, G.S. (2009). Constraints on the amplitude of Mid-Pliocene (3.6-2.4 Ma) eustatic sea-level fluctuations from the New Zealand shallow-marine sediment record. *Philosophical Transactions of the Royal Society A: Mathematical, Physical and Engineering Sciences*. 367 (1886). pp. 169–187.

O'Brien, C.L., Foster, G.L., Martínez-Botí, M.A., Abell, R., Rae, J.W.B. & Pancost, R.D. (2014). High sea surface temperatures in tropical warm pools during the Pliocene. *Nature Geoscience*. [Online]. 7 (8). pp. 606–611.

Pachauri, R.K., Meyer, L., Van Ypersele, J.-P., Brinkman, S., Van Kesteren, L., Leprince-Ringuet, N. & Van Boxmeer, F. (2014). *Climate Change 2014: Synthesis Report. Contribution of Working Groups I, II and III to the Fifth Assessment Report of the Intergovernmental Panel on Climate Change.* IPCC, Geneva, Switzerland, 151 pp.

Pagani, M., Liu, Z., LaRiviere, J. & Ravelo, A.C. (2010). High Earth-system climate sensitivity determined from Pliocene carbon dioxide concentrations. *Nature Geoscience*. [Online]. 3 (1). pp. 27–30.

Raymo, M.E., Grant, B., Horowitz, M. & Rau, G.H. (1996). Mid-Pliocene warmth: stronger greenhouse and stronger conveyor. *Marine Micropaleontology*. 27 (1–4). pp. 313–326.

Raymo, M.E., Hearty, P., De Conto, R., O'Leary, M., Dowsett, H.J., Robinson, M.H. & Mitrovica, J.X. (2009). PLIOMAX: Pliocene maximum sea level project. *PAGES News*. 17 (2). pp. 58–59.

Robinson, M.M., Dowsett, H.J., Dwyer, G.S. & Lawrence, K.T. (2008). Reevaluation of mid-Pliocene North Atlantic sea surface temperatures. *Paleoceanography*. 23 (3).

Robinson, M. (2011). Pliocene Climate Lessons: An ongoing reconstruction of a warmer Earth 3

million years ago helps test climate-change forecasts. *American Scientist*. 99. pp. 228–235.

Salzmann, U., Haywood, A.M., Lunt, D.J., Valdes, P.J. & Hill, D.J. (2008). A new global biome reconstruction and data-model comparison for the Middle Pliocene. *Global Ecology and Biogeography*. 17 (3). pp. 432–447.

Salzmann, U., Dolan, A.M., Haywood, A.M., Chan, W.-L., Voss, J., Hill, D.J., Abe-Ouchi, A., Otto-Bliesner, B., Bragg, F.J., Chandler, M.A., Contoux, C., Dowsett, H.J., Jost, A., Kamae, Y., Lohmann, G., Lunt, D.J., Pickering, S.J., Pound, M.J., Ramstein, G., Rosenbloom, N.A., Sohl, L., Stepanek, C., Ueda, H. & Zhang, Z. (2013). Challenges in quantifying Pliocene terrestrial warming revealed by data–model discord. *Nature Climate Change*. 3 (11). pp. 969–974.

Seki, O., Foster, G.L., Schmidt, D.N., Mackensen, A., Kawamura, K. & Pancost, R.D. (2010). Alkenone and boron-based Pliocene pCO2 records. *Earth and Planetary Science Letters*. 292 (1–2). pp. 201–211.

Sloan, L.C., Crowley, T.J. & Pollard, D. (1996). Modeling of middle Pliocene climate with the NCAR GENESIS general circulation model. *Marine Micropaleontology*. 27 (1–4). pp. 51–61.

Sohl, L.E., Chandler, M.A., Schmunk, R.B., Mankoff, K., Jonas, J.A., Foley, K.M. & Dowsett, H.J. (2009). PRISM3/GISS Topographic Reconstruction. *U.S. Geological Survey Data Series 419*. 6 pp.

Sosdian, S. & Rosenthal, Y. (2009). Deep-Sea Temperature and Ice Volume Changes Across the Pliocene-Pleistocene Climate Transitions. *Science*. 325 (5938). pp. 306–310.

Su, T., Jacques, F.M.B., Spicer, R.A., Liu, Y.-S., Huang, Y.-J., Xing, Y.-W. & Zhou, Z.-K. (2013). Post-Pliocene establishment of the present monsoonal climate in SW China: evidence from the late Pliocene Longmen megaflora. *Climate of the Past*. 9 (4). pp. 1911–1920.

Suarez, M.B., Passey, B.H. & Kaakinen, A. (2011). Paleosol carbonate multiple isotopologue signature of active east asian summer monsoons during the late Miocene and Pliocene. *Geology*. 39 (12). pp. 1151–1154.

Tarasov, P.E., Andreev, A.A., Anderson, P.M., Lozhkin, A. V., Leipe, C., Haltia, E., Nowaczyk, N.R., Wennrich, V., Brigham-Grette, J. & Melles, M. (2013). A pollen-based biome reconstruction over the last 3.562 million years in the Far East Russian Arctic – new insights into climate–vegetation relationships at the regional scale. *Climate of the Past*. 9 (6). pp. 2759–2775.

Thompson, R.S. & Fleming, R.F. (1996). Middle Pliocene vegetation: reconstructions, paleoclimatic inferences, and boundary conditions for climate modeling. *Marine Micropaleontology*. 27 (1–4). pp. 27–49.

Tripati, A.K., Roberts, C.D. & Eagle, R.A. (2009). Coupling of CO2 and Ice Sheet Stability Over Major Climate Transitions of the Last 20 Million Years. *Science*. 326 (5958). pp. 1394–1397.

Turner, A.G., Inness, P.M. & Slingo, J.M. (2007). The effect of doubled CO2 and model basic state biases on the monsoon-ENSO system. I: Mean response and interannual variability. *Quarterly Journal of the Royal Meteorological Society*. 133 (626). pp. 1143–1157.

Tzedakis, P.C. (2005). Towards an understanding of the response of southern European vegetation to orbital and suborbital climate variability. *Quaternary Science Reviews*. 24 (14–15). pp. 1585–1599.

Tzedakis, P.C., Raynaud, D., McManus, J.F., Berger, A., Brovkin, V. & Kiefer, T. (2009). Interglacial diversity. *Nature Geoscience*. 2 (11). pp. 751–755.

Valdes, P.J. & Glover, R.W. (1999). Modelling the climate response to orbital forcing. *Philosophical Transactions of the Royal Society of London A: Mathematical, Physical and Engineering Sciences*. 357. pp. 1873-1890.

Volkman, J.K., Eglinton, G., Corner, E.D.S. & Forsberg, T.E. V (1980). Long-chain alkenes and alkenones in the marine coccolithophorid Emiliania huxleyi. *Phytochemistry*. 19 (12). pp. 2619–2622.

Wan, S., Tian, J., Steinke, S., Li, A. & Li, T. (2010). Evolution and variability of the East Asian summer monsoon during the Pliocene: Evidence from clay mineral records of the South China Sea. *Palaeogeography, Palaeoclimatology, Palaeoecology*. 293 (1–2). pp. 237–247.

Wang, P., Clemens, S., Beaufort, L., Braconnot, P., Ganssen, G., Jian, Z., Kershaw, P. & Sarnthein, M. (2005). Evolution and variability of the Asian monsoon system: state of the art and outstanding issues. *Quaternary Science Reviews*. 24 (5). pp. 595–629.

Wanner, H., Mercolli, L., Grosjean, M. & Ritz, S.P. (2015). Holocene climate variability and change; a data-based review. *Journal of the Geological Society*. 172 (2). pp. 254–263.

Wardlaw, B.R. & Quinn, T.M. (1991). The record of Pliocene sea-level change at Enewetak Atoll. *Quaternary Science Reviews*. 10 (2–3). pp. 247–258.

Willis, K.J., Kleczkowski, A. & Crowhurst, S.J. (1999). 124,000-year periodicity in terrestrial vegetation change during the late Pliocene epoch. *Nature*. 397 (6721). pp. 685–688.

Zhang, R., Yan, Q., Zhang, Z.S., Jiang, D., Otto-Bliesner, B.L., Haywood, A.M., Hill, D.J., Dolan, A.M., Stepanek, C., Lohmann, G., Contoux, C., Bragg, F., Chan, C.L., Chandler, M.A., Jost, A., Kamae, Y., Abe-Ouchi, A., Ramstein, G., Rosenbloom, N.A., Sohl, L. & Ueda, H. (2013). Mid-Pliocene East Asian monsoon climate simulated in the PlioMIP. *Climate of the Past*. 9 (5). pp. 2085–2099.

Zhang, R., Jiang, D. & Zhang, Z. (2015). Causes of mid-Pliocene strengthened summer and weakened winter monsoons over East Asia. *Advances in Atmospheric Sciences*. 32 (7). pp. 1016–1026.

Zheng, H., Powell, C.M., Rea, D.K., Wang, J. & Wang, P. (2004). Late Miocene and mid-Pliocene

enhancement of the East Asian monsoon as viewed from the land and sea. *Global and Planetary Change*. 41 (3). pp. 147–155.

CHAPTER 2

ASSESSING ORBITALLY-FORCED INTERGLACIAL CLIMATE VARIABILITY DURING THE MID-PLIOCENE WARM PERIOD

Preface

This chapter has been published in Earth and Planetary Letters as:

Prescott C.L., Haywood A.M., Dolan A.M., Hunter S.J., Pope J.O., Pickering S.J. (2014) Assessing orbitally-forced interglacial climate variability during the mid-Pliocene Warm Period. *Earth and Planetary Science Letters*, 400, pp. 261-271.

The co-authors are my supervisors and colleagues. The experimental design was planned by A.H. and C.P.. The experiments, processing, analysis and interpretation was completed by the candidate as well as the figures and written manuscript. The co-authors, A.H., A.D. and S.H. contributed specific expertise and with how to place the work into the broader scientific content. J.P. and S.P. gave technical help with the experiments.

Abstract

The traditional view of the Pliocene is one of an epoch with higher than present global mean annual temperatures (~2 to 3°C) and stable climate conditions. Published data-model comparisons for the mid-Pliocene Warm Period (mPWP: ~3.3 to 3 million years ago) have identified specific regions of concordance and discord between climate model outputs and marine/terrestrial proxy data. Due to the time averaged nature of global palaeoenvironmental syntheses, it has been hypothesised that climate variability during interglacial events within the mPWP could contribute to site-specific data-model disagreement. The Hadley Centre Coupled Climate Model Version 3 (HadCM3) is used to assess the nature of climate variability around two interglacial events within the mPWP that have different characteristics of orbital forcing (Marine Isotope Stages KM5c and K1). Model results indicate that +/- 20 kyr on either side of the MIS KM5c, orbital forcing produced a less than 1°C change in global mean annual temperatures. Regionally, mean annual surface air temperature (SAT) variability can reach 2 to 3°C. Seasonal variations exceed those predicted for the annual mean and can locally exceed 5°C. Simulations 20 kyr on either side of MIS K1 show considerably increased variability in relation to KM5c.

We demonstrate that orbitally-forced changes in surface air temperature during interglacial events within the mPWP can be substantial, and could therefore contribute to data-model discord. This is especially likely if proxies preserve growing season rather than mean annual temperatures.

Model results indicate that peak MIS KM5c and K1 interglacial temperatures were not globally synchronous, highlighting leads and lags in temperature in different regions. This highlights the potential pitfalls in aligning peaks in proxy-derived temperature across geographically diverse data sites, and indicates that a single climate model simulation for an interglacial event is inadequate to capture peak temperature change in all regions.

We conclude that the premise of sustained global warmth and stable Pliocene climate conditions is incomplete. We also contend that the likely nature of Pliocene interglacial climate variability is more akin to interglacial events within the Quaternary, where the

character of interglacials is known to be diverse. In the future, the utility of Pliocene data-model comparisons is dependent upon 1) establishing precise chronology of the proxy data, 2) providing climate models with fully proxy-consistent boundary conditions and 3) in utilising ensembles of climate simulations that can adequately capture orbital variability around any studied interval.

2.1 Introduction

2.1.1 Modelling Pliocene climate

Geological data, as well as climate model outputs, have shed considerable light on the nature of Pliocene climate and environments. During Pliocene warmth, highlighted by negative excursions in $\delta^{18}O$ from benthic foraminifera, Antarctic and/or Greenland ice volume may have been reduced (Shackleton & Hall, 1984; Lunt et al., 2008; Naish et al., 2009; Pollard & DeConto, 2009; Hill et al., 2010; Dolan et al., 2011). Peak sea-level high stands have been estimated to have been 22 ± 5 m higher than modern (Miller et al., 2012). Sea surface temperatures (SSTs) were warmer (Dowsett et al., 2010), particularly in the higher latitudes and upwelling zones (e.g. Dekens et al., 2007; Dowsett et al., 2012; Rosell-Melé et al., 2014). Sea-ice cover also declined substantially (e.g. Cronin et al., 1993; Moran et al., 2006; Polyak et al., 2010). On land, the global extent of arid deserts decreased, and forests replaced tundra in the Northern Hemisphere (e.g. Salzmann et al., 2008). The global mean annual temperature may have increased by 2 to 3°C (e.g. Haywood & Valdes, 2004; Haywood et al., 2013a). Meridional and zonal temperature gradients may have been reduced, which had a significant impact on the Hadley and Walker circulation (e.g. Haywood et al., 2000; Chan et al., 2011). The East Asian Summer monsoon, as well as other monsoon systems, may have been enhanced (e.g. Wan et al., 2010).

Arguably the best geologically studied interval of the Pliocene is the mid-Pliocene warm period (mPWP) between 3264 and 3025 ka (Dowsett et al., 2010; Haywood et al., 2010). It sits within the Piacenzian age of the Late Pliocene according to the geological timescale of Gradstein et al. (2005). The mPWP has been the focus of a number of modelling efforts that have employed individual snap-shot style climate simulations to explore the nature of global

climate at this time, as well as the sensitivity of simulated global and regional climates to imposed Pliocene boundary conditions (e.g. Haywood et al., 2013). The mPWP has also been a focus for a specific targeted campaign of data collection as well as modelling, under the PRISM (Pliocene Research Interpretations and Synoptic Mapping) approach.

2.1.2 Data-model comparison and climate variability

Given the abundance of proxy data, the mPWP has become a focus for data-model comparisons that attempt to analyse the ability of climate models to reproduce a warm climate state in Earth history (e.g. Haywood & Valdes, 2004; Salzmann et al., 2008b; Dowsett et al., 2011, 2012; Haywood et al., 2013; Salzmann et al., 2013). Whilst these studies have shown areas of agreement between climate model outputs and geological proxy temperature estimates, discord has been noted in the North Atlantic, as well as the high-latitudes in general. In these areas climate models underestimate the degree of polar amplification recorded in proxy data (Dowsett et al., 2012; Salzmann et al., 2013). If true these results are potentially of great importance in understanding the sensitivity of models for simulating warm climate states.

In any palaeo data-model comparison the cause of data-model discord will be complex and not easily attributable to a single factor in either the models or proxy data. One aspect that requires consideration is the proxy data that provide surface temperature estimates which are compared with climate model outputs. In the Pliocene, and in deep time in general (pre-Quaternary), some of the most important uncertainty in proxy data used for data model comparison can be attributed to chronology, correlation and the time averaged nature of existing global palaeoenvironmental syntheses. This is in addition to inherent uncertainties with proxies stemming from non-modern analogue environments, evolutionary changes of ecological tolerance and methodological problems. In the context of the Pliocene, limitations in correlating one marine or land site to another over large geographical distances originally favoured the establishment of a time slab to which the ages of marine or terrestrial sites could be more confidently attributed (Dowsett & Poore, 1991). The time slab for the PRISM3D (Pliocene Research, Interpretation and Synoptic Mapping) global marine synthesis was ~240 kyr long (Dowsett et al., 2010; Fig. 2.1). The global vegetation reconstruction within PRISM3D was constructed by considering information from the entire Piacenzian Stage of the Pliocene epoch, ~1000 kyr in duration (Salzmann et al., 2008).

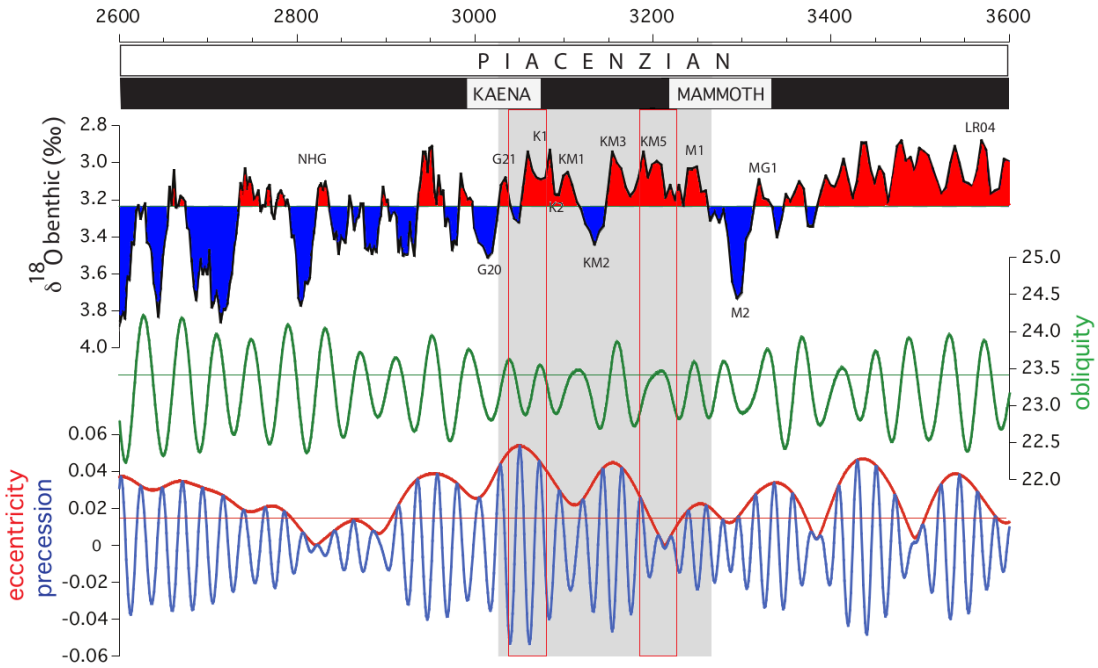

Figure 2.1 Position of the K1 and KM5c interglacials and the PRISM3D time slab (grey shaded band) on the Lisiecki & Raymo (2005) benthic oxygen isotope stratigraphy horizontal line showing the Holocene average. Obliquity, precession and eccentricity as derived from the astronomical solution of Laskar et al. (2004; La04) are also shown with the horizontal lines showing the modern orbital values.

The PRISM mPWP global environmental syntheses represent an average of warm climate signals from site to site for a defined time slab (Salzmann et al., 2008; Dowsett et al., 2010). They should not be considered as reconstructions of environmental conditions that existed together at a discrete moment in time. Climate model simulations are run for short integration periods (i.e. several centuries) using a single realisation of orbital, CO_2 and other forcings, and are not able to reproduce syntheses of average warm climate conditions (e.g. spanning ~240 to 1000 kyr), which must by definition reflect multiple changing and interacting forcing mechanisms (i.e. show climate variability). Haywood et al. (2013b) hypothesise that a component of currently noted data-model inconsistencies are related to the time slab nature of the global environmental syntheses and the limited characterisation of Pliocene climate variability in existing proxy data and climate model simulations.

Here we explore this hypothesis by completing a series of orbital forcing sensitivity experiments using the Hadley Centre Coupled Climate Model version 3 (HadCM3) around

two discrete interglacial events within the mPWP (Marine Isotope Stages KM5c (3205 ka) and K1 (3060 ka); Fig. 2.1). For the purposes of this paper we define a Pliocene interglacial as any isotope excursion which results in more negative $\delta^{18}O$ than the Holocene average. Whilst the nature of discrete boundary conditions (e.g. the ice sheet configuration) for individual interglacial events within the mPWP remains unknown, we are able to quantify the magnitude of orbitally-forced climate variability in each interglacial event, and how the variability in each interglacial differs. Haywood et al. (2013b) show that the peak of Marine Isotope Stage (MIS) KM5c is characterised by a near modern orbital forcing within a period of low eccentricity and low precession. In contrast MIS K1 occurred during an interval where the total global mean annual insolation was ~0.5 Wm^{-2} higher than the modern. It is characterised by one of the lightest benthic oxygen isotope excursions evident in the mPWP.

2.2 Methodology

2.2.1 Model description – HadCM3

The particulars of the UK Met Office Hadley Centre Coupled Climate Model Version 3 (HadCM3) used in this study are well documented (Gordon et al., 2000). The model requires no flux corrections, even for simulations of a thousand years or more (Gregory & Mitchell, 1997). HadCM3 consists of a coupled atmosphere, ocean and sea ice model components. The horizontal resolution of the atmospheric model is 2.5 degrees in latitude by 3.75 degrees in longitude. This gives a grid spacing at the equator of 278 km in the north-south direction and 417 km east-west and is approximately comparable to a T42 spectral model resolution. The atmospheric model consists of 19 layers. The atmospheric model has a time step of 30 minutes and includes a radiation scheme that can represent the effects of minor trace gases (Edwards & Slingo, 1996). A parameterization of simple background aerosol climatology is also included (Cusack et al., 1998). The convection scheme is described in Gregory et al. (1997). A land-surface scheme includes the representation of the freezing and melting of soil moisture. The representation of evaporation includes the dependence of stomatal resistance on temperature, vapour pressure and CO_2 concentration (Cox et al., 1999).

The spatial resolution of the ocean is 1.25 by 1.25 degrees. The model has 20 layers and includes the use of the Gent-McWilliams mixing scheme (Gent & Mcwilliams, 1990). The sea ice model uses a simple thermodynamic scheme and contains parameterisations of ice drift and leads (Cattle et al., 1995).

2.2.2 Boundary conditions & experimental design

Essential boundary conditions for our Pliocene simulations are based on, or modified from, those used within the Pliocene Model Intercomparison Project (PlioMIP) coupled atmosphere-ocean simulation, which is described in detail in Haywood et al. (2011). In brief this PlioMIP simulation uses the US Geological Survey PRISM3D boundary condition data set (Dowsett et al., 2010) and the PlioMIP submission for HadCM3 is presented in Bragg et al., (2012).

In PlioMIP a modern orbital configuration is specified and atmospheric trace gasses are set to pre-industrial levels, except CO_2 which is specified at 405 ppmv. All simulations were integrated for 500 years (unless otherwise stated), with the final 100 years used to calculate the required climatological means. Table 2.1 provides summary details of all HadCM3 experiments included in this study. Time series analyses show no significant globally integrated trends in surface climate for the averaging period, indicating that the surface climatology of the model has reached an equilibrium state.

2.2.3 KM5c and K1 orbital forcing sensitivity experiments

Initially we have performed two control simulations for the KM5c ($Plio^{CTL}KM5c^{3205}$) and K1 ($Plio^{CTL}K1^{3060}$) interglacials. Using orbital parameters derived from the astronomical solution of Laskar et al. (2004), we have modified HadCM3 to be representative of orbital forcing at the interglacial events, 3205 and 3060 ka. Due to precessional effects amplified by changes in eccentricity, the length of seasons evolves through time (Joussaume & Braconnot, 1997). This "calendar effect" has no impact on the mean annual SATs but has potential to introduce inaccuracy/bias to the interpretation of seasonal SATs. In this study, we have assessed that the seasonal results shown are not sensitive to this "calendar effect".

Experiment name	Eccentricity	Precession	Obliquity	MAT (°C)	JJA (°C)	DJF (°C)
Plio_KM5c^{3225}	0.01	−0.003998	22.92704	18.05	20.11	15.92
Plio_KM5c^{3223}	0.01	0.001968	23.01538	18.04	20.00	15.99
Plio_KM5c^{3221}	0.01	0.005338	23.12036	18.10	19.99	16.12
Plio_KM5c^{3219}	0.01	0.005455	23.22784	18.05	19.98	16.02
Plio_KM5c^{3217}	0.00	0.003253	23.32529	18.06	20.05	15.98
Plio_KM5c^{3215}	0.00	0.000577	23.40339	18.07	20.13	15.91
Plio_KM5c^{3213}	0.00	−0.000684	23.45685	18.13	20.20	15.99
Plio_KM5c^{3211}	0.00	0.000348	23.48581	18.07	20.11	15.96
Plio_KM5c^{3209}	0.00	0.003001	23.49423	18.14	20.11	16.09
Plio_KM5c^{3207}	0.01	0.005561	23.48812	18.09	20.02	16.06
Plio^{CTL}KM5c^{3205}	**0.01**	**0.006048**	**23.47363**	**18.04**	**20.00**	**15.98**
Plio_KM5c^{3203}	0.01	0.003145	23.45559	18.08	20.11	15.94
Plio_KM5c^{3201}	0.01	−0.002863	23.43613	18.14	20.34	15.86
PlioKM5c^{3199}	0.01	−0.009965	23.41459	18.16	20.48	15.78
Plio_KM5c^{3197}	0.02	−0.015177	23.38809	18.20	20.59	15.78
Plio_KM5c^{3195}	0.02	−0.015627	23.35229	18.22	20.57	15.84
Plio_KM5c^{3193}	0.02	−0.009880	23.30298	18.24	20.39	16.05
Plio_KM5c^{3191}	0.02	0.001086	23.23714	18.21	20.09	16.26
Plio_KM5c^{3189}	0.02	0.013936	23.15446	18.16	19.78	16.44
Plio_KM5c^{3187}	0.03	0.023878	23.05862	18.12	19.59	16.50
Plio_KM5c^{3185}	0.03	0.026414	22.95756	18.11	19.64	16.43
Plio_K1^{3080}	0.04	−0.024808	23.31512	18.50	20.91	16.11
Plio_K1^{3076}	0.04	0.019597	23.51012	18.51	19.86	17.05
Plio_K1^{3072}	0.05	0.046580	23.57159	18.41	19.48	17.18
Plio_K1^{3068}	0.05	0.021245	23.46148	18.60	20.49	16.49
Plio_K1^{3064}	0.05	−0.032116	23.23327	18.71	21.65	15.75
Plio^{CTL}K1^{3060}	**0.05**	**−0.050860**	**23.00698**	**18.79**	**21.89**	**15.87**
Plio_K1^{3056}	0.05	−0.008461	22.90429	18.76	20.58	16.88
Plio_K1^{3052}	0.05	0.045905	22.98374	18.58	19.43	17.61
Plio_K1^{3048}	0.05	0.045280	23.20710	18.60	19.92	17.07
Plio_K1^{3044}	0.05	−0.009171	23.46148	18.76	21.31	16.06
Plio_K1^{3040}	0.05	−0.050801	23.62471	18.88	22.13	15.73

Table 2.1 Summary of experiments including orbital parameters implemented in HadCM3 and global mean annual and seasonal temperatures, controls indicated in bold.

Additionally, we have carried out a suite of 30 orbital sensitivity simulations that are centred on the two selected isotope excursions. For 20 kyr preceding and postdating KM5c a total of 20 simulations were carried out (a simulation every 2 kyr). The 20 kyr window was selected in order to best capture a plausible scenario of uncertainty in chronological control for new proxy records produced. Using the experience gained from the KM5c sensitivity experiments, we were able to determine that a 4 kyr spacing between experiments was sufficient to capture the nature of orbitally forced SAT variability. Therefore, we have only

performed experiments every 4 kyr around K1 (see Table 1). These sensitivity experiments enable us to quantify the orbital forcing contribution to climate change for two intervals of time spanning 40 kyr each. For convenience we have adopted the notation Plio_KM5c^{Year} to describe each KM5c sensitivity experiment. For example, Plio_KM5c^{3203} represents the orbital sensitivity experiment 2 kyr after the peak of the KM5c interglacial event (see Table 2.1). We have also followed a similar notation system for the K1 sensitivity experiments, whereby Plio_K1^{3056} denotes the simulations 2 kyr after the K1 peak.

2.3 Results

2.3.1 Magnitude of orbitally forced changes in SAT (KM5c 3185 to 3225 ka)

Figure 2.2 shows the difference in mean annual SAT between the KM5c/K1 control simulations and the standard pre-industrial control simulation (see also Haywood et al. 2013b). Figure 2.3 displays global mean annual SAT anomalies (compared to Plio^{CTL}KM5c^{3205}) predicted by HadCM3 for 10 of the orbital sensitivity simulations.

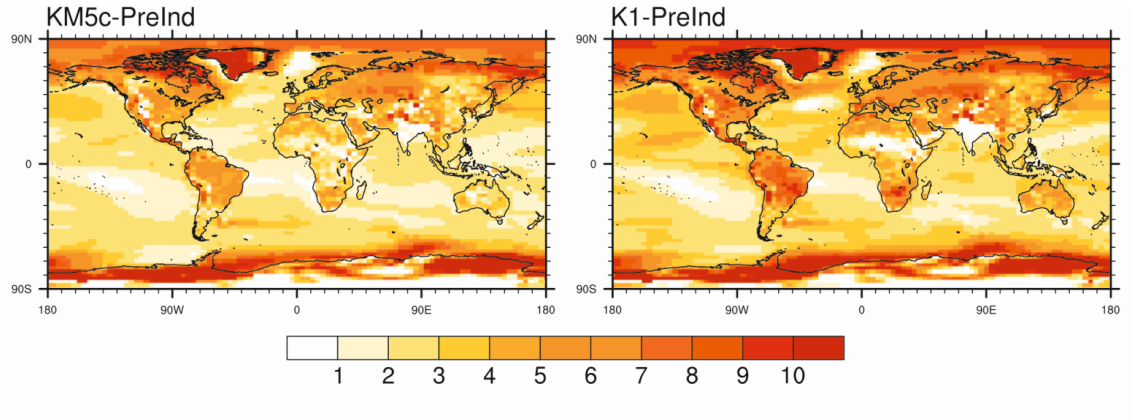

Figure 2.2 Annual mean Pliocene SAT predictions from HadCM3: (left) interglacial MIS KM5c minus a pre-industrial experiment; (right) interglacial MIS K1 minus a pre-industrial experiment.

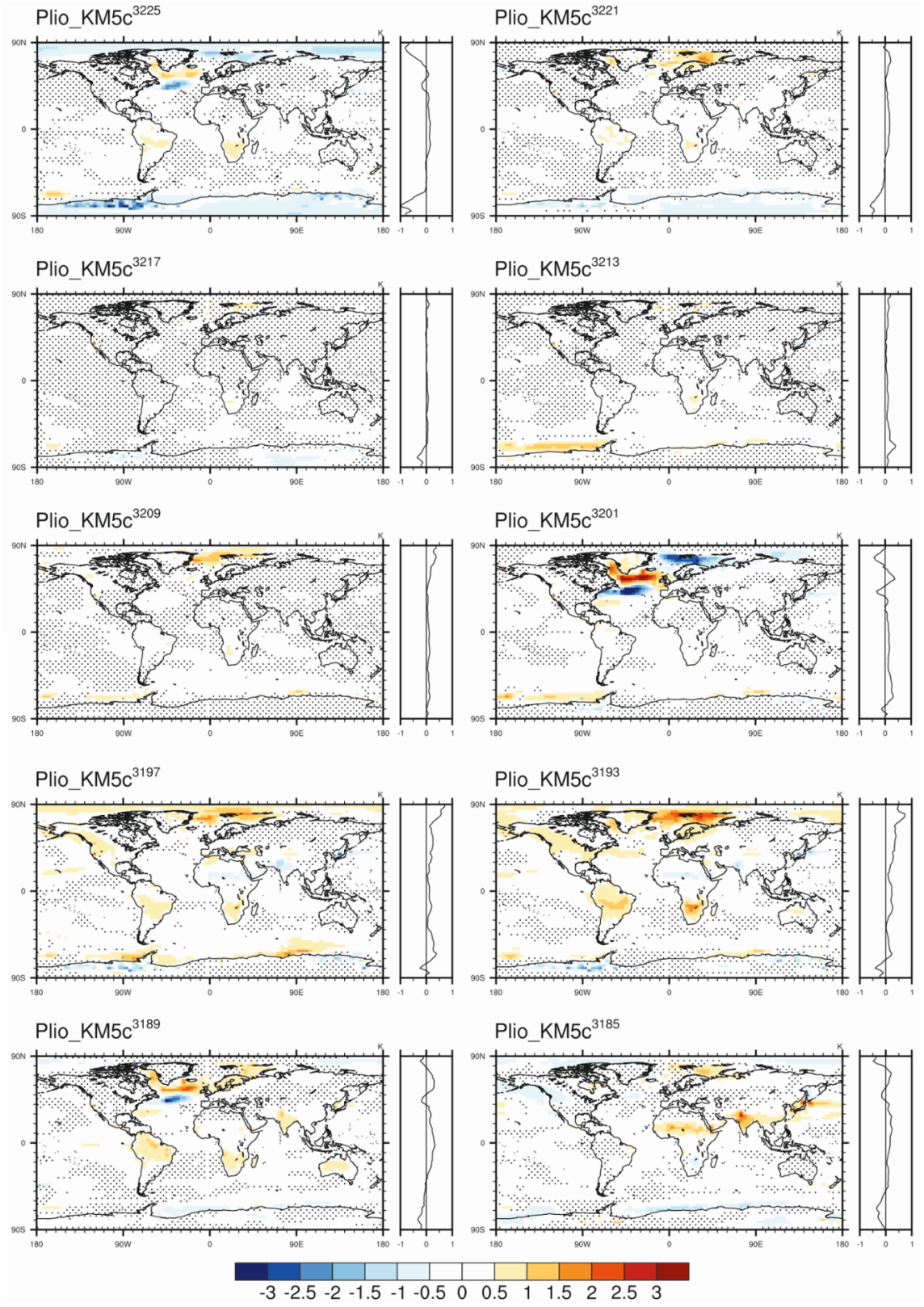

Figure 2.3 Annual mean Pliocene SAT (°C) predictions from HadCM3 for 10 orbital sensitivity simulations minus the MIS KM5c control ($Plio^{CTL}KM5c^{3205}$). Stippling indicates the SAT changes that are statistically insignificant according to the Student's t-test. Zonal SAT anomalies are shown to the right of each simulation.

During the 40 kyr interval sampled around KM5c, the global annual mean temperature ranges from 18.04°C (Plio^{CTL}KM5c^{3205}) to 18.25°C (Plio_KM5c$^{3197,3193 \text{ and } 3191}$), see Table 2.1. The most striking observation from the results displayed in Figure 2.3 is the vast areas of the Earth's surface that do not show any statistical significant differences from the KM5c control experiment. In general, experiments representative of the time window prior to the KM5c interglacial peak (i.e. Plio_KM5c^{3225} to Plio_KM5c^{3209}) are cooler than peak itself. Those after KM5c (i.e. Plio_KM5c^{3201} to Plio_KM5c^{3185}) are warmer (Fig. 2.3). The spatial patterns exhibited in the temperature anomalies can be broadly categorised into three groups; (i) nominal differences, (ii) experiments which display a dipole feature of temperature change in the North Atlantic, and (iii) experiments which display terrestrial surface temperature changes of greater than 1°C.

Experiments exhibiting nominal, or statistically insignificant (when assessed by a Student's t-test at the 95% confidence interval), deviation from Plio^{CTL}KM5c^{3205} include, Plio_KM5c^{3217}, Plio_KM5c^{3213}, Plio_KM5c^{3209}. One of the major features predicted by HadCM3 to varying degrees is a dipole in temperature change in the North Atlantic. This feature of cooling, which begins at the coast of Newfoundland and propagates Eastward across the Atlantic, coupled with a warming centred off the Southern tip of Greenland and into the Labrador Sea is apparent in eight of the twenty KM5c sensitivity simulations. Often this pattern of temperature change is also associated with a large temperature anomaly around Svalbard (e.g. Plio_KM5c^{3215}). The temperature dipole is strongest (>2°C) in experiments Plio_KM5c^{3201} and Plio_KM5c^{3189}. Simulations conducted for the time period between Plio_KM5c^{3197} and Plio_KM5c^{3185} all demonstrate a significant terrestrial warming over parts of South America, South Africa and India of up to 2°C. Please refer to Appendix A, Figure A.2 for the further 10 KM5c orbital sensitivity anomaly plots.

Some experiments do not easily fall into one of the categories identified above. In Plio_KM5c^{3225} significant changes (up to 2°C cooling) are limited to the high latitudes including Antarctica, sea ice marginal regions and the North Atlantic. Plio_KM5c^{3221} displays a cooling over the interior of Antarctica and a moderate (less than -1°C) warming around Svalbard. Finally, Plio_KM5c^{3197} displays isolated regions of warming, for example over Svalbard and the wider Arctic sea ice region, in North America and around the Antarctic margins.

2.3.2 Magnitude of orbitally forced changes in SAT (K1 3040 to 3080 ka)

Figure 2.4 shows the global SAT anomalies from $Plio^{CTL}K1^{3060}$ for 10 orbital sensitivity experiments with HadCM3. The global mean annual temperature ranges from 18.4°C ($Plio\_K1^{3072}$) to 18.85°C ($Plio\_K1^{3040}$). The spatial patterns shown in Figure 2.4 can be approximately grouped as (i) patterns of warming and cooling exceeding 2°C and (ii) patterns of warming and cooling not exceeding 2°C.

Experiments showing the strongest SAT anomalies were $Plio\_K1^{3048}$, $Plio\_K1^{3052}$, $Plio\_K1^{3068}$ and $Plio\_K1^{3072}$ with most differences demonstrated to be statistically significant. There is cooling at the high northern latitudes (-1.5°C) with areas of terrestrial cooling over North and South America, Southern Africa, Europe, Greenland and Australia, with some temperature anomalies (such as over South America and Southern Africa) reaching 4°C. Equatorial terrestrial regions such as India and Central Africa exhibit a warming of up to 4°C and 3°C over Antarctica. Simulations $Plio\_K1^{3044}$, $Plio\_K1^{3056}$, $Plio\_K1^{3064}$ and $Plio\_K1^{3076}$ show a very similar pattern of temperature change to the previously discussed simulations, but with most temperature variations not exceeding +/-2°C and larger areas showing statistically insignificant temperature changes. $Plio\_K1^{3044}$ and $Plio\_K1^{3064}$ predict warming in the Svalbard area of up to 2°C, whereas $Plio\_K1^{3056}$ and $Plio\_K1^{3076}$ show cooling in this area of up to 2°C. $Plio\_K1^{3076}$ displays high latitude warming in the southern hemisphere of up to 4°C. The simulations $Plio\_K1^{3040}$ and $Plio\_K1^{3080}$ show the least amount of temperature change in Figure 2.4. $Plio\_K1^{3040}$ predicts predominantly cooling of up to 1.5°C and $Plio\_K1^{3080}$, warming in the high latitudes of up to 2°C.

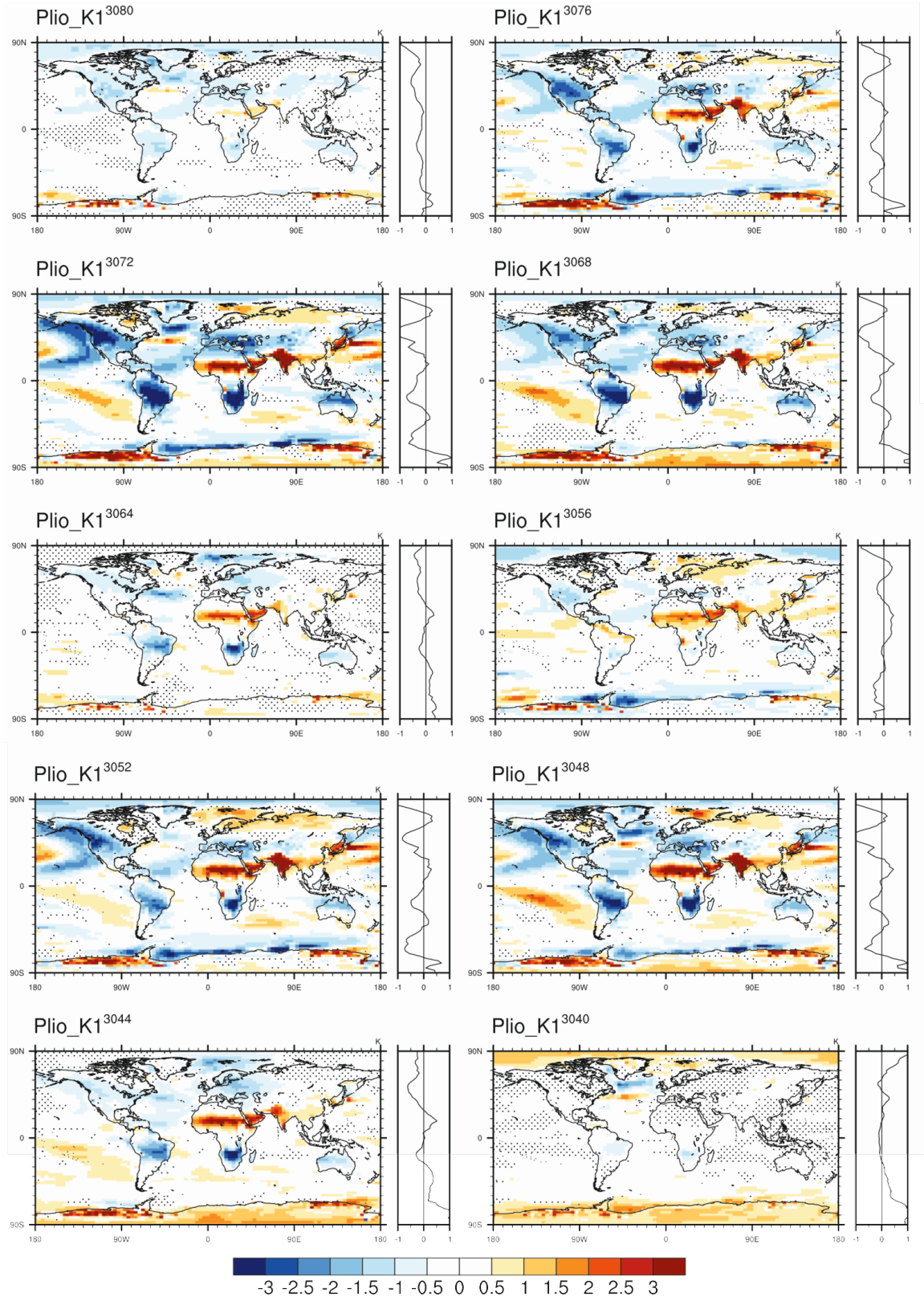

Figure 2.4 Annual mean Pliocene SAT (°C) predictions from HadCM3 for 10 orbital sensitivity simulations minus the MIS K1 control ($Plio^{CTL}K1^{3060}$). Stippling indicates the SAT changes that are statistically insignificant according to the Student's t-test. Zonal SAT anomalies are shown to the right of each simulation.

2.3.3 Patterns of maximum spatial variation in SAT

In order to determine the maximum difference in SAT within the two ensembles (KM5c and K1) we have examined all of the sensitivity experiments, and for each grid box selected the experiment that displays the maximum deviation from the associated control simulation (i.e. $Plio^{CTL}KM5c^{3205}$ and $Plio^{CTL}K1^{3060}$). Using this information, we have constructed a composite figure (Fig. 2.5) that demonstrates the spatial variation in maximum SAT difference.

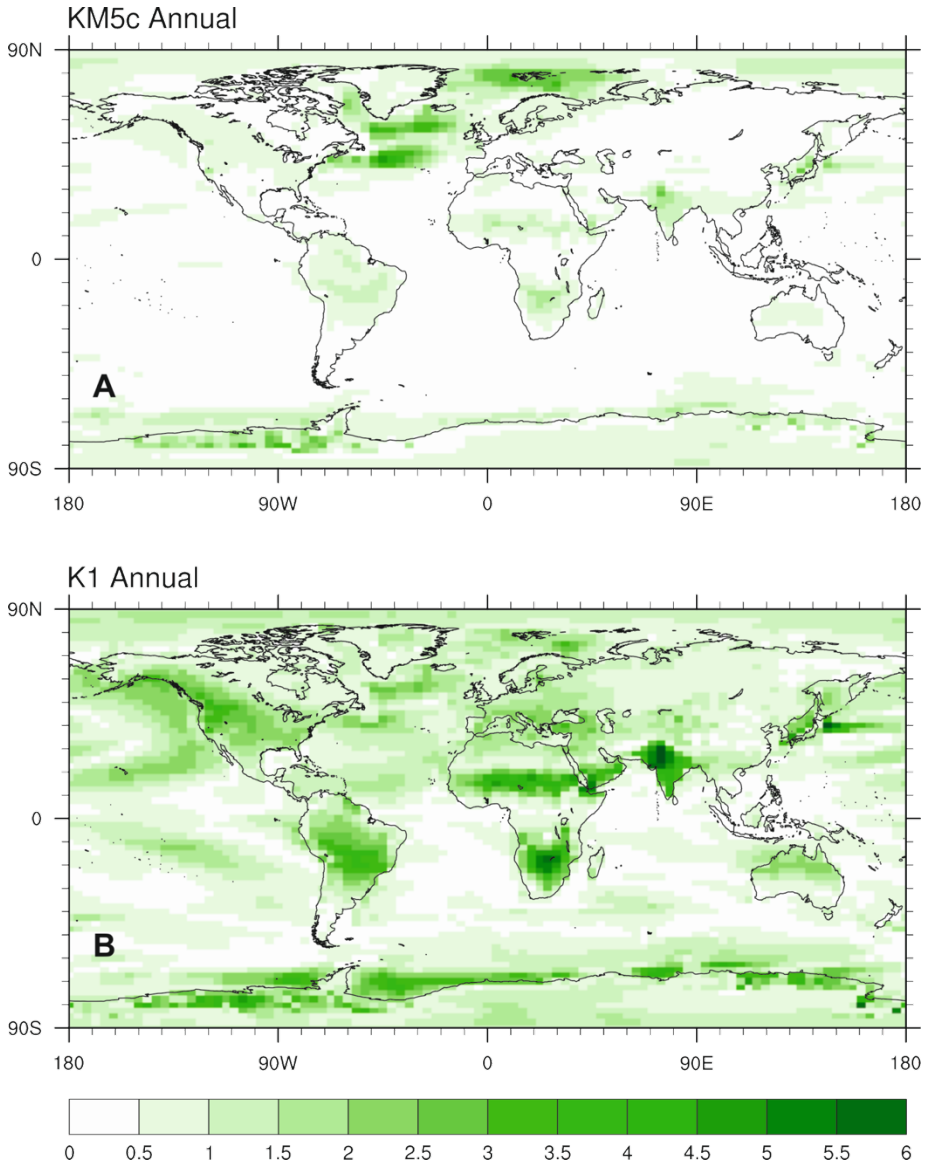

Figure 2.5 Maximum Annual SAT change (°C) derived from 10 orbital sensitivity simulations differenced from the MIS KM5c (A) and the K1 (B) controls, in each grid square. See text in Section 2.3.3 for further explanation.

There is a maximum orbitally induced variation in SATs of less than 1°C around KM5c. An exception is the North Atlantic, Labrador Sea and Arctic Ocean where HadCM3 predicts differences of up to 4.8°C. This is associated with the experiments that displayed the dipole in North Atlantic SATs discussed in section 2.3.1. The variation in these regions is linked to changes in the geographical location of deep water formation, which itself is associated with a seasonal redistribution in sea ice cover, brine rejection and salinity.

To examine the dipole, feature further simulations showing high variation in these regions were continued for an additional 500 simulated years. Following a greater integration length, the amount of variation displayed in these regions declined. For example, differences in SAT are reduced from a maximum of 5°C in the North Atlantic to 2°C in the same grid squares. Thus, the higher variation predicted in these regions, compared to other regions, could simply be an artefact of model spin up. However, this is difficult to conclude with certainty. Given the transient nature of orbital forcing it could be argued that a suite of 1 kyr simulations using fixed astronomical forcing might be expected to predict less variation than a transient simulation covering the same time interval where orbital forcing was continuously updated in the model. Thus continuing simulations to 1 kyr years without altering orbital forcing could bias our results towards stability. To ensure consistency in our model results that are used in our calculations of maximum SAT variation, we utilise the results from the 500 year simulations in all cases (the impact of this choice is demonstrated in Appendix A, Figure A.9.).

The maximum difference in SAT around the K1 interglacial is in general, much larger than around KM5c (Fig. 2.5). The changes in terrestrial SATs are also larger reaching 7.7°C in India. There are also substantial changes over Central and Southern Africa (5.6°C), North and South America (4°C) and Antarctica (5.1°C). Globally there is a 2°C maximum orbitally induced variation over the oceans.

In K1 there is a similar dipole pattern in the North Atlantic, although less intense, in three simulations are also associated with changes in salinity, sea ice and ocean mixed layer depth. Other differences in the K1 sensitivity experiments such as cooling over Antarctica are associated with increases in sea ice in this region. Large terrestrial SAT changes are effected by orbit and insolation. It is worthwhile noting that the Earth as global annual mean received

0.5 wm-2 insolation at the top of the atmosphere compared to present day or the KM5c time slice. This is also demonstrated in Appendix A, Figure A.4 showing incoming short-wave radiation for the K1 orbital sensitivity experiments. These strong orbitally forced terrestrial changes in SATs shown in 7 of the simulations in Figure 2.4, are also linked to increased changes in precipitation, especially in regions of South America, South Africa and Northern Africa. The patterns of SAT change in the orbital sensitivity experiment also indicate a possible shift in the position of the inter-tropical convergence zone in response to the altered equator to pole temperature gradient.

2.3.4 Patterns of maximum spatial variation in seasonal mean SAT (summer and winter)

Using the procedure described in section 2.3.3 we are able to determine that the maximum changes in seasonal SAT driven by orbital forcing (Fig. 2.6) are larger than the annual maximum difference (Fig. 2.5) for both KM5c and K1. For KM5c, temperature differences reach 6°C in DJF (December, January, February) in the sea ice regions with JJA (June, July, August) showing larger SAT differences of up to 5°C over terrestrial areas (South America, South Africa and Australia). The seasonal SAT differences around the K1 interglacial show greater variation than KM5c, reaching 13°C over Antarctica and 10°C over India and Australia in DJF, and 12°C during JJA over the land.

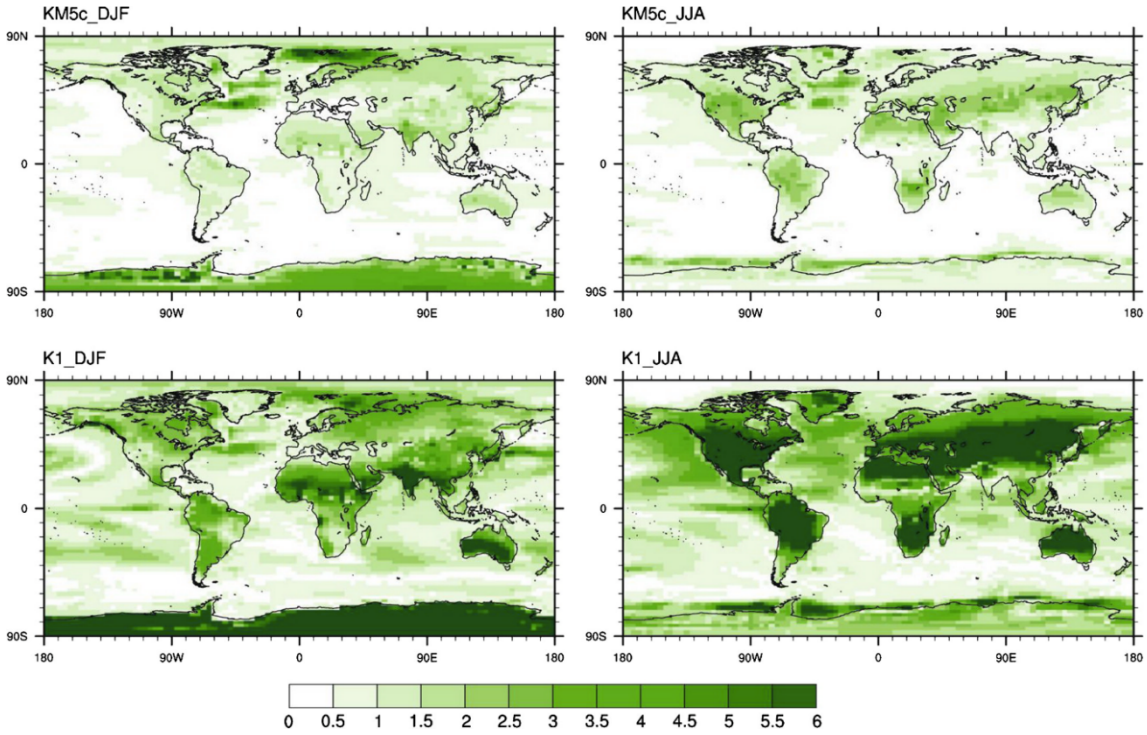

Figure 2.6 Maximum Seasonal SAT change (°C) derived from 10 orbital sensitivity simulations differenced from the MIS KM5c (left) and the K1 (right) controls, in each grid square. (Top left) KM5c_December, January, February (DJF); (top right) KM5c_June, July, August (JJA); (bottom left) K1_DJF; (bottom right) K1_JJA.

In summary, the maximum annual variation in SAT around K1 (7.9°C) is shown to be higher than for KM5c (4.8°C). This is also reflected within the seasonal SAT analysis (Fig. 2.6), which shows a maximum difference of 21.7°C in SATs for K1 and 9.3°C for KM5c. These results are consistent with the changes in insolation at the top of the atmosphere shown in Appendix A, Figure A.1.

2.4 Discussion

2.4.1 Interglacials in the Pliocene

From Quaternary science we understand that interglacial events can be diverse in character and such a broad term as 'interglacial' can encompass warm episodes of different duration, stability and climatic characteristics (Schreve & Candy, 2010). For the first time we have explored the nature of discrete interglacial events within the Pliocene epoch. Our analyses

have demonstrated that the KM5c and K1 interglacial events are different in nature. Therefore, the results discussed here suggest that treating the mPWP as a single 'average stable interglacial' is not representative of this time as each interglacial is likely to display its own unique characteristics. Additionally, there are an increasing number of proxy records documenting orbital variability in Pliocene surface temperatures (e.g. Lawrence et al., 2006; Dekens et al., 2008; Etourneau et al., 2009; Naafs et al., 2012; Rosell-Melé et al., 2014).

2.4.2 Implications for data-model comparison

Traditionally, data-model comparison (DMC) studies for the Pliocene have focused on mean annual temperatures for a defined time slab encompassing different orbital forcing (e.g. Dowsett et al., 2013; Salzmann et al., 2013). The differences we have seen in model predictions for KM5c and K1 demonstrate the complications of comparing time averaged proxy data to time specific model simulations. For the purpose of DMC this underlines the importance of new initiatives to reconstruct discrete time slices within the mPWP (Dowsett et al., 2013; Haywood et al., 2013b). KM5c has been identified as a reconstruction target for next phase of the PRISM project (PRISM4: Dowsett et al., 2013). Assuming that it will not be possible to precisely correlate all proxy records to the peak of the KM5c event, our results indicate that as long as proxy data reflect mean annual SAT, then the effect of variations in SAT around the benthic oxygen isotope peak KM5c will have an overall small effect on DMC. For example, in Figure 2.5 most areas show maximum SAT deviation from $Plio^{CTL}$-$KM5c^{3205}$ of less than 1°C. However, the magnitude of SAT change around K1 is larger, dictating the necessity for even higher resolution chronology compared to KM5c, although this may be difficult to achieve.

However, if proxy data represent seasonal temperatures the SAT variation is more significant with regard to DMC, especially at higher latitudes. Figure 2.6 shows up to 7°C of SAT change in the Nordic Seas and Antarctica for DJF and up to 3.5°C change in most terrestrial areas in JJA for the KM5c interglacial.

2.4.3 Assessing the synchroneity of peak temperatures

In this study we have assessed the synchroneity of peak warming around two interglacial events. Our results show that peak warmth is not synchronous, instead we see a complex

mosaic of responses whereby in specific regions maximum temperature change is largely synchronous, yet in other regions maximum temperature may be diachronous by as much as 40 kyr. This can be seen in Figure 2.7 for both KM5c and K1. The diachronous nature of warming demonstrated in our model results implies that aligning or adjusting proxy temperature time series (so that warm/cold peaks always correlate) can result in significant temporal miscorrelation. The end result would be a reconstruction of maximum temperatures at multiple locations that did not coexist in a temporal sense. This has implications for both regional and global synoptic temperature reconstruction, as well as studies investigating dominant drivers of climate.

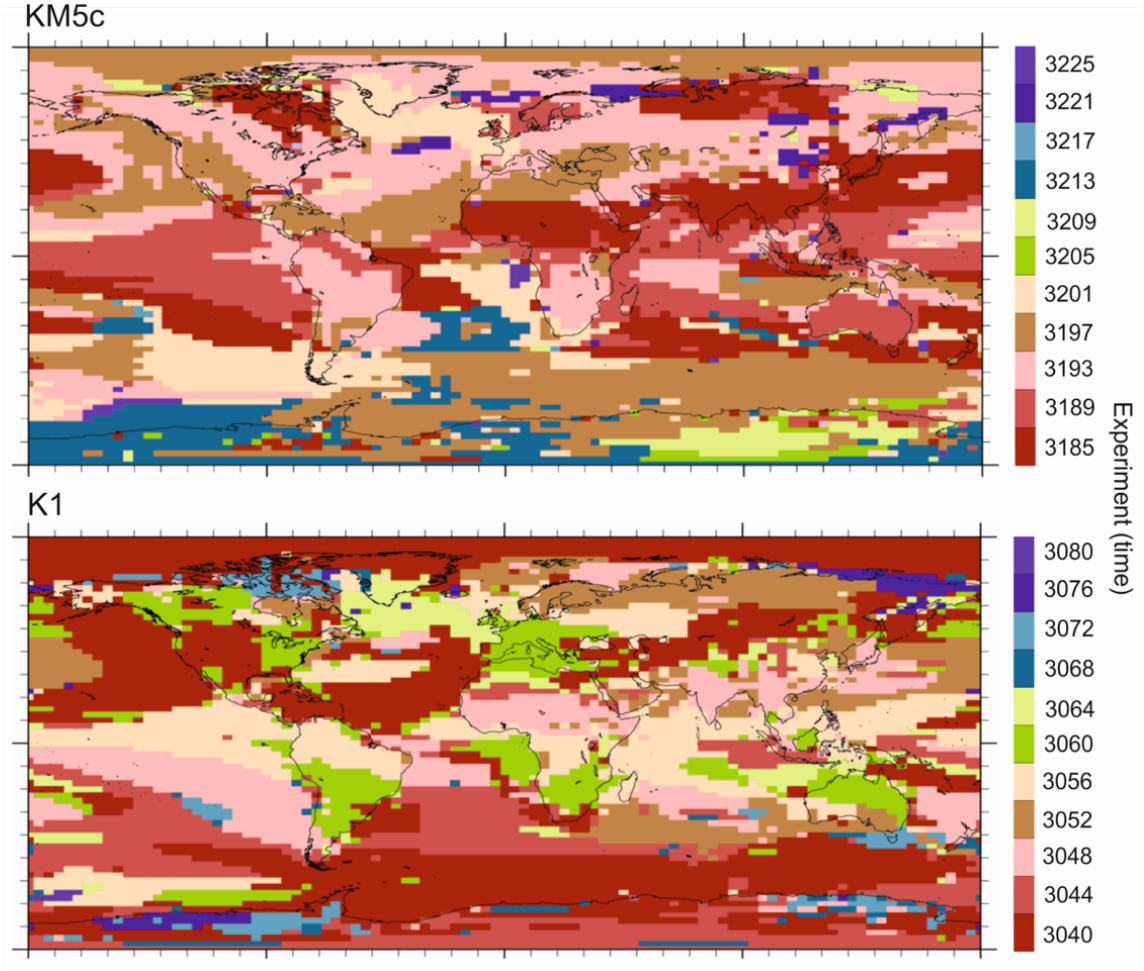

Figure 2.7 Maximum SAT around each interglacial peak: colours denote model simulations in which maximum temperature occurred per model grid square. This indicates that maximum temperature for each interglacial was not synchronous and also varied between KM5c and K1.

At this time, the majority of disagreements between Pliocene simulations and proxy estimates of temperature imply that models underestimate the magnitude of change (Sloan et al., 1996; Dowsett et al., 2010; Lunt et al., 2012; Salzmann et al., 2013). If peak warming is diachronous, then this provides a mechanism to at least partly account for this discrepancy. Independent determination of synchroneity in peak temperatures in marine/terrestrial records is difficult to achieve. Thus pre-Quaternary DMC requires a methodology which incorporates the effects of orbital forcing on climate variability and the potential effects of diachronous proxy-based temperature estimates.

2.4.4 Caveats and future work

In this study we have looked at the effects of orbital forcing. We have not incorporated additional feedbacks associated with changes in orbital forcing (i.e. those associated with ice-sheet evolution and vegetation change). It is therefore possible that our maximum changes in SAT could be under or overestimated. Given the nature of the K1 event and the changes in orbital forcing compared to modern, the assumption of limited feedbacks from ice sheets and vegetation cover around this interglacial is more difficult to justify than KM5c. Future work will look at these two additional feedbacks alongside changing orbit. We have not run simulations in which CO_2 covaried with orbit, but we do know there is a relationship between CO_2 and orbital forcing from the late Pleistocene (Saltzman & Maasch, 1988; Berger et al., 1999). However, most CO_2 reconstructions have relatively low temporal resolution. Therefore, accounting for this in a meaningful way in our experimental design is difficult. New records of atmospheric CO_2 such as Badger et al. (2013) show relatively stable levels of CO_2 using an alkenone carbon isotope-based record at high temporal but more records are needed.

2.5 Conclusion

In this paper we query the traditional view of the mPWP as having stable climate conditions. Using HadCM3 we present the first suite of orbital sensitivity experiments around the KM5c and K1 interglacial peaks in order to assess the nature of climate variability around two discrete interglacial events within the mPWP. We find that:

- Maximum mean annual temperature variation around the K1 interglacial is higher than around KM5c, and the spatial patterns of these SAT differences vary between the two interglacials.

- In a seasonal analysis, the maximum difference in temperature around the KM5c and K1 interglacials are larger than the mean annual changes.

- The maximum warming shown in the simulations 40 kyr around the interglacial peaks, both spatially and temporally were not consistent between the two interglacial events: this implies that the variation in maximum warming are dependent upon the nature of orbital forcing.

In the context of future climate change, orbital forcing is not a significant factor that will influence climate over politically or socially meaningful timescales. Therefore, for the Pliocene to inform us about the long-term effects of near modern CO_2 concentrations, it is necessary to reconstruct an interglacial event(s) in the Pliocene that displays modern/near modern orbital forcing (Haywood et al., 2013b). The results presented here have highlighted diversity in the nature of Pliocene interglacials. While the averaging of these interglacial events (Dowsett & Poore, 1991; Dowsett, 2007) may generally show the same broad patterns of global mean annual SAT change, it will mask significant variations in regional and seasonal temperature change critical to the robust assessment of climate model performance. In order to successfully compare model results and proxy data to form significant conclusions about model fidelity, a time slice rather than a time-averaged approach is needed. The issues discussed here are not only relevant to Pliocene climate, but to any pre-Quaternary interval, and the effects of time averaging and non-synchroneity are likely to be exacerbated further back in time due to weaker chronological constraints on proxy data.

References

Badger, M.P.S., Schmidt, D.N., Mackensen, A. & Pancost, R.D. (2013). High-resolution alkenone palaeobarometry indicates relatively stable pCO2 during the Pliocene (3.3–2.8 Ma). *Philosophical Transactions of the Royal Society of London A: Mathematical, Physical and Engineering Sciences*. 371 (2001).

Berger, A., Li, X.S. & Loutre, M.F. (1999). Modelling northern hemisphere ice volume over the last 3Ma. *Quaternary Science Reviews*. 18 (1). pp. 1–11.

Bragg, F.J., Lunt, D.J. & Haywood, A.M. (2012). Mid-Pliocene climate modelled using the UK Hadley Centre Model: PlioMIP Experiments 1 and 2. *Geoscientific Model Development Discussions*. 5 (2). pp. 837–871.

Cattle, H., Crossley, J. & Drewry, D.J. (1995). Modelling Arctic Climate Change [and Discussion]. *Philosophical Transactions of the Royal Society A: Mathematical, Physical and Engineering Sciences*. 352 (1699). pp. 201–213.

Chan, W.-L., Abe-Ouchi, A. & Ohgaito, R. (2011). Simulating the mid-Pliocene climate with the MIROC general circulation model: experimental design and initial results. *Geoscientific Model Development*. 4 (4). pp. 1035–1049.

Cox, P.M., Betts, R.A., Bunton, C.B., Essery, R.L.H., Rowntree, P.R. & Smith, J. (1999). The impact of new land surface physics on the GCM simulation of climate and climate sensitivity. *Climate Dynamics*. 15 (3). pp. 183–203.

Cronin, T.M., Whatley, R., Wood, A., Tsukagoshi, A., Ikeya, N., Brouwers, E.M. & Briggs, W.M. (1993). Microfaunal Evidence for Elevated Pliocene Temperatures in the Arctic Ocean. *Paleoceanography*. 8 (2). pp. 161–173.

Cusack, S., Slingo, A., Edwards, J.M. & Wild, M. (1998). The radiative impact of a simple aerosol climatology on the Hadley Centre atmospheric GCM. *Quarterly Journal of the Royal Meteorological Society*. 124 (551). pp. 2517–2526.

Dekens, P.S., Ravelo, A.C. & McCarthy, M.D. (2007). Warm upwelling regions in the Pliocene warm period. *Paleoceanography*. 22 (3). p.p. PA3211

Dekens, P.S., Ravelo, A.C., McCarthy, M.D. & Edwards, C.A. (2008). A 5 million year comparison of Mg/Ca and alkenone paleothermometers. *Geochemistry, Geophysics, Geosystems*. 9 (10). p.p. Q10001.

Dolan, A.M., Haywood, A.M., Hill, D.J., Dowsett, H.J., Hunter, S.J., Lunt, D.J. & Pickering, S.J. (2011). Sensitivity of Pliocene ice sheets to orbital forcing. *Palaeogeography, Palaeoclimatology, Palaeoecology*. 309 (1–2)..pp. 98–110.

Dowsett, H.J. & Poore, R.Z. (1991). Pliocene sea surface temperatures of the north atlantic ocean at 3.0 Ma. *Quaternary Science Reviews*. 10 (2–3). pp. 189–204.

Dowsett, H.J. (2007). The PRISM palaeoclimate reconstruction and Pliocene sea-surface temperature. In: M. Williams, A. M. Haywood, F. J. Gregory, & D. N. Schmidt (eds.). *Deep-time perspectives on climate change : marrying the signal from computer models and biological proxies*. London: Published for the Micropalaeontological Society by the Geological Society, p. 589.

Dowsett, H., Robinson, M., Haywood, A.M., Salzmann, U., Hill, D., Sohl, L., Chandler, M., Williams, M., Foley, K. & Stoll, D. (2010). The PRISM3D paleoenvironmental reconstruction. *Stratigraphy*. 7 (2-3). pp. 123-139.

Dowsett, H.J., Haywood, A.M., Valdes, P.J., Robinson, M.M., Lunt, D.J., Hill, D.J., Stoll, D.K. & Foley, K.M. (2011). Sea surface temperatures of the mid-Piacenzian Warm Period: A comparison of PRISM3 and HadCM3. *Palaeogeography, Palaeoclimatology, Palaeoecology*. 309 (1–2). pp. 83–91.

Dowsett, H.J., Robinson, M.M., Haywood, A.M., Hill, D.J., Dolan, A.M., Stoll, D.K., Chan, W.-L., Abe-Ouchi, A., Chandler, M.A., Rosenbloom, N.A., Otto-Bliesner, B.L., Bragg, F.J., Lunt, D.J., Foley, K.M. & Riesselman, C.R. (2012). Assessing confidence in Pliocene sea surface temperatures to evaluate predictive models. *Nature Climate Change*. 2 (5). pp. 365–371.

Dowsett, H.J., Foley, K.M., Stoll, D.K., Chandler, M.A., Sohl, L.E., Bentsen, M., Otto-Bliesner, B.L., Bragg, F.J., Chan, W.-L., Contoux, C., Dolan, A.M., Haywood, A.M., Jonas, J.A., Jost, A., Kamae, Y., Lohmann, G., Lunt, D.J., Nisancioglu, K.H., Abe-Ouchi, A., Ramstein, G., Riesselman, C.R., Robinson, M.M., Rosenbloom, N.A., Salzmann, U., Stepanek, C., Strother, S.L., Ueda, H., Yan, Q. & Zhang, Z. (2013). Sea surface temperature of the mid-Piacenzian ocean: a data-model comparison. *Scientific reports*. 3. p.p. 2013.

Edwards, J.M. & Slingo, A. (1996). Studies with a flexible new radiation code. I: Choosing a configuration for a large-scale model. *Quarterly Journal of the Royal Meteorological Society*. 122 (531). pp. 689–719.

Etourneau, J., Martinez, P., Blanz, T. & Schneider, R. (2009). Pliocene-Pleistocene variability of upwelling activity, productivity, and nutrient cycling in the Benguela region. *Geology*. 37 (10). pp. 871–874.

Gent, P.R. & Mcwilliams, J.C. (1990). Isopycnal Mixing in Ocean Circulation Models. *Journal of Physical Oceanography*. 20 (1). pp. 150–155.

Gordon, C., Cooper, C., Senior, C.A., Banks, H., Gregory, J.M., Johns, T.C., Mitchell, J.F.B. & Wood, R.A. (2000).The simulation of SST, sea ice extents and ocean heat transports in a version of the Hadley Centre coupled model without flux adjustments.*Climate Dynamics*.16 (2–3).pp.147–168.

Gradstein, F., Ogg, J. & Smith, A. (2005). *A Geologic Time Scale 2004*. [Online]. Cambridge University Press.

Gregory, D., Kershaw, R. & Inness, P.M. (1997). Parametrization of momentum transport by convection. II: Tests in single-column and general circulation models. *Quarterly Journal of the Royal Meteorological Society*. 123 (541). pp. 1153–1183.

Gregory, J.M. & Mitchell, J.F.B. (1997). The climate response to CO_2 of the Hadley Centre coupled AOGCM with and without flux adjustment. *Geophysical Research Letters*. 24 (15). pp. 1943–1946.

Haywood, A.M., Valdes, P.J. & Sellwood, B.W. (2000). Global scale palaeoclimate reconstruction of the middle Pliocene climate using the UKMO GCM: Initial results. *Global and Planetary Change*. 25 (3–4). pp. 239–256.

Haywood, A.M. & Valdes, P.J. (2004). Modelling Pliocene warmth: contribution of atmosphere, oceans and cryosphere. *Earth and Planetary Science Letters*. 218 (3–4). pp. 363–377.

Haywood, A.M., Dowsett, H.J., Otto-Bliesner, B., Chandler, M.A., Dolan, A.M., Hill, D.J., Lunt, D.J., Robinson, M.M., Rosenbloom, N., Salzmann, U. & Sohl, L.E. (2010). Pliocene Model Intercomparison Project (PlioMIP): experimental design and boundary conditions (Experiment 1). *Geoscientific Model Development*. 3 (1). pp. 227–242.

Haywood, A.M., Dowsett, H.J., Robinson, M.M., Stoll, D.K., Dolan, A.M., Lunt, D.J., Otto-Bliesner, B. & Chandler, M.A. (2011). Pliocene Model Intercomparison Project (PlioMIP): experimental design and boundary conditions (Experiment 2). *Geoscientific Model Development*. 4 (3). pp. 571–577.

Haywood, A.M., Dolan, A.M., Pickering, S.J., Dowsett, H.J., McClymont, E.L., Prescott, C.L., Salzmann, U., Hill, D.J., Hunter, S.J., Lunt, D.J., Pope, J.O. & Valdes, P.J. (2013a). On the identification of a Pliocene time slice for data-model comparison. *Philosophical transactions. Series A, Mathematical, physical, and engineering sciences*. 371 (2001). p.p. 20120515.

Haywood, A.M., Hill, D.J., Dolan, A.M., Otto-Bliesner, B.L., Bragg, F., Chan, W.-L., Chandler, M.A., Contoux, C., Dowsett, H.J., Jost, A., Kamae, Y., Lohmann, G., Lunt, D.J., Abe-Ouchi, A., Pickering, S.J., Ramstein, G., Rosenbloom, N.A., Salzmann, U., Sohl, L., Stepanek, C., Ueda, H., Yan, Q. & Zhang, Z. (2013b). Large-scale features of Pliocene climate: results from the Pliocene Model Intercomparison Project. *Climate of the Past*. 9 (1). pp. 191–209.

Hill, D.J., Dolan, A.M., Haywood, A.M., Hunter, S.J. & Stoll, D.K. (2010). Sensitivity of the Greenland Ice Sheet to Pliocene sea surface temperatures. *Stratigraphy*. 7. pp. 111–122.

Joussaume, S. & Braconnot, P. (1997). Sensitivity of paleoclimate simulation results to season definitions. *Journal of Geophysical Research*. 102 (D2). p.p. 1943.

Laskar, J., Robutel, P., Joutel, F., Gastineau, M., Correia, A.C.M. & Levrard, B. (2004). A long-term

numerical solution for the insolation quantities of the Earth. *Astronomy & Astrophysics*. 428 (1). pp. 261–285.

Lawrence, K.T., Liu, Z. & Herbert, T.D. (2006). Evolution of the eastern tropical Pacific through Plio-Pleistocene glaciation. *Science (New York, N.Y.)*. 312 (5770). pp. 79–83.

Lisiecki, L.E. & Raymo, M.E. (2005). A Pliocene-Pleistocene stack of 57 globally distributed benthic $\delta^{18}O$ records. *Paleoceanography*. 20 (1). p.p. PA1003

Lunt, D.J., Foster, G.L., Haywood, A.M. & Stone, E.J. (2008). Late Pliocene Greenland glaciation controlled by a decline in atmospheric CO2 levels. *Nature*. 454 (7208). pp. 1102–1105.

Lunt, D.J., Haywood, A.M., Schmidt, G.A., Salzmann, U., Valdes, P.J., Dowsett, H.J. & Loptson, C.A. (2012). On the causes of mid-Pliocene warmth and polar amplification. *Earth and Planetary Science Letters*. 321–322. pp. 128–138.

Miller, K.G., Wright, J.D., Browning, J. V., Kulpecz, A., Kominz, M., Naish, T.R., Cramer, B.S., Rosenthal, Y., Peltier, W.R. & Sosdian, S. (2012). High tide of the warm Pliocene: Implications of global sea level for Antarctic deglaciation. *Geology*. 40 (5). pp. 407–410.

Moran, K., Backman, J., Brinkhuis, H., Clemens, S.C., Cronin, T., Dickens, G.R., Eynaud, F., Gattacceca, J., Jakobsson, M., Jordan, R.W., Kaminski, M., King, J., Koc, N., Krylov, A., Martinez, N., Matthiessen, J., McInroy, D., Moore, T.C., Onodera, J., O'Regan, M., Pälike, H., Rea, B., Rio, D., Sakamoto, T., Smith, D.C., Stein, R., St John, K., Suto, I., Suzuki, N., Takahashi, K., Watanabe, M., Yamamoto, M., Farrell, J., Frank, M., Kubik, P., Jokat, W. & Kristoffersen, Y. (2006). The Cenozoic palaeoenvironment of the Arctic Ocean. *Nature*. 441 (7093). pp. 601–605.

Naafs, B.D.A., Hefter, J., Acton, G., Haug, G.H., Martínez-Garcia, A., Pancost, R. & Stein, R. (2012). Strengthening of North American dust sources during the late Pliocene (2.7Ma). *Earth and Planetary Science Letters*. 317–318. pp. 8–19.

Naish, T., Powell, R., Levy, R., Wilson, G., Scherer, R., Talarico, F., Krissek, L., Niessen, F., Pompilio, M., Wilson, T., Carter, L., DeConto, R., Huybers, P., McKay, R., Pollard, D., Ross, J., Winter, D., Barrett, P., Browne, G., Cody, R., Cowan, E., Crampton, J., Dunbar, G., Dunbar, N., Florindo, F., Gebhardt, C., Graham, I., Hannah, M., Hansaraj, D., Harwood, D., Helling, D., Henrys, S., Hinnov, L., Kuhn, G., Kyle, P., Läufer, A., Maffioli, P., Magens, D., Mandernack, K., McIntosh, W., Millan, C., Morin, R., Ohneiser, C., Paulsen, T., Persico, D., Raine, I., Reed, J., Riesselman, C., Sagnotti, L., Schmitt, D., Sjunneskog, C., Strong, P., Taviani, M., Vogel, S., Wilch, T. & Williams, T. (2009). Obliquity-paced Pliocene West Antarctic ice sheet oscillations. *Nature*. 458 (7236). pp. 322–328.

Pollard, D. & DeConto, R.M. (2009). Modelling West Antarctic ice sheet growth and collapse

through the past five million years. *Nature*. 458 (7236). pp. 329–332.

Polyak, L., Alley, R.B., Andrews, J.T., Brigham-Grette, J., Cronin, T.M., Darby, D.A., Dyke, A.S., Fitzpatrick, J.J., Funder, S., Holland, M., Jennings, A.E., Miller, G.H., O'Regan, M., Savelle, J., Serreze, M., St. John, K., White, J.W.C. & Wolff, E. (2010). History of sea ice in the Arctic. *Quaternary Science Reviews*. 29 (15–16). pp. 1757–1778.

Rosell-Melé, A., Martínez-Garcia, A. & McClymont, E.L. (2014). Persistent warmth across the Benguela upwelling system during the Pliocene epoch. *Earth and Planetary Science Letters*. 386. pp. 10–20.

Saltzman, B. & Maasch, K.A. (1988). Carbon cycle instability as a cause of the Late Pleistocene Ice Age Oscillations: Modeling the asymmetric response. *Global Biogeochemical Cycles*. 2 (2). pp. 177–185.

Salzmann, U., Haywood, A.M., Lunt, D.J., Valdes, P.J. & Hill, D.J. (2008). A new global biome reconstruction and data-model comparison for the Middle Pliocene. *Global Ecology and Biogeography*. 17 (3). pp. 432–447.

Salzmann, U., Dolan, A.M., Haywood, A.M., Chan, W.-L., Voss, J., Hill, D.J., Abe-Ouchi, A., Otto-Bliesner, B., Bragg, F.J., Chandler, M.A., Contoux, C., Dowsett, H.J., Jost, A., Kamae, Y., Lohmann, G., Lunt, D.J., Pickering, S.J., Pound, M.J., Ramstein, G., Rosenbloom, N.A., Sohl, L., Stepanek, C., Ueda, H. & Zhang, Z. (2013). Challenges in quantifying Pliocene terrestrial warming revealed by data–model discord. *Nature Climate Change*. 3 (11). pp. 969–974.

Schreve, D. & Candy, I. (2010). Interglacial climates: Advances in our understanding of warm climate episodes. *Progress in Physical Geography*. 34 (6). pp. 845–856.

Shackleton, N.J. & Hall, M.A. (1984). *Oxygen and Carbon Isotope stratigraphy of deep sea drilling project hole 552A: Plio-Pleistocene glacial history. Initial Reports of the Deep Sea Drilling Project*. Washington.

Sloan, L.C., Crowley, T.J. & Pollard, D. (1996). Modeling of middle Pliocene climate with the NCAR GENESIS general circulation model. *Marine Micropaleontology*. 27 (1–4). pp. 51–61.

Wan, S., Tian, J., Steinke, S., Li, A. & Li, T. (2010). Evolution and variability of the East Asian summer monsoon during the Pliocene: Evidence from clay mineral records of the South China Sea. *Palaeogeography, Palaeoclimatology, Palaeoecology*. 293 (1–2). pp. 237–247.

CHAPTER 3

REGIONAL CLIMATE AND VEGETATION RESPONSE TO ORBITAL FORCING WITHIN THE MID-PLIOCENE WARM PERIOD: A STUDY USING HADCM3

Preface

This chapter has been published in Global and Planetary Change as:

Prescott C.L., Dolan A.M., Haywood A.M., Hunter S.J., Tindall J.C.. (2018) Regional climate and vegetation response to orbital forcing within the mid-Pliocene Warm Period: a study using HadCM3. *Global and Planetary Change*, 161, pp. 231-243.

The experiment design and implementation, data analysis and presentation and the written manuscript was completed by the candidate. A.D. and A.H. advised on the experiment design and suggested improvements and advice on the manuscript. S.H. and J.T. provided technical support for the climate modelling and analysis of model output.

Abstract

Regional climate and environmental variability in response to orbital forcing during interglacial events within the mid-Piacenzian (Pliocene) Warm Period (mPWP; 3.264-3.025 Ma) has been rarely studied using climate and vegetation models. Here we use climate and vegetation model simulations to predict changes in regional vegetation patterns in response to orbital forcing for four different interglacial events within the mPWP (Marine Isotope Stages (MIS) G17, K1, KM3 and KM5c). The efficacy of model-predicted changes in regional vegetation are assessed by reference to selected high temporal resolution palaeobotanical studies that are theoretically capable of discerning vegetation patterns for the selected interglacial stages.

Annual mean surface air temperatures for the studied interglacials are between 0.4°C to 0.7°C higher than a comparable Pliocene experiment using modern orbital parameters. Increased spring/summer and reduced autumn/winter insolation in the Northern Hemisphere during MIS G17, K1 and KM3 enhances seasonality in surface air temperature. The two most robust and notable regional responses to this in vegetation cover occur in North America and continental Eurasia, where forests are replaced by more open-types of vegetation (grasslands and shrubland). In these regions our model results appear to be inconsistent with local palaeobotanical data. The orbitally driven changes in seasonal temperature and precipitation lead to a ~30% annual reduction in available deep soil moisture (2.0 m from surface), a critical parameter for forest growth, and subsequent reduction in the geographical coverage of forest-type vegetation; a phenomenon not seen in comparable simulations of Pliocene climate and vegetation run with a modern orbital configuration. Our results demonstrate the importance of examining model performance under a range of realistic orbital forcing scenarios within any defined time interval (e.g. mPWP). Additional orbitally resolved records of regional vegetation are needed to further examine the validity of model-predicted regional climate and vegetation responses in greater detail.

3.1 Introduction

3.1.1 Vegetation in the mPWP

The mid-Piacenzian (Pliocene) Warm Period (mPWP), approximately 3.264 to 3.025 million years ago, was the most recent interval in Earth history when global annual mean temperatures are considered to have been higher than the pre-industrial (Haywood et al., 2013a; Dowsett et al., 2013). A continually updated and large palaeoenvironmental reconstruction produced by the Pliocene Research Investigations and Synoptic Mapping (PRISM) project (e.g. Dowsett et al. 1994), in combination with numerous additional proxy data studies and modelling investigations, has enabled the mPWP to become a well-studied warm interval in Earth history (Haywood et al., 2013b). Primarily, the PRISM palaeoenvironmental reconstruction focussed on sea surface temperatures (SST), originally just for the North Atlantic (Dowsett & Poore, 1991) before further developing into a global reconstruction including vegetation cover. Applying a time slab approach (Dowsett & Poore 1991), the PRISM project reconstructed average interglacial conditions throughout the mPWP and found warming concentrated in the high latitudes, with minimal change in the tropics (Dowsett & Poore, 1991; Dowsett et al., 1994, 1996).

The PRISM vegetation reconstruction indicates a warmer and moister climate than today (Salzmann et al., 2008), with the largest differences found in the high latitudes related to a pronounced warming in this region (Thompson & Fleming, 1996). The warmer and wetter climate, on average, during the mPWP resulted in a northward shift of the taiga-tundra boundary and a spread of tropical savannahs and woodland in Africa and Australia at the expense of arid deserts (Salzmann et al., 2008).

To generate a satisfactory distribution of global vegetation data, the PRISM3 vegetation reconstruction incorporated records from the whole Piacenzian Stage of the Pliocene (~1 million years in duration; Salzmann et al. 2008). Most records within the reconstruction are not dated on orbital timescales and could potentially represent interglacial or glacial conditions. However, where it was possible to reconstruct more than one potential biome from an individual locality, the biome representing the warmest climate condition was chosen (Salzmann et al. 2008).

While the PRISM3 vegetation synthesis is representative of the entire Piacenzian Stage, published vegetation records are available that can provide an indication of terrestrial climate variability in response to orbital forcing. For example, the joint pollen and marine faunal study in Japan by Heusser and Morley (1996), found temperatures varying between dry and humid conditions on top of an overall drying and cooling trend. Wu et al. (2011) found a general drying trend over the interior of central Asia reconstructed from sporopollen records. The Willis et al. (1999) sequence from Pula Maar (Hungary) showed significant fluctuations in vegetation between boreal and temperate forest, as well as dust data, thought to directly reflect changes in continental aridity and vegetation. Leroy and Dupont (1994) identified cyclic fluctuations between dry and humid periods in sediments dated 3.7 to 1.7 Ma in North West Africa and attributed these to marine isotope stages. The vegetation record from the James Bay Lowland in Canada shows fluctuations between deciduous and boreal forests in tune with the benthic oxygen isotope record (Gao et al., 2012). Tarasov et al. (2013) derived biome reconstructions based on pollen results from Lake El'gygytgyn in north-east Russia and found millennial-scale vegetation changes in the region that corresponded well with alternating cool and warm marine isotope stages during the mPWP. Finally, the record from Lake Baikal in south-central Siberia found short term intervals of climate deterioration controlling forest development and advances in open vegetation that overlay long term trends of cooling during the Pliocene (Demske et al., 2002).

3.1.2 Research questions

Here we investigate interglacial climate variability within the mPWP through examining the four most negative benthic oxygen isotope excursions. These are MIS G17, K1, KM3 and KM5c (Fig. 3.1) as seen in the LR04 benthic oxygen isotope stack (Lisiecki & Raymo, 2005). These 'super-interglacial' events (Raymo et al., 2009) have also been targeted by the PLIOMAX (Pliocene Maximum Sea Level) project in a multidisciplinary approach to investigate Pliocene sea level high stands.

In this study, we analyse and compare the effect of orbital forcing on terrestrial climate and vegetation during these four interglacial events within the mPWP. We use a climate model with and without a dynamic vegetation component to answer the following questions:

- How important is the effect of orbitally-driven seasonality changes for regional climate and land cover response during the interglacials studied, and how does the addition of a dynamic vegetation model alter the climatological as well as land cover response?
- Looking at specific high-resolution records (Lake Baikal and Lake El'gygytgyn), do our simulations capture similar variability shown in the geological record?

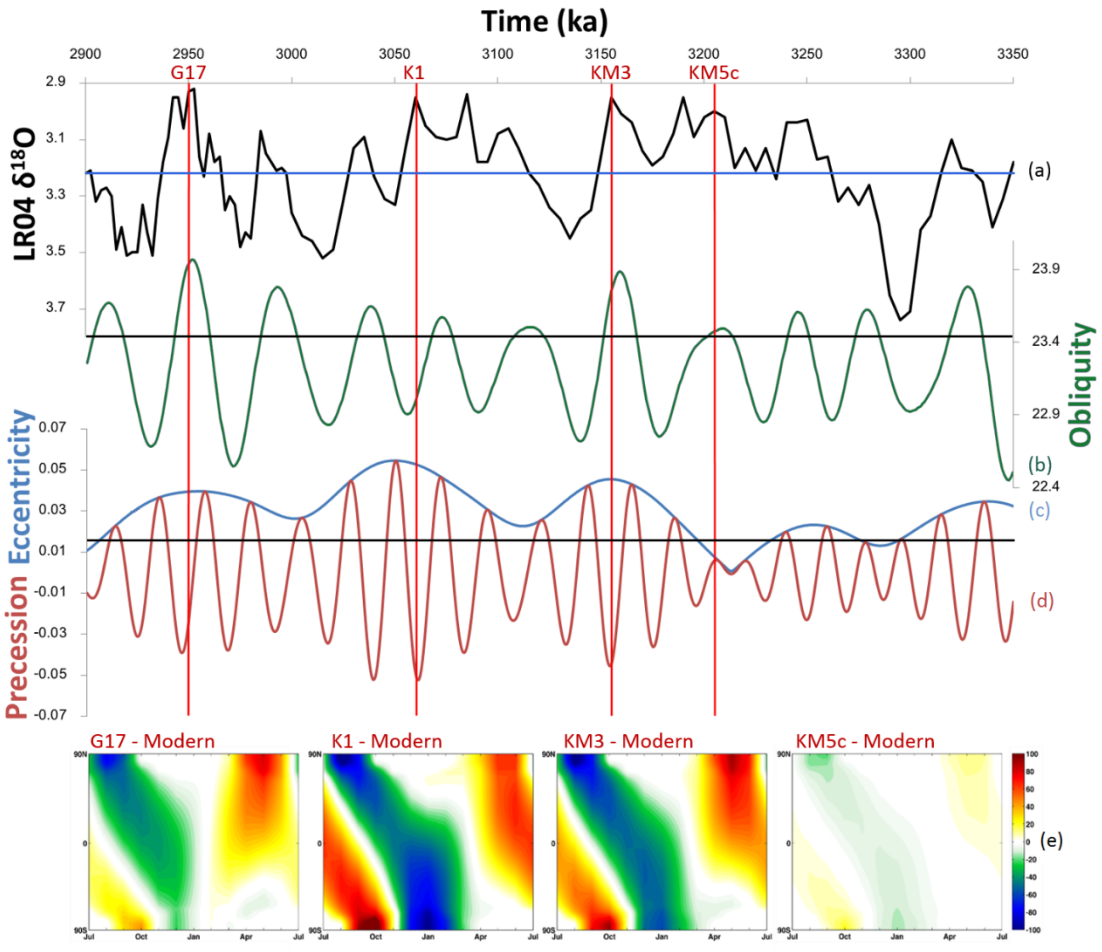

Figure 3.1 Marine isotope stages G17, K1, KM3 and KM5c plotted on (a) the benthic isotope record of Lisiecki and Raymo (2005). (b) obliquity (c) eccentricity (d) precession as derived from the astronomical solution of Laskar et al. (2004). Black horizontal lines show modern orbit with blue horizontal line showing the Holocene oxygen isotope average. (e) Incoming short-wave radiation flux derived from HadCM3 (Wm^{-2}) for MIS G17 minus modern; MIS K1 minus modern, MIS KM3 minus modern; MIS KM5c minus modern.

3.2 Methods

3.2.1 Model description

The Hadley Centre Coupled Climate Model Version 3 (HadCM3) is combined with either a dynamic vegetation model (Top-down Representation of Interactive Foliage and Flora Including Dynamics (TRIFFID)) or with a prescribed vegetation scheme. Two versions of the Met Office Surface Exchange Scheme (MOSES) are used; simulations with the dynamic vegetation model use the MOSES2.1 land surface scheme, and those with prescribed vegetation use MOSES1 to remain consistent with previous studies (e.g. Bragg et al., 2012; Prescott et al. 2014). We use the resulting modelled climatology to drive the BIOME4 model, which is an offline coupled biogeography and biogeochemistry model that simulates natural vegetation types (biomes). This allows a comparison of predicted biomes for all simulations directly to the Salzmann et al (2008) vegetation reconstruction (PRISM3 vegetation reconstruction).

3.2.1.1 HadCM3

A comprehensive description of the UK Met Office Hadley Centre Coupled Model Version 3 (HadCM3) used in this study is available in Gordon et al. (2000) and Cox et al. (1999). HadCM3 has been widely used for palaeoclimate modelling, with simulations of the Last-Glacial Maximum and Mid-Holocene climates as well as the mPWP (Braconnot et al., 2007; Bragg et al., 2012; Valdes et al., 2017) and deeper time. HadCM3 is a dynamically and thermodynamically coupled atmosphere, ocean and sea ice model. The resolution of the atmosphere component is 2.5° in latitude by 3.75° in longitude, which translates to a grid spacing of 278 km by 417 km at the equator. The atmosphere model is composed of 19 layers with a time step of 30 minutes. The ocean model has a spatial resolution of 1.25 by 1.25° with 20 layers. The sea ice model contains parameterisation of ice drift and leads (Cattle et al., 1995) with a simple thermodynamic scheme.

3.2.1.2 MOSES land surface scheme

A land surface scheme calculates the exchange of heat, moisture, momentum and CO_2 between the surface and atmosphere (Essery et al., 2003). The simulations included in this study use two different version of the Met Office (land) Surface Exchange Scheme (MOSES; versions 1 and 2.1) MOSES1 primarily differs from MOSES2.1 by its use of effective

parameters to calculate a single surface energy balance for each grid box, while MOSES 2.1 includes a tile model (Essery et al., 2003; Best et al., 2006). In MOSES2.1, the grid boxes which were previously treated as whole are now characterised as mosaics of distinct surface types. Separate surface temperatures, shortwave and longwave radiative fluxes, sensible and latent heat fluxes, ground heat fluxes, canopy moisture contents, snow masses and snow melt rates are computed for each surface type or tile in a grid box. The different surface types recognised are broadleaf and needle leaf trees, C_3 and C_4 grasses, shrub, inland water, bare soil and ice. A grid box can be made of any combination of surface types apart from those classified as land-ice. The fractions of surface types within each grid box are modelled by TRIFFID (Falloon et al., 2011).

3.2.1.3 TRIFFID vegetation model

The dynamic global vegetation model (DGVM) TRIFFID computes the structure and distribution of six plant functional types (broadleaf tree, needle leaf tree, C_3 grass, C_4 grass, shrub and bare soil). The areal coverage, leaf index and canopy height of each plant type is updated using a carbon balance approach whereby vegetation change is directed by net carbon fluxes calculated within the MOSES 2.1 land surface scheme (Cox, 2001). The carbon fluxes are derived using the coupled photosynthesis-stomatal conductance model developed by Cox et al. (1998) that utilises existing models of leaf-level photosynthesis in C_3 and C_4 plants (Collatz et al., 1991, 1992). Climate and CO_2 drive the resulting rates of photosynthesis and plant respiration. Each plant functional type (PFT) is updated over a grid box (normally every 10 model days) based on competition from other plant types, modelled using the Lotka-Volterra approach and the net carbon available. Soil carbon is increased by litter fall and is returned to the atmosphere by microbial respiration at a rate based on temperature and soil moisture (Cox 2001).

TRIFFID can be run in equilibrium and dynamic mode. The equilibrium mode is coupled asynchronously to the atmosphere model, with accumulated carbon fluxes passing though MOSES2.1 (Cox 2001). Using the equilibrium method has been shown to be successful in producing equilibrium states for the slowest variables in the model (for example, soil carbon and forest cover) by offline tests. This is often followed by a dynamic run to allow faster varying components (such as grasses) to reach equilibrium with seasonally varying climate (Cox 2001). The modes used in this study are detailed in the methodology of this paper.

3.2.1.4 BIOME4

BIOME4 is a carbon and water flux model that predicts the interaction of vegetation distribution, structure and biogeochemistry (Kaplan, 2003). The model is driven by long term averages of monthly mean temperature, sunshine and precipitation and requires information on soil texture and depth to determine water holding capacity and percolation rates. There are twelve plant functional types (PFTs) whose bioclimatic limits determine whether it could be present in each grid cell. The seasonal maximum leaf area index (LAI) that maximises net primary production (NPP) for each PFT is calculated based on a daily time step simulation of soil water balance and monthly processes based calculations of canopy conductance, photosynthesis, respiration and phenological state (Haxeltine & Prentice, 1996; Kaplan, 2003). The PFT with the highest NPP is selected as the dominant plant type. For the biome to be identified, the PFTs are ranked according to a set of rules based on a number of computed biogeochemical variables, including NPP, LAI and mean annual soil moisture (Kaplan 2003). This ranking in each grid cell controls the selection of one of twenty-seven biomes.

3.2.2 Boundary conditions and experimental design

In this paper, we present results from ten climate model simulations (Table 3.1). Four experiments were run with HadCM3 based on experimental design from the PlioMIP project (Haywood et al., 2010; Bragg et al., 2012), using PRISM3D boundary conditions (Dowsett et al., 2010) and the MOSES 1 land surface scheme with prescribed vegetation from Salzmann et al. (2008). While the PlioMIP project specified a modern orbital configuration, here we have performed simulations for MIS G17, K1, KM3 and KM5c interglacials using orbital parameters derived from the Laskar et al. (2004) astronomical solution. For these interglacials the specific orbit used in the simulations represents the peak of the interglacial according to the LR04 benthic oxygen isotope stack. An additional four experiments were run with the same set up but this time in conjunction with the dynamic vegetation model TRIFFID and the MOSES 2.1 land surface scheme. All experiments were run for five hundred years with the final 100 years used to calculate the required climatological averages. Table 1 details the simulations included in this study. There were two pre-industrial experiments also run as a comparison, one with MOSES 1 land surface scheme and the other with MOSES2.1.

Experiment name	Land Surface Scheme	Vegetation	Orbit (kyr)	Eccentricity	Precession	Obliquity (degrees)	MAT (°C)	MAP mm/day	JJA (°C)	DJF (°C)	JJA mm/day	DJF mm/day
Plio-G17^{Dynamic}	MOSES 2.1	Dynamic	2950	0.04	-0.01776	23.96	19.35	3.04	22.45	16.35	3.10	2.99
Plio-K1^{Dynamic}	MOSES 2.1	Dynamic	3060	0.05	-0.05086	23.01	19.35	3.04	22.95	16.05	2.95	3.11
Plio-KM3^{Dynamic}	MOSES 2.1	Dynamic	3155	0.05	-0.04350	23.76	19.45	3.02	23.15	16.15	3.01	3.02
Plio-KM5c^{Dynamic}	MOSES 2.1	Dynamic	3205	0.01	0.00605	23.47	18.85	3.01	21.25	16.55	3.06	2.98
Pre-Ind^{Dynamic}	MOSES 2.1	Dynamic	Pre-Industrial	0.02	0.01628	23.44	14.85	2.91	17.15	13.05	2.98	2.87
Plio-G17^{Prescribed}	MOSES 1	Prescribed	2950	0.04	-0.01776	23.96	18.55	3.10	21.25	15.85	3.18	3.02
Plio-K1^{Prescribed}	MOSES 1	Prescribed	3060	0.05	-0.05086	23.01	18.75	3.10	21.85	15.85	3.07	3.11
Plio-KM3^{Prescribed}	MOSES 1	Prescribed	3155	0.05	-0.04350	23.76	18.75	3.11	21.85	15.75	3.13	3.07
Plio-KM5c^{Prescribed}	MOSES 1	Prescribed	3205	0.01	0.00605	23.47	18.05	3.06	20.05	15.95	3.14	3.00
Pre-Ind^{Prescribed}	MOSES 1	Prescribed	Pre-Industrial	0.02	0.01628	23.44	13.85	2.88	15.65	11.95	2.96	2.83

Table 3.1 Summary of experiments including orbital parameters implemented in HadCM3, also showing global mean annual and seasonal temperatures and precipitation. Control experiments indicated in bold.

The experiments using TRIFFID were run using equilibrium mode (where TRIFFID is coupled to the atmospheric model, with accumulated carbon fluxes passing through MOSES 2.1 (Cox, 2001) for the first 50 years and subsequently run in dynamic mode for the remainder of the simulation (450 years). All simulations were subsequently run through BIOME4 to compare biome types between those run with prescribed vegetation and those with dynamic vegetation.

When running BIOME4 a standard anomaly method was used, which subtracts the control climate simulation from the palaeo simulation and adds the resulting 'anomaly' to the present-day baseline climatology. This approach compensates for first order bias in the HadCM3 control simulations (Kaplan, 2003). Due to the lack of sufficient observational climatological data this method could not be employed over Antarctica, therefore biomes are only predicted up to 60°S in the Southern Hemisphere.

Haywood et al., (2013a) show that the peak of MIS KM5c is characterised by a near modern orbital forcing within a period of low eccentricity and low precession (Laskar et al., 2004; Prescott et al., 2014). In this study, therefore, when examining changes in the climatology in the simulations of the four interglacials, KM5c is considered as the control Pliocene experiment.

3.3 Results – Climatological response to orbital forcing

3.3.1 Pliocene interglacial climate differences

We have simulated four interglacials within the mPWP using prescribed (HadCM3 MOSES1) and dynamic vegetation models (HadCM3 MOSES2.1 coupled with TRIFFID). Using both versions of the model, all interglacials are warmer than the pre-industrial control experiments (range of 18.05°C to 19.45°C global annual mean temperatures). Our experiments for KM5c are similar to previous mPWP climate simulations that have modern orbit (in terms of the large-scale features of temperature and precipitation change; (Haywood et al., 2013b), due to the near modern orbital configuration during MIS KM5c (3.205 Ma). The other interglacials are between 0.54°C and 0.71°C warmer as a global annual mean

average than KM5c for the prescribed vegetation experiments and between 0.51°C and 0.64°C warmer for the dynamic vegetation experiments (Table 3.1). Global annual mean total precipitation rate increases are between 0.04mm/day and 0.05mm/day for prescribed and 0.01mm/day and 0.03mm/day for dynamic vegetation experiments (Table 3.1). Experiments incorporating dynamic vegetation are on average 0.73°C warmer, as a global annual mean average, than those using prescribed, which may be attributable to either general differences in the model or the feedbacks on climate associated with the implementation of dynamic vegetation. Broadly all regional patterns of temperature and precipitation change are enhanced in the MOSES2.1 experiments relative to MOSES1 for each of the studied interglacials. The detailed climate response associated with each interglacial will be described alongside the vegetation (biome and PFT) predictions below.

3.3.1.1 MOSES1 prescribed vegetation experiments

The large-scale features of surface temperature change and precipitation (relative to the pre-industrial experiment) are seen in all four experiments (Figs. 3.2d and 3.2h), however the patterns of change in Plio-G17^{Prescribed}, Plio-K1^{Prescribed}, Plio-KM3^{Prescribed} are intensified (Fig. 3.2a-c, 3.2e-g). The dominant features include progressive warming towards the higher latitudes of both hemispheres, more surface warming over the land versus the oceans. There is also cooling over tropical Africa and India which is related to increases in precipitation and associated evaporative cooling and an enhanced di-pole pattern in the North Atlantic (linked to a change in the mode of sinking/deep-water formation, which has been observed previously using this version of the model (see Prescott et al., 2014)).

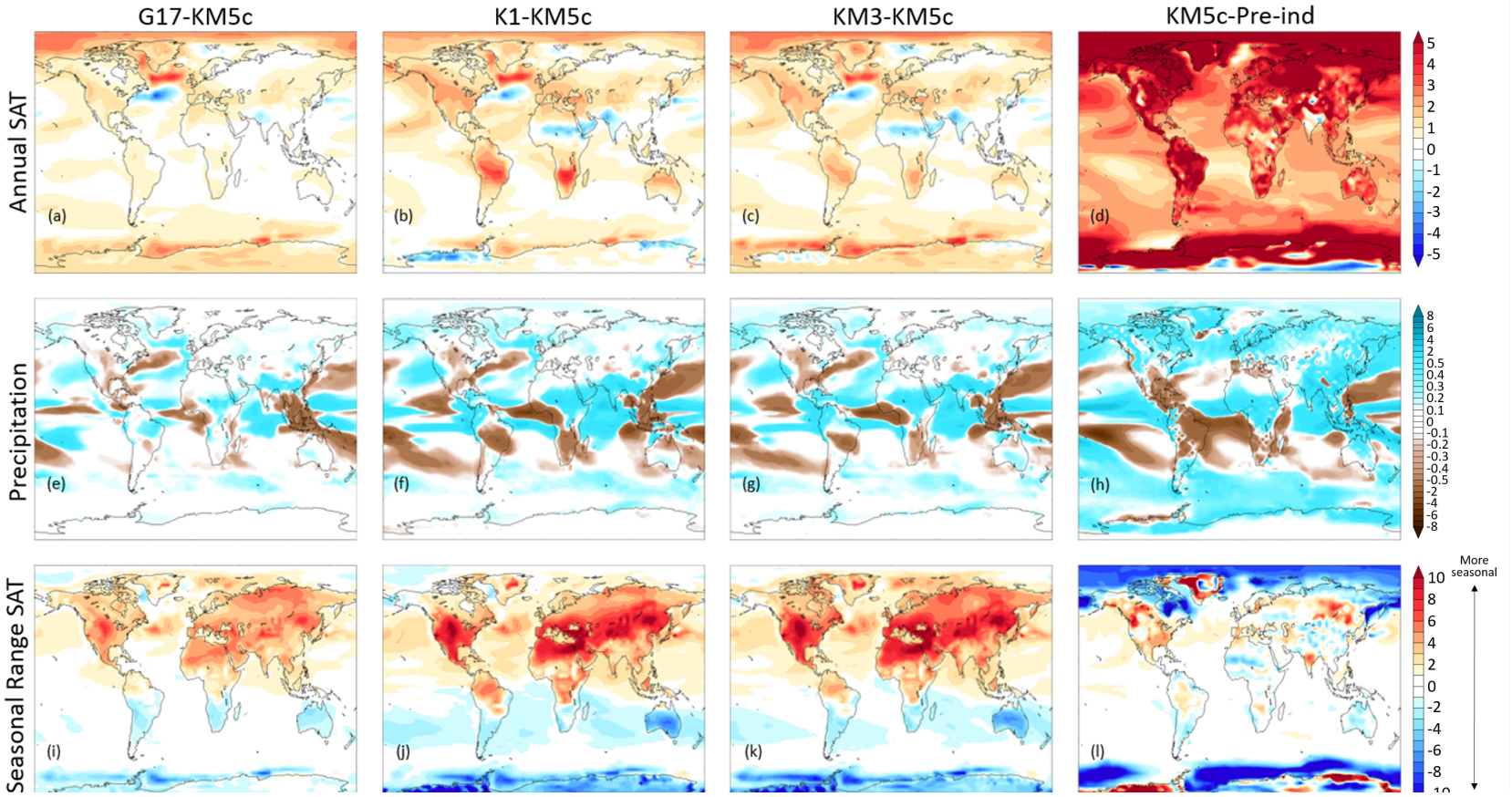

Figure 3.2 HadCM3 results run with MOSES1 surface scheme showing (a – d) Annual SAT anomalies (°C) for (a) Plio-G17^{Prescribed} – Plio-KM5c^{Prescribed}, (b) Plio-K1^{Prescribed} – Plio-KM5c^{Prescribed}, (c) Plio-KM3^{Prescribed} – Plio-KM5c^{Prescribed}, (d) Plio-KM5c^{Prescribed} – Pre-Ind^{Prescribed}. (e – h) Annual precipitation anomalies (mm/day) for (e) Plio-G17^{Prescribed} – Plio-KM5c^{Prescribed}, (f) Plio-K1^{Prescribed} – Plio-KM5c^{Prescribed}, (g) Plio-KM3^{Prescribed} – Plio-KM5c^{Prescribed}, (h) Plio-KM5c^{Prescribed} – Pre-Ind^{Prescribed}. (i – l) Seasonal range surface temperature anomalies (°C); each figure shows warm monthly mean minus cold monthly mean minus the same for the control. (i) Plio-G17^{Prescribed} – Plio-KM5c^{Prescribed}, (j) Plio-K1^{Prescribed} – Plio-KM5c^{Prescribed}, (k) Plio-KM3^{Prescribed} – Plio-KM5c^{Prescribed}, (l) Plio-KM5c^{Prescribed} – Pre-Ind^{Prescribed}.

A key difference between experiments Plio-G17^{Prescribed}, Plio-K1^{Prescribed}, Plio-KM3^{Prescribed} and Plio-KM5c^{Prescribed} is the generally reduced seasonal range of temperature in the Southern Hemisphere versus the increased seasonal range of temperatures in the Northern Hemisphere (particularly over land). This bipolar response is understandable given the changes in orbital forcing shown in Figure 3.1 (b-e).

The four interglacial experiments (Plio-G17^{Prescribed}, Plio-K1^{Prescribed}, Plio-KM3^{Prescribed} and Plio-KM5c^{Prescribed}) with prescribed vegetation were run through the offline vegetation model BIOME4 to classify them into different biomes for comparison purposes (Figure 3.3b – e). Figure 3.3a shows the PRISM3 vegetation reconstruction from Salzmann et al. (2008) for reference. As the PRISM3 vegetation reconstruction is a model boundary condition, the subsequent biome reconstructions are, in some respects, constrained to the PRISM3 dataset. Any differences are due to inconsistencies between the simulated Pliocene climate and the original vegetation reconstruction (PRISM3) or are a function of the climate response to the orbital forcing imposed.

There are regional differences in biome distribution when compared to the PRISM3 reconstruction. In all four interglacial experiments, South Africa is dominated by shrubland and desert instead of forest and woodland in the PRISM3 reconstruction. All interglacials show a larger expanse of grassland in North America and Asia, as well as enhanced desert over Australia and a loss of trees to shrubland in South America. Plio-KM5c^{Prescribed} predicts the most similar biome reconstruction to PRISM3. This is to be expected as this interglacial has the least difference from modern orbital conditions (Haywood et al. 2013a; Prescott et al., 2014).

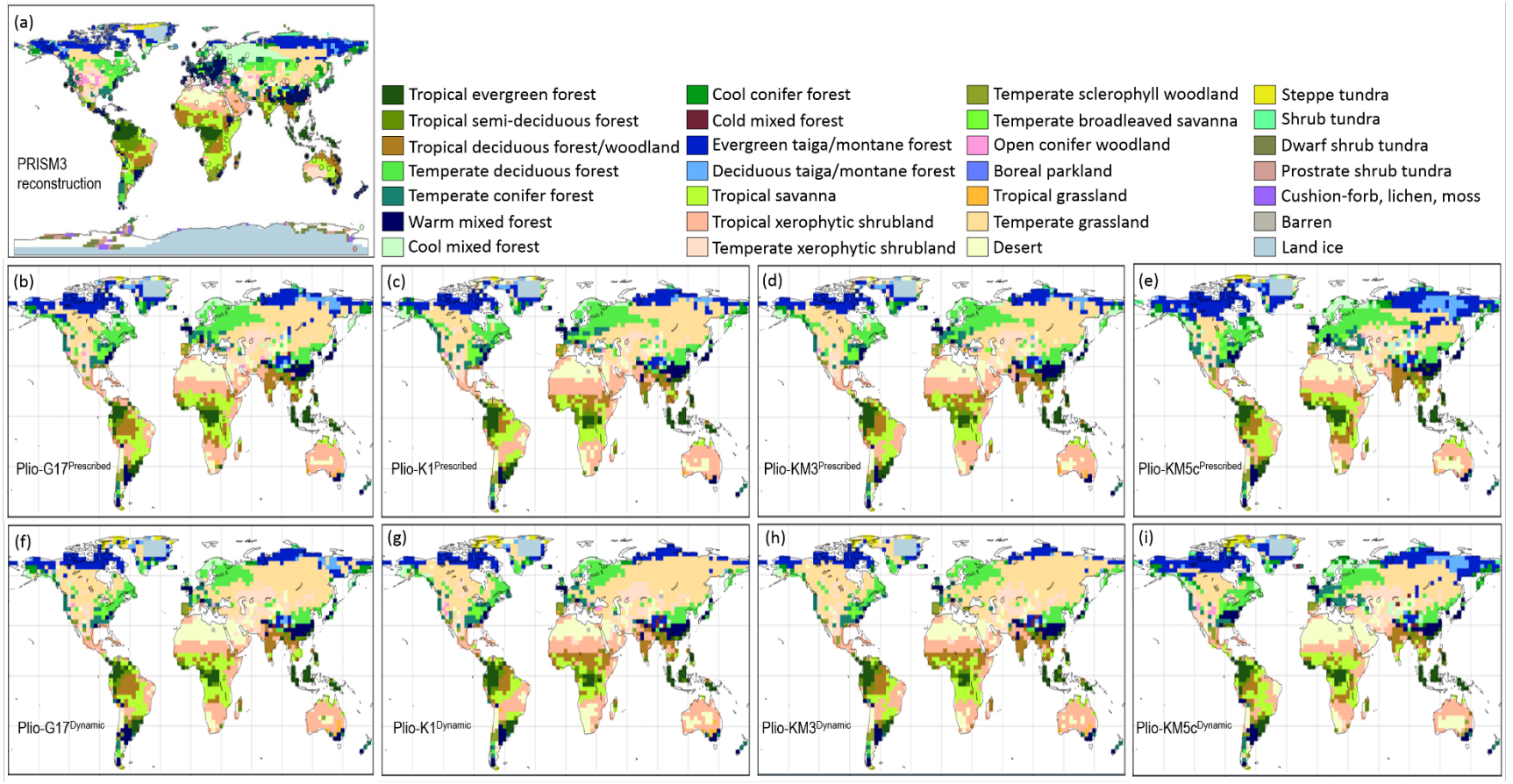

Figure 3.3 (a) Model/data hybrid PRISM3 vegetation reconstruction from Salzmann et al. (2008). (b – e) Global Pliocene predicted biomes simulated by BIOME4 with experiments run with prescribed vegetation with HadCM3 and land surface scheme MOSES1. (f – i) Global Pliocene predicted biomes simulated by BIOME4 with experiments run with HadCM3 coupled to TRIFFID vegetation model and Land surface scheme MOSES2. Note the larger expanse of grassland throughout Asia, especially with experiments where vegetation could run dynamically (f – i).

3.3.1.2 MOSES2.1 dynamic vegetation experiments

To understand how the addition of dynamic vegetation can impact the modelled climate response to orbital forcing, as well as to further understand the changes seen in vegetation distribution, we investigate annual and seasonal surface air temperature (SAT) and precipitation changes in the four interglacials (Fig. 3.4) alongside the changes in the simulated vegetation (Fig. 3.5 and 3.3f-3i).

The annual SAT differences (the interglacials minus the Plio-KM5c^{Dynamic} control) show a similar pattern to the Plio-KM5c^{Dynamic} minus Pre-Ind^{Dynamic} (Fig. 3.4d) but with a greater magnitude of change. Interglacials Plio-G17^{Dynamic} and Plio-KM3^{Dynamic} present greater high latitude warming compared to Plio-KM5c^{Dynamic} than Plio-K1^{Dynamic}. For Plio-G17^{Dynamic} warming of ~2°C is modelled, and in Plio-KM3^{Dynamic} warming reaches 3.5°C at the high latitudes (60°N – 90°N) relative to the Plio-KM5c^{Dynamic} control experiment. Patterns of temperature change such as high latitude warming and tropical cooling are seen in all the interglacials (when differenced to Plio-KM5c^{Dynamic}) and are generally consistent with the simulations using prescribed vegetation (Fig. 3.2).

TRIFFID's predictions of PFTs are described to better understand the differences between the interglacials due to orbital changes and dynamic vegetation feedbacks (Fig.3.5). Here we discuss the results in relation to how they are different to the Plio-KM5c^{Dynamic} control broken down into different regional responses.

3.3.1.2.1 Africa

In Plio-KM5c^{Dynamic} there is 80-90% broadleaf forest over southern and central Africa with 100% bare soil (desert) in North Africa, Arabia and the west coast of southern Africa. The forest and bare soil are separated by a thin band of grassland at approximately 15°N. Plio-K1^{Dynamic} and Plio-KM3^{Dynamic} show 80 – 90% increase of broadleaf trees across southern North Africa relative to the Plio-KM5c^{Dynamic} control. This replaces bare soil and the grasses therefore pushing the boundary between forest and grassland northwards. Plio-G17^{Dynamic} shows this same pattern but broadleaf increase is over a much smaller area and is less intense. In the Plio-K1^{Dynamic} interglacial Southern Africa shows a loss of 80-100% broadleaf to bare soil and grassland, with Plio-KM3^{Dynamic} showing a slight loss of broadleaf and the occurrence of grasses.

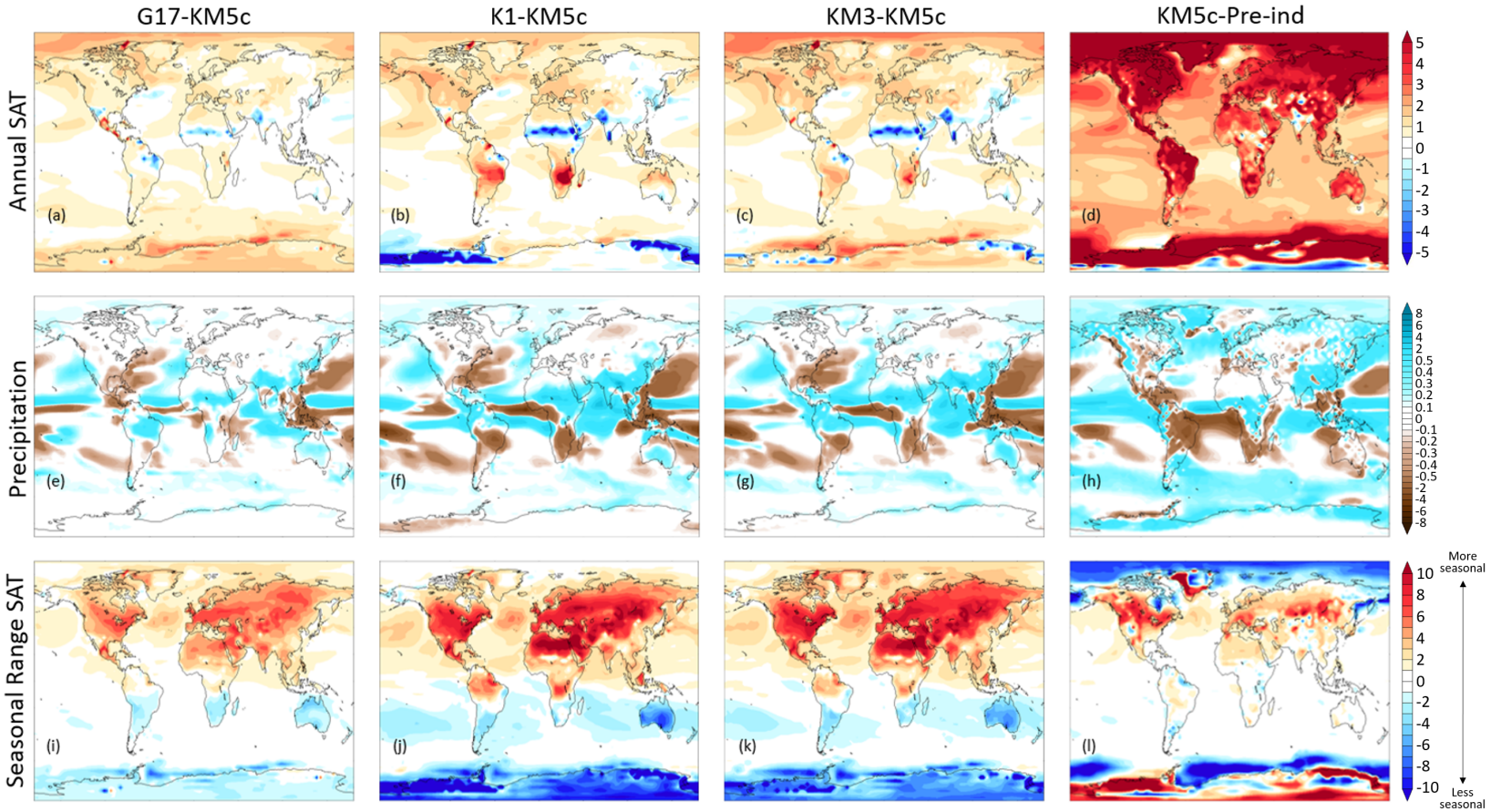

Figure 3.4 HadCM3 results run with MOSES2 surface scheme showing (a – d) Annual SAT anomalies (°C) for (a) Plio-G17^{Dynamic} – Plio-KM5c^{Dynamic}, (b) Plio-K1^{Dynamic} – Plio-KM5c^{Dynamic}, (c) Plio-KM3^{Dynamic} – Plio-KM5c^{Dynamic}, (d) Plio-KM5c^{Dynamic} – Pre-Ind^{Dynamic}. (e – h) Annual precipitation anomalies (mm/day) for (e) Plio-G17^{Dynamic} – Plio-KM5c^{Dynamic}, (f) Plio-K1^{Dynamic} – Plio-KM5c^{Dynamic}, (g) Plio-KM3^{Dynamic} – Plio-KM5c^{Dynamic}, (h) Plio-KM5c^{Dynamic} – Pre-Ind^{Dynamic}. (i – l) Seasonal range surface temperature anomalies (°C); each figure shows warm monthly mean minus cold monthly mean minus the same for the control. (i) Plio-G17^{Dynamic} – Plio-KM5c^{Dynamic}, (j) Plio-K1^{Dynamic} – Plio-KM5c^{Dynamic}, (k) Plio-KM3^{Dynamic} – Plio-KM5c^{Dynamic}, (l) Plio-KM5c^{Dynamic} – Pre-Ind^{Dynamic}.

3.3.1.2.2 North America

Plio-KM5c^{Dynamic} has a mixed forest of broadleaf and needle leaf trees in North America with the highest percentage of broadleaf trees predominately focussed in the northern continental interior and South-East America and Mexico. The rest of America, Canada and Greenland (outside of the ice sheet) is dominated by needle leaf trees.

Plio-G17^{Dynamic}, Plio-K1^{Dynamic} and Plio-KM3^{Dynamic} share similar spatial changes in vegetation over North America. Relative to Plio-KM5c^{Dynamic}, they present 30–50% more broadleaf trees over Canada and Alaska and a reduction of the same PFT of 30-40% in Central and Eastern America. This increase of broadleaf is associated with a decrease of needle leaf trees over the same areas. There are also areas of increasing shrub (up to 60%) to the west of America replacing needle leaf trees.

3.3.1.2.3 South America

Within the Plio-KM5c^{Dynamic} control simulation there is forest of up to 90% broadleaf trees over most of South America. Over the remaining areas, predominantly the interior of Northern Brazil, there are areas of 85% grassland and along the east coast of Brazil, 100% bare soil. Chile and southern Argentina are dominated by needle leaf trees.

Over South America, the differences in PFTs compared to Plio-KM5c^{Dynamic} seen in interglacial peaks Plio-G17^{Dynamic}, Plio-K1^{Dynamic} and Plio-KM3^{Dynamic} are minor. However, over Brazil, Plio-G17^{Dynamic} and Plio-KM3^{Dynamic} show increases in broadleaf trees (between 20% and 60%), whereas Plio-K1^{Dynamic} shows a decrease of up to 60% over the southern east coast of Brazil.

3.3.1.2.4 Eurasia

Plio-KM5c^{Dynamic} shows Eurasia largely covered in forest, including 70% broadleaf forest over Spain and south-western Europe. Central Siberia and areas of southern Asia (e.g. South China and Indonesia) have broadleaf forest concentrations reaching 95%. The remaining areas of Northern Eurasia have 50 - 75% of needle leaf trees. Grassland can be seen in India and in central Asia south of the simulated forest line. There are shrubs found in small areas throughout Asia, particularly in the north-eastern region.

All three interglacials exhibit localised increases in broadleaf trees in northern Eurasia, however, the dominant response is up to 60% decline in needle leaf trees that are replaced by grasses (20% increase) and shrubs (up to 60% increase). The largest difference in PFTs for the interglacials is in the Northern region of India where there is a 100% reduction in bare soil, replaced by grassland and broadleaf trees.

3.3.1.2.5 Australia

Australia in the Plio-KM5c^{Dynamic} control experiment includes large areas of broadleaf forest to the north and east of the country, grassland through the centre, surrounded by shrubland and bare soil in the south east.

Plio-G17^{Dynamic}, Plio-K1^{Dynamic} and Plio-KM3^{Dynamic} all predict a reduction in grassland in central Australia which is replaced with broadleaf forest to the north and shrub to the south. Plio-K1^{Dynamic} has a slightly more pronounced pattern of change, comprising a 60% reduction in broadleaf forest along the north-east coastline with grassland growing instead.

3.3.1.2.6 Antarctica

Plio-KM5c^{Dynamic} and Plio-G17^{Dynamic} predict mainly shrub and grassland over non-glaciated regions of Antarctica with small areas of bare soil. The largest changes predicted over Antarctica are within the Plio-K1^{Dynamic} interglacial. Experiment Plio-K1^{Dynamic} suggests that all grasses and shrubs on the Antarctic margins are replaced by bare soil. Experiment Plio-KM3^{Dynamic} has a similar predicted vegetation distribution with a smaller area of increased bare soil and grassland.

The addition of dynamic vegetation results in a spatially complex climatic response. There are some areas where adding vegetation causes positive feedbacks, for example, increases the temperature signal (be that, positive or negative) and examples of negative feedbacks where this signal is reduced with the addition of dynamic vegetation. There is enhanced warming over central South America (5°C anomaly in Plio-K1^{Dynamic}) and southern Africa (up to 10°C anomaly in Plio-K1^{Dynamic}) compared to the Plio-KM5c^{Dynamic} control. This is due to feedbacks through partial replacement of forest with grasses in South America, and with grasses, shrubs and bare soil in southern Africa. The occurrence of more open type vegetation (in Africa

and South America; Fig. 3.5) is caused by the orbitally forced warming in these areas (in Plio-K1^{Prescribed}; Fig. 3.2b) and enhanced by decreases in evapotranspiration (not shown). This is linked with a decrease in precipitation in the Plio-K1^{Prescribed} experiment (Fig. 3.2f). The larger temperature change seen in central Africa is a result of a positive feedback between vegetation and surface temperature brought about through the northward shift of the Sahara Desert and its replacement with broadleaf forest and grasses (Fig. 3.4 and Fig. 3.5).

Over India, bare soil is replaced with broadleaf forest and grasses and this change amplifies the local evapotranspiration-driven cooling demonstrated in the prescribed vegetation experiments. The largest positive feedback effect is seen in Plio-K1^{Dynamic} over Antarctica. This area shows higher albedo (not shown) due to snow cover and a temperature decrease of 3.5°C compared to Plio-KM5c^{Prescribed}. When using dynamic vegetation, the simulated albedo over Antarctica is increased further due to the total loss of vegetation (shrub and grass) and its replacement with bare soil leading to further cooling in these regions, Plio-K1^{Dynamic} is up to 9°C colder than Plio-KM5c^{Dynamic}.

In the prescribed vegetation experiments we demonstrate a trend towards more open vegetation in Eurasia (Fig. 3.3b-e), linked primarily to changes in insolation patterns. The differences in vegetation (in terms of PFT, Fig. 3.5) are enhanced further by positive feedbacks in dynamic vegetation (reduction of precipitation, evapotranspiration and soil moisture associated with the loss of forest).

There are however, also areas of cooling seen in the MOSES2.1 simulations when run with dynamic vegetation that are not seen in the simulations run solely with changing orbital forcing and prescribed vegetation. For example, in all interglacial experiments, coastal northeast Brazil shows a cooling of approximate 5°C when compared to Plio-KM5c^{Dynamic} (Fig. 3.4a-c). This appears to be due to an orbitally driven vegetation switch from bare soil and grasses to broadleaf forest which results in an increase in evapotranspiration (and a resulting increase of the latent heat flux). Coupling the simulations to a dynamic vegetation model also induces a cooling of 2°C (in all interglacials) on the coastline of South Australia. This temperature change occurs with the replacement of bare soil and grass with shrub, and is associated with an increase of evaporative cooling in this region (not shown).

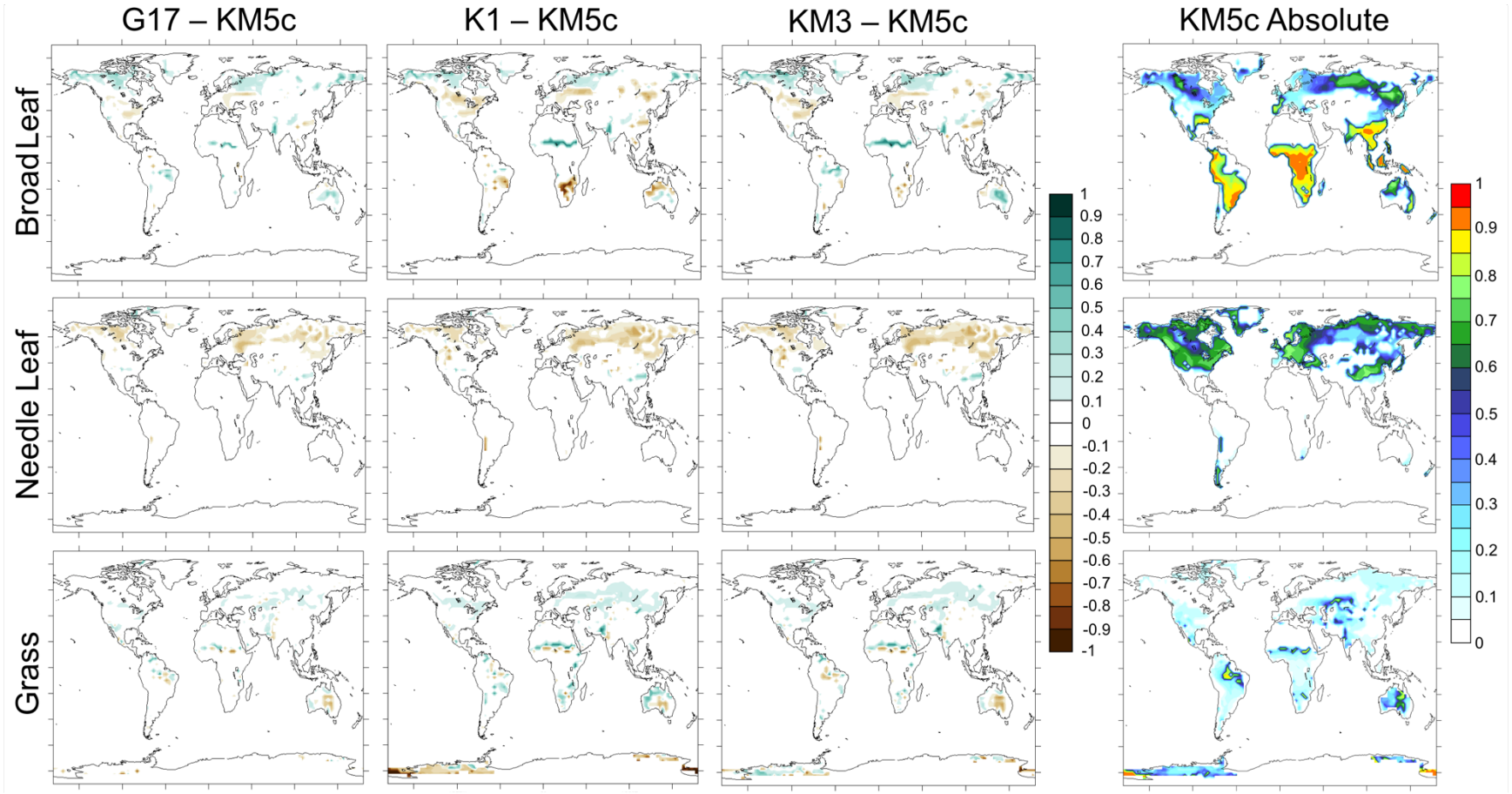
G17 – KM5c
K1 – KM5c
KM3 – KM5c
KM5c Absolute
Broad Leaf
Needle Leaf
Grass
1
0.9
0.8
0.7
0.6
0.5
0.4
0.3
0.2
0.1
0
-0.1
-0.2
-0.3
-0.4
-0.5
-0.6
-0.7
-0.8
-0.9
-1
1
0.9
0.8
0.7
0.6
0.5
0.4
0.3
0.2
0.1
0

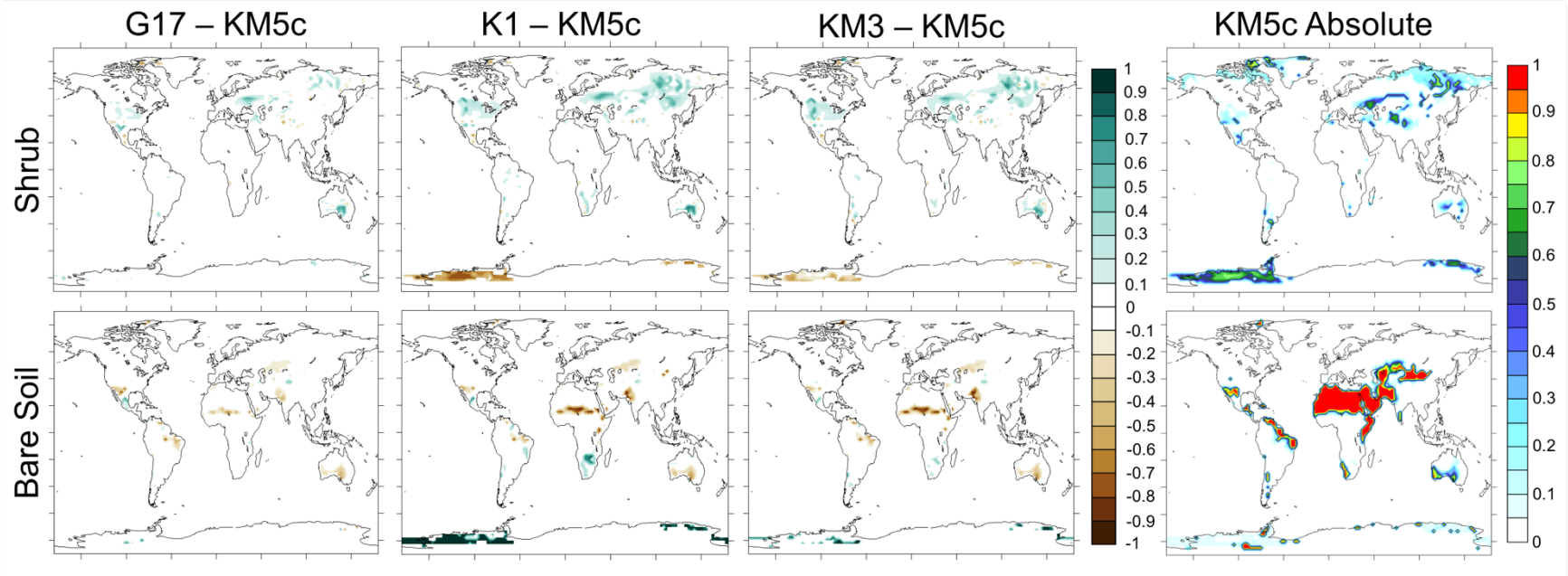

Figure 3.5 Model predictions from experiments run with dynamic vegetation for TRIFFID simulated Plant Functional Types (PFTs) shown as percentage anomalies from control run MIS KM5c (Plio-KM5c^{Dynamic}) for (left) Plio-G17^{Dynamic} – Plio-KM5c^{Dynamic}; (middle-left) Plio-K1^{Dynamic} – Plio-KM5c^{Dynamic}; (middle-right) Plio-KM3^{Dynamic} – Plio-KM5c^{Dynamic}; (right) Control Plio-KM5c^{Dynamic} absolute plant functional types.

There is a reduction in the level of high latitude warming seen with the introduction of dynamic vegetation, especially in two interglacials (Plio-KM3^{Dynamic} and Plio-G17^{Dynamic}) that show greater high latitude warming than Plio-KM5c^{Dynamic}. Broadleaf trees in the Arctic have twice the albedo and 50 – 80% greater evapotranspiration rates when leafed-out than their evergreen needle leaf counterparts (Swann et al., 2010). Therefore, more broadleaf forest replacing needle leaf along the Arctic coast has a cooling effect due to increased evapotranspiration, moderating the high northern latitude warming signal.

The cause and effect of the simulated climate response to orbit and vegetation changes is complicated when introducing the dynamic vegetation model, as this also involves a switch in land surface schemes. Where the inclusion of dynamic vegetation has made the terrestrial areas generally warmer, this could be arguably due to the use of MOSES2.1 (over MOSES1), which in previous analysis has been found to be a warmer model (not shown). However, we can suggest that the areas where the introduction of dynamic vegetation simulates an increased cooling, to be solely a signal from vegetation feedbacks.

3.3.2 MOSES2.1 Dynamic large-scale biome changes (BIOME4)

The four interglacial experiments (Plio-G17^{Dynamic}, Plio-K1 ^{Dynamic}, Plio-KM3 ^{Dynamic} and Plio-KM5c ^{Dynamic}) with dynamic vegetation were run through the offline vegetation model BIOME4 to classify them into different biomes for comparison purposes.

Patterns of biome distribution appears similar between the four interglacials (using dynamic vegetation). They all have expanded grassland over Asia and North America, with Eastern Europe/Scandinavia predominantly showing temperate deciduous forest. They all show large areas of desert in northern and southern Africa, however three experiments (Plio-G17^{Dynamic}, Plio-K1 ^{Dynamic}, and Plio-KM3 ^{Dynamic}) show smaller desert areas with more xerophytic shrubland than Plio-KM5c ^{Dynamic} over central Australia. The Arctic coastline has predominantly evergreen taiga/montane forest. South America has tropical forest biome to the north and shrubland and mixed forest types to the south.

There are detailed differences between the BIOME4 reconstructions for the dynamic vegetation experiments. For example, across central Africa Plio-K1^{Dynamic} and Plio-KM3^{Dynamic} show a band of deciduous forest, whereas Plio-G17^{Dynamic} and Plio-KM5c^{Dynamic} are more dominated by tropical savannah and shrubland biomes. In Plio-KM5c^{Dynamic}, taiga montane forest reaches the Arctic coastline and stretches latitudinally across north Asia. The other three interglacials also have taiga montane forest in this region but covering a smaller area. In experiments Plio-K1^{Dynamic} and Plio-KM3^{Dynamic} the band of forest across the coast is broken and pushed north by grassland which can reach the Arctic coast of eastern Asia. North America shows a similar pattern, with evergreen taiga/montane forest again being pushed north by grasslands which in Plio-K1^{Dynamic} and Plio-KM3^{Dynamic} reaches the northern Canadian coastline. Arid desert regions in Australia shrink in Plio-G17^{Dynamic} and Plio-KM3^{Dynamic}, whereas Plio-KM5c^{Dynamic} and Plio-K1^{Dynamic} show a distribution which is similar to the PRISM3 reconstruction of desert in this region.

In summary, the BIOME4 output for Plio-KM5c^{Dynamic} is the most like the PRISM3 reconstruction due to the stable and near modern orbital forcing. The other three interglacials run with dynamic vegetation show a very different terrestrial environment to Plio-KM5c^{Dynamic} (and the PRISM3 reconstruction). The biomes are more stratified in a latitudinal sense and are less heterogeneous with large areas of grass in the northern hemisphere mid to high latitudes.

3.4 Discussion

The exploration of discrete interglacial events within the mPWP was investigated in Prescott et al. (2014), which looked at both the MIS K1 and KM5c interglacial peaks and demonstrated that the two events are different in nature in terms of their climatology (Prescott et al., 2014). Here we continue with the incorporation of two more Pliocene interglacial events (MIS G17 and KM3) to build a fuller picture of mPWP interglacial climate variability, but with the addition of dynamic vegetation responses. We focus our discussion on addressing the importance of orbitally driven changes in seasonality as a driver for

regional land cover response, and the validity of model predictions regarding regional palaeobotanical data.

3.4.1 How important is the effect of orbitally-driven seasonality changes for understanding regional climate and land cover responses, and how does the addition of a dynamic vegetation model alter the climatological and land cover response?

The simulated SATs in Figure 3.2 shows notably large increases in seasonal range in relation to the Plio-KM5c^{Prescribed} control simulation. For all three interglacials (G17, K1, and KM3), the larger amplitude of the Northern Hemisphere seasonal signal is forced by both the higher eccentricity (Fig. 3.1), when compared to MIS KM5c, and the perihelion falling during the boreal spring (MIS G17) and summer (MIS K1 and KM3).

Given the increased seasonality in all MIS G17, K1 and KM3 simulations, there is a need to understand the seasonal response of temperature in relation to predicted vegetation. For example, the cooling over Antarctica in Plio-K1^{Prescribed} is due to a large insolation reduction (of up to 100 Wm^{-2}; Fig. 3.1) over the Southern Hemisphere during the summer months that is not seen to the same extent in the other interglacials. The similarities seen between all the interglacials such as the northern hemisphere high latitude warming is caused by increases of up to 95 Wm^{-2} in the spring/summer months.

Changes in the seasonality of surface temperature and precipitation response is especially amplified in simulations run with dynamic vegetation (Fig. 3.4). In these experiments, the Northern Hemisphere shows an enhanced seasonality in all three interglacials compared to the Plio-KM5c^{Dynamic} control. While this is seen most strongly on land due to the lower heat capacity of land versus the oceans, the oceans also show the same signal. This is most clearly expressed in Plio-K1^{Dynamic} and Plio-KM3^{Dynamic} due to the largest seasonal differences in orbitally driven incoming insolation (Fig, 3.1).

The larger seasonal range (colder autumn/winters and warmer spring/summers) over the Northern hemisphere coincides with the reduction of forest seen in both BIOME4 output

and TRIFFID PFTs in favour of more open vegetation over Eurasia. This region presented the largest vegetation change.

The colder temperatures in winter over North America/Eurasia do not reduce winter precipitation for MIS K1, G17 and KM3 compared to Plio-KM5c (in both the prescribed and dynamic vegetation simulations). Springtime precipitation for MIS K1, G17 and KM3 increase compared to KM5c in large areas of Eurasia in experiments using prescribed vegetation. However, this is not the case for the same experiments run using dynamic vegetation were during the boreal spring and summer large areas of Eurasia receive either the same or less precipitation than the KM5c experiments, even though summer surface temperatures increase substantially. This reduced seasonal surface moisture availability can affect the seasonal patterns of warming through changes in latent heat flux, and decreased deeper soil moisture availability favouring grass/shrub occurrence over trees (Fig. 3.4).

Grasses have an intense but shallow root system using water from upper soil layers whereas trees roots access deeper soil moisture (Ward et al., 2013). Winter precipitation is critical to recharge deeper soil layers for trees to access (Schwinning et al., 2005), and this process would be especially important in a scenario where summer temperatures increase due to a change in seasonality. Therefore, in these results the warmer spring/summers and lack of associated increase in winter/summer precipitation favours the simulation of grass rather than trees in our model simulations (Figs. 3.3 and 3.5). The reduction in available soil moisture in the deepest soil layer (on average 308 mm less in all 4 interglacials than the pre-industrial annual mean, and a decrease to 327 mm less in winter) is seen most acutely in the dynamic vegetation simulations (Appx Fig. B.8). Given that soil moisture and temperature are fundamental drivers in TRIFFID (Cox, 2001) in the prediction of vegetation types, this reduction in soil moisture provides a partial explanation for the large-scale tree retreat in Eurasia and North America.

Additionally, the higher summer temperatures seen over Eurasia and North America favours the existence of grass in the BIOME4 model. In BIOME4, through the identification of the 2 most successful PFTs each model grid cell is assigned a biome (Haxeltine & Prentice, 1996). The BIOME4 look up table sets a value of 21°C as a maximum warm monthly mean temperature for boreal evergreen and deciduous trees to grow. The simulated mean

temperature of the warmest month in our HadCM3 results often exceeds 21°C. When this threshold parameter is increased within BIOME4, the predicted forest/grass boundary moves equatorward). It appears that this empirical threshold in BIOME4 is another explanation as to why trees are replaced with grasses in all experiments for MIS K1, KM3 and G17.

BIOME4 simulates the vegetation distribution that is in equilibrium with a particular climate and atmospheric CO_2 concentration (Haxeltine & Prentice, 1996), it does not incorporate ecological successional processes which increases the uncertainty in the results. For prediction of rapidly changing climate response, BIOME4 can suggest the general direction and maximum extent of change to be expected but this may be oversimplified. Whereas the BIOME4 model has been used offline and forced with the climatology from HadCM3 the interaction between climate and vegetation is not fully resolved. Arguably, a more realistic approach is to allow vegetation to grow and interact with the climate.

We therefore use TRIFFID, a DGVM to treat the land cover as an interactive element to ascertain the magnitude of vegetation feedbacks from orbitally forced changes in seasonality and the variability between interglacials in the mPWP. TRIFFID separates the vegetation into PFT per the physical response to climate conditions and runs interactively with the climate model, therefore enabling vegetation feedbacks that are not possible when solely running the climate through BIOME4 without TRIFFID enabled.

When considering large scale vegetation changes predicted by TRIFFID, the decline of forest to more open vegetation (i.e. the combination of grasses, shrubs and bare soil) over Asia represents a significant change. This is consistent with the BIOME4 output which shows large expanses of grassland pushing the forest margin northwards in North America and Asia. While BIOME4 predicts temperate grassland across much of Asia, TRIFFID shows the main difference to be increased shrub causing a northward shift in broadleaf tree and an overall reduction of needle leaf at Northern high latitudes. Given that there are such large changes of vegetation seen over Eurasia in both TRIFFID and BIOME4 we compare the general trend in these results to published palaeobotanical sites that capture variability in this region.

3.4.2 Looking at specific high-resolution records (Lake Baikal and Lake El'gygytgyn), do our simulations capture similar variability shown in the geological record?

We now consider high resolution palaeobotanical data specifically where our models simulate the clearest change due to orbitally forcing (in central and eastern Asia). A similar response is also predicted over central North America but this region currently lacks a palaeobotanical record of sufficient temporal resolution to resolve the specific interglacials we have modelled. Given the difficulty of precise age controls for land-based records we look to proxy time series to estimate the range of vegetation expressed during the four Pliocene interglacials at Lake El'gygytgyn in Northeast Russia and Lake Baikal in Siberia, and this range is then compared to the range in vegetation simulated by the model. Note that we appreciate that TRIFFID PFTs cannot be directly compared to abundances of pollen due to differential pollen production rates across plant types. In concert with our BIOME4 results, we instead restrict any inference regarding PFTs and reconstructed pollen types simply as a relative measure of a more open or forest covered environment. Comparison of the model output to site specific proxy data may not be statistically robust due to differences in the representation of spatial scales in the model versus the spatial regime represented by the data. In order to circumvent these limitations, we compare the vegetation reconstruction to the model grid square corresponding to the specific geographical location of the proxy data site, as well as adjacent model grid squares to better represent the overall response of the simulated vegetation in the region.

3.4.2.1 Lake El'gygytgyn

The high Arctic is particularly sensitive of late Pliocene high latitude continental climate (Brigham-Grette et al., 2013; Andreev et al., 2016). There is some suggestion from contemporary pollen studies that the lake traps pollen from a source area of several thousand square kilometres and therefore the lake provides reliable information into regional and/or even over regional vegetation changes (Lozhkin & Anderson, 2013; Andreev et al., 2016).

Detailed pollen analysis and regional climate reconstructions have been published for the late Pliocene period ~3.58 – 2.15 Ma in Andreev et al. (2014) and Brigham-Grette et al. (2013) presents a summary of multiproxy evidence from 3.58 – 2.2 Ma. Extreme warmth

and polar amplification, compared to modern climate, was reconstructed from the record at Lake El'gygytgyn (67.5°, 72°) during the mPWP with a stepped cooling event during the Pliocene-Pleistocene transition (Brigham-Grette et al., 2013) and Arctic summer warmth with forest cover at both warm and cold summer orbits.

We examine pollen-based biome reconstructions of Lake El'gygytgyn (Tarasov et al., 2013) to facilitate comparison with our model results, however the fossil pollen data used for the biome reconstruction has also been the basis for other climate reconstructions (for details of this pollen analysis see (Melles et al., 2012; Brigham-Grette et al., 2013; Andreev et al., 2014).

Biome reconstructions at Lake El'gygytgyn indicate that the late Pliocene to early Pleistocene can be characterised by six vegetation types- four forest and two open vegetation biomes (Tarasov et al., 2013). The four biomes representing forest found at Lake El'gygytgyn in the Pliocene are either boreal or a mixture of boreal and temperate. The other two biomes are tundra and steppe and are dominated by boreal or arctic herb and shrub communities (Tarasov et al., 2013).

The pollen based biome reconstruction at Lake El'gygytgyn (Tarasov et al., 2013) indicates that MIS KM5c coincides with a transition from a cold deciduous biome to taiga. The pollen based biome reconstruction at KM3 is cool conifer forest (Tarasov et al., 2013) and K1 is on the boundary between cool mixed and cold deciduous forest and tundra (Tarasov et al., 2013) whereas there is both taiga and cool conifer forest at MIS G17 (Tarasov et al., 2013).

In this modelling study, the PFTs predicted by TRIFFID for Plio-KM5c^{Dynamic} are 64% needle leaf tree, 21% shrub and 13% grass (remainder bare soil) with BIOME4 simulating a cold evergreen needle leaf forest. The surrounding grid squares show biomes varying between cold evergreen and cool evergreen needle leaf forest, and low and high shrub tundra. The main simulated biome (cold evergreen needle leaf forest), is arguably interchangeable with the taiga, predicted from the pollen data (Tarasov et al., 2013). The cold deciduous biome interpreted from the pollen data, is not represented in the simulated biomes at or around Lake El'gygytgyn in our modelling results.

The biome simulated for Plio-KM3^{Dynamic} is cold evergreen needle leaf forest at Lake El'gygytgyn, with cool conifer forest interpreted from the pollen data. The PFTs predicted by TRIFFID also show 65% needle leaf trees. For Plio-K1^{Dynamic} BIOME4 simulates cold evergreen needle leaf forest, with biomes of temperate grassland, temperate deciduous and cool mixed forest simulated in the surrounding grid squares. The pollen-based biome reconstruction shows cool mixed and cold deciduous forest moving to a tundra biome. For this interglacial the simulation of forest biome types in BIOME4 matches well with the data. TRIFFID predicts 23% shrub and 12% grass at this site which is the highest shrub percentage simulated of the interglacials.

For Plio-G17^{Dynamic} BIOME4 simulates cold evergreen needle leaf forest with cool evergreen needle leaf forest and cool mixed forest predicted in the adjacent grid squares. The pollen-based biome reconstruction shows taiga and cool conifer forest, indicating consistency with the modelling results. TRIFFID simulated PFTs also predict 67% needle leaf trees (highest of the simulated interglacials) and a drop to 19% shrub (from 23% at Plio-K1^{Dynamic}).

3.4.2.2 Lake Baikal

Lake Baikal is situated in the continental interior of north-eastern Eurasia (53°, 108°) and has a long continuous depositional history (Demske et al., 2002). Proxies suggest it was located at the boundary between different vegetation zones during the Pliocene with shifts in distribution of coniferous forests, steppe and mountain vegetation. There is an overall cooling trend between the warm early Pliocene and the onset of Northern Hemisphere Glaciation shown by the reduction of broadleaf trees throughout the record with periods of open vegetation interpreted to have been cool, dry conditions (Demske et al., 2002).

After MIS M2 and leading up to KM5c, the proxy derived vegetation reconstruction suggests a gradual increase in spruce/hemlock forests due to an increase in precipitation. Around the KM5c event (between 3.26 and 3.18 Ma) the record indicates a decrease in forests and the spread of boreal taxa such as birches and dwarf shrubs. This corresponds to a macro fauna assemblage in West Siberia reconstructing drier and/or cooler conditions (Zykin et al., 1995).

Around KM3 there are large fluctuations in spruce abundances and pine forests begin to appear in the record leading to a reduction of spruce/hemlock forest. There is evidence of a severely dry interval five thousand years after KM3 (3.150 Ma) with low palaeo-temperatures. More open vegetation spreads between KM3 and K1, with further expansion of open vegetation and dry steppe continuing to increase after K1. The pollen reconstruction at G17 shows a development of mixed coniferous forest with a specific increase in hemlock indicating a return to warmer conditions (Demske et al., 2002). There were also warm optimum conditions indicated in the record between 3.3 and 3.15 Ma and 3.01 and 2.94 Ma that envelopes all the interglacials studied here. The record in general between 3.3 and 2.9 Ma indicates variability between warm-moist conditions and cold-dry fluctuations and does not support a dry-warm climate regime.

The TRIFFID vegetation results simulate no shrub for Plio-KM5c^{Dynamic} with high percentages of broad and needle leaf trees (57% and 30% respectively). In contrast, the simulated PFTs at Plio-KM3^{Dynamic} and Plio-K1^{Dynamic} predict no broadleaf or needle leaf trees, instead predicting high shrub percentages (~60 - 70%) with the remaining vegetation simulated as grass. The simulated plant functional types show an increase of broadleaf forest (24%) at Plio-G17^{Dynamic} compared to Plio-KM3^{Dynamic} and Plio-K1^{Dynamic} with the remainder of PFTs simulated as shrub (54%) and grass (20%).

The Lake Baikal record reconstructs a varying open steppe type vegetation with mixed coniferous forest throughout the mPWP, attributing the open vegetation with MIS glacial stages. Whereas the modelled PFTs in this study simulate a mixture of predominantly forest in Plio-KM5c^{Dynamic}, no forest and mainly shrub in Plio-KM3^{Dynamic} and Plio-K1^{Dynamic} and a mix of both forest, shrub and grass for Plio-G17^{Dynamic}. The simulated biome from BIOME4 for all four interglacials is temperate grassland at the Lake Baikal location and the surrounding area. At a glance the general trends in vegetation variability from proxy records and the PFTs simulated with TRIFFID are comparable with both indicating switches between open and forest type vegetation. The proxy based vegetation reconstruction in Demske et al. (2002) interpreted the forest vegetation to indicate warm and moist conditions and the open steppe type vegetation cold and dry. Following this, one might expect the warm interglacials modelled to simulated mainly forest vegetation at this location, however it is the two warmest of the interglacials (Plio-KM3^{Dynamic} and Plio-K1^{Dynamic}) that simulate no forest PFTs with all open vegetation types and the cooler of the two interglacials (Plio-KM5c^{Dynamic}

and Plio-G17^{Dynamic}) that simulate a mixture of shrub, grass and forest PFTs. The BIOME4 results all simulate temperate grassland across this location and the surrounding areas with no variability in biomes between the interglacials.

In general, the simulated vegetation appears to be more favourable comparable to the Lake El'gygytgyn record than Lake Baikal, where in the simulated Asian continental interior a large expanse of the grassland biome is predicted by the model but not supported in the geological record. The degree to which the regional patterns of vegetation change shown in our model results truly reflect what happened during the four interglacial events in question is difficult to ascertain. Some palaeobotanical sites in the literature, especially those close to palaeogeographic transitions of major vegetation zones (Salzmann et al., 2013) present a fluctuating climate that swings between an annual climate signal of warm-wet, and cool-dry (Leroy & Dupont, 1994; Heusser & Morley, 1996; Willis et al., 1999; Gao et al., 2012). Whereas our model results in Eurasia for the interglacials in question show a more warm and dry signal, especially, in the northern hemisphere, where there are warmer summers of up to 14°C (relative to the control summer temperatures) as well as cooler winters (up to 5°C cooler than the control).

Palaeoclimate modelling studies by Loptson et al. (2014) and Hunter et al. (2013), both using HadCM3L coupled with TRIFFID, describe a model dry bias (associated with TRIFFID) within their results. Here, the predicted biomes also appear to reflect a dry bias but further investigation shows this loss of trees to grassland in the northern hemisphere is due to an increase of seasonality driven principally by changes in the orbital forcing. The hotter spring and summers combined with colder autumn and winters appears to favour grass/shrub vegetation types in our simulations.

The data-model mismatch found at Lake Baikal could also be due to the proxy record not capturing the simulated interglacial peaks we have modelled here. Orbital sensitivity simulations run for the Eocene (Sloan & Morrill, 1998) also found increased seasonality in the continental temperatures which was not reflected in the proxy records. The study postulates that while this could be due to the simulations incorrectly predicting seasonal cycles, it could also be due to biases in the preservation of complete orbital cycles that prevents the stronger signals being seen in the proxy record (Sloan & Morrill, 1998). While

this could also be the case for this study, the magnitude of the data-model mismatch is so substantial at Lake Baikal that it is more likely that fundamental issues with the simulations in this area and the Eurasian continental interior. The better match of data-model comparison at Lake El'gygytgyn, which is located on the Asian Arctic coastline (under a maritime influence) also suggests that the mismatch at Lake Baikal could be related to issues associated with modelling continental interiors, which has emerged in a Pliocene scenario when different to modern orbital forcing configurations have been employed.

Biases in model representations of Eurasian hydrology in response to orbital forcing have been reported before. For example, Holocene CMIP5 simulations also found drier conditions in Eurasia compared to palaeo observations that indicate this area was wetter than today (Harrison et al., 2015; Bartlein et al., 2017). For the mid-Holocene climate models simulated a significant increase in the summer temperatures in Eurasia, and therefore seasonality, whereas the observations suggest cooler summers (lower seasonality). Temperature biases in the CMIP5 modern simulations have been linked to systematic biases in evapotranspiration with an oversimplification of precipitation leading to cold temperature biases (Mueller & Seneviratne, 2014; Harrison et al., 2015). Harrison et al. (2015) suggests that some climate models do not produce a sufficient increase in regional precipitation for the mid-Holocene in Eurasia and therefore underestimate evapotranspiration causing higher summer temperatures. Interestingly, a modelling study on future climate change over Siberia using HadCM3 anomalies for a number of future scenarios, coupled to the Siberian BioClimatic model, found the climate to be drier with a reduction in forest replaced by increased steppe as a result of decreased precipitation and increasing temperatures (Tchebakova et al., 2009).

Within this study for the Pliocene we see similar trends with the simulated climate to the studies above. Increased seasonality combined with warmer summers and insufficient precipitation and a resulting significant reduction in soil moisture appears to create a scenario where our modelled climate is unable to sustain forest seen consistently in published records of Eurasian vegetation distribution.

3.5 Conclusions

The mid-Pliocene Warm Period (mPWP) is an important interval to investigate the long-term response of vegetation patterns to a CO_2 induced warming. However, the nature of vegetation change in response to orbital variability during this interval is only partially constrained. Understanding orbitally induced vegetation variability is important to understand the Pliocene overall, and for identifying the degree to which climate and vegetation models are able to reproduce climate states in Earth history.

We have investigated the degree to which orbital forcing drives changes in surface climatological and land cover response between four of the largest interglacial events within the mPWP. The degree of surface temperature warming and precipitation response regionally is strongly controlled by orbital forcing. This translates into variations in seasonality and moisture availability that can have profound effects on the predictions of land cover regionally. In our study this is clearly expressed in North America and Eurasia where mid-Pliocene experiments with increased insolation during the northern hemisphere spring/summer and decreased insolation during autumn/winter (compared to a mid-Pliocene scenario with near modern orbital forcing) led to a strong climate response and associated vegetation climate feedbacks, resulting in replacement of forest with open types of vegetation. However, available high temporal resolution palaeobotanical data from Eurasia indicate that whilst variations in forest cover versus more open type vegetation are possible between interglacial events in the mPWP, trees remained a dominant feature of the landscape. This suggests that the climate and vegetation response in this region in our model is overestimated, and this conclusion is similar to studies for the mid-Holocene, using a variety of climate models, that indicate similar regional biases in climate and predicted vegetation response to orbital forcing.

This highlights the importance of evaluating model predictions using a variety of orbital scenarios and underlines the urgent requirement for additional high resolution palynological studies from around the world to better quantify the nature of land cover variability during the mPWP and the ability of climate and vegetation models to reproduce geological evidence.

References

Andreev, A.A., Tarasov, P.E., Wennrich, V. & Melles, M. (2016). Millennial-scale vegetation changes in the north-eastern Russian Arctic during the Pliocene/Pleistocene transition (2.7 - 2.5 Ma) inferred from the pollen record of Lake El'gygytgyn. *Quaternary Science Reviews*. 147. pp. 245–258.

Andreev, A.A., Tarasov, P.E., Wennrich, V., Raschke, E., Herzschuh, U., Nowaczyk, N.R., Brigham-Grette, J. & Melles, M. (2014). Late Pliocene and Early Pleistocene vegetation history of northeastern Russian Arctic inferred from the Lake El'gygytgyn pollen record. *Climate of the Past*. 10 (3). pp. 1017–1039.

Bartlein, P.J., Harrison, S.P. & Izumi, K. (2017). Underlying causes of Eurasian midcontinental aridity in simulations of mid-Holocene climate. *Geophysical Research Letters*. 44 (17). pp. 9020–9028.

Best, M.J., Grimmond, C.S.B. & Villani, M.G. (2006). Evaluation of the Urban Tile in MOSES using Surface Energy Balance Observations. *Boundary-Layer Meteorology*. 118 (3). pp. 503–525.

Braconnot, P., Otto-Bliesner, B., Harrison, S., Joussaume, S., Peterchmitt, J.-Y., Abe-Ouchi, A., Crucifix, M., Driesschaert, E., Fichefet, T., Hewitt, C.D., Kageyama, M., Kitoh, A., Laîné, A., Loutre, M.-F., Marti, O., Merkel, U., Ramstein, G., Valdes, P., Weber, S.L., Yu, Y. & Zhao, Y. (2007). Results of PMIP2 coupled simulations of the Mid-Holocene and Last Glacial Maximum – Part 1: experiments and large-scale features. *Climate of the Past*. 3 (2). pp. 261–277.

Bragg, F.J., Lunt, D.J. & Haywood, A.M. (2012). Mid-Pliocene climate modelled using the UK Hadley Centre Model: PlioMIP Experiments 1 and 2. *Geoscientific Model Development Discussions*. 5 (2). pp. 837–871.

Brigham-Grette, J., Melles, M., Minyuk, P., Andreev, A., Tarasov, P., DeConto, R., Koenig, S., Nowaczyk, N., Wennrich, V., Rosén, P., Haltia, E., Cook, T., Gebhardt, C., Meyer-Jacob, C., Snyder, J. & Herzschuh, U. (2013). Pliocene Warmth, Polar Amplification, and Stepped Pleistocene Cooling Recorded in NE Arctic Russia. *Science*. 340 (6139). pp. 1421–1427.

Cattle, H., Crossley, J. & Drewry, D.J. (1995). Modelling Arctic Climate Change [and Discussion]. *Philosophical Transactions of the Royal Society A: Mathematical, Physical and Engineering Sciences*. 352 (1699). pp. 201–213.

Collatz, G.J., Ball, J.T., Grivet, C. & Berry, J.A. (1991). Physiological and environmental regulation of stomatal conductance, photosynthesis and transpiration: a model that includes a laminar boundary layer. *Agricultural and Forest Meteorology*. 54 (2–4). pp. 107–136.

Collatz, G.J., Ribas-Carbo, M. & Berry, J. (1992). Coupled Photosynthesis-Stomatal Conductance

Model for Leaves of C 4 Plants. *Australian Journal of Plant Physiology*. 19 (5). pp. 519-538.

Cox, P.M., Huntingford, C. & Harding, R.. (1998). A canopy conductance and photosynthesis model for use in a GCM land surface scheme. *Journal of Hydrology*. 212–213. pp. 79–94.

Cox, P.M., Betts, R.A., Bunton, C.B., Essery, R.L.H., Rowntree, P.R. & Smith, J. (1999). The impact of new land surface physics on the GCM simulation of climate and climate sensitivity. *Climate Dynamics*. 15 (3). pp. 183–203.

Cox, P.M. (2001). Description of the TRIFFID dynamic global vegetation model: Hadley Centre Technical Note 24. Hadley Centre, Met Office.

Demske, D., Mohr, B. & Oberhänsli, H. (2002). Late Pliocene vegetation and climate of the Lake Baikal region, southern East Siberia, reconstructed from palynological data. *Palaeogeography, Palaeoclimatology, Palaeoecology*. 184 (1–2). pp. 107–129.

Dowsett, H.J. & Poore, R.Z. (1991). Pliocene sea surface temperatures of the north atlantic ocean at 3.0 Ma. *Quaternary Science Reviews*. 10 (2–3). pp. 189–204.

Dowsett, H.J., Thompson, R., Barron, J., Cronin, T., Fleming, F., Ishman, S., Poore, R., Willard, D. & Holtz, T. (1994). Joint investigations of the Middle Pliocene climate I: PRISM paleoenvironmental reconstructions. *Global and Planetary Change*. 9 (3–4). pp. 169–195.

Dowsett, H.J, Barron, J. & Poore, R. (1996). Middle Pliocene sea surface temperatures: a global reconstruction. *Marine Micropaleontology*. 27 (1–4)..pp. 13–25.

Dowsett, H.J., Robinson, M., Haywood, A.M., Salzmann, U., Hill, D., Sohl, L., Chandler, M., Williams, M., Foley, K. & Stoll, D. (2010). The PRISM3D paleoenvironmental reconstruction. *Stratigraphy*. 7 (2-3). pp. 123-139.

Dowsett, H.J., Robinson, M.M., Stoll, D.K., Foley, K.M., Johnson, A.L.A., Williams, M. & Riesselman, C.R. (2013). The PRISM (Pliocene palaeoclimate) reconstruction: time for a paradigm shift. *Philosophical transactions. Series A, Mathematical, physical, and engineering sciences*. 371 (2001). p.p. 20120524.

Essery, R.L.H., Best, M.J., Betts, R.A., Cox, P.M. & Taylor, C.M. (2003). Explicit Representation of Subgrid Heterogeneity in a GCM Land Surface Scheme. *Journal of Hydrometeorology*. 4 (3). pp. 530–543.

Falloon, P., Betts, R., Wiltshire, A., Dankers, R., Mathison, C., McNeall, D., Bates, P. & Trigg, M. (2011). Validation of River Flows in HadGEM1 and HadCM3 with the TRIP River Flow Model. *Journal of Hydrometeorology*. 12 (6). pp. 1157–1180.

Gao, C., McAndrews, J.H., Wang, X., Menzies, J., Turton, C.L., Wood, B.D., Pei, J. & Kodors, C. (2012). Glaciation of North America in the James Bay Lowland, Canada, 3.5 Ma. *Geology*. 40

(11). pp. 975–978.

Gordon, C., Cooper, C., Senior, C.A., Banks, H., Gregory, J.M., Johns, T.C., Mitchell, J.F.B. & Wood, R.A. (2000). The simulation of SST, sea ice extents and ocean heat transports in a version of the Hadley Centre coupled model without flux adjustments. *Climate Dynamics*. 16 (2–3). pp. 147–168.

Harrison, S.P., Bartlein, P.J., Izumi, K., Li, G., Annan, J., Hargreaves, J., Braconnot, P. & Kageyama, M. (2015). Evaluation of CMIP5 palaeo-simulations to improve climate projections. *Nature Climate Change*. 5 (8). pp. 735–743.

Haxeltine, A. & Prentice, I.C. (1996). BIOME3: An equilibrium terrestrial biosphere model based on ecophysiological constraints, resource availability, and competition among plant functional types. *Global Biogeochemical Cycles*. 10 (4). pp. 693–709.

Haywood, A.M., Dowsett, H.J., Otto-Bliesner, B., Chandler, M.A., Dolan, A.M., Hill, D.J., Lunt, D.J., Robinson, M.M., Rosenbloom, N., Salzmann, U. & Sohl, L.E. (2010). Pliocene Model Intercomparison Project (PlioMIP): experimental design and boundary conditions (Experiment 1). *Geoscientific Model Development*. 3 (1). pp. 227–242.

Haywood, A.M., Dolan, A.M., Pickering, S.J., Dowsett, H.J., McClymont, E.L., Prescott, C.L., Salzmann, U., Hill, D.J., Hunter, S.J., Lunt, D.J., Pope, J.O. & Valdes, P.J. (2013a). On the identification of a Pliocene time slice for data-model comparison. *Philosophical transactions. Series A, Mathematical, physical, and engineering sciences*. 371 (2001). p.p. 20120515.

Haywood, A.M., Hill, D.J., Dolan, A.M., Otto-Bliesner, B.L., Bragg, F., Chan, W.-L., Chandler, M.A., Contoux, C., Dowsett, H.J., Jost, A., Kamae, Y., Lohmann, G., Lunt, D.J., Abe-Ouchi, A., Pickering, S.J., Ramstein, G., Rosenbloom, N.A., Salzmann, U., Sohl, L., Stepanek, C., Ueda, H., Yan, Q. & Zhang, Z. (2013b). Large-scale features of Pliocene climate: results from the Pliocene Model Intercomparison Project. *Climate of the Past*. 9 (1). pp. 191–209.

Heusser, L.E. & Morley, J.J. (1996). Pliocene climate of Japan and environs between 4.8 and 2.8 Ma: A joint pollen and marine faunal study. *Marine Micropaleontology*. 27 (1–4). pp. 85–106.

Hunter, S., Haywood, A.M., Valdes, P., Francis, J. & Pound, M. (2013). Modelling equable climates of the Late Cretaceous: Can new boundary conditions resolve data-model discrepancies? *Palaeogeography, Palaeoclimatology, Palaeoecology*. 392. pp. 41-51

Kaplan, J.O. (2003). Climate change and Arctic ecosystems: 2. Modeling, paleodata-model comparisons, and future projections. *Journal of Geophysical Research*. 108 (D19). p.p. 8171.

Laskar, J., Robutel, P., Joutel, F., Gastineau, M., Correia, A.C.M. & Levrard, B. (2004). A long-term numerical solution for the insolation quantities of the Earth. *Astronomy & Astrophysics*. 428 (1). pp. 261–285.

Leroy, S. & Dupont, L. (1994). Development of vegetation and continental aridity in northwestern Africa during the Late Pliocene: the pollen record of ODP site 658. *Palaeogeography, Palaeoclimatology, Palaeoecology*. 109 (2–4). pp. 295–316.

Lisiecki, L.E. & Raymo, M.E. (2005). A Pliocene-Pleistocene stack of 57 globally distributed benthic $\delta^{18}O$ records. *Paleoceanography*. 20 (1). p.p. PA1003.

Loptson, C.A., Lunt, D.J. & Francis, J.E. (2014). Investigating vegetation–climate feedbacks during the early Eocene. *Climate of the Past*. 10 (2). pp. 419–436.

Lozhkin, A. V. & Anderson, P.M. (2013). Vegetation responses to interglacial warming in the Arctic: Examples from Lake El'gygytgyn, Far East Russian Arctic. *Climate of the Past*. 9 (3). pp. 1211–1219.

Lunt, D.J., Haywood, A.M., Schmidt, G.A., Salzmann, U., Valdes, P.J., Dowsett, H.J. & Loptson, C.A. (2012). On the causes of mid-Pliocene warmth and polar amplification. *Earth and Planetary Science Letters*. 321–322. pp. 128–138.

Melles, M., Brigham-Grette, J., Minyuk, P.S., Nowaczyk, N.R., Wennrich, V., DeConto, R.M., Anderson, P.M., Andreev, A.A., Coletti, A., Cook, T.L., Haltia-Hovi, E., Kukkonen, M., Lozhkin, A. V., Rosén, P., Tarasov, P., Vogel, H. & Wagner, B. (2012). 2.8 Million Years of Arctic Climate Change from Lake El'gygytgyn, NE Russia. *Science*. 337 (6092).

Mueller, B. & Seneviratne, S.I. (2014). Systematic land climate and evapotranspiration biases in CMIP5 simulations. *Geophysical research letters*. 41 (1). pp. 128–134.

Prescott, C.L., Haywood, A.M., Dolan, A.M., Hunter, S.J., Pope, J.O. & Pickering, S.J. (2014). Assessing orbitally-forced interglacial climate variability during the mid-Pliocene Warm Period. *Earth and Planetary Science Letters*. 400. pp. 261–271.

Raymo, M.E., Hearty, P., De Conto, R., O'Leary, M., Dowsett, H.J., Robinson, M.H. & Mitrovica, J.X. (2009). PLIOMAX: Pliocene maximum sea level project. *PAGES News*. 17 (2). pp. 58–59.

Salzmann, U., Haywood, A.M., Lunt, D.J., Valdes, P.J. & Hill, D.J. (2008). A new global biome reconstruction and data-model comparison for the Middle Pliocene. *Global Ecology and Biogeography*. 17 (3). pp. 432–447.

Salzmann, U., Dolan, A.M., Haywood, A.M., Chan, W.-L., Voss, J., Hill, D.J., Abe-Ouchi, A., Otto-Bliesner, B., Bragg, F.J., Chandler, M.A., Contoux, C., Dowsett, H.J., Jost, A., Kamae, Y., Lohmann, G., Lunt, D.J., Pickering, S.J., Pound, M.J., Ramstein, G., Rosenbloom, N.A., Sohl, L., Stepanek, C., Ueda, H. & Zhang, Z. (2013). Challenges in quantifying Pliocene terrestrial warming revealed by data–model discord. *Nature Climate Change*. 3 (11). pp. 969–974.

Schwinning, S., Starr, B.I. & Ehleringer, J.R. (2005). Summer and winter drought in a cold desert ecosystem (Colorado Plateau) part I: effects on soil water and plant water uptake. *Journal of Arid*

Environments. 60 (4). pp. 547–566.

Sloan, L.C. & Morrill, C. (1998). Orbital forcing and Eocene continental temperatures. *Palaeogeography, Palaeoclimatology, Palaeoecology*. 144 (1–2). pp. 21–35.

Swann, A.L., Fung, I.Y., Levis, S., Bonan, G.B. & Doney, S.C. (2010). Changes in Arctic vegetation amplify high-latitude warming through the greenhouse effect. *Proceedings of the National Academy of Sciences of the United States of America*. 107 (4). pp. 1295–300.

Tarasov, P.E., Andreev, A.A., Anderson, P.M., Lozhkin, A. V., Leipe, C., Haltia, E., Nowaczyk, N.R., Wennrich, V., Brigham-Grette, J. & Melles, M. (2013). A pollen-based biome reconstruction over the last 3.562 million years in the Far East Russian Arctic – new insights into climate–vegetation relationships at the regional scale. *Climate of the Past*. 9 (6). pp. 2759–2775.

Tchebakova, N.M., Parfenova, E. & Soja, A.J. (2009). The effects of climate, permafrost and fire on vegetation change in Siberia in a changing climate. *Environmental Research Letters*. 4 (4). p.p. 45013.

Thompson, R.S. & Fleming, R.F. (1996). Middle Pliocene vegetation: reconstructions, paleoclimatic inferences, and boundary conditions for climate modeling. *Marine Micropaleontology*. 27 (1–4). pp. 27–49.

Valdes, P.J., Armstrong, E., Badger, M.P.S., Bradshaw, C.D., Bragg, F., Davies-Barnard, T., Day, J.J., Farnsworth, A., Hopcroft, P.O., Kennedy, A.T., Lord, N.S., Lunt, D.J., Marzocchi, A., Parry, L.M., Roberts, W.H.G., Stone, E.J., Tourte, G.J.L. & Williams, J.H.T. (2017). The BRIDGE HadCM3 family of climate models: HadCM3@Bristol v1.0. *Geoscientific Model Development Discussions*. pp. 1–42.

Ward, D., Wiegand, K. & Getzin, S. (2013). Walter's two-layer hypothesis revisited: back to the roots! *Oecologia*. 172 (3). pp. 617–30.

Willis, K.J., Kleczkowski, A. & Crowhurst, S.J. (1999). 124,000-year periodicity in terrestrial vegetation change during the late Pliocene epoch. *Nature*. 397 (6721). pp. 685–688.

Wu, F., Fang, X., Herrmann, M., Mosbrugger, V. & Miao, Y. (2011). Extended drought in the interior of Central Asia since the Pliocene reconstructed from sporopollen records. *Global and Planetary Change*. 76 (1–2). pp. 16–21.

Zykin, V.S., Zazhigin, V.S. & Zykina, V.S. (1995). Changes in environment and climate during early Pliocene in the southern West-Siberian Plain. *Russ. Geol. Geophys*. 36. pp. 37–47.

CHAPTER 4

ORBITAL FORCING AND THE VARIABILITY OF THE INDIAN MONSOON DURING INTERGLACIALS OF THE PLIOCENE

Preface

Chapter 4 has been prepared for submission to *Global and Planetary Change*. The co-authors are my supervisors: Alan Haywood, Aisling Dolan, Stephen Hunter and colleague Julia Tindall. The work presented in this chapter including experiment design, data analysis and the written manuscript was completed by the candidate. A.H., and A.D. suggested improvements on the written manuscript and data presentation.

Abstract

The Asian monsoon represents a major component of the global climate system and can be divided into two subsystems: The Indian monsoon and the East Asian monsoon. Valuable insights have been gained through looking at monsoon behaviour during past warm intervals in Earth's history. One such interval is the Pliocene epoch and the Piacenzian Stage (3.6 – 2.58 Ma) specifically. This time is characterised as a period of sustained warmth, with annual mean temperatures 2-3°C higher than pre-industrial levels. Many studies have been published regarding the East Asian monsoon during the Pliocene from both geological data and climate modelling perspectives. However, there has been less investigation into the behaviour of the Indian monsoon during the Pliocene. Using a coupled atmosphere-ocean global climate model (HadCM3) how the Indian summer monsoon may have varied in response to orbital forcing during discrete interglacial events within the Piacenzian Stage is investigated.

Of the simulated interglacial peaks, Marine Isotope Stages (MIS KM5c, KM3, K1 and G17), MIS KM5c is differentiated by a near-modern orbital forcing, and is compared to a pre-industrial simulation to ascertain the character of a Piacenzian Indian summer monsoon without a strong orbital forcing. The monsoon at MIS KM5c, is simulated to be stronger than pre-industrial, with higher surface air temperatures and precipitation over terrestrial areas due to higher levels of CO_2. While MIS G17, K1, and KM3 are negative isotope excursions of similar magnitude, the monsoon is simulated to be significantly stronger in K1 and KM3. This is due to stronger precession forcing causing an increase in summer surface air temperature and precipitation. The simulated difference in climatology over the Indian monsoon area is significantly larger between K1 and KM3, and KM5c, where the only difference is orbital forcing than they are between the pre-industrial simulation and KM5c, where Pliocene boundary conditions have been implemented. This displays the significant effect of orbital forcing on the strength of the Indian summer monsoon when combined with Pliocene boundary conditions which increased monsoon strength. As this study compared only four interglacial time slices in the Piacenzian, in order to understand a more complete picture of Indian monsoon variability throughout this time, further studies simulating the Indian monsoon should be conducted. The demonstrated response of the Indian monsoon to orbital forcing has important implications if looking to the Pliocene to

draw parallels about future monsoon behaviour; any assumptions about future monsoons based on the Pliocene would need to concentrate on interglacials with a near modern orbit.

4.1 Introduction:

4.1.1 Pliocene Asian monsoon

The Intergovernmental Panel on Climate Change (IPCC) defines monsoons as a seasonal phenomenon responsible for producing the majority of wet season rainfall within the tropics (Christensen et al., 2013). The monsoon circulation is driven by the difference in temperature between land and sea, which varies seasonally with the distribution of solar heating (Christensen et al., 2013). The duration and amount of rainfall depends on the moisture content of the air and on the configuration and strength of atmospheric circulation (Christensen et al., 2013). The Asian monsoon represents a major component of the global climate system and influences societal and economic activity for almost two thirds of the world's population (Webster et al., 1998; Ao et al., 2016). The strength and variability of the Asian monsoon has been, and will continue to be, crucial to the prosperity of the region (Clift & Plumb, 2008). The Asian monsoon includes at least two subsystems: The Indian monsoon (or South Asian monsoon) and the East Asian monsoon, roughly divided at ~105°E (Wang et al., 2005). The two systems both respond to the strength of the continental high and low-pressure cells and are therefore linked, however they also have significant differences due to different land-sea distributions (Wang et al., 2005).

By looking at monsoon behaviour during past warm intervals valuable insights on potential monsoon behaviour in the future may be extracted. One of these past warm intervals is the Pliocene epoch (5.33-2.58 Ma). The Pliocene is particularly useful for understanding future climate due to similar continental configurations, land elevations and ocean bathymetries to the present day (Haywood et al., 2013a). The Late Pliocene specifically, (3.6-2.58 Ma; Piacenzian Stage) is characterised as a period of sustained warmth in Earth's history with annual mean temperatures thought to be 2-3°C higher than pre-industrial (Haywood & Valdes, 2004; Haywood et al., 2013b). There has been considerable effort to understand the climate of the Pliocene through a combination of climate modelling and data reconstruction, particularly in the mid Pliocene Warm Period (mPWP; 3.264 – 3.025 Ma) also defined as the Pliocene Research Interpretation and Synoptic Mapping (PRISM) time slab. As well as a

focus for data-model comparison, the mPWP has been proposed as an important interval to assess the sensitivity of climate to current or near future concentrations of CO_2 (Haywood et al., 2013a).

There are many studies of the South East Asian monsoon in the Pliocene from both a data and modelling perspective. Published work on the Chinese Loess Plateau indicate an enhanced East Asian Summer monsoon (EASM) during the Piacenzian Stage (Ding et al., 2001; Ao et al., 2016) and a relatively weak East Asian Winter monsoon (EAWM; Chen et al., 2006; Wang et al., 2007). Yan et al. (2012) found a stronger than present EASM using the Community Atmosphere Model version 3.1 (CAM3.1) but could not reproduce the weakened EAWM seen in the proxy data. A multi-model comparison of the East Asian monsoon from the Pliocene Model Intercomparison Project (PlioMIP) project (Zhang et al., 2013) found that East Asian summer winds largely strengthen in monsoonal China which agrees with the reconstructions. A discrepancy between the different models was noted when simulating the East Asian winter winds. Six models simulated weakened mid-Pliocene East Asian winter winds and nine models more intense (Zhang et al., 2013). The simulated weakened East Asian winter winds were caused by larger decreases in the sea level pressure gradient in the boreal winter due to stronger winter warming over China than the multi-model mean. These different responses to the same radiative forcing in the PlioMIP ensemble are speculated to be related to independent changes in boundary conditions (e.g. land-cover/vegetation) and/or physical processes and parameterisation in the models (Zhang et al., 2013).

4.1.2 Indian monsoon

There has been far less investigation into the behaviour of the Indian monsoon in the Pliocene and this study will focus on that sub-system of the Asian monsoon (Fig.4.1).

The present day Indian monsoon is driven by large seasonal variations in wind direction over the Indian subcontinent and surrounding oceans (Gadgil et al., 2003). Due to the seasonal cycle of solar heating during boreal spring, the south Asian landmass is warmed faster than the ocean, owing to differences in heat capacity (Turner & Annamalai, 2012). This results in the formation of a surface heat low over northern India and winds are therefore driven from the southwest to northeast towards the continent. In contrast, in winter (November to

February) the pressure cells reverse and winds flow from northeast to southwest (Gupta & Anderson, 2005). The seasonal variation of rainfall associated with monsoons is of greater importance to modern society than the variation in winds (Gadgil et al., 2003). This pattern of seasonally reversing winds transport moisture from over the warm Indian Ocean and ultimately contributes 80% of annual rainfall to south Asia between June and September (Turner & Annamalai, 2012). In contrast, during winter the dry continental air blows from the northeast resulting in very low rainfall.

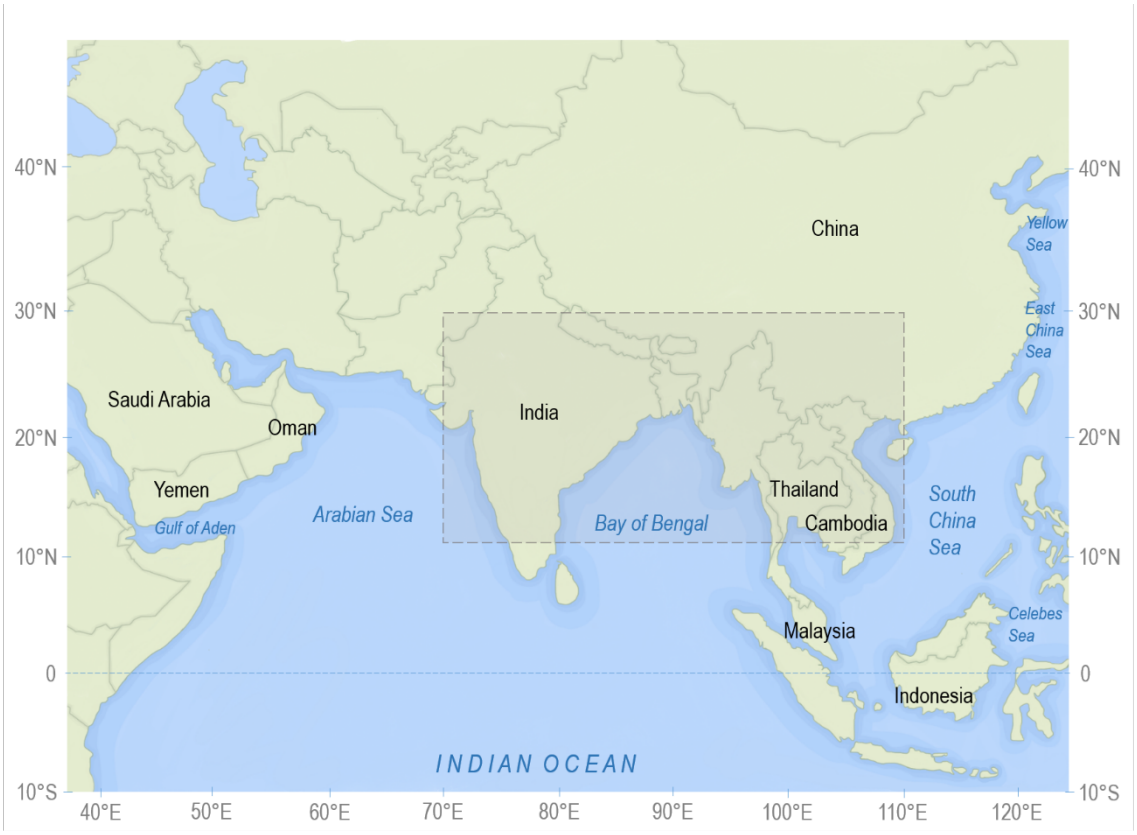

Figure 4.1 Map of the Indian monsoon area. The shaded area indicating the geographical area used to calculate the monsoon indices (described in section 4.2.3).

4.1.2.1 Pliocene Indian monsoon

Due to limited availability of high temporal resolution marine sediments and few terrestrial records related to the Pliocene history of the Indian monsoon variability, the nature of Indian monsoon variability in the Pliocene remains largely unknown. A terrestrial sedimentary sequence from the Yanmou Basin in Southwest China, where the climate is thought to be controlled by the Indian monsoon in summer bringing rainfall from the tropical Indian Ocean to the Basin, was presented in Chang et al. (2010). A general trend of increased clay

and clay plus fine silt fractions accompanied by an increase in sedimentation rate was found, suggesting a gradual intensification of the Indian summer monsoon at the interval 3.57 to 2.78 Ma. A terrestrial study using the leaf physiognomic spectrum examined the late Pliocene Longmen flora on the eastern side of Mt Gaoligong and Mt Nu in western Yunnan (Western China) (Su et al., 2013). Since the western Yunnan experiences both the East Asian monsoon and the Indian monsoon (Wang, 2006) this study could not robustly distinguish the East Asian from the Indian monsoon. The results indicated that the Asian monsoon during the late Pliocene was not as strong as present day in western Yunnan. There was however, an amplification from the late Miocene to the late Pliocene (Su et al., 2013).

Sediments deposited in the Himalayas foreland of early Miocene - Pliocene age are known as the Siwalik group. Carbon and oxygen isotope ratios of soil carbonate nodules, and carbon isotope ratio of associated organic matter, were measured from three Indian Siwalik successions. Variations in soil carbonate $\delta^{18}O$ suggest a clear onset of the monsoon system at 6 Ma, with a peak of intensity at 5.5 Ma, followed by a gradual decrease in monsoon strength until modern-like conditions were attained with minor fluctuations (Sanyal et al., 2004).

Mohan and Gupta (2011) analysed a 5.6-million-year proxy record of surface dwelling planktic foraminifera from the Deep Sea Drilling Project (DSDP) Site 219. They suggest that the monsoon regime over Site 219 in the southeast Arabian Sea switched between summer (southwest) and winter (northeast) monsoons on glacial-interglacial timescales with more influence of the summer monsoon during warm periods and the winter monsoon during cold periods. A major shift in the physical character of the surface ocean in the southeast Arabian Sea was observed at ~3.4 Ma, indicating a change in monsoon wind intensities and a switch to surface productivity being driven by winter monsoon winds linked to the expansion of the Northern Hemisphere glaciation (Mohan & Gupta, 2011). Gupta and Thomas (2003) found an important change in monsoon behaviour between 3.2 and 2.5 Ma in their analysis of benthic foraminifera from Site 758 in the northern Indian Ocean. They found indications of high seasonality, demonstrated by a faunal change between 3.2 and 2.5 Ma consisting of a change from overall high-productivity, nonopportunistic-species-dominated biofacies to biofacies dominated by opportunist species (Gupta & Thomas, 2003).

In a multi-proxy organic geochemical record from DSDP Site 231 in the Gulf of Aden spanning 5.3 – 2 Ma, warm subsurface ocean temperatures were found in the earliest Pliocene with ocean temperatures cooling after 5 Ma (Liddy et al., 2016). A transition to arid conditions on land was found at 4.3 Ma appearing to be due to an atmospheric response to cooling ocean temperatures. The authors suggest this may reflect changes in tropical ocean circulation or the intensification of Indian monsoon winds (Liddy et al., 2016). Another multiproxy study of a sediment core from Ocean Drilling Program (ODP) Site 722 in the Arabian Sea found an alkenone sea surface temperature (SST) record with similar trends to the global benthic foraminifera $\delta^{18}O$ record over the past 11 Ma showing low amplitude variations from 11 to 5 Ma, a slight decrease in temperature from 5 to 4 Ma, followed by high amplitude variability from 4 to 0.7 Ma (Huang et al., 2007).

The nature of the Indian monsoon and its variability during the Pliocene remains unclear but could be interpreted a number of ways. The proxy reconstructions indicate high variability in the Indian monsoon throughout the Pliocene with some proxies suggesting an intensification from the Miocene while others indicate a decrease in strength.

In the first modelling study on the Indian monsoon in the Pliocene the atmosphere only Community Atmosphere Model version 4 (CAM4) was used to investigate the effects of different PRISM3 boundary conditions on the simulation of the summer Indian monsoon (Zhang & Zhang, 2017). The impact of altered mid-Piacenzian topography, land cover and combined CO_2 and SSTs were compared to each other and to a pre-industrial simulation. The study found the combined CO_2 concentration (405 ppm) and PRISM3 SSTs to be the most important factor responsible for simulating the largest difference between the mid-Piacenzian and pre-industrial summer monsoons (Zhang & Zhang, 2017). In comparison, the changes in vegetation and topography had a limited effect on the intensification of the Indian monsoon (Zhang & Zhang, 2017). The simulations analysed in this study all had a modern orbit and in the concluding remarks the authors suggest that further investigation into the effect of orbital forcing on the predicted monsoon is necessary.

4.1.2.2 The effect of orbital forcing on the Indian monsoon:

There is a wide range of evidence from different environmental indicators over land, ice and ocean that the Asian monsoon varies depending on insolation (Wang et al., 2005; Braconnot

et al., 2008) and that orbital forcing has affected the long term evolution of the Asian monsoon (Liu & Shi, 2009). Variations in the Earth's orbit cause shifts in the distribution of incoming solar radiation to Earth (Hays et al., 1976; Berger, 1978). Precession, obliquity and eccentricity are three parameters of the earth's orbit controlling this distribution of solar radiation at the top of the atmosphere (Liu & Shi, 2009). Precession controls the amount of insolation that reaches Earth specifically as a function of seasons (Overpeck et al., 1996). It is the key parameter that determines at which time in the year maximum or minimum insolation occurs, as well as length of the seasons (Berger, 1988). Summer insolation is largest for periods where the Earth is near the perihelion of its orbit in summer. The resulting continental heating over the Northern Hemisphere causes an intensification of monsoon flow. There is a clear link between orbital forcing, specifically the precession cycle, and the strength of monsoons (Clemens & Prell, 1990; Braconnot & Marti, 2003). Changes in climate boundary conditions, such as ice volume, snow cover in the Himalayas, sea surface temperatures (SSTs), albedo, and atmospheric gas concentrations, modulate the response of the monsoon to solar insolation (Prell & Kutzbach, 1992; deMenocal & Rind, 1993; Overpeck et al., 1996). It is therefore an oversimplification to assume that all summer monsoons during interglacials are strong in the same way that not all summer monsoons during glacial times are weak (Prell & Kutzbach, 1992).

In general, efforts in modelling and reconstructing the Piacenzian stage (including the PlioMIP project) have predominantly focused on reconstructing an average Pliocene climate. This includes Pliocene modelling studies looking at monsoon systems; such as Zhang et al., (2013). Recently however, efforts have started to try to understand how the climate varies, even within this 'stable' warm period. In Prescott et al. (2014), large seasonal temperature differences were seen between simulations of two interglacials with different orbital forcings. Building on this, how the monsoon varies within the Piacenzian Stage is investigated by simulating the Indian monsoon with a changing orbit relating to four interglacial time slices in this time and assessing how they compare. An aspect of this study that differs from the majority of current Pliocene literature is that instead of analysing idealised orbital forcing experiments or hypothetical scenarios, actual orbital forcing parameters corresponding to the four largest interglacial peaks seen in the LR04 benthic oxygen isotope stack (Lisiecki & Raymo, 2005) within the Piacenzian stage have been used. While it might be expected for interglacial periods to have stronger monsoons, as has been shown in the Quaternary (Prell & Campo, 1986), the orbital forcing study of Prescott et al. (2014) found that interglacials within the Piacenzian stage can vary in magnitude and nature. More specifically, a recent

vegetation modelling study looking at the same four largest interglacial peaks (Prescott et al., 2018) found particularly large seasonal changes in surface air temperatures (SAT) and vegetation over the Asian continent.

To better understand the nature of the Indian monsoon during the mPWP, four Pliocene interglacials are simulated using the Met Office Hadley Centre Global Coupled model, HadCM3; Marine Isotope Stages (MIS) KM5c (3.205 Ma), KM3 (3.155 Ma), K1 (3.060 Ma) and G17 (2.950 Ma) (Fig. 4.2). These are the four most negative benthic oxygen isotope excursions seen in the LR04 benthic oxygen isotope stack (Lisiecki & Raymo, 2005) during the middle Piacenzian Stage. The specific orbit used in the simulations represents the peak of each interglacial event. Haywood et al. (2013a) show that the peak of MIS KM5c is characterised by a near modern orbital forcing within a period of low eccentricity and low precession (Laskar et al., 2004; Prescott et al., 2014). In this study, therefore, when examining changes in the climatology in the simulations of the four interglacials, KM5c is considered as the control Pliocene experiment. The Indian monsoon of KM5c is compared to the pre-industrial and then KM5c is compared to the other three interglacials (G17, K1, and KM3) that display different orbital forcing parameters.

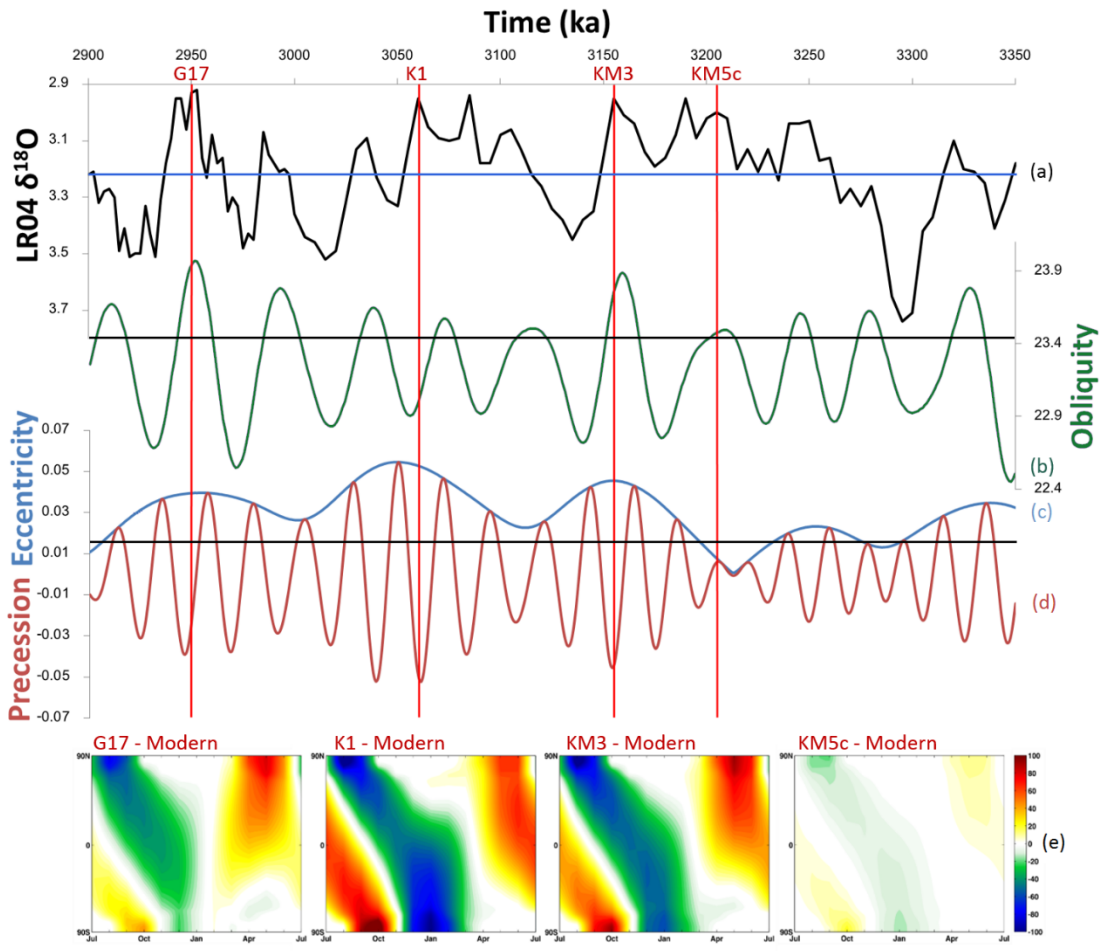

Figure 4.2 Marine Isotope stages (MIS) G17, K1, KM3 and KM5c plotted on (a) the benthic isotope record of Lisiecki and Raymo (2005). (b) obliquity (c) eccentricity (d) precession as derived from the astronomical solution of Laskar et al. (2004). Black horizontal lines show modern orbit with blue horizontal line showing the Holocene oxygen isotope average. (e) Incoming short wave radiation flux derived from HadCM3 (Wm^{-2}) for MIS G17 minus modern; MIS K1 minus modern, MIS KM3 minus modern; MIS KM5c minus modern.

4.1.3 The specific research questions addressed are:

1) How does HadCM3 simulate the Indian monsoon in the Pliocene for MIS KM5c (an interglacial with a near modern orbit) compared to pre-industrial?
2) How does the simulation of the Indian monsoon change when simulating three further Pliocene interglacials with stronger orbital forcing?
3) What does the modelled variability in the Indian monsoon behaviour imply about interpreting discrete and often time specific proxy records of Indian monsoon behaviour?

4.2 Methods

The simulations described in this study were all carried out using HadCM3. HadCM3 is a dynamically and thermodynamically coupled atmosphere, ocean and sea ice model. The resolution of the atmosphere is 2.5° in latitude by 3.75° in longitude and contains 19 layers with a time step of 30 minutes. The ocean model has a resolution of 1.25 by 1.25 with 20 layers. A full description of the model can be found in Gordon et al. (2000), Cox et al. (1999) and Valdes et al. (2017). HadCM3 has been widely used for palaeoclimate modelling, with simulations of the Last Glacial Maximum and Mid-Holocene climates as well as the mPWP and deeper time. The model represents the seasonal cycle of the Indian monsoon well for the modern compared to other similarly complex models. (Turner et al., 2007). The experiments were run for 500 years with the final 100 years used to calculate the required climatological averages.

In this version of HadCM3, the Met Office Surface Exchange Scheme version 2.1 (MOSES2.1) was used coupled to a dynamic vegetation model (Top-down Representation of Interactive Foliage and Flora Including Dynamics; TRIFFID). TRIFFID computes the structure and distribution of six plant functional types and can be run in both equilibrium and dynamic mode. The equilibrium mode is coupled asynchronously to the atmosphere model, with accumulated carbon fluxes passing through MOSES2.1 (Cox 2001). The experiments were run using equilibrium mode for the first 50 years and then run with dynamic mode for the remainder of

the simulation. Previous modelling studies have demonstrated that the inclusion of dynamic vegetation could contribute to the enhancement of the orbitally-induced monsoon change for both the Holocene and modern (Li et al., 2009). Similarly, Braconnot et al. (1999) determined the importance of including vegetation feedbacks in simulations of the African monsoon, yielding model results in better agreement with observations.

4.2.1 Boundary conditions

In this paper, results are presented from 5 climate model simulations (Table 4.1.). Four experiments were run with HadCM3 based on the experimental design from the PlioMIP project (Haywood et al., 2010; Bragg et al., 2012), using PRISM3D boundary conditions (Dowsett et al., 2010) but with the addition of dynamic vegetation and the MOSES2.1 land surface scheme. An experiment with pre-industrial boundary conditions was also run for comparison purposes. As in the PlioMIP project the Pliocene experiments CO_2 concentration is set to 405 ppmv with other trace gases and aerosols consistent at pre-industrial levels. The PRISM3D ice sheet reconstruction includes a much reduced Greenland ice sheet with East Antarctica showing little change and significant retreat in the Wilkes and Aurora sub-glacial basins compared to modern (Haywood et al., 2010). The PRISM3D topographic reconstruction was used to provide palaeogeographic boundary conditions (Sohl et al., 2009). This is quite similar to modern apart from the coastline adjusted for the 25 m higher than modern sea level, the Hudson Bay filled to low elevation and an absent West Antarctic ice. Most relevant to this study, the elevations for the Tibetan Plateau were made roughly consistent with modern day due to uncertainty over the timing of plateau uplift (Sohl et al., 2009).

Experiment	Orbit (kyr)	Eccentricity	Precession	Obliquity	JJAS NH Insolation (Wm^{-2})	EIMR Index (mm/day)	MHI (m/s)
G17	2950	0.04	-0.01776	23.96	422.00	9.20	2.34
K1	3060	0.05	-0.05086	23.01	459.50	11.01	4.15
KM3	3155	0.05	-0.04350	23.76	443.40	10.44	3.69
KM5c	3205	0.01	0.00605	23.47	419.50	8.42	1.78
Pre-ind	Modern	Modern	Modern	Modern	419.10	7.28	1.44

Table 4.1 Summary of experiments including orbital parameters implemented in HadCM3 (Laskar et al., 2004), also showing average summer (June, July, August, September; JJAS) Northern Hemisphere insolation, extended Indian monsoon rainfall (EIMR) index and Monsoon Hadley Index (MHI).

4.2.2 Orbit

While the PlioMIP project specified a modern orbital configuration, here, the simulations for Marine Isotope Stages (MIS) G17, K1, KM3 and KM5c have been performed using orbital parameters derived from the Laskar et al. (2004) astronomical solution. In order to take into account the changes in the length of the seasons determined by variations in the date of perihelion along a precession cycle, a calendar correction from the modern day calendar is applied as discussed in Marzocchi et al. (2015) using the method documented in Pollard & Reusch (2002). This conversion method estimates angular calendar monthly means from the model output means which are on a modern calendar, therefore reducing incorrect calendar effects (Pollard & Reusch, 2002). There is also a modification from the Pollard and Reush (2002) method as detailed in Marzocchi et al. (2015) to take the 360-day model year simulated in HadCM3 into account.

4.2.3 Monsoon indices

In order to compare the five experiments beyond climatological patterns, monsoon indices have been calculated (Table 4.1). The Extended Indian Monsoon Rainfall (EIMR) index, rather than just looking at the rainfall over the Indian subcontinent, includes precipitation over the neighbouring land and seas that are affected by the Indian monsoon (Goswami et al., 1999). The EIMR index is the average precipitation per day over the area 70°E – 110°E, 10°N – 30°N

(shown by the shaded area in Fig. 4.1). As well as the precipitation based index, Goswami et al. (1999) proposed that the Hadley circulation represents the strength of the Indian summer monsoon circulation. The shear of meridional wind between the lower and upper troposphere (between 850 and 200 hPa) was found to be a good measure of the Hadley circulation averaged over the same region as the EIMR index (70°E – 110°E, 10°N – 30°N), therefore the Monsoon Hadley Index (MHI) is also used here:

$$MHI = V_{850} - V_{200}$$

Where V_{850} and V_{200} are the meridional wind anomalies at 850 hPa and 200 hPa averaged over the summer months (June – September) and over the monsoon region (70°E – 110°E, 10°N – 30°N) (Goswami et al., 1999).

4.3 Results

4.3.1 Comparing the KM5c and pre-industrial simulation.

The simulated climate over the Indian monsoon region during summer (JJAS) for KM5c and pre-industrial overall share similar patterns in predicted climate variables but with different intensities (Fig. 4.3). The simulated surface air temperature (SAT) for KM5c is higher for both land and ocean than pre-industrial (Fig. 4.3a). Simulated temperatures reached 43.7°C in KM5c and 43.0°C in pre-industrial over northwest India and 49.1°C in KM5c and 45.5°C in pre-industrial over the Middle East (Fig. 4.3a). When looking at the SAT difference between KM5c and pre-industrial there are individual grid boxes showing SAT differences of up to 8°C higher in KM5c than the pre-industrial (Fig. 4.3a). The highest SATs are predominantly seen north of 30°N in KM5c, when compared to pre-industrial, whereas overall there are similar temperatures over India (31.0°C in KM5c compared to 29.6°C in pre-industrial) with some areas to the northwest of India simulating cooler temperatures in KM5c than pre-industrial (up to ~4°C) (Fig. 4.3a).

For both KM5c and pre-industrial the highest precipitation amounts occur in the South China Sea (reaching a maximum of 26.4 mm/day in KM5c and 22.9 mm/day in pre-industrial) and

Bay of Bengal (reaching 18.8 mm/day in KM5c and 15.6 mm/day in pre-industrial) (Fig. 4.3b). There is also a band of high rainfall between 2 – 10°N across the Indian Ocean (Fig. 4.3b). A similar pattern of precipitation over terrestrial areas is predicted in both experiments with high rainfall over most of South and Southeast Asia, on average 10.3 mm/day for pre-industrial and 10.8 mm/day for KM5c (Fig. 4.3b). For KM5c however, the model does simulate more precipitation (of up to ~5 mm/day) across India, into Southern China and the northern Bay of Bengal with further increases in the Indian Ocean. The simulated precipitation in KM5c is on average 2.0 mm/day less than pre-industrial across Thailand, Cambodia and into the South China Sea (Fig. 4.3b). The precipitation differences between the two experiments is driven by differences in convective rainfall (Appx Fig. C.3d).

Over the high topographic area of western China (between 30 – 35°N) there is the lowest mean sea level pressure (MSLP) in summer for the KM5c (985 hPa) and pre-industrial (990 hPa) with the surrounding areas simulating higher pressure (on average 1011 hPa over Indian Ocean in pre-industrial with KM5c simulating 1008 hPa for the same area) (Fig. 4.3c).

KM5c has lower pressure than pre-industrial throughout the whole monsoon area with the largest difference between 32°N and 45°N over continental Asia where the pressure is on average 6.4 hPa lower than the pre-industrial simulation. Whereas between 5°S and 5°N over the Indian Ocean the simulated MSLP for KM5c is only 3.0 hPa lower than the pre-industrial simulation (Fig. 4.3c).

Both KM5c and the pre-industrial simulate the same pattern of surface winds blowing inland from the equatorial Indian Ocean, across the Horn of Africa and into continental Asia blowing eastwards across the Arabian Sea into India and across the Bay of Bengal (Fig. 4.3c). In KM5c the winds are weaker than those simulated in the pre-industrial across India and Bay of Bengal but stronger across the Horn of Africa and the Arabian Sea (Fig. 4.3c) following a pattern of decreased pressure in this area in KM5c than pre-industrial.

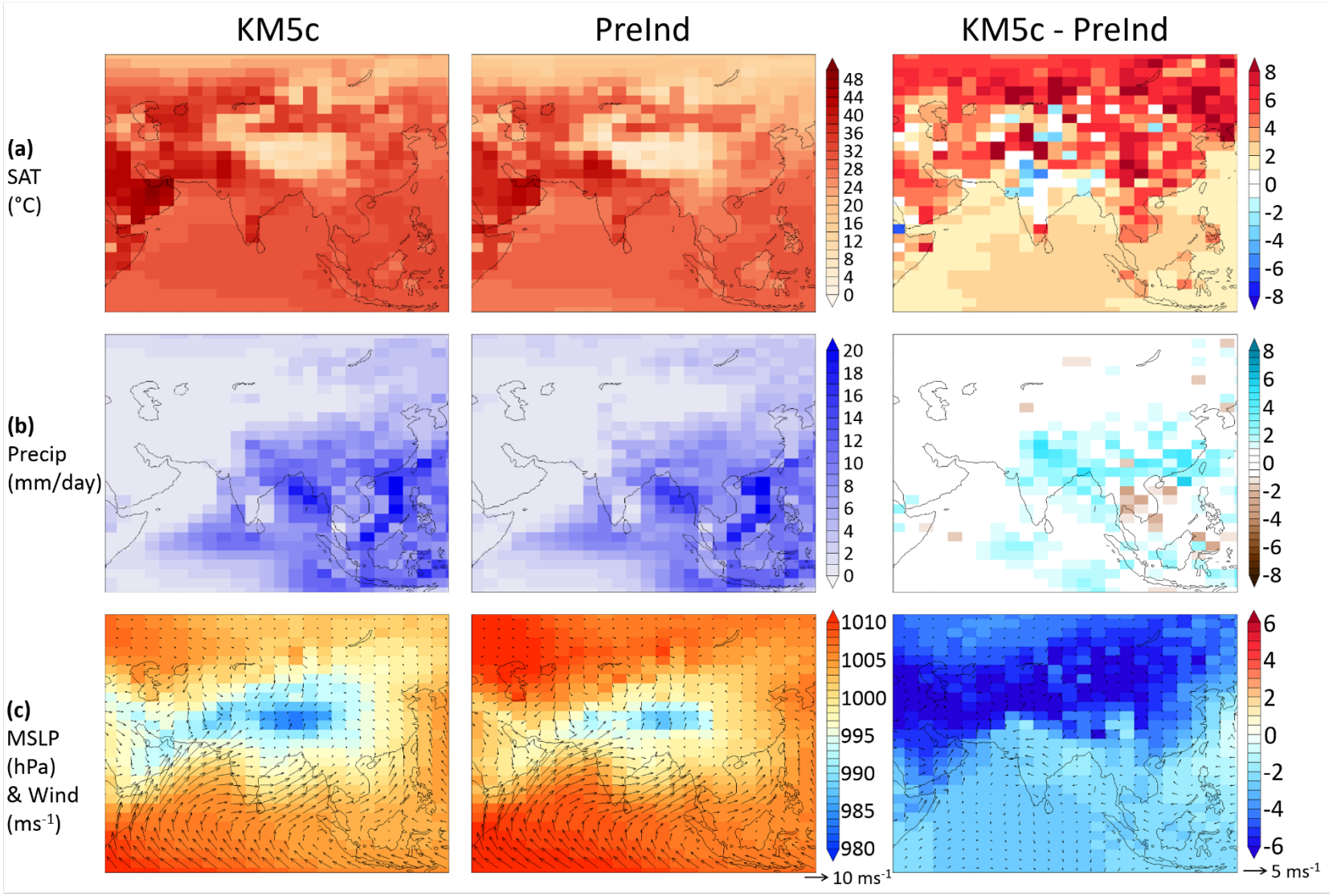
KM5c
PreInd
KM5c - PreInd
(a)
SAT
(°C)
48
44
40
36
32
28
24
20
16
12
8
4
0
8
6
4
2
0
-2
-4
-6
-8
(b)
Precip
(mm/day)
20
18
16
14
12
10
8
6
4
2
0
8
6
4
2
0
-2
-4
-6
-8
(c)
MSLP
(hPa)
& Wind
(ms-1)
1010
1005
1000
995
990
985
980
10 ms-1
6
4
2
0
-2
-4
-6
5 ms-1

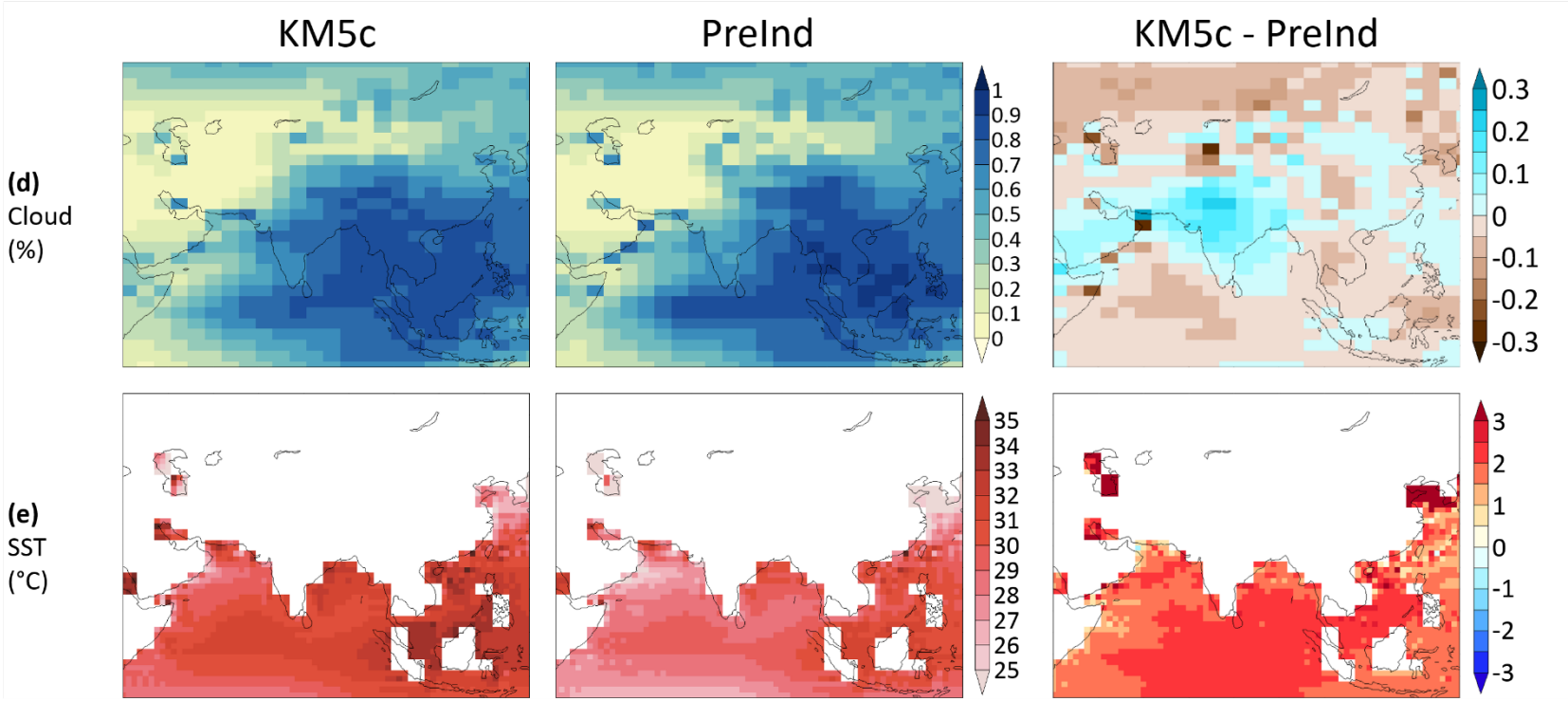

Figure 4.3 Left column: Average absolute JJAS (June – September) results for the MIS KM5c simulation. Middle column: Average absolute JJAS results for pre-industrial simulation. Right column: Average anomaly JJAS results for MIS KM5c minus pre-industrial, showing (a) surface air temperature (SAT) (°C), (b) precipitation (mm/day), (c) mean sea level pressure (MSLP) (hPa) and arrows showing surface winds (ms^{-1}), (d) percentage cloud cover and (e) sea surface temperatures (SSTs) (°C).

The sea surface temperatures (SSTs) are on average 2.1°C higher in KM5c than pre-industrial with the temperature increase mainly focussed in the Indian Ocean and Bay of Bengal (Fig. 4.3e). Both KM5c and pre-industrial are most saline in the Arabian Sea and Western Indian Ocean (both approximately 37 PSU) and least saline in the Yellow Sea and the Southeast Asian Seas (KM5c on average 26.3 PSU and pre-industrial 27.6 PSU) (Appx. Fig. C.3b). KM5c simulates very similar salinity to pre-industrial throughout the monsoon area, apart from in the Yellow Sea which is up to 5 PSUs less saline (Appx. Fig. C.4b). The simulated runoff for both KM5c and pre-industrial predicts high runoff in areas with the highest simulated precipitation, Southern China, Northeast India and Southeast Asia (Appx. Fig. C.3c). KM5c shows on average 4.7 mm/day over these areas (on average 1.8 mm/day more than pre-industrial) and reaches a maximum of 11mm/day (Appx. Fig. C.2c and C.3c). There is a decrease in mixed layer depth in KM5c compared to pre-industrial across the Indian Ocean of up to 8m and decrease across the Bay of Bengal of up to 7.5 m and south-east Asia of 11 m less (Appx. Fig. C.4f). KM5c simulates an increase of up to 21.11 m compared to pre-industrial over the Gulf of Aden in the western Arabian Sea in mixed layer depth (Appx. Fig. C.4f). High percentages of cloud cover are simulated over South and Southeast Asia (on average ~80%) for both KM5c and pre-industrial with little cloud simulated to western Asia and western Indian Ocean, approximately 24% for both (Fig. 4.3d). KM5c simulates more cloud cover over India (6% more) but in general simulates minimal differences from the pre-industrial simulation (Fig. 4.3d).

4.3.2 Comparing G17, K1 and KM3 with the KM5c control

Superficially the patterns of summer SAT are very similar between all the simulated interglacials as seen in the figures of absolute model results (Fig. 4.3 & 4.4). There are however, some changes in temperature between KM5c and the other three interglacials. G17, K1 and KM3 simulate higher temperatures over continental Asia than KM5c (average increases of 2.9°C in G17, 6.6°C in K1 and 5.9°C in KM3), especially over west Asia/Middle East and 35°N and above over the rest of Asia (Fig. 4.4). K1 and KM3 simulate the largest temperature differences from KM5c with a maximum SAT change of 9.2°C in K1 and 10.4°C in KM3 over Asia (Fig. 4.4). All three interglacials simulate some warming over the ocean compared to KM5c, on average 1.2°C warmer in G17, 2.2°C warmer in K1 and 2.0°C warmer in KM3 (averaged over 10°S to 5°N) (Fig. 4.4). Whereas, for all three interglacials, the SAT predicted over latitudes 20°N to 30°N

show little change from the KM5c control (Fig. 4.4). There are also areas simulating cooling compared to KM5c. The north west of India (maximum decrease of 4.7°C in G17, 5.3°C in K1 and 7.1°C in KM3), the southern tip of India (increase of 0.3°C in G17 but up to 4.9°C cooler in K1 and 4.4°C in KM3), and Oman and Yemen (maximum decrease of 4.4°C in G17, 5.3°C in K1 and 6.3°C in KM3) (Fig. 4.4).

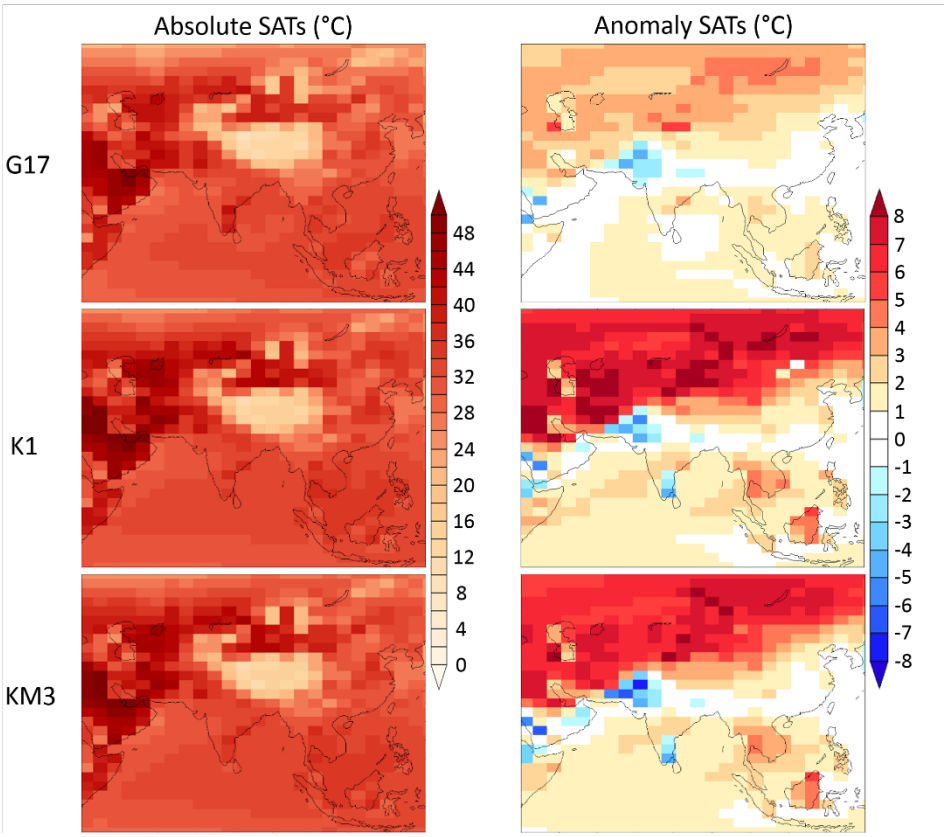

Figure 4.4 HadCM3 surface air temperature for JJAS (June – September) (°C). Left column: three Piacenzian interglacials (MIS G17, K1, KM3) absolute results. Right column: MIS G17, K1 and KM3 minus the MIS KM5c control.

The interglacials simulate even lower MSLP than KM5c from 25°N and above, with average decreases of 1.9 hPa in G17, 5.2 hPa in K1 and 4.4 hPa in KM3 (Fig. 4.5). Slightly lower pressure than KM5c is also predicted over the Indian Ocean (10°S to 5°N), 0.5 hPa in G17, 0.8 hPa in K1 and 0.9 hPa in KM3 (Fig. 4.5). There is, however, an area of higher pressure reaching 5.6 hPa in G17, 7.1 hPa in K1 and 7.0 hPa in KM3 more than KM5c in East China Sea (Fig. 4.5). This area of higher pressure is the largest between 25°N and 40°N in the West Pacific Ocean and extends latitudinally across eastern Asia to northern India. There is lower pressure than

KM5c across the Middle East but higher pressure across northern and eastern India (Fig. 4.5). Because of this, there is a decrease in surface wind strength moving from the Arabian Sea into the Indian subcontinent in the interglacials compared to KM5c in addition to the weaker winds that flow across the Bay of Bengal into East Asia (Fig. 4.5). Due to the lower pressure than KM5c over the Middle East there is an increase in wind strength from the Gulf of Aden into Yemen, Oman and Saudi Arabia (Fig. 4.5).

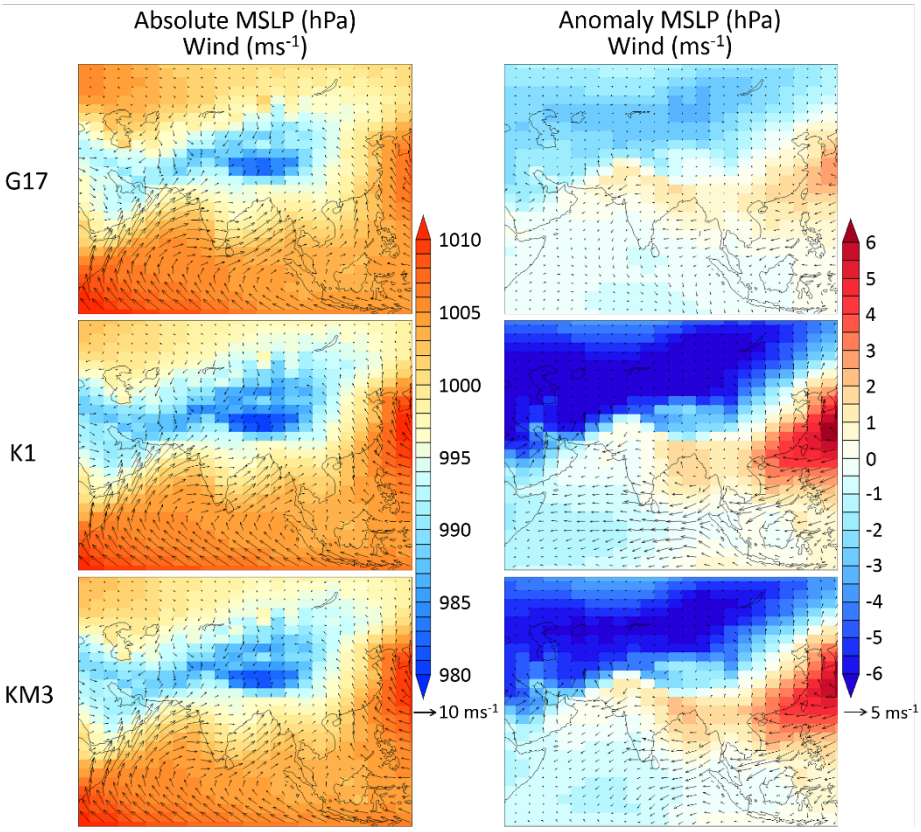

Figure 4.5 HadCM3 mean sea level pressure (MSLP) (hPa) for JJAS (June – September) and arrows indicating surface wind direction and strength (ms^{-1}). Left column: three Piacenzian interglacials (MIS G17, K1, KM3) absolute results. Right column: MIS G17, K1 and KM3 minus the MIS KM5c control.

The precipitation changes simulated between the three interglacials and KM5c (Fig. 4.6) show greater differences than between the Pliocene KM5c control and pre-industrial simulation (Fig. 4.3). In contrast to the SAT results (Fig. 4.4), the largest increases of summer precipitation compared to KM5c is seen across northern India and in general between 20°N and 30°N across

the south Asian terrestrial areas reaching maximum increases of 4.2 mm/day in G17, 13.0 mm/day in K1 and 11.4 mm/day in KM3 (Fig. 4.6). The area over India (the All Indian Rainfall (AIR) lats 7 - 30°N, lon 65 - 95°E) simulates on average increases from KM5c of 1.0 mm/day in G17, 2.9 mm/day in K1 and 2.4 mm/day in KM3 (Fig. 4.6). With some decreases in precipitation over the Bay of Bengal (approximately 0.8 mm/day less than KM5c in K1 and KM3) and the East and South China Seas (decrease from KM5c of up to 5.2 mm/day in G17, 8.6 mm/day in K1 and 9.0 mm/day in KM3) and to the east of equatorial Indian Ocean (Fig. 4.6). There are also increases of up to 3.5 mm/day in G17, 4.4 mm/day in K1 and 5.3 mm/day in KM3 in the northern Indian Ocean (Fig. 4.6).

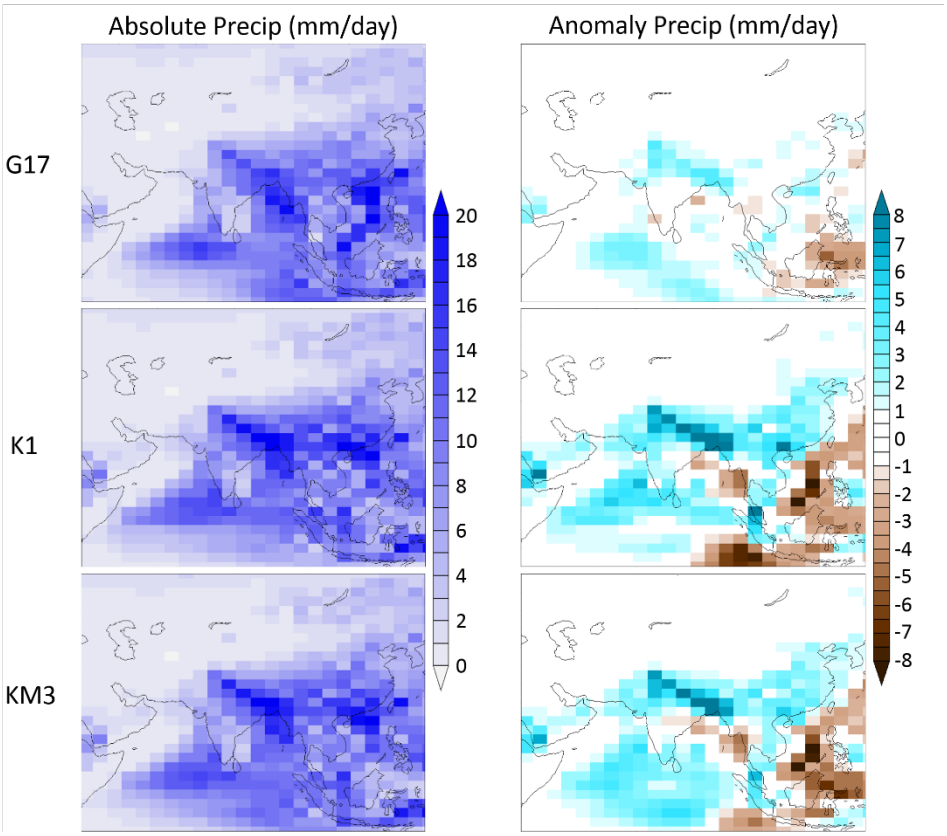

Figure 4.6 HadCM3 precipitation for JJAS (June – September) (mm/day). Left column: three Piacenzian interglacials (MIS G17, K1, KM3) absolute results. Right column: MIS G17, K1 and KM3 minus the MIS KM5c control.

The increases in precipitation compared to KM5c are driven by a combination of convective rainfall and largescale rainfall, with the changes in largescale rainfall mainly driving the increased

band of precipitation across northern India and the decreases of precipitation over oceanic areas due to less convective rainfall in these areas (Appx. Fig. C.4d and C.4e). The increased precipitation across terrestrial southern Asia is strongly matched by increases in runoff throughout northern India and across China reaching the eastern coast in all three interglacials predicting average runoff increases from KM5c of 1.5 mm/day in G17, 4.0 mm/day in K1 and 3.7 mm/day in KM3 (Appx. Fig. C.4c). These increases in precipitation and runoff cause localised decreases in salinity just off the coast of the Bay of Bengal and Arabian Sea of up to 4.5 PSUs in G17, 8.9 PSUs in K1 and 8.5 PSUs in KM3 less than KM5c (Appx. Fig. C.4b). There is also decreased salinity of on average 0.9 PSU in G17, 3.0 PSU in K1 and 2.2 PSU in the Indian Ocean (largest between 3°N and 6°N) (Appx. Fig. C.4b). Some increases in salinity is simulated in the South Asian seas, on average 0.6 PSUs in G17, 1.7 PSUs in K1 and 1.5 PSUs in KM3 more than KM5c, in the areas where a decrease of precipitation is simulated (Fig. 4.6 and Appx. Fig. C.4b. The interglacials all show increased cloud cover compared to KM5c over terrestrial areas, reaching increases of 19% in G17, 33% in K1 and 32% in KM3 over Northern India and the Middle East, with increases in the Arabian Sea and western Indian Ocean (increases of 28% in K1 and 24% in KM3 compared to KM5c) (Fig. 4.7). There is also a decrease in cloud cover simulated in the southeast Asia region in the interglacials compared to KM5c (Fig. 4.7).

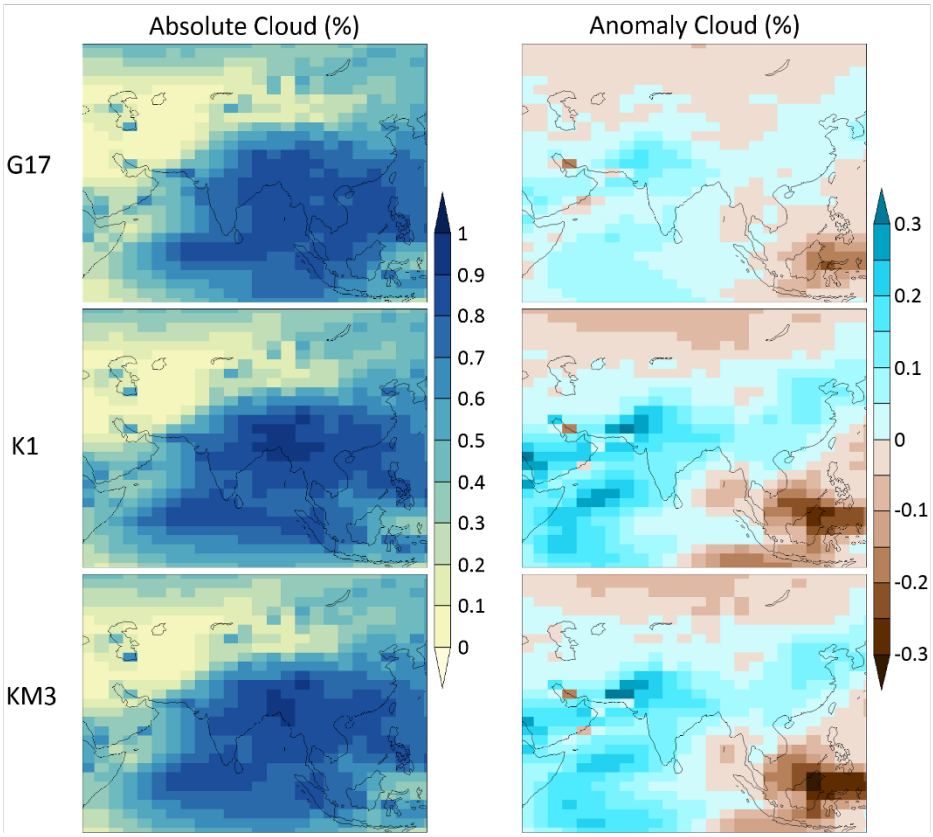

Figure 4.7 HadCM3 cloud cover for JJAS (June – September) (%). Left column: three Piacenzian interglacials (MIS G17, K1, KM3) absolute results. Right column: MIS G17, K1 and KM3 minus the MIS KM5c control.

Higher SSTs are simulated in the three interglacials compared to KM5c (Fig. 4.8). This increase of SSTs is on average 1°C in G17, 1.4°C in K1 and 1.5°C in KM3 higher than KM5c over the Indian Ocean between 10°S and 5°N (Fig. 4.8). There is a larger difference in SSTs over the Arabian Sea with the interglacials reaching up to 2.2°C in G17, 2.8°C in K1 and 2.4°C in KM3 higher than KM5c (Fig. 4.8). There are large decreases in the mixed layer depth for particularly K1 and KM3 and to a lesser extent G17 over the whole monsoon region (Appx. Fig. C.4f). The largest differences are predicted in the Bay of Bengal where compared to the KM5c average for mixed layer depth, 64.7 m, the other interglacials on average simulate shallower mixed layer depths of 49.8 m for G17, 28.1 m for K1 and 32.7 m for KM3 (Appx. Fig. C.4f). The only area with simulated increases in mixed layer depth are the Celebes and Molucca seas in east Asia where the interglacials simulate 11.2 m in G17, 9.0 m in K1 and 15.1 m in KM3 more than KM5c (Appx. Fig. C.4f).

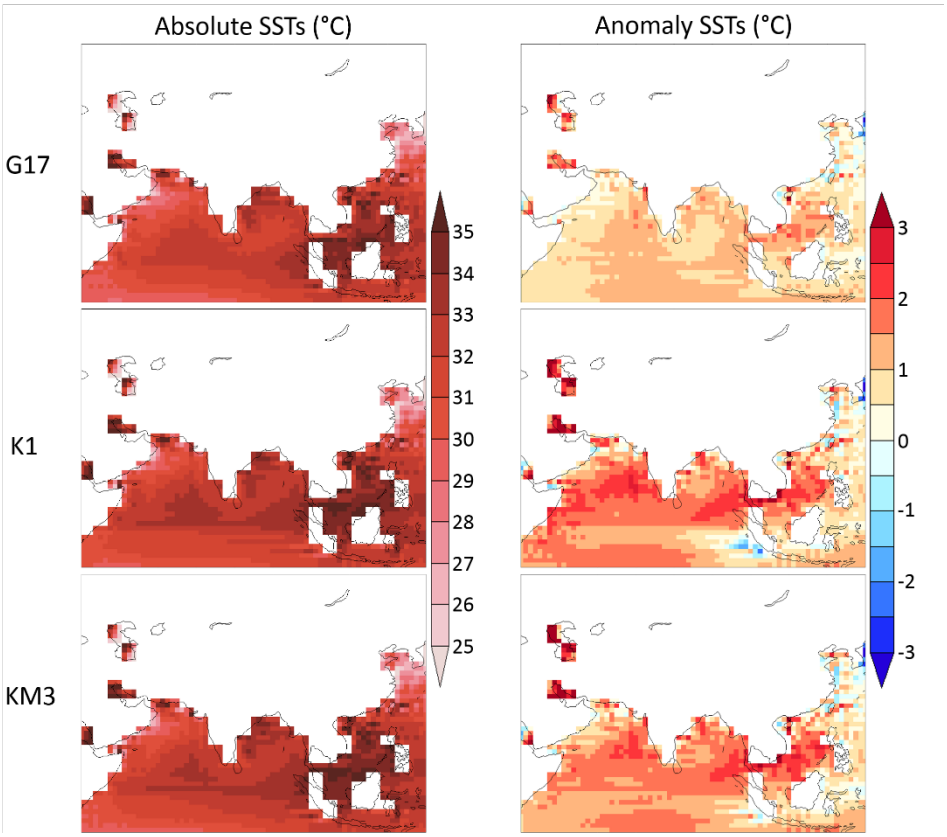

Figure 4.8 HadCM3 sea surface temperatures (SSTs) for JJAS (June – September) (°C). Left column: three Piacenzian interglacials (MIS G17, K1, KM3) absolute results. Right column: MIS G17, K1 and KM3 minus the MIS KM5c control.

4.4 Discussion

4.4.1 How does HadCM3 simulate the Indian monsoon in the Pliocene for MIS KM5c (an interglacial with a near modern orbit) compared to pre-industrial?

Rather than just looking at the rainfall over the Indian subcontinent, the Extended Indian Monsoon Rainfall (EIMR) index includes precipitation over the neighbouring oceans and land that are affected by the Indian monsoon (Goswami et al., 1999). The EIMR index is the average precipitation per day over the area 70°E - 110°E, 10°N - 30°N. As well as the precipitation based index, the Monsoon Hadley Index (MHI) represents the strength of the Indian summer

monsoon circulation by measuring the shear of meridional wind between the lower and upper troposphere averaged over the same region as the EIMR index (70°E - 110°E, 10°N - 30°N). Large positive values of MHI indicate a strong monsoon with negative values corresponding to a weak monsoon (Fig.4.9).

In Fig. 4.9b and c the points indicate the average index for the summer months for each interglacial for 100 years of the simulation and the bars either side show the summer minimum and maximum indices throughout the 100 simulated years. Both the EIMR and MHI indices are higher in KM5c than the pre-industrial simulation for the summer months, indicating a stronger summer monsoon in the Pliocene simulation KM5c than the pre-industrial. Looking to Fig. 4.3, the terrestrial areas simulate overall higher SATs and precipitation in the JJAS summer months. Although the Hadley circulation is predicted to be stronger in KM5c than pre-industrial (as seen in the MHI; Fig. 4.9c), the simulated changes in surface winds are very small between KM5c and pre-industrial with slight decreases in wind strength across the eastern Arabian Sea and India simulated in summer months. The increased surface winds moving from Somalia into the Middle East in KM5c compared to pre-industrial is the only area where increased summer monsoon winds are simulated in KM5c (Fig.4.3c). The higher SAT simulated over terrestrial areas in summer is not seen over India where increased cloud cover counteracts the increased insolation in this area (Fig.4.3a). This, combined with an increase in SSTs in KM5c summer compared to pre-industrial, decreases the pressure gradient between ocean and land causing weaker winds moving from the Arabian Sea into India, despite higher precipitation still simulated over most of the Indian sub-continent in summer.

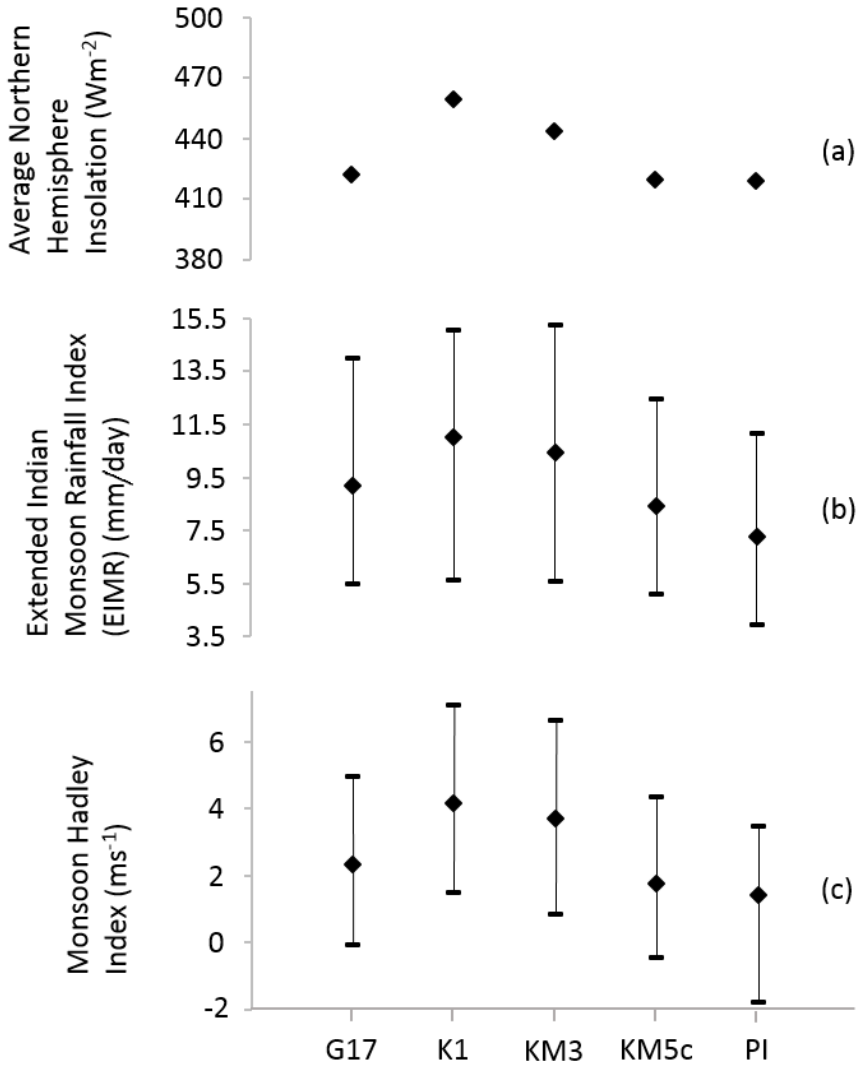

Figure 4.9 HadCM3 results for the four Piacenzian interglacials MIS G17, K1, KM3, KM5c and a pre-industrial simulation (PI) showing (a) the average northern hemisphere insolation (Wm^{-2}) for JJAS, (b) The Extended Indian Monsoon Rainfall (EIMR) Index (mm/day) and (c) The Monsoon Hadley Index (MHI) (ms^{-1}). In (b) and (c) diamonds indicate average monsoon index for simulated 100 years model years of the JJAS (June, July, August September) summer season. Bars show the minimum and maximum index throughout the 100 years for the EIMR and Monsoon Hadley Index for JJAS.

As KM5c has an orbital forcing very close to modern, any changes between the Indian monsoon in KM5c and the pre-industrial simulation are due to the implementation of other Pliocene boundary conditions. The difference in the simulated Indian monsoon is likely due to the higher CO_2 forcing in the Pliocene simulations. It has been well established in the literature that increases in greenhouse gas concentrations intensified the Asian summer monsoon due to

enhanced moisture transport into the Asian monsoon region (Kitoh et al., 1997; Annamalai et al., 2007; Kripalani et al., 2007). The higher moisture capacity of warmer air (a rate of 6-7% increase per degree) as set by the Clausius-Clapeyron equation is responsible for the intensified precipitation simulated (Xie et al., 2014). This increase in seasonal precipitation even in regions of weaker flow has been noted in the literature since Kitoh et al. (1997) described weakening of the low level monsoon winds over the Arabian sea despite an increase in summer monsoon rainfall over India in a study using the Meteorological Research Institute (MRI) coupled climate model. This level of increased summer precipitation over India with no change or weakened surface winds has been repeated in other modelling studies for future climate change (May, 2002; Ueda et al., 2006) and has been found in experiments using HadCM3 with doubled CO_2 (Turner et al., 2007).

The main difference forcing a stronger Indian monsoon in the KM5c experiment compared to the pre-industrial is higher CO_2 causing higher temperatures and enhanced moisture transport and therefore increased precipitation. To keep this investigation consistent with previous modelling studies such as Prescott et al. (2014) and the PlioMIP project, the CO_2 value was chosen to be 405 ppm. Estimates of CO_2 for the Piacenzian have been in the range 305-415 ppm (Pagani et al., 2009) with a more recent estimate suggesting a range of 280 – 420 ppm (Martínez-Botí et al., 2015). The CO_2 concentration is kept at 405 ppm for all the experiments in this study. While it has been demonstrated that the CO_2 levels varied throughout the Pliocene which would have influenced the intensity of the Indian monsoon any variation has not been accounted for in this study.

4.4.2 How does the simulation of the Indian monsoon change when simulating three further Pliocene interglacials with stronger orbital forcing?

G17, K1 and KM3 are negative isotope excursions of similar magnitude, however when compared to KM5c, the climate signal over the monsoon area in G17 is much smaller in JJAS than K1 and KM3. The differences between the interglacials are due to orbital forcing; K1 and KM3 simulate very similar summer signals and both have stronger precession forcing than G17. In K1 and KM3, the Northern Hemisphere receives 10% and 6% respectively more summer

insolation than the pre-industrial simulation compared to 1% in G17 and only 0.1% in KM5c. The resulting monsoon indices EIMR and MHI follow the same pattern of distribution with the indices for the pre-industrial being the lowest consistently, as an average as well as minimum and maximum (Table 4.1; Fig. 4.9). The pattern of average EIMR and MHI follow the same pattern as the average Northern Hemisphere insolation. The interglacials with the highest average EIMR index (K1 and KM3), and therefore strongest average monsoon, also result in the largest difference between the maximum and minimum EIMR, with the opposite being the case for the pre-industrial simulation and KM5c interglacial which indicate a weaker monsoon signal. This suggests the stronger precession forcing causes on average higher precipitation and a stronger monsoon but also a larger spread of possible monsoon strengths. The MHI similarly shows this pattern with the difference between minimum and maximum MHI in K1 and KM3 larger than G17 and KM5c. The minimum summer MHI for pre-industrial however is much lower than the other simulations at -1.8 ms^{-1} which corresponds to a simulated weak summer monsoon (Fig. 4.9).

G17, K1 and KM3 all display higher precipitation over both terrestrial areas and the surrounding ocean, with northern Indian summer precipitation levels in K1 and KM3 reaching 13 and 11 mm/day more than KM5c respectively. While strong increases in summer SAT are simulated over the terrestrial areas particularly in K1 and KM3, these temperature increases are not seen over India specifically. Increases in cloud cover reduces the amount of solar radiation reaching the surface in this area and enhanced precipitation increases evaporative cooling.

The reduced temperature and pressure gradients over India cause a reduction in wind speed across the Arabian Sea and Bay of Bengal in the interglacials, as also discussed above between KM5c and pre-industrial. The increases in precipitation over the Indian ocean during summer follow a 'warmer-gets-wetter' pattern (Xie et al., 2010; Huang et al., 2013), whereby SST patterns are the dominant mechanism for tropical precipitation response in areas where local warming in SSTs exceeds the tropical average (Xie et al., 2014).

All the interglacials showed higher summer SSTs over the Indian Ocean than pre-industrial by ~2°C in KM5c and 3°C and higher in G17, K1 and KM3. Proxy data from the monsoon area can be used to compare these average changes; Dowsett et al. (2013) compared SSTs between

the PlioMIP ensemble and the PRISM3 reconstruction. The PRISM SSTs used in the comparison have undergone a warm peak average method (Dowsett & Poore, 1991) to develop an 'average interglacial' for the mPWP. The ODP sites 709, 716, 722 and 758 in the Indian monsoon area have been assigned 'high confidence' using the λ-confidence scheme (Dowsett et al., 2012) and despite representing an average warm interglacial still reconstruct lower SSTs than the multi-model mean (MMM) at all sites, suggesting that the models in the PlioMIP ensemble may overestimate SSTs in this area. HadCM3 specifically, simulates the highest SSTs out of the MMM at all these sites, simulating approximate 2°C higher than the PRISM SST reconstruction. The 2°C and 3°C SST warming simulated in the interglacials in this study therefore may be too high due to model sensitivity in HadCM3 over this area. Overly warm SSTs would influence the simulation of the monsoon by reducing the pressure and temperature gradient between the land and ocean and reducing wind speed. However, caution should be applied when interpreting this as due to the time slab nature of the PRISM SSTs, there is the potential that the PRISM data does not capture the interglacial peaks that have been simulated in this study.

The data-model discord in SSTs between the PlioMIP project and PRISM3 dataset is not solely seen in the Indian monsoon area but has also been noted throughout the low latitudes. In line with current understanding, the higher CO_2 concentration in the Pliocene would be expected to cause warmer tropical SSTs, which is the temperature pattern simulated by climate models. Data reconstructions find tropical SSTs to be little or no warmer than present day (Haywood et al., 2016), however, interpretation of the tropical proxy data in the Pliocene is evolving. Recent work by O'Brien et al. (2015) and Evans et al (2016) detailed the impact of changing seawater chemistry on Mg/Ca derived SST estimates and found that the previous SST reconstructions to be underestimated. The alkenone proxy reaches saturation at about 28°C which inhibits its use for producing records from the warmest locations. Faunal assemblage techniques (used to determine the SST estimates in the Indian monsoon area) can be affected by increased dissolution in the warm end members of assemblages which result in cooler SST estimates. Overall, these uncertainties in SST reconstructions highlight the need for further study before concrete conclusions can be drawn about the models ability to simulate SST in this area.

Here, the simulated differences in SAT, precipitation, MSLP, salinity and mixed layer depth are larger between K1 and KM3, and KM5c, where the only difference is orbital forcing, than they

are between the pre-industrial simulation and KM5c, where Pliocene boundary conditions have been implemented. This shows the high potential for orbital forcing to affect the strength of the Indian summer monsoon, especially in addition to Pliocene boundary conditions that already cause intensified Indian summer monsoon due to increased CO_2. This is in line with previous work as far back as Prell & Kutzbach (1992) in a study to identify the sensitivity of the Indian monsoon to various boundary conditions which showed the monsoon is most sensitive to elevation and orbital changes. As the simulations for the mPWP interglacials in this manuscript use a topography very similar to modern it would follow that the interglacials with very different orbital forcing caused a more significant change in Indian monsoon than the rest of the changed Pliocene boundary conditions combined.

4.4.3 What does the modelled variability in the Indian monsoon behaviour imply about interpreting discrete and often time specific proxy records of Indian monsoon behaviour?

It is not possible to compare the specific interglacial time slices with geological data by looking at the proxy data for the Pliocene over the Indian Ocean, due to insufficient dating and chronological control. In general, the trends seen in the proxy data suggest that the Pliocene simulations should show a stronger monsoon than modern (Sanyal et al., 2004; Chang et al., 2010), and this is reflected in the Indian monsoon EIMR and MHI indices for all simulated interglacials.

KM5c does have a stronger summer Indian monsoon than pre-industrial but this signal is surpassed by the signals in G17, K1 and KM3 due to the strong precession especially in K1 and KM3. This could be important for proxy reconstructions with a large signal of increased monsoon strength in the Pliocene but without the temporal resolution to pinpoint when in time that was. Such records could incorrectly interpret the large signal as relevant for the whole Pliocene and potentially, future climate change. In contrast, this study finds that orbital forcing has a large effect on the Pliocene Indian monsoon and therefore any assumptions about future monsoon behaviour based on the Pliocene need to concentrate on interglacials without strong orbital forcing. An obvious target for this is KM5c which has a very near modern orbit and in

HadCM3 simulates a stronger summer Indian monsoon than pre-industrial and is now the focus for modelling and data efforts within the PlioMIP2 and PRISM4 projects.

A caveat of this study is the uncertainty surrounding the topography of the Tibetan Plateau. There is some dispute about whether the Tibetan Plateau had reached near modern elevation by the Miocene or Pliocene. Overall, most of the evidence seems to suggest the Tibetan Plateau having reached its modern height by 3.6 Ma, which is before the interglacials simulated in this study. A recent high resolution ostracod record from Lake Qinghai of the northeast margin of the Tibetan Plateau found that the deep lacustrine ostracod fauna disappeared abruptly at ~3.6 Ma (Lu et al., 2017) and the sediment lithology from Lake Qinghai changed from deep lacustrine sub-facies to a shallower facies also at this time (Fu et al., 2013). The authors attribute these changes to uplift of the Qinghai Nanshan, indicating an overall extension of north-eastern Tibetan Plateau at 3.6 Ma (Lu et al., 2017). Regarding the Indian monsoon specifically, model simulations by Prell and Kutzbach (1992) suggested that the uplift of the Tibetan Plateau had dramatic effects on the Indian monsoon. The PRISM3D topography used for the simulations here was with a Tibetan Plateau kept roughly consistent with modern day (Sohl et al., 2009). Therefore, if the uplift did occur after 3.6 Ma the elevation of the Tibetan Plateau used in the simulations may be too high and model could therefore be simulating stronger monsoons than is realistic.

4.4.4 Future work

Here, the Indian monsoon is simulated for four interglacials in the Piacenzian. To understand a more complete picture of monsoon variability throughout this time, it would be informative to also simulate the Indian monsoon in cooler or glacial events in the Piacenzian. While this study has looked at interglacial monsoon variability on orbital timescales, there are also short-term changes in monsoon intensity on sub-orbital timescales. For example, variability due to oscillations in the thermohaline circulation, atmospheric energy and moisture transfer all happen on decadal timescales (Wang et al., 2005) and would add to a fuller picture of potential Pliocene monsoon variability. More proxy reconstructions from the monsoon area with the temporal resolution necessary to be able to compare to these simulations would further this analysis. The future PlioMIP2 project will run simulations with the orbital forcing for KM5c is a further

opportunity for the investigation of the mid-Piacenzian monsoons with an ensemble of models and would also reduce potential for model bias.

4.5 Conclusion

This paper presents the modelled climatological results of four interglacials in the mPWP (MIS G17, K1, KM3, KM5c) summer Indian monsoon using HadCM3. MIS KM5c has a near modern orbit (Fig. 4.2) and indicates stronger monsoon indices and increased SAT and precipitation over terrestrial areas but small decreases in wind when compared to a pre-industrial simulation. These changes are due to a higher CO_2 level of 405ppm in the simulation for KM5c. The very different-from-modern orbital forcing in the other three interglacials, especially MIS K1 and KM3, triggers a stronger climate signal and resulting summer monsoon with significant increases in temperatures. The results from this paper also suggest that the stronger orbital forcing triggers a more variable summer monsoon as well as, on average, a stronger summer monsoon. This shows large potential for orbital forcing (especially precession) to affect the Indian summer monsoon particularly when simulated on top of mPWP boundary conditions and high CO_2 levels.

Currently the chronological control of proxy data from the Indian monsoon area is insufficient to compare to these modelled time slices. If the focus of geological reconstructions from the mPWP is to understand the Indian summer monsoon in a warmer, high CO_2 world for the relevance of future climate change, these results indicate a strong influence of orbit in simulating the Indian monsoon in the mPWP. Therefore, care must be taken when interpreting past records for the understanding of future monsoon behaviour to concentrate on times where orbital forcing is similar to today such as MIS KM5c.

References

Annamalai, H., Hamilton, K., Sperber, K.R., Annamalai, H., Hamilton, K. & Sperber, K.R. (2007). The South Asian Summer Monsoon and Its Relationship with ENSO in the IPCC AR4 Simulations. *Journal of Climate*. 20 (6). pp. 1071–1092.

Ao, H., Roberts, A.P., Dekkers, M.J., Liu, X., Rohling, E.J., Shi, Z., An, Z. & Zhao, X. (2016). Late Miocene–Pliocene Asian monsoon intensification linked to Antarctic ice-sheet growth. *Earth and Planetary Science Letters*. 444. pp. 75-87.

Berger, A.L. (1978). Long-Term Variations of Caloric Insolation Resulting from the Earth's Orbital Elements. *Quaternary Research*. 9 (2). pp. 139–167.

Berger, A. (1988). Milankovitch Theory and climate. *Reviews of Geophysics*. 26 (4). p.p. 624.

Braconnot, P., Joussaume, S., Marti, O. & de Noblet, N. (1999). Synergistic feedbacks from ocean and vegetation on the African Monsoon response to Mid-Holocene insolation. *Geophysical Research Letters*. 26 (16). pp. 2481–2484.

Braconnot, P. & Marti, O. (2003). Impact of precession on monsoon characteristics from coupled ocean atmosphere experiments: changes in Indian monsoon and Indian ocean climatology. *Marine Geology*. 201 (1). pp. 23–34.

Braconnot, P., Marzin, C., Grégoire, L., Mosquet, E. & Marti, O. (2008). Monsoon response to changes in Earth's orbital parameters: comparisons between simulations of the Eemian and of the Holocene. *Clim. Past*. 4. pp. 281–294.

Bragg, F.J., Lunt, D.J. & Haywood, A.M. (2012). Mid-Pliocene climate modelled using the UK Hadley Centre Model: PlioMIP Experiments 1 and 2. *Geoscientific Model Development Discussions*. 5 (2). pp. 837–871.

Chang, Z., Xiao, J., Lü, L. & Yao, H. (2010). Abrupt shifts in the Indian monsoon during the Pliocene marked by high-resolution terrestrial records from the Yuanmou Basin in southwest China. *Journal of Asian Earth Sciences*. 37 (2). pp. 166–175.

Chen, J., Chen, Y., Liu, L., Ji, J., Balsam, W., Sun, Y. & Lu, H. (2006). Zr/Rb ratio in the Chinese loess sequences and its implication for changes in the East Asian winter monsoon strength. *Geochimica et Cosmochimica Acta*. 70 (6). pp. 1471–1482.

Christensen, J.H., Kumar, K.K., Aldrian, E., An, S.-I., Cavalcanti, I.F.A., De Castro, M., Dong, W., Goswami, P., Hall, A., Kanyanga, J.K., Kitoh, A., Kossin, J., Lau, N.-C., Renwick, J., Stephenson,

D.B., Xie, S.-P. & Zhou, T. (2013). Climate Phenomena and their Relevance for Future Regional Climate Change. In: T. F. Stocker, D. Qin, G.-K. Plattner, M. Tignor, S. K. Allen, J. Boschung, A. Nauels, Y. Xia, V. Bex, & P. M. Midgley (eds.). *Climate Change 2013 - The Physical Science Basis. Contribution of Working Group I to the Fifth Assessment Report of the International Panel on Climate Change*. [Online]. Cambridge, United Kingdom and New York, NY, USA: Cambridge University Press, pp. 1217–1308.

Clemens, S.C. & Prell, W.L. (1990). Late Pleistocene variability of Arabian Sea summer monsoon winds and continental aridity: Eolian records from the lithogenic component of deep-sea sediments. *Paleoceanography*. 5 (2). pp. 109–145.

Clift, P.D. & Plumb, R.A. (2008). *The Asian Monsoon, Causes History and Effects*. Cambridge University Press.

Cox, P.M., Betts, R.A., Bunton, C.B., Essery, R.L.H., Rowntree, P.R. & Smith, J. (1999). The impact of new land surface physics on the GCM simulation of climate and climate sensitivity. *Climate Dynamics*. 15 (3). pp. 183–203.

deMenocal, P.B. & Rind, D. (1993). Sensitivity of Asian and African climate to variations in seasonal insolation, glacial ice cover, sea surface temperature, and Asian orography. *Journal of Geophysical Research*. 98 (D4). p.p. 7265.

Ding, Z.L., Yang, S.L., Sun, J.M. & Liu, T.S. (2001). Iron geochemistry of loess and red clay deposits in the Chinese Loess Plateau and implications for long-term Asian monsoon evolution in the last 7.0 Ma. *Earth and Planetary Science Letters*. 185 (1). pp. 99–109.

Dowsett, H.J. & Poore, R.Z. (1991). Pliocene sea surface temperatures of the north atlantic ocean at 3.0 Ma. *Quaternary Science Reviews*. 10 (2–3). pp. 189–204.

Dowsett, H., Robinson, M., Haywood, A.M., Salzmann, U., Hill, D., Sohl, L., Chandler, M., Williams, M., Foley, K. & Stoll, D. (2010). The PRISM3D paleoenvironmental reconstruction. *Stratigraphy*. 7 (2-3). pp. 123-139.

Dowsett, H.J., Robinson, M.M., Haywood, A.M., Hill, D.J., Dolan, A.M., Stoll, D.K., Chan, W.-L., Abe-Ouchi, A., Chandler, M.A., Rosenbloom, N.A., Otto-Bliesner, B.L., Bragg, F.J., Lunt, D.J., Foley, K.M. & Riesselman, C.R. (2012). Assessing confidence in Pliocene sea surface temperatures to evaluate predictive models. *Nature Climate Change*. 2 (5). pp. 365–371.

Dowsett, H.J., Foley, K.M., Stoll, D.K., Chandler, M.A., Sohl, L.E., Bentsen, M., Otto-Bliesner, B.L., Bragg, F.J., Chan, W.-L., Contoux, C., Dolan, A.M., Haywood, A.M., Jonas, J.A., Jost, A., Kamae, Y., Lohmann, G., Lunt, D.J., Nisancioglu, K.H., Abe-Ouchi, A., Ramstein, G., Riesselman, C.R., Robinson, M.M., Rosenbloom, N.A., Salzmann, U., Stepanek, C., Strother, S.L., Ueda, H., Yan, Q.

& Zhang, Z. (2013). Sea surface temperature of the mid-Piacenzian ocean: a data-model comparison. *Scientific reports*. 3. p.p. 2013.

Fu, C., An, Z., Qiang, X., Bloemendal, J., Song, Y. & Chang, H. (2013). Magnetostratigraphic determination of the age of ancient Lake Qinghai, and record of the East Asian monsoon since 4.63 Ma. *Geology*. 41 (8). pp. 875–878.

Gadgil, S., Vinayachandran, P. & Francis, P. (2003). Droughts of the Indian summer monsoon: Role of clouds over the Indian Ocean. *Current Science*. 85 (12). pp 1713-1719.

Gordon, C., Cooper, C., Senior, C.A., Banks, H., Gregory, J.M., Johns, T.C., Mitchell, J.F.B. & Wood, R.A. (2000). The simulation of SST, sea ice extents and ocean heat transports in a version of the Hadley Centre coupled model without flux adjustments. *Climate Dynamics*. 16 (2–3). pp. 147–168.

Goswami, B.N., Krishnamurthy, V. & Annmalai, H. (1999). A broad-scale circulation index for the interannual variability of the Indian summer monsoon. *Quarterly Journal of the Royal Meteorological Society*. 125 (554). pp. 611–633.

Gupta, A.K. & Thomas, E. (2003). Initiation of Northern Hemisphere glaciation and strengthening of the northeast Indian monsoon: Ocean drilling program site 758, eastern equatorial Indian Ocean. *Geology*. 31 (1). pp. 47–50.

Gupta, A.K. & Anderson, D.M. (2005). Mysteries of the Indian Ocean Monsoon System. *Geological Society of India*. 65 (1). pp. 54–60.

Hays, J.D., Imbrie, J. & Shackleton, N.J. (1976). Variations in the Earth's Orbit: Pacemaker of the Ice Ages. *Science*. 194 (4270). p.pp. 1121–1132.

Haywood, A.M. & Valdes, P.J. (2004). Modelling Pliocene warmth: contribution of atmosphere, oceans and cryosphere. *Earth and Planetary Science Letters*. 218 (3–4). pp. 363–377.

Haywood, A.M., Dowsett, H.J., Otto-Bliesner, B., Chandler, M.A., Dolan, A.M., Hill, D.J., Lunt, D.J., Robinson, M.M., Rosenbloom, N., Salzmann, U. & Sohl, L.E. (2010). Pliocene Model Intercomparison Project (PlioMIP): experimental design and boundary conditions (Experiment 1). *Geoscientific Model Development*. 3 (1). pp. 227–242.

Haywood, A.M., Dolan, A.M., Pickering, S.J., Dowsett, H.J., McClymont, E.L., Prescott, C.L., Salzmann, U., Hill, D.J., Hunter, S.J., Lunt, D.J., Pope, J.O. & Valdes, P.J. (2013a). On the identification of a Pliocene time slice for data-model comparison. *Philosophical transactions. Series A, Mathematical, physical, and engineering sciences*. 371 (2001). p.p. 20120515.

Haywood, A.M., Hill, D.J., Dolan, A.M., Otto-Bliesner, B.L., Bragg, F., Chan, W.-L., Chandler, M.A., Contoux, C., Dowsett, H.J., Jost, A., Kamae, Y., Lohmann, G., Lunt, D.J., Abe-Ouchi, A.,

Pickering, S.J., Ramstein, G., Rosenbloom, N.A., Salzmann, U., Sohl, L., Stepanek, C., Ueda, H., Yan, Q. & Zhang, Z. (2013b). Large-scale features of Pliocene climate: results from the Pliocene Model Intercomparison Project. *Climate of the Past*. 9 (1). pp. 191–209.

Haywood, A.M., Dowsett, H.J. & Dolan, A.M. (2016). Integrating geological archives and climate models for the mid-Pliocene warm period. *Nature Communications*. 7. p.p. 10646.

Huang, Y., Clemens, S.C., Liu, W., Wang, Y. & Prell, W.L. (2007). Large-scale hydrological change drove the late Miocene C4 plant expansion in the Himalayan foreland and Arabian Peninsula. *Geology*. 35 (6). p.p. 531.

Huang, P., Xie, S.-P., Hu, K., Huang, G. & Huang, R. (2013). Patterns of the seasonal response of tropical rainfall to global warming. *Nature Geoscience*. 6 (5). pp. 357–361.

Kitoh, A., Yukimoto, S., Noda, A. & Motoi, T. (1997). Simulated Changes in the Asian Summer Monsoon at Times of Increased Atmospheric CO2. *Journal of the Meteorological Society of Japan. Ser. II*. 75 (6). pp. 1019–1031.

Kripalani, R.H., Oh, J.H., Kulkarni, A., Sabade, S.S. & Chaudhari, H.S. (2007). South Asian summer monsoon precipitation variability: Coupled climate model simulations and projections under IPCC AR4. *Theoretical and Applied Climatology*. 90 (3–4). pp. 133–159.

Laskar, J., Robutel, P., Joutel, F., Gastineau, M., Correia, A.C.M. & Levrard, B. (2004). A long-term numerical solution for the insolation quantities of the Earth. *Astronomy & Astrophysics*. 428 (1). pp. 261–285.

Li, Y., Harrison, S.P., Zhao, P. & Ju, J. (2009). Simulations of the impacts of dynamic vegetation on interannual and interdecadal variability of Asian summer monsoon with modern and mid-Holocene orbital forcings. *Global and Planetary Change*. 66 (3–4). pp. 235–252.

Liddy, H.M., Feakins, S.J. & Tierney, J.E. (2016). Cooling and drying in northeast Africa across the Pliocene. *Earth and Planetary Science Letters*. 449. pp. 430–438.

Lisiecki, L.E. & Raymo, M.E. (2005). A Pliocene-Pleistocene stack of 57 globally distributed benthic δ 18 O records. *Paleoceanography*. [Online]. 20 (1). p.p. PA1003

Liu, X. & Shi, Z. (2009). Effect of precession on the Asian summer monsoon evolution: A systematic review. *Chinese Science Bulletin*. 54 (20) pp. 3720–3730.

Lu, F., An, Z., Chang, H., Dodson, J., Qiang, X., Yan, H., Dong, J., Song, Y., Fu, C. & Li, X. (2017). Climate change and tectonic activity during the early Pliocene Warm Period from the ostracod record at Lake Qinghai, northeastern Tibetan Plateau. *Journal of Asian Earth Sciences*. 138. pp. 466–476.

Martínez-Botí, M.A., Foster, G.L., Chalk, T.B., Rohling, E.J., Sexton, P.F., Lunt, D.J., Pancost, R.D., Badger, M.P.S. & Schmidt, D.N. (2015). Plio-Pleistocene climate sensitivity evaluated using high-resolution CO2 records. *Nature*. 518 (7537). pp. 49–54.

Marzocchi, A., Lunt, D.J., Flecker, R., Bradshaw, C.D., Farnsworth, A. & Hilgen, F.J. (2015). Orbital control on late Miocene climate and the North African monsoon: insight from an ensemble of sub-precessional simulations. *Clim. Past*. 11. pp. 1271–1295.

May, W. (2002). Simulated changes of the Indian summer monsoon under enhanced greenhouse gas conditions in a global time-slice experiment. *Geophysical Research Letters*. 29 (7). pp. 22–24.

Mohan, K. & Gupta, A.K. (2011). Intense deep convective mixing in the Southeast Arabian Sea linked to strengthening of the Northeast Indian monsoon during the middle Pliocene (3.4 Ma). *Current Science*. 101 (4). pp. 543-548.

Overpeck, J., Anderson, D., Trumbore, S. & Prell, W. (1996). The southwest Indian Monsoon over the last 18 000 years. *Climate Dynamics*. 12 (3). pp. 213–225.

Pagani, M., Liu, Z., LaRiviere, J. & Ravelo, A.C. (2009). High Earth-system climate sensitivity determined from Pliocene carbon dioxide concentrations. *Nature Geoscience*. 3 (1). pp. 27–30.

Pollard, D. & Reusch, D.B. (2002). A calendar conversion method for monthly mean paleoclimate model output with orbital forcing. *Journal of Geophysical Research Atmospheres*. [Online]. 107 (22). p.p. 4615.

Prell, W.L. & Campo, E. Van (1986). Coherent response of Arabian Sea upwelling and pollen transport to late Quaternary monsoonal winds. *Nature*. 323 (6088). pp. 526–528.

Prell, W.L. & Kutzbach, J.E. (1992). Sensitivity of the Indian monsoon to forcing parameters and implications for its evolution. *Nature*. 360 (6405). pp. 647–652.

Prescott, C.L., Haywood, A.M., Dolan, A.M., Hunter, S.J., Pope, J.O. & Pickering, S.J. (2014). Assessing orbitally-forced interglacial climate variability during the mid-Pliocene Warm Period. *Earth and Planetary Science Letters*. 400. pp. 261–271.

Prescott, C.L., Dolan, A.M., Haywood, A.M., Hunter, S.J. & Tindall, J.C. (2018). Regional climate and vegetation response to orbital forcing within the mid-Pliocene Warm Period: a study using HadCM3. *Global and and Planetary Change*. 161. pp. 231–243.

Sanyal, P., Bhattacharya, S.., Kumar, R., Ghosh, S.. & Sangode, S.. (2004). Mio–Pliocene monsoonal record from Himalayan foreland basin (Indian Siwalik) and its relation to vegetational change. *Palaeogeography, Palaeoclimatology, Palaeoecology*. 205 (1). pp. 23–41.

Sohl, L.E., Chandler, M.A., Schmunk, R.B., Mankoff, K., Jonas, J.A., Foley, K.M. & Dowsett, H.J. (2009). PRISM3/GISS Topographic Reconstruction. *U.S. Geological Survey Data Series 419*. 6 pp.

Su, T., Jacques, F.M.B., Spicer, R.A., Liu, Y.-S., Huang, Y.-J., Xing, Y.-W. & Zhou, Z.-K. (2013). Post-Pliocene establishment of the present monsoonal climate in SW China: evidence from the late Pliocene Longmen megaflora. *Climate of the Past*. 9 (4). pp. 1911–1920.

Turner, A.G., Inness, P.M. & Slingo, J.M. (2007). The effect of doubled CO2 and model basic state biases on the monsoon-ENSO system. I: Mean response and interannual variability. *Quarterly Journal of the Royal Meteorological Society*. 133 (626). pp. 1143–1157.

Turner, A.G. & Annamalai, H. (2012). Climate change and the South Asian summer monsoon. *Nature Climate Change*. 2 (8). pp. 587–595.

Ueda, H., Iwai, A., Kuwako, K. & Hori, M.E. (2006). Impact of anthropogenic forcing on the Asian summer monsoon as simulated by eight GCMs. *Geophysical Research Letters*. 33 (6). p.p. L06703.

Valdes, P.J., Armstrong, E., Badger, M.P.S., Bradshaw, C.D., Bragg, F., Davies-Barnard, T., Day, J.J., Farnsworth, A., Hopcroft, P.O., Kennedy, A.T., Lord, N.S., Lunt, D.J., Marzocchi, A., Parry, L.M., Roberts, W.H.G., Stone, E.J., Tourte, G.J.L. & Williams, J.H.T. (2017). The BRIDGE HadCM3 family of climate models: HadCM3@Bristol v1.0. *Geoscientific Model Development Discussions*. pp. 1–42.

Wang, B. (2006). *The Asian monsoon*. Springer-Verlag Berlin Heidelberg New York.

Wang, P., Clemens, S., Beaufort, L., Braconnot, P., Ganssen, G., Jian, Z., Kershaw, P. & Sarnthein, M. (2005). Evolution and variability of the Asian monsoon system: state of the art and outstanding issues. *Quaternary Science Reviews*. 24 (5). pp. 595–629.

Wang, Y.-X., Yang, J.-D., Chen, J., Zhang, K.-J. & Rao, W.-B. (2007). The Sr and Nd isotopic variations of the Chinese Loess Plateau during the past 7 Ma: Implications for the East Asian winter monsoon and source areas of loess. *Palaeogeography, Palaeoclimatology, Palaeoecology*. 249 (3). pp. 351–361.

Webster, P.J., Magaña, V.O., Palmer, T.N., Shukla, J., Tomas, R.A., Yanai, M. & Yasunari, T. (1998). Monsoons: Processes, predictability, and the prospects for prediction. *Journal of Geophysical Research: Oceans*. 103 (C7). pp. 14451–14510.

Xie, S.-P., Deser, C., Vecchi, G.A., Ma, J., Teng, H., Wittenberg, A.T., Xie, S.-P., Deser, C., Vecchi, G.A., Ma, J., Teng, H. & Wittenberg, A.T. (2010). Global Warming Pattern Formation: Sea Surface Temperature and Rainfall*. *Journal of Climate*. 23 (4). pp. 966–986.

Xie, S., Deser, C., Vecchi, G.A., Collins, M., Tom, L., Hall, A., Hawkins, E., Johnson, N.C. & Cassou, C. (2014). Towards predictive understanding of regional climate change: Issues and opportunities for progress. *Nature Publishing Group*. 5 (10). pp. 1–29.

Yan, Q., Zhang, Z.-S. & Gao, Y.-Q. (2012). An East Asian Monsoon in the Mid-Pliocene. *Atmospheric*

and Oceanic Science Letters. 5 (6). pp. 449-454.

Zhang, R., Yan, Q., Zhang, Z.S., Jiang, D., Otto-Bliesner, B.L., Haywood, A.M., Hill, D.J., Dolan, A.M., Stepanek, C., Lohmann, G., Contoux, C., Bragg, F., Chan, C.L., Chandler, M.A., Jost, A., Kamae, Y., Abe-Ouchi, A., Ramstein, G., Rosenbloom, N.A., Sohl, L. & Ueda, H. (2013). Mid-Pliocene East Asian monsoon climate simulated in the PlioMIP. *Climate of the Past*. 9 (5). pp. 2085–2099.

Zhang, R. & Zhang, Q. (2017). Non-uniform spatial difference in the South Asian summer monsoon during the mid-Piacenzian. *Atmospheric and Oceanic Science Letters*. 10 (4). pp. 269–275.

CHAPTER 5

CONCLUSIONS AND DISCUSSION

5.1 Summary

The aim of this thesis was to investigate orbit-driven climate variability through the mPWP. The overall aim was broken into three research questions. Chapter 1 commenced by discussing the relevant literature on Pliocene climate and continued with the specific scientific background for each research question. The following chapters answered each of the three research questions. Each of the results chapters contain discussion and conclusion sections so within this summary only the main points will be discussed again for each of the research questions outlined in chapter 1. This chapter will summarise how the chapters link together to address the thesis aim. It will also answer the research questions, explore the wider implications and scientific advances of this thesis and finally, discuss the limitations of the study and the possibilities for future work.

While the reconstruction and modelling of the mPWP as an average warm 'time slab' was necessary at the time, and significant advances were made from this method, it is essential to begin to understand the climate variability through this time. Chapter 2 concentrated on modelling two interglacials within the mPWP with different orbital characteristics, MIS KM5c and K1. In assessing and comparing the simulated surface temperatures around these interglacials it was shown that the spatial patterns and magnitude of the SAT changes varied significantly between the two interglacials. This investigation also found highly variable seasonal differences, particularly over terrestrial areas around both MIS KM5c and K1. The simulations in chapter 2 only changed orbital parameters for the two simulations and it is known that there

are feedbacks that would have dampened or enhanced the temperature signal derived from orbital forcing. This is especially relevant for vegetation feedbacks as large seasonal temperature changes were seen over terrestrial areas in the results. Building on the results of chapter 2, a dynamic vegetation element was added to the simulations analysed in chapter 3.

Chapter 2 looked at the interglacials MIS K1 and KM5c and demonstrated that the two events are dissimilar in terms of their climatology due to the differences in orbital forcing. Chapter 3 is a development of this, with the incorporation of two more Pliocene interglacial events, MIS G17 and KM3 to build a fuller picture of potential mPWP interglacial climate variability. To further explore these large terrestrial differences shown between the interglacial MIS KM5c and K1 in chapter 2, the simulated vegetation is compared between the four interglacials simulated in chapter 3 with a more in-depth investigation into the seasonal range of temperatures. The results of both chapter 2 and 3 displayed high levels of seasonal variability between the four interglacials. This was especially evident over the continental interiors of North America and Eurasia in the interglacials MIS K1 and KM3 that have a near minimum precession causing increasing seasonality. In chapter 4 therefore, a seasonal event, the Indian monsoon was investigated and compared between the interglacials. While chapter 2 and 3 investigated the climate changes due to orbit on global scales, chapter 4 concentrated on the orbital variability of the regional climate system of the Indian monsoon.

5.2 Answering the research questions

5.2.1 RQ1: What is the predicted temperature variability around two interglacial events with different characteristics of orbital forcing in the mPWP and what are the implications for terrestrial and marine data-model comparison?

The work in chapter 2 analysed the results of a series of 30 orbital sensitivity experiments centred on two interglacial events in the mPWP with different characteristics of orbital forcing. The magnitude of orbitally-forced temperature changes across both interglacial events was quantified and compared. The analysis determined that the MIS KM5c and K1 interglacial events were different in nature; 20kyr either side of the MIS KM5c, changes in orbital forcing produced less

than a 1°C change in global annual mean temperatures and regionally less than 3°C. In contrast, 20kyr either side of MIS K1 had considerably more variability with annual temperatures exceeding 7°C over terrestrial regions. Similarly, the seasonal analysis displayed maximum differences in surface temperatures in the 20kyr surrounding each interglacial peak of ~10°C for KM5c but reaching ~20°C for K1.

The temperature differences shown in chapter 2 around the modelled interglacials KM5c and K1 demonstrate the complications of comparing time averaged proxy data to time specific model simulations. New initiatives reconstructing time slices within the mPWP are therefore a more appropriate target for future data-model comparison (Haywood et al., 2013). More specifically, the results in chapter 2 suggest that when selecting a target for a time slice reconstruction it would be prudent to pick MIS KM5c (or similar) rather than an interglacial more akin to K1. As has been shown in chapter 2, MIS K1 has highly variable temperatures solely due to orbital forcing in the surrounding 20kyrs. Any miscorrelation of proxy records around K1 would result in larger temperature differences than for an interglacial like KM5c that is surrounded by less variable temperature changes. The larger variation in seasonal temperatures also has important implications for DMC if the proxy data reflects the growing season rather than mean annual.

Chapter 2 also assessed the timing of peak warming in the simulations 20kyr before and after the interglacial peaks. This showed that the warmest temperatures in the 40kyr window are not necessarily synchronous. This has important implications for aligning globally distributed proxy temperature time series (so that warm peaks correlate). In DMC, there are many areas where Pliocene model simulations appear to underestimate warming compared to the geological data, such as the high latitudes. Given that peak warming was diachronous then this can explain some of this discrepancy when comparing the geological data representing multiple orbits to a single model simulation. This has potential implications for older time periods as the effects of time averaging or miscorrelation are likely to be exacerbated further back in time due to weaker chronological constraints on proxy data.

5.2.2 RQ2: To what degree does orbital forcing drive changes in surface climatological and land cover response between four interglacial events in the mPWP and how does the addition of vegetation feedbacks in a model alter this?

The nature of vegetation change in response to orbital forcing has not been fully constrained in Pliocene modelling studies to date. The initial results presented in chapter 3 are based on four simulations run with HadCM3 with the specific orbit representing the peak of four interglacials in the middle Piacenzian stage of the LR04 stack, MIS G17, K1, KM3 and KM5c. The simulated vegetation is predicted by running an offline vegetation model (BIOME4) with the HadCM3 climatology for each interglacial and compared to each other interglacial and also the PRISM3 vegetation reconstruction. To better understand the link between orbital forcing and vegetation changes this chapter also includes analysis of the seasonal range of surface temperatures of the interglacials. The vegetation feedback with orbital forcing is also examined, with a further four simulations of the interglacials MIS G17, K1, KM3 and KM5c completed with a dynamic vegetation model (TRIFFID). The surface temperature and precipitation, seasonal temperature range and predicted vegetation from both the BIOME4 and TRIFFID models were compared between the interglacials, with and without the inclusion of dynamic vegetation.

The degree of surface temperature warming and precipitation response in the results was strongly controlled by orbital forcing. This translated into variations in seasonality and moisture availability which had a large effect on the prediction of land cover regionally. Changes in the seasonality of surface temperature and precipitation response is especially amplified in the simulations run with dynamic vegetation. This is seen most strongly over terrestrial areas, particularly in MIS K1 and KM3, due to the largest seasonal differences in insolation. In chapter 3 this is shown in North America and Eurasia where mid-Pliocene experiments with increased insolation during northern hemisphere spring/summer and decreased insolation during autumn/winter (compared to a mid-Pliocene scenario with a near modern orbital forcing) led to a strong climate response and associated vegetation climate feedbacks, resulting in replacement of forest with open types of vegetation. Palaeobotanical data from Eurasia shows that while there were variations between forest cover and more open vegetation, the trees remained a dominant feature of the landscape, especially during warmer periods. This indicates that the modelled climate and vegetation response is overestimated in these continental interiors,

potentially linked to a large reduction in soil moisture due to increased surface temperatures alongside little or no increase in precipitation. This response has been noted in other models for different time periods such as the Holocene CMIP5 simulations (Harrison et al., 2015; Bartlein et al., 2017).

5.2.3 RQ3: How does orbital forcing influence a critical component of the climate system, the Indian monsoon, during mPWP interglacials?

In general, efforts in climate modelling and proxy reconstructions during the Piacenzian Stage have focused on reconstructing an average East Asian Pliocene monsoon. There has been relatively little attention dedicated to the Indian Monsoon system in the proxy and climate modelling communities and no specific work dedicated to modelling monsoon variability due to orbital forcing in the Pliocene.

The results in chapter 4 are the first time the Indian monsoon is simulated for warm interglacials of the Piacenzian Stage. An average summer monsoon is simulated for the same four interglacials investigated in the previous chapter 3 and a pre-industrial simulation. Chapter 4 was structured to compare the MIS KM5c simulations (near modern orbit) to the pre-industrial and then the three interglacials with stronger orbital forcing compared to MIS KM5c. To compare the simulated monsoons quantitatively, monsoon indices are calculated. The Extended Indian Monsoon Rainfall (EIMR) index is the precipitation over the Indian subcontinent and neighbouring oceans and lands affected by the Indian monsoon. The Monsoon Hadley Index (MHI) is a measure of the Hadley circulation averaged over the same region as the EIMR (Goswami et al., 1999). The monsoon indices were compared along with the simulated climatological patterns of Indian monsoon for the four interglacial periods.

While both monsoon indices are higher for MIS KM5c than the pre-industrial simulation for the summer Indian monsoon, there is not a significant difference. This indicates there may have been a slightly more intense summer monsoon in the Pliocene simulation with a near modern orbit, likely due to higher CO_2 increasing temperatures and precipitation. Whereas, the other three interglacials with stronger orbital forcing simulate a more intense summer monsoon than KM5c, particularly in K1 and KM3 with dramatic increases in seasonal temperatures. The results

also indicated that a stronger orbital forcing triggers a more variable summer monsoon. The model results of chapter 4 showed how much orbital forcing in combination with Pliocene boundary conditions can affect the strength of the summer monsoon during the interglacials simulated. There were stronger differences in the simulated summer monsoon between the interglacials with the strongest orbital forcing (K1 and KM3) compared to the KM5c interglacial, where the only difference between the simulations was orbital forcing, than there was between KM5c and the pre-industrial simulation, where the difference was the implementation of all the other Pliocene boundary conditions.

5.3 Wider implications and scientific advances

The overall conclusions of all the chapters in this thesis found the simulated climate of the interglacials to be variable, in both magnitude of change and spatial distribution. From the results of this thesis there is increased understanding about the climate variability driven by orbit in the Pliocene. This variability, shown in the results chapters, promotes the general importance of no longer thinking of the Pliocene as a homogenous stable climate interval. The work presented here both aids understanding and demonstrates the need to shift the interpretation of Pliocene climate to be more akin to how we understand the Quaternary; how the climate shifts between glacial and interglacial cycles and how one glacial or interglacial is not necessarily like another, with unique regional features and responses. Continuing to think of the Pliocene as a warm stable period is not conducive to furthering our understanding of how past warm climates evolve nor the ability of models to simulate them. More specifically, in terms of data-model comparison, this thesis has conclusively shown the impact of variations in orbit is considerable throughout the mPWP. If evaluating the performance of climate models is the purpose of the data-model comparison, comparing it with time averaged proxy data does not yield reliable enough results to draw conclusions on model performance.

One of the results in chapter 3, the widespread loss of forest vegetation types simulated over the continental interiors of North America and Eurasia particularly in the interglacials MIS K1 and KM3, differs from reconstructed vegetation from palaeobotanical records. This contrasts with

previous Pliocene simulations with modern orbit that compared quite favourably with the geological data, such as in the data-model comparison in Salzmann et al. (2008). In this case, if a series of palaeo experiments (run with a modern orbit) were used to test model performance and compared to data, the resulting predicted vegetation would indicate good model performance. In chapter 3, it was only after the interglacials were simulated with a very different orbit to modern, causing increased seasonality in an area with existing high seasonal contrasts, that a change in the hydrological regime was observed. This result therefore suggests, if palaeo experiments are used as a benchmark for model performance, multiple palaeo scenarios with different forcings (including orbit) are necessary to fully evaluate model ability.

In the literature, there have been discussions in general terms about enhanced monsoons in the Pliocene, often followed by a suggestion about the potential for increased monsoon strength in the future. What has been explored in chapter 4, however, is that within the interglacial simulated that is most relevant in the context of the immediate future, i.e. the interval with near modern orbit, there is some increase in the strength of the Indian monsoon, but this change is not significant. The interglacials where the larger changes in summer Indian monsoon strength are shown, are the intervals with the stronger orbital forcing (MIS K1 and KM3) due to increased summer insolation. The assumption that Pliocene monsoon studies demonstrate that in a warmer world you have enhanced monsoons is therefore an oversimplification. Arguably, if studies aim to enhance the connections between Pliocene climates and lessons for the future, one way would be to concentrate on time intervals where the warming is due to CO_2 rather than a strong orbital forcing. The results throughout this thesis have added to the understanding of the differences between interglacials in the Pliocene and what interglacial to target in the Pliocene if seeking to compare to current/future climate change.

Before the start of this thesis, work had been undertaken to select a new 'time slice' for future data-model comparisons. The time slice selected in Haywood et al. (2013) was MIS KM5c. This time slice is a target for both the PRISM4 and PlioMIP2 projects (Dowsett et al., 2016; Haywood et al., 2016). The analysis in this thesis, which concentrated on four interglacials, found that even after further analysis KM5c remained the best choice of interglacials within the mPWP for future study. As discussed in section 5.2.1, the surface temperatures simulated around KM5c were less variable than around K1, due the stability in orbital forcing immediately before and after KM5c.

There is, therefore, a window in which palaeotemperature information from geological data can be imperfectly correlated to KM5c, but may still be essentially representative of the general conditions that existed during this interglacial (Haywood et al., 2013). In chapter 3, due to this stable orbit, the considerable increase in seasonality leading to intense summer temperatures and large reductions in forest vegetation cover is not simulated to the same extent for KM5c as it is for the other interglacials. One aim of the future PRISM4 and PlioMIP2 projects is to undertake another joint data-model comparison, centred on the MIS KM5c. If the target was another of the interglacials simulated in chapter 3, this potential model bias of simulating too arid climate in the continental interiors would be a more significant issue in the data-model comparison.

5.4 Limitations and future work

As described above, the future PlioMIP2 and PRISM4 projects will be centred on MIS KM5c (3.205 Ma). The future data-model comparison will avoid the issue discussed in this thesis of comparing a time slab of the average of multiple orbital configurations with a simulation with one specific orbit. This will be a more accurate way of ascertaining model performance in the Pliocene and enable further discussion into the areas that show discord, knowing it is not due to the orbital variability not previously considered.

As there is now a better understanding of the potential climate variability in the Pliocene, there is a need for different ways to approach this uncertainty. It is not always practical to run many snapshot experiments, as in chapter 1 of this thesis, especially with newer versions of GCMs. To constrain this orbital uncertainty for data-model comparisons, where data cannot be confidently placed in time, there is a need for new methodologies. One such method is the development of an emulator to reconstruct the behaviour of a climate model, a fast, computationally cheap statistical model to measure uncertainty and enable a more direct comparison between model output and time averaged data. In a recent study by Lord et al. (2017) an emulator was applied to the Late Pliocene and compared to palaeo proxy data. The authors found the emulator provided a useful and powerful tool for rapidly simulating long-term evolution of climate (Lord et al., 2017).

Another area where there is potential for further work in understanding Pliocene climate variability, is running transient simulations to enable an easier comparison to time series data. A recent example of the potential of this is seen in De Boer et al. (2017), where a 3-D ice sheet model is used to simulate ice volume over Greenland and Antarctica forced with the snapshot experiments around MIS KM5c and K1 described in chapter 2. The transient ice-sheet predictions indicated the Antarctic and Greenland ice sheets were relatively stable during KM5c and both contributed to sea level rise relative to present day (De Boer et al., 2017). Whereas, during MIS K1 the ice sheets varied out of phase, with maxima and minima of the Antarctic and Greenland ice sheets not occurring at the same time (De Boer et al., 2017).

Two key variables that have not been changed in the model are CO_2 concentrations and ice sheets. New high-resolution CO_2 records indicate a level of variability that has not been accounted for here. The $\delta^{11}B$ pCO_2 record from Martínez-Botí et al. (2015) observed orbital-scale variations of similar magnitude to that exhibited by published late and mid-Pleistocene records with the pCO_2 varying between 280 and 420ppm through the mid-Pliocene. Therefore, keeping the CO_2 at 405ppm in all the simulations is an oversimplification as its demonstrated variation would have impacted the predicted climate. In all the simulations, ice sheets were set to the PRISM3D reconstruction and had no dynamic element. As indicated in the compilation sea level curve of Miller et al. (2012) (Fig. 1.3) the sea level, and therefore ice sheets, were changing in the Pliocene. In addition, if the ice sheets were waxing and waning throughout the Pliocene as is suggested in Fig.1.3, it would also be expected that the palaeogeography would change which has not been included in this study.

A large amount of climate variability has been seen in the simulations of interglacials in the Pliocene because of orbital forcing alone (chapter 2) and including vegetation feedback to the orbital forcing (chapters 3 and 4). There are however, many other climate feedbacks associated with orbital forcing that have not been considered which have the potential to either suppress or enhance the patterns of climate change simulated in this thesis. Therefore, further work using a model with additional earth system feedbacks may simulate a more realistic impact of orbital forcing on Pliocene climate. One example of feedbacks omitted from this study includes the chemistry-climate feedbacks. An Earth system model used to simulate terrestrial ecosystem emissions and atmospheric chemical composition in the mid-Pliocene indicate the potential for

chemistry-climate feedbacks to have a large impact on the resulting simulated climate (Unger & Yue, 2014). These feedbacks were found to operate on centennial and millennial timescales and contributed a net global warming that is +30-250% of the carbon dioxide effect (Unger & Yue, 2014). Another factor not accounted for is the representation of dust in the climate model and the inclusion of the indirect effect of dust through its role as ice nuclei in cloud formation. A study by Sagoo & Storelvmo (2017) suggested that the inclusion of dust as an aerosol indirect effect may improve regional deficiencies in palaeoclimate simulations and showed how an inclusion of this feedback led to increased warming in a mid-Pliocene simulation.

While the focus of Pliocene study has predominantly been to investigate the climate of a warmer world, episodic glaciation events and accompanying sea-level fluctuations have been recorded in benthic isotope records (De Schepper et al., 2013). A review paper collating the available terrestrial and marine evidence for these glacial events identified major glacial expansion on four occasions during the Pliocene (c. 4.9-4.8, 4.0, 3.6 and 3.3 Ma) prior to the intensification of the Northern Hemisphere glaciation in the latest Pliocene (De Schepper et al., 2013). These events are exceptions to the globally warm conditions and high CO_2 concentrations in the Pliocene. Indeed, the mechanisms causing the glacials are not currently understood. The preservation of the terrestrial evidence of glacial events is a problem in the Pliocene due to their removal by more extensive Quaternary glacial advances (De Schepper et al., 2013). Dolan et al., (2015) undertook the first AOGCM experiments into one of these identified glacial events, MIS M2 by implementing plausible ice sheet configurations into the model to test whether larger-than-modern ice sheets may have existed during this event. A comparison to the available data reinforced the possibility of larger ice sheets in the Northern and Southern Hemisphere during the M2 event. The study highlighted however, a need for more proxy data that recorded this event (Dolan et al., 2015). A study testing the hypothesis proposed by De Schepper et al. (2013), that re-opening and closing of the shallow Central America Seaway explained both the onset and termination of the M2 event, was undertaken using a fully coupled AOGCM and dynamic ice sheet model (Tan et al., 2017). The results found that even with the most favourable conditions for ice sheet growth and associated feedbacks (low CO_2, orbit, vegetation and ice sheets) a sea level drop of 16m was simulated which corresponds to the lowest estimates of the proxy derived estimates (Tan et al., 2017). It was also found that the closure of the Central America Seaway

had a negligible effect on ice sheet melt and cannot explain the termination of the MIS M2 event (Tan et al., 2017).

If the aim is for a full understanding of climate variability throughout the Pliocene, then this needs to be inclusive of the colder events. It is clear the understanding of the mechanisms and causes for these glacial events needs further investigation. There is huge potential for both modelling and data groups to investigate these glacials in the Pliocene which would significantly add to the current understanding of Pliocene climate variability. As shown in this thesis, not all interglacials are similar in nature and the same would be expected for Pliocene glacials.

Another area that would significantly add to the understanding of Pliocene climate variability is investigation into the mechanism and causes of the transition from the MIS M2 glacial into the KM3 interglacial. In general, the shift from comparing absolute numbers in both modelling and proxy data to exploring the amplitude of change throughout the Pliocene has started to provide a more nuanced appreciation of climate variability in this time and future studies continuing this theme will only improve understanding.

References

Bartlein, P.J., Harrison, S.P. & Izumi, K. (2017). Underlying causes of Eurasian midcontinental aridity in simulations of mid-Holocene climate. *Geophysical Research Letters*. 44 (17). pp. 9020–9028.

De Boer, B., Haywood, A.M., Dolan, A.M., Hunter, S.J. & Prescott, C.L. (2017). The transient response of ice volume to orbital forcing during the warm Late Pliocene. *Geophysical Research Letters*. 44.

Dolan, A.M., Haywood, A.M., Hunter, S.J., Tindall, J.C., Dowsett, H.J., Hill, D.J. & Pickering, S.J. (2015). Modelling the enigmatic Late Pliocene Glacial Event - Marine Isotope Stage M2. *Global and Planetary Change*. 128. pp. 47–60.

Dowsett, H., Dolan, A., Rowley, D., Moucha, R., Forte, A.M., Mitrovica, J.X., Pound, M., Salzmann, U., Robinson, M., Chandler, M., Foley, K. & Haywood, A. (2016). The PRISM4 (mid-Piacenzian) paleoenvironmental reconstruction. *Climate of the Past*. 12 (7). pp. 1519–1538.

Goswami, B.N., Krishnamurthy, V. & Annmalai, H. (1999). A broad-scale circulation index for the interannual variability of the Indian summer monsoon. *Quarterly Journal of the Royal Meteorological Society*. 125 (554). pp. 611–633.

Harrison, S.P., Bartlein, P.J., Izumi, K., Li, G., Annan, J., Hargreaves, J., Braconnot, P. & Kageyama, M. (2015). Evaluation of CMIP5 palaeo-simulations to improve climate projections. *Nature Climate Change*. 5 (8). pp. 735–743.

Haywood, A.M., Dolan, A.M., Pickering, S.J., Dowsett, H.J., McClymont, E.L., Prescott, C.L., Salzmann, U., Hill, D.J., Hunter, S.J., Lunt, D.J., Pope, J.O. & Valdes, P.J. (2013). On the identification of a Pliocene time slice for data-model comparison. *Philosophical transactions. Series A, Mathematical, physical, and engineering sciences*. 371 (2001). p.p. 20120515.

Haywood, A.M., Dowsett, H.J., Dolan, A.M., Rowley, D., Abe-Ouchi, A., Otto-Bliesner, B., Chandler, M.A., Hunter, S.J., Lunt, D.J., Pound, M. & Salzmann, U. (2016). The Pliocene Model Intercomparison Project (PlioMIP) Phase 2: Scientific objectives and experimental design. *Climate of the Past*. 12 (3). pp. 663–675.

Lord, N.S., Crucifix, M., Lunt, D.J., Thorne, M.C., Bounceur, N., Dowsett, H., O'Brien, C.L. & Ridgwell, A. (2017). Emulation of long-term changes in global climate: Application to the late Pliocene and future. *Climate of the Past Discussions*. pp. 1–47.

Martínez-Botí, M.A., Foster, G.L., Chalk, T.B., Rohling, E.J., Sexton, P.F., Lunt, D.J., Pancost, R.D., Badger, M.P.S. & Schmidt, D.N. (2015). Plio-Pleistocene climate sensitivity evaluated using high-

resolution CO2 records. *Nature*. 518 (7537). pp. 49–54.

Miller, K.G., Wright, J.D., Browning, J. V., Kulpecz, A., Kominz, M., Naish, T.R., Cramer, B.S., Rosenthal, Y., Peltier, W.R. & Sosdian, S. (2012). High tide of the warm Pliocene: Implications of global sea level for Antarctic deglaciation. *Geology*. 40 (5). pp. 407–410.

Sagoo, N. & Storelvmo, T. (2017). Testing the sensitivity of past climates to the indirect effects of dust. *Geophysical Research Letters*. 44 (11). pp. 5807–5817.

Salzmann, U., Haywood, A.M., Lunt, D.J., Valdes, P.J. & Hill, D.J. (2008). A new global biome reconstruction and data-model comparison for the Middle Pliocene. *Global Ecology and Biogeography*. 17 (3). pp. 432–447.

De Schepper, S., Gibbard, P.L., Salzmann, U. & Ehlers, J. (2013). A global synthesis of the marine and terrestrial evidence for glaciation during the Pliocene Epoch. *Earth-Science Reviews*. 135. pp. 83–102.

Tan, N., Ramstein, G., Dumas, C., Contoux, C., Ladant, J.B., Sepulchre, P., Zhang, Z. & De Schepper, S. (2017). Exploring the MIS M2 glaciation occurring during a warm and high atmospheric CO2 Pliocene background climate. *Earth and Planetary Science Letters*. 472. pp. 266–276.

Unger, N. & Yue, X. (2014). Strong chemistry-climate feedbacks in the Pliocene. *Geophysical Research Letters*. 41 (2). pp. 527–533.

APPENDIX A

SUPPLEMENTARY FIGURES FOR CHAPTER 2

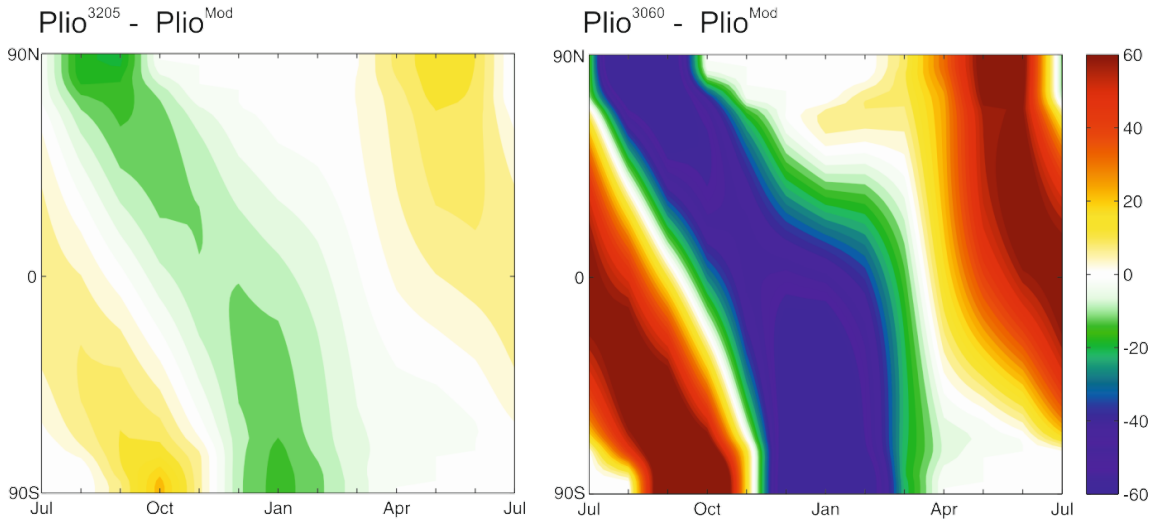

Figure A.1 Incoming short wave radiation flux derived from HadCM3 (Wm^{-2}) for the MIS KM5c ($Plio^{CTL}KM5c^{3205}$) (Left) and MIS K1 ($Plio^{CTL}K1^{3060}$) (Right) minus a Pliocene experiment with a modern orbit.

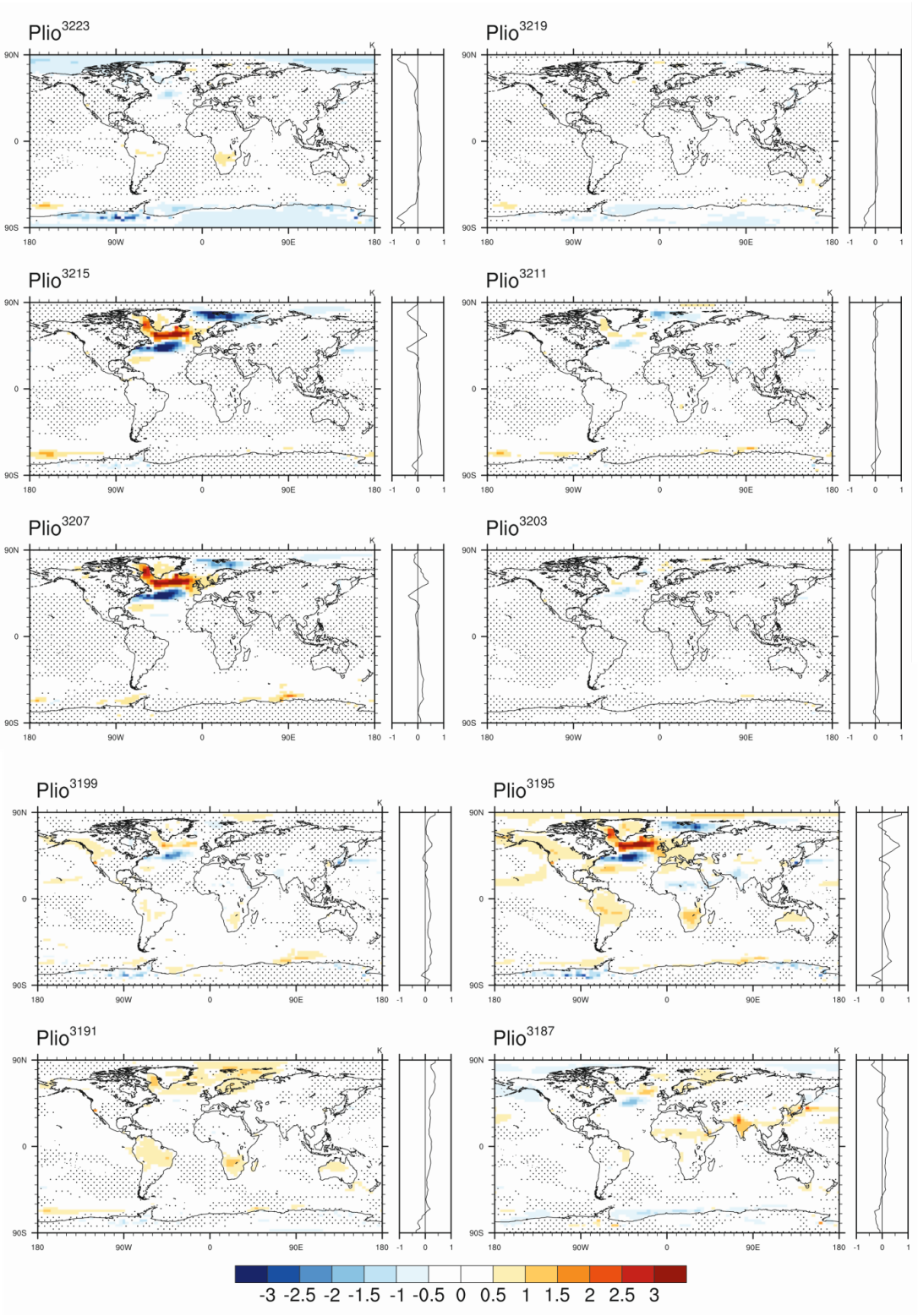

Figure A.2 Annual mean Pliocene SAT (°C) predictions from HadCM3 for 10 additional orbital sensitivity simulations minus the MIS KM5c control ($Plio^{CTL}KM5c^{3205}$). Stippling indicates the SAT changes that are statistically insignificant according to the Student's t-test. Zonal SAT anomalies are shown to the right of each simulation.

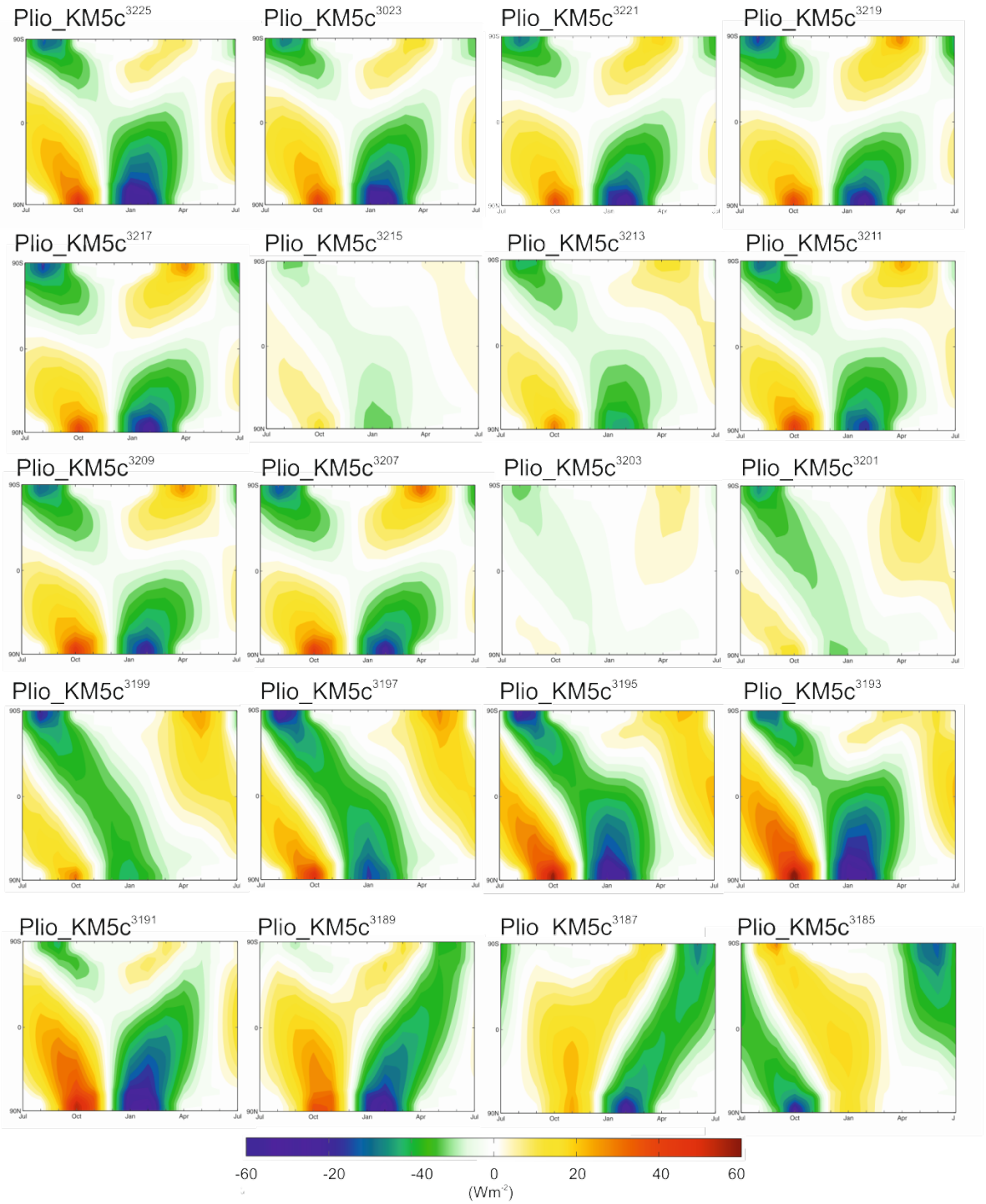

Figure A.3 Incoming short wave radiation flux derived from HadCM3 (Wm^{-2}) for 20 orbital sensitivity experiments minus the MIS KM5c control ($Plio^{CTL}KM5c^{3205}$).

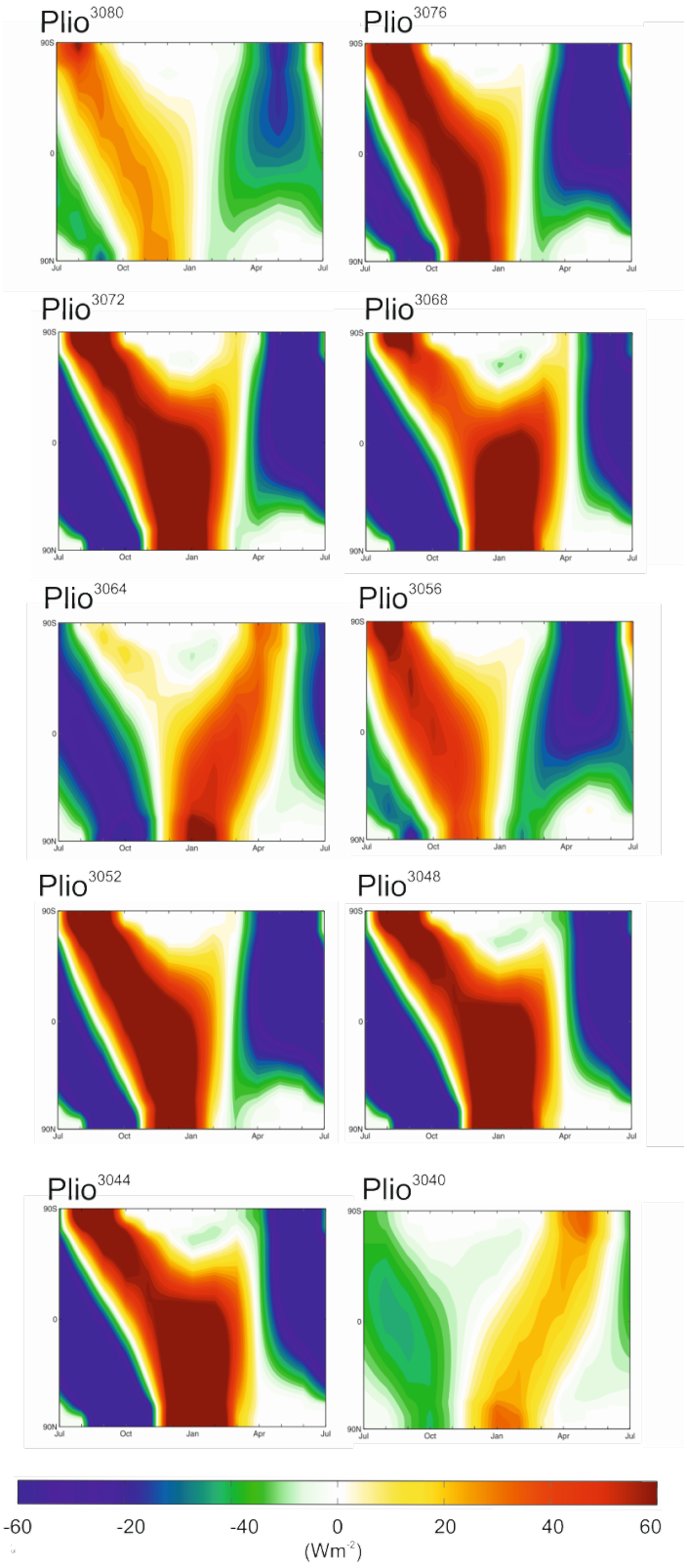

Figure A.4 Incoming short wave radiation flux derived from HadCM3 (Wm^{-2}) for 10 orbital sensitivity experiments minus the MIS K1 control ($Plio^{CTL}K1^{3060}$).

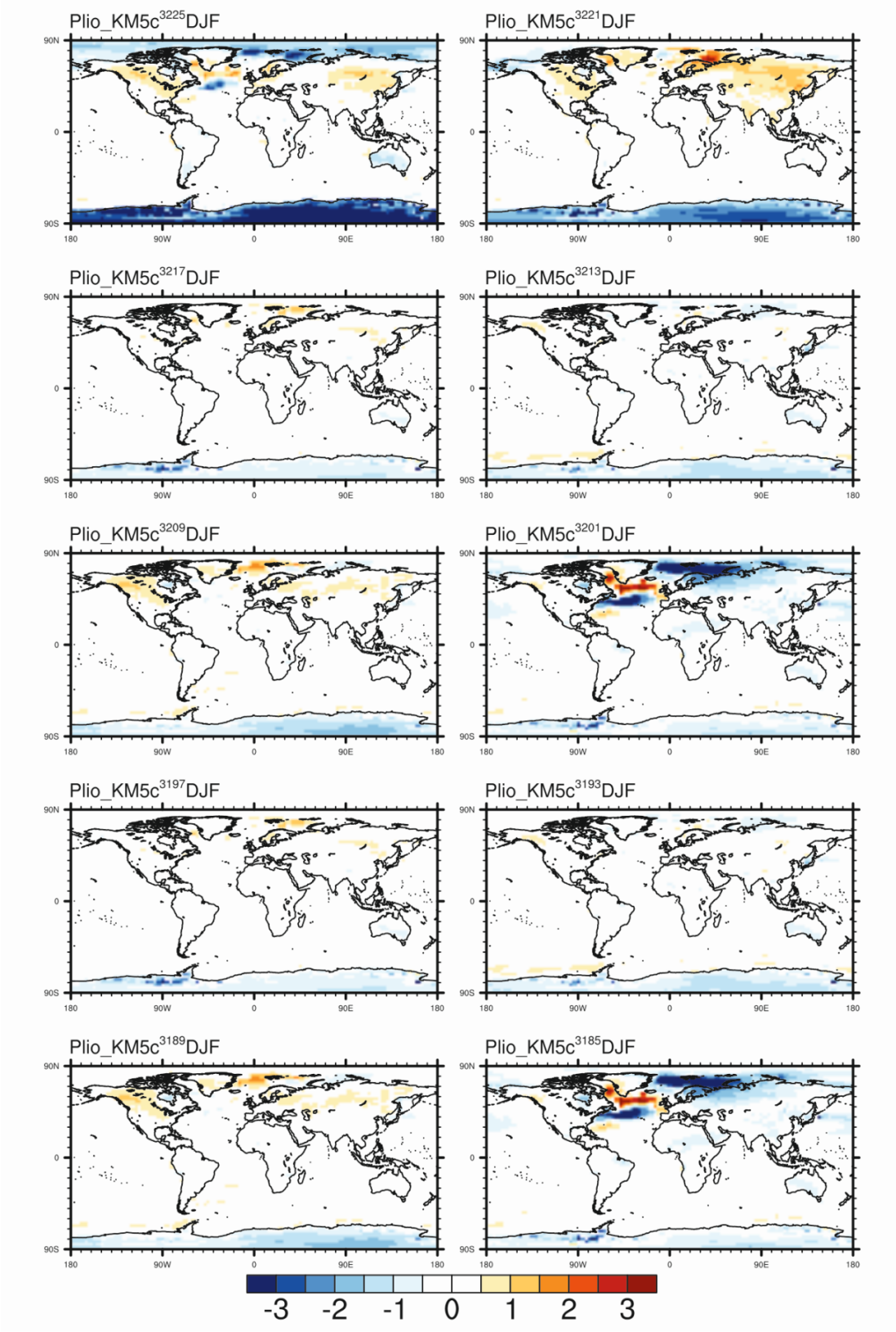

Figure A.5 Mean Pliocene SAT for December, January and February (°C) predictions from HadCM3 for 10 orbital sensitivity simulations minus the MIS KM5c control ($Plio^{CTL}KM5c^{3205}$).

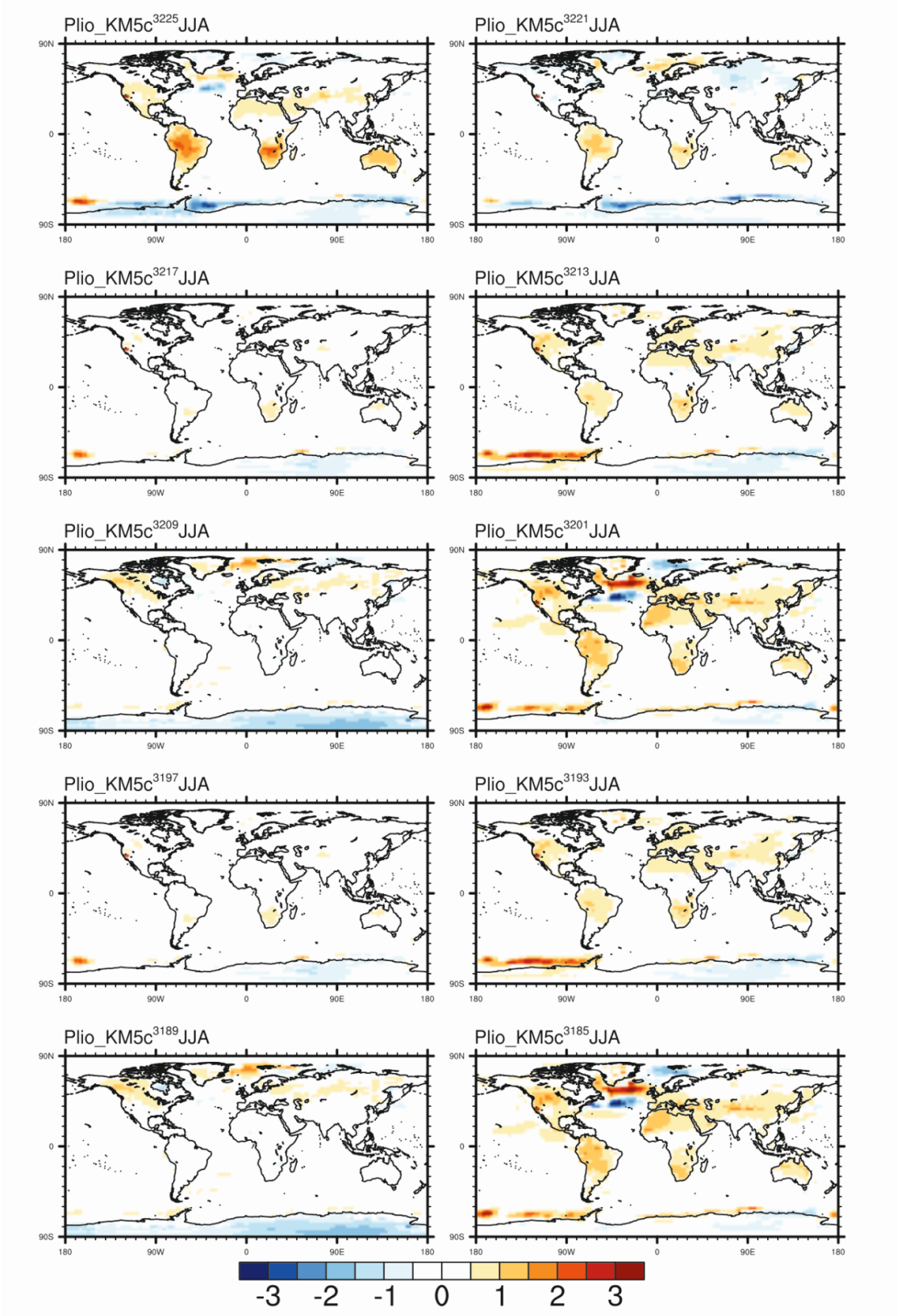

Figure A.6 Mean Pliocene SAT for June, July and August (°C) predictions from HadCM3 for 10 orbital sensitivity simulations minus the MIS KM5c control ($Plio^{CTL}KM5c^{3205}$).

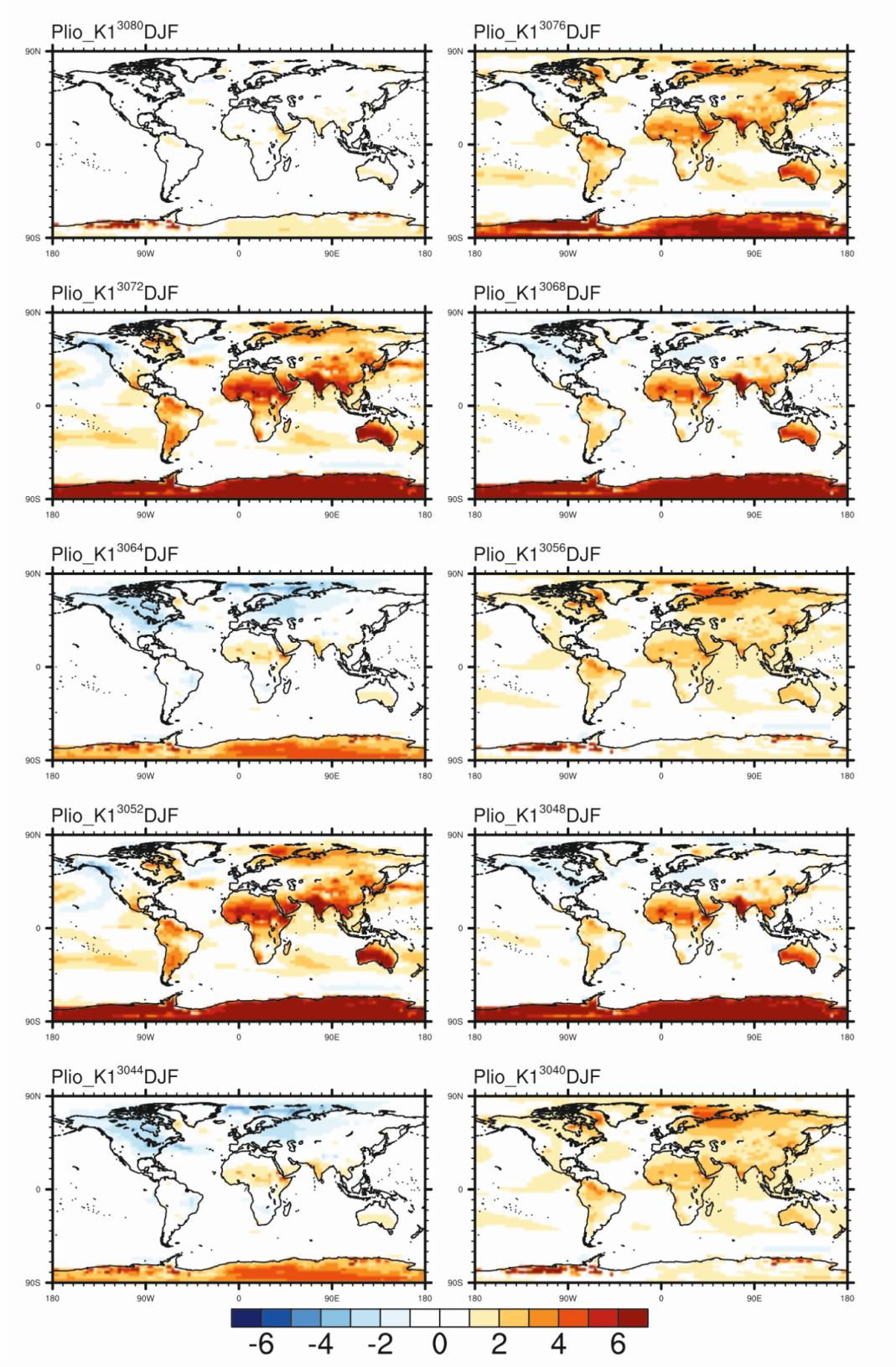

Figure A.7 Mean Pliocene SAT for December, January and February (°C) predictions from HadCM3 for 10 orbital sensitivity simulations minus the MIS K1 control ($Plio^{CTL}K1^{3060}$).

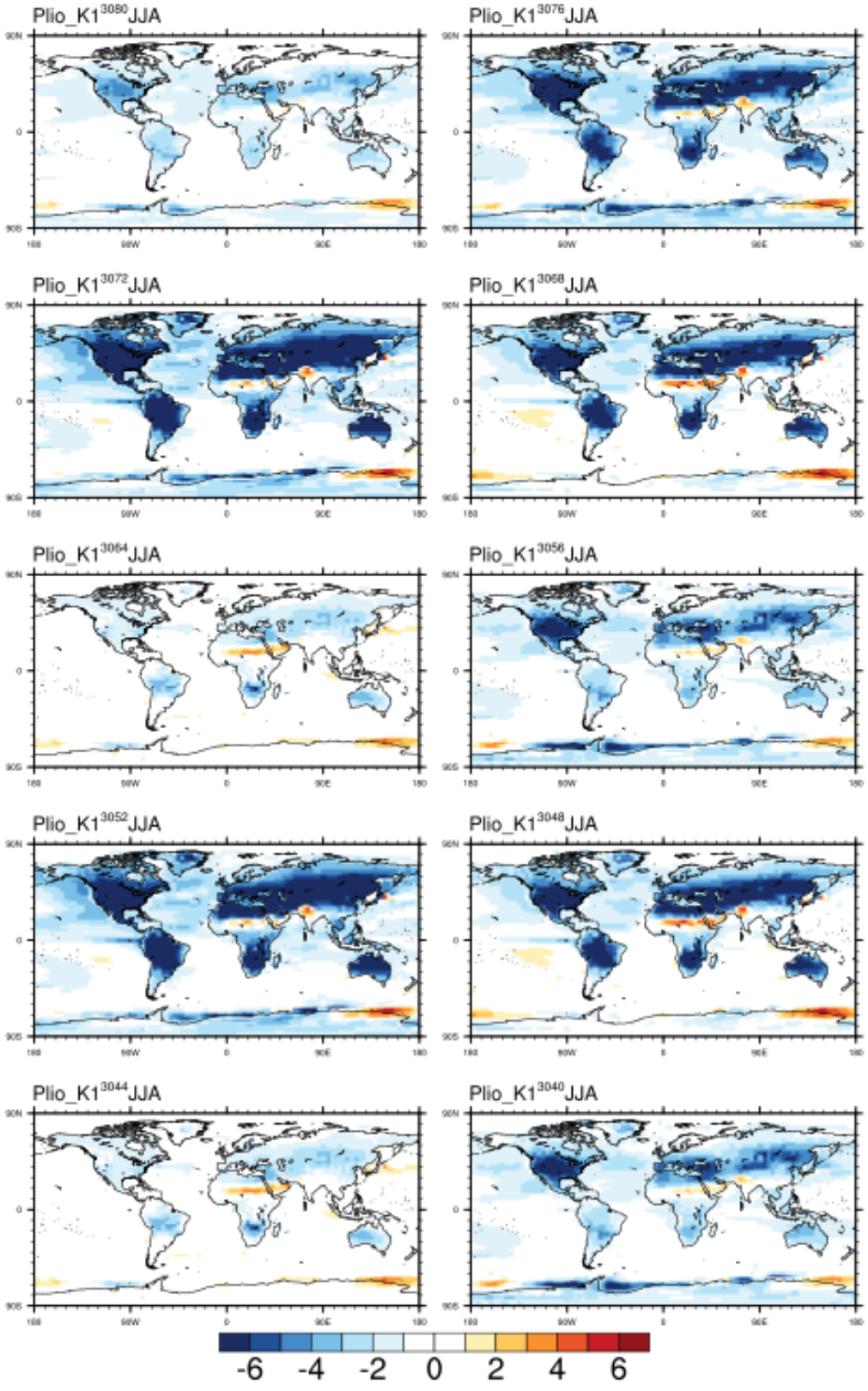

Figure A.8 Mean Pliocene SAT for June, July and August (°C) predictions from HadCM3 for 10 orbital sensitivity simulations minus the MIS K1 control ($Plio^{CTL}K1^{3060}$).

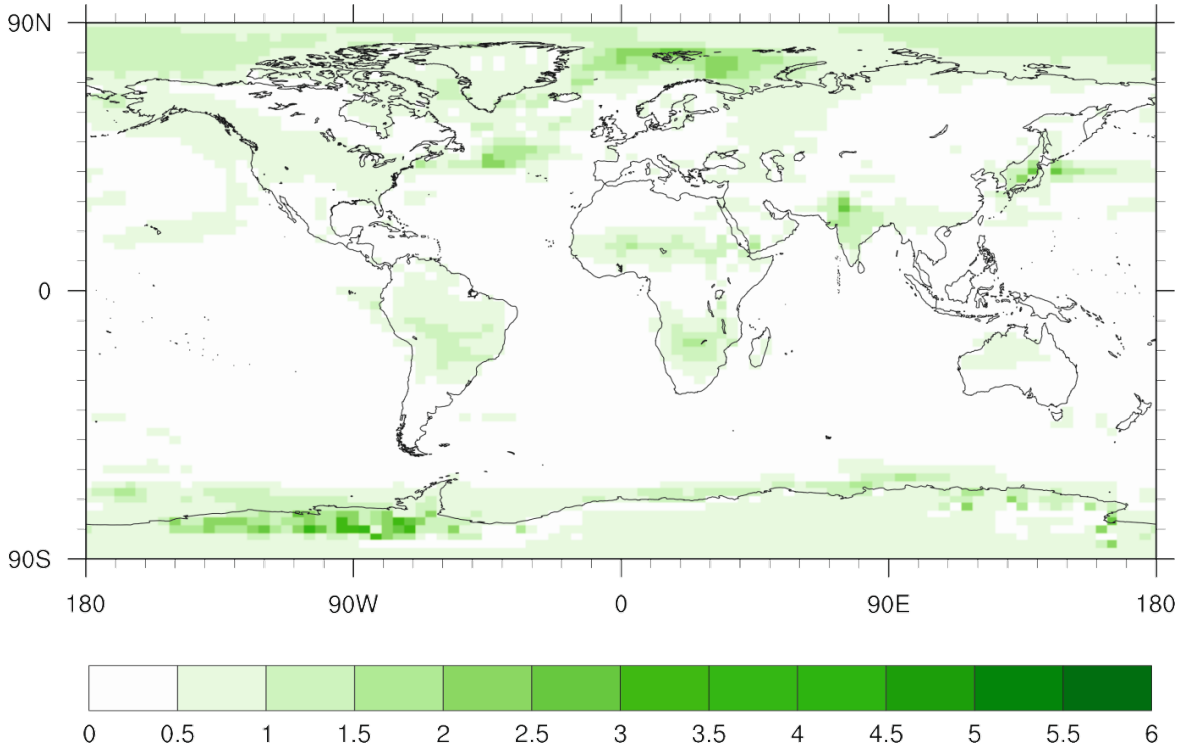

Figure A.9 Maximum Annual SAT change (°C) derived from 10 orbital sensitivity simulations differenced from the MIS KM5c control ($Plio^{CTL}KM5c^{3205}$) in each grid square using results from the combination of the 500 year simulations as well as the smaller number of simulations run for 1000 years

Appendix B

Supplementary Figures for Chapter 3

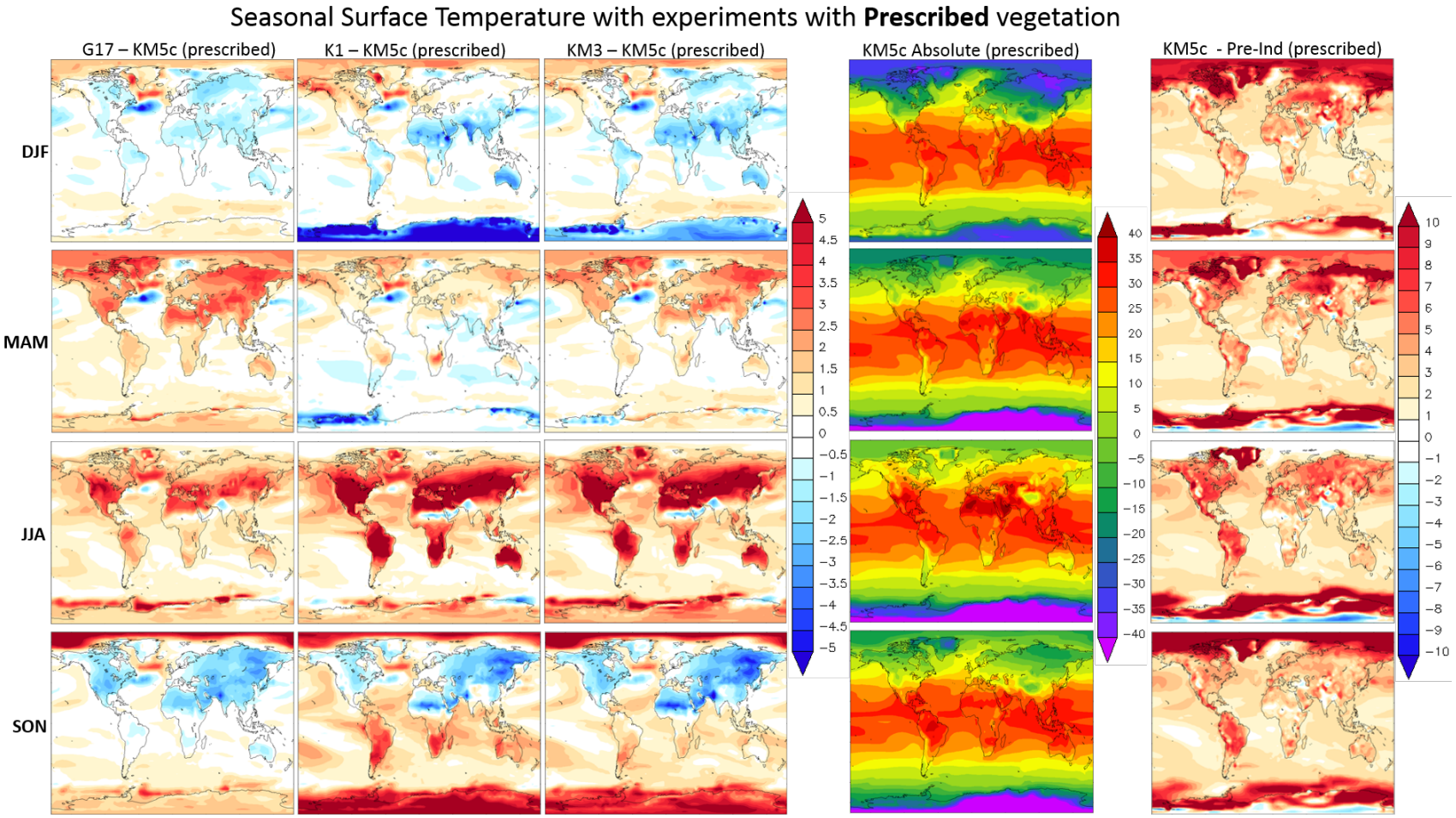

Figure B.1 HadCM3 results with MOSES1 land surface scheme (and prescribed vegetation) showing average seasonal SAT anomalies (°C). DJF (December, January, February), MAM (March, April, May), JJA (June, July, August) and SON (September, October, November).

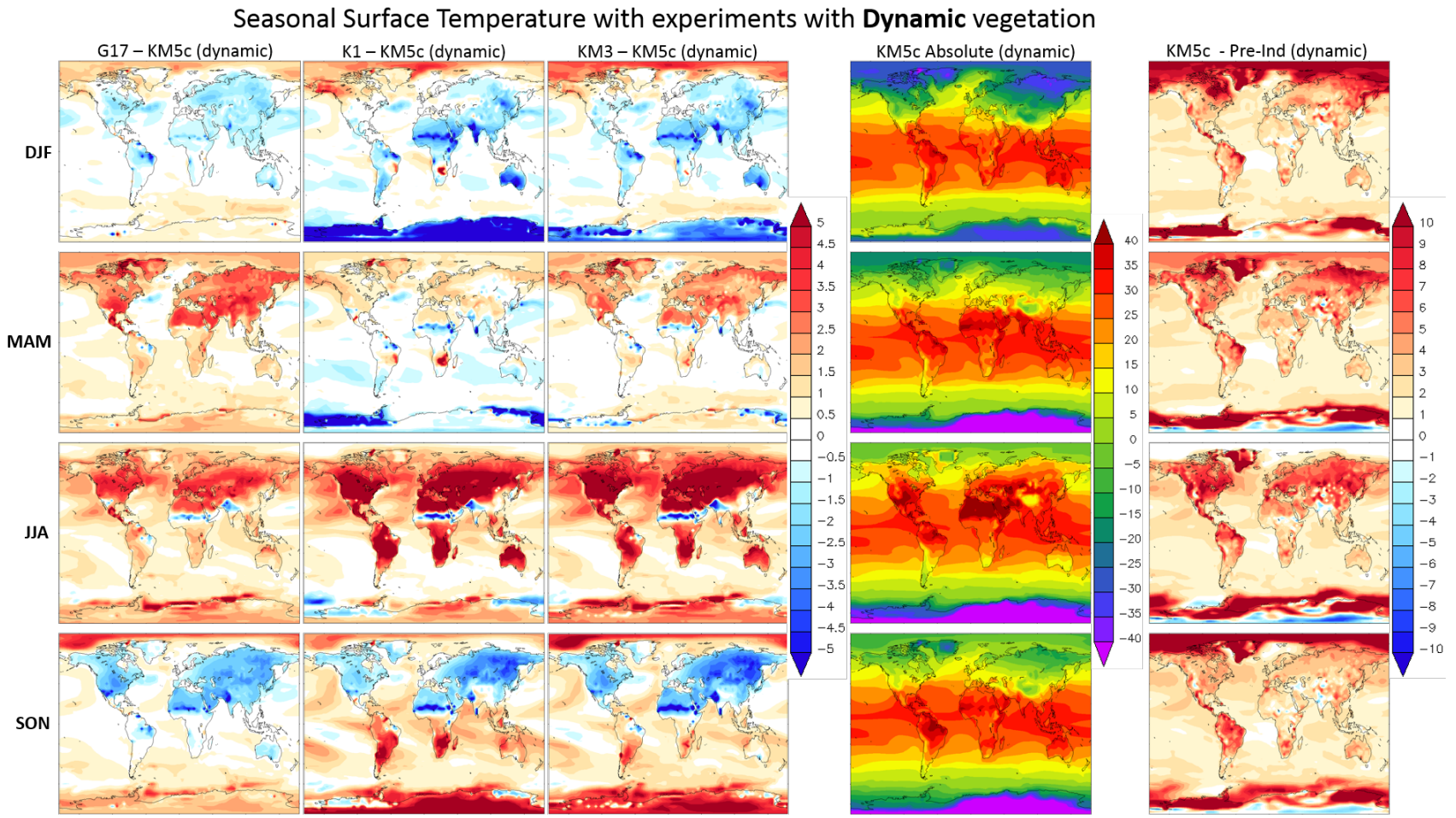

Figure B.2 HadCM3 results with MOSES2.1 land surface scheme (and dynamic vegetation) showing average seasonal SAT anomalies (°C). DJF (December, January, February), MAM (March, April, May), JJA (June, July, August) and SON (September, October, November).

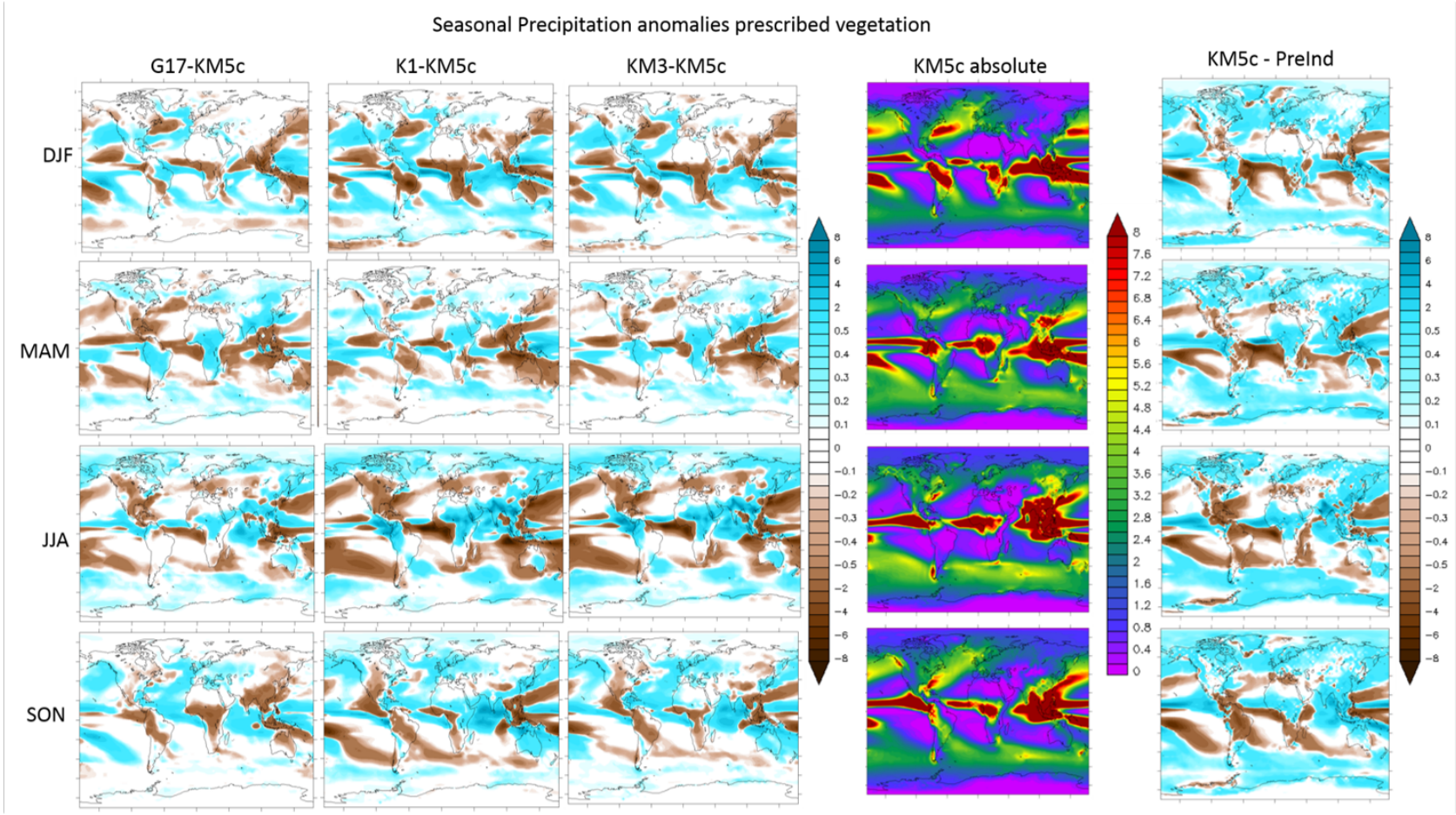

Figure B.3 HadCM3 results with MOSES1 land surface scheme (and prescribed vegetation) showing average seasonal precipitation anomalies (mm/day). DJF (December, January, February), MAM (March, April, May), JJA (June, July, August) and SON (September, October, November).

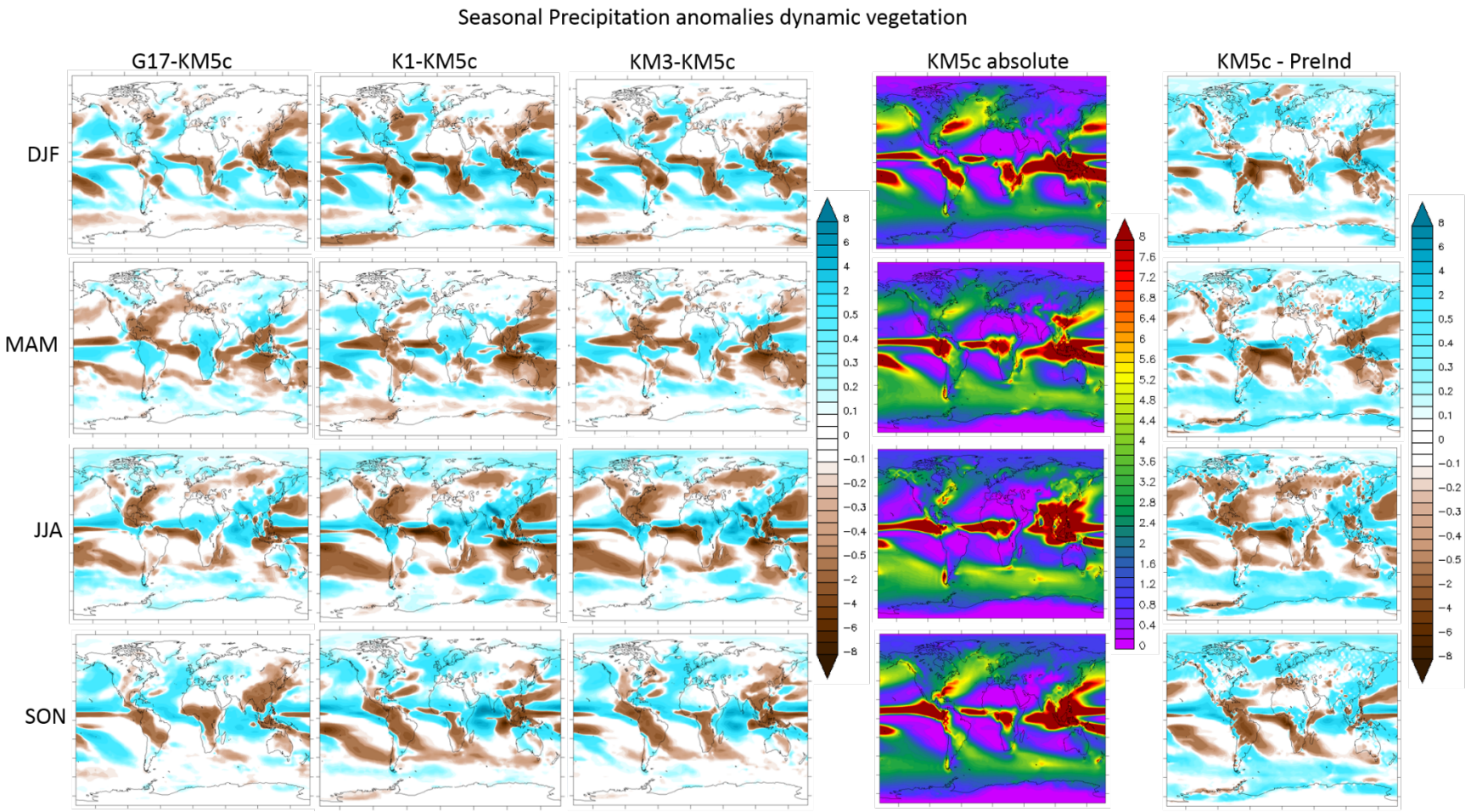

Figure B.4 HadCM3 results with MOSES2.1 land surface scheme (and dynamic vegetation) showing average seasonal precipitation anomalies (mm/day). DJF (December, January, February), MAM (March, April, May), JJA (June, July, August) and SON (September, October, November).

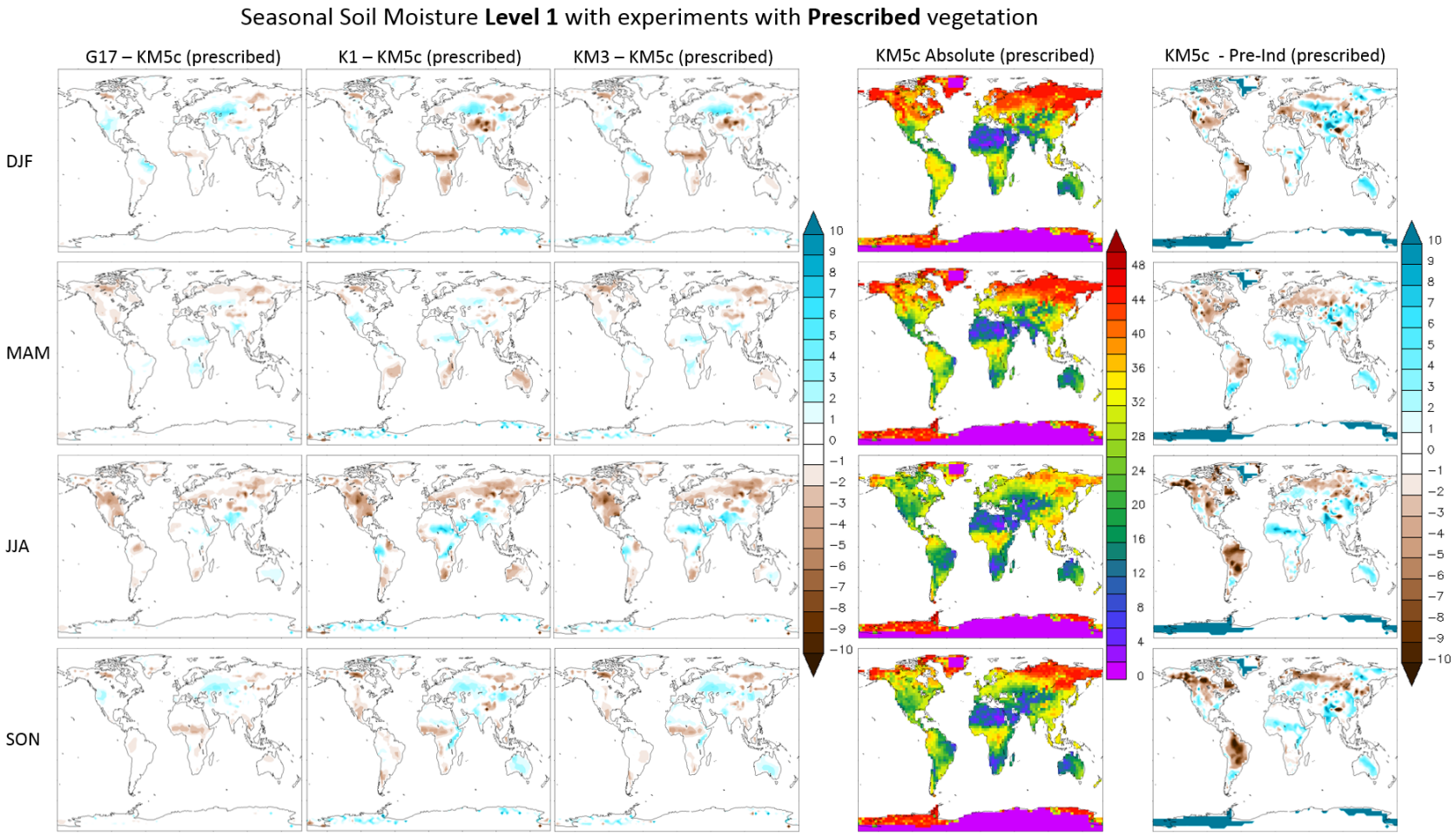

Figure B.5 HadCM3 results with MOSES1 land surface scheme (and prescribed vegetation) showing average seasonal soil moisture anomalies 0.1m from surface (mm/day). DJF (December, January, February), MAM (March, April, May), JJA (June, July, August) and SON (September, October, November).

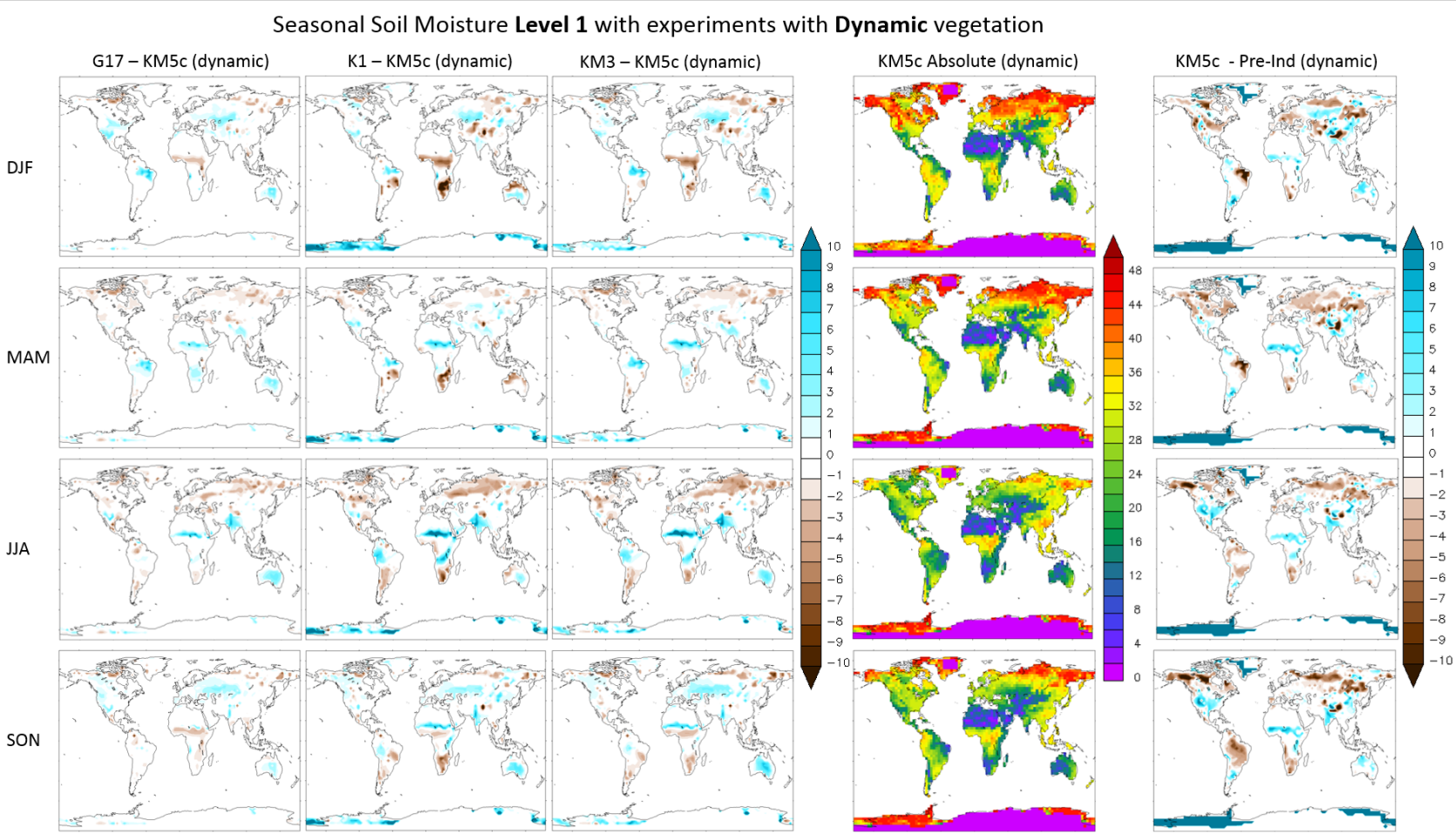

Figure B.6 HadCM3 results with MOSES2.1 land surface scheme (and dynamic vegetation) showing average seasonal soil moisture anomalies 0.1m from surface (mm/day). DJF (December, January, February), MAM (March, April, May), JJA (June, July, August) and SON (September, October, November).

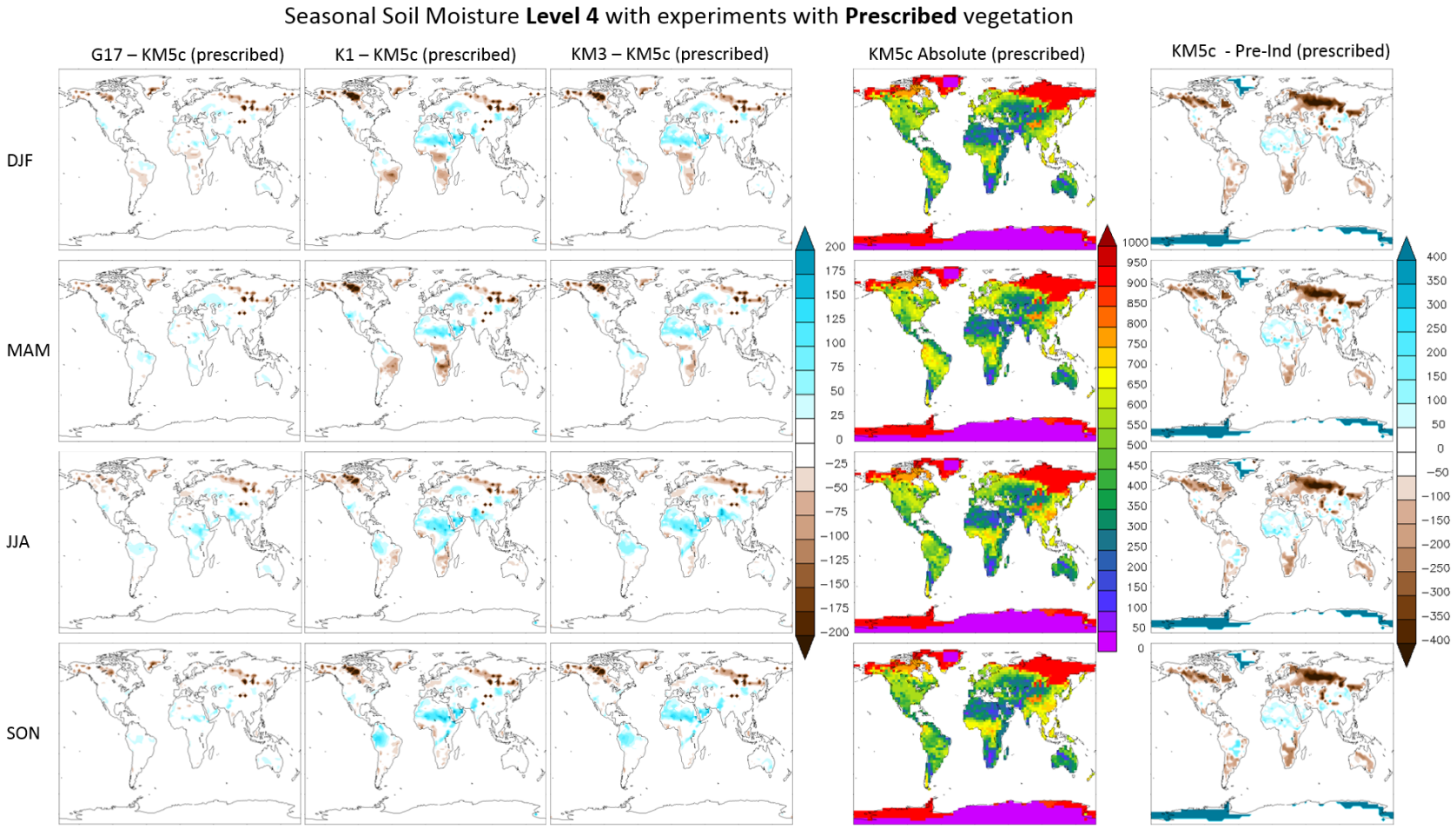

Figure B.7 HadCM3 results with MOSES1 land surface scheme (and prescribed vegetation) showing average seasonal soil moisture anomalies 2m from surface (mm/day). DJF (December, January, February), MAM (March, April, May), JJA (June, July, August) and SON (September, October, November).

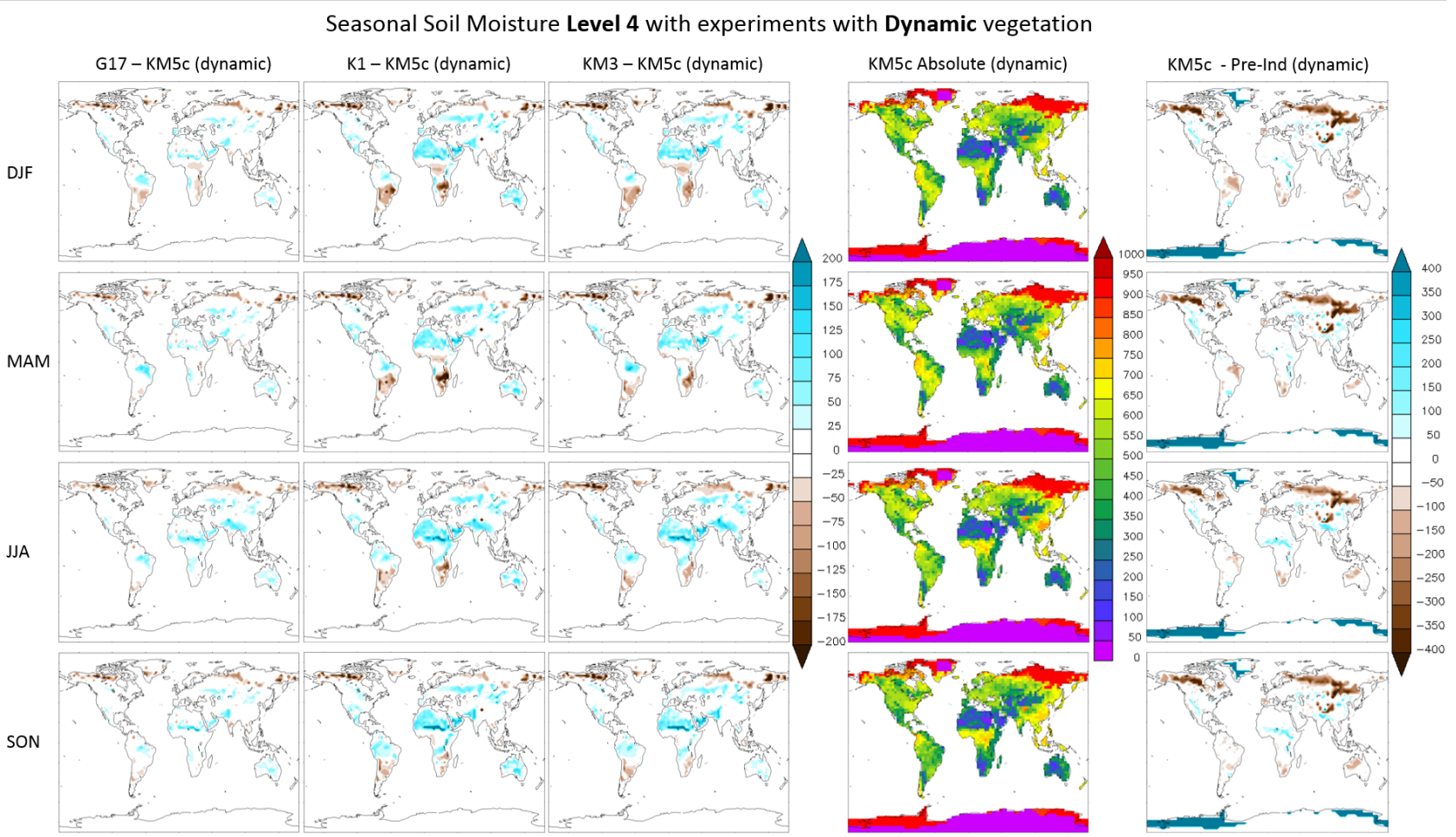

Figure B.8 HadCM3 results with MOSES2.1 land surface scheme (and dynamic vegetation) showing average seasonal soil moisture anomalies 2m from surface (mm/day). DJF (December, January, February), MAM (March, April, May), JJA (June, July, August) and SON (September, October, November).

Appendix C

Supplementary Figures for Chapter 4

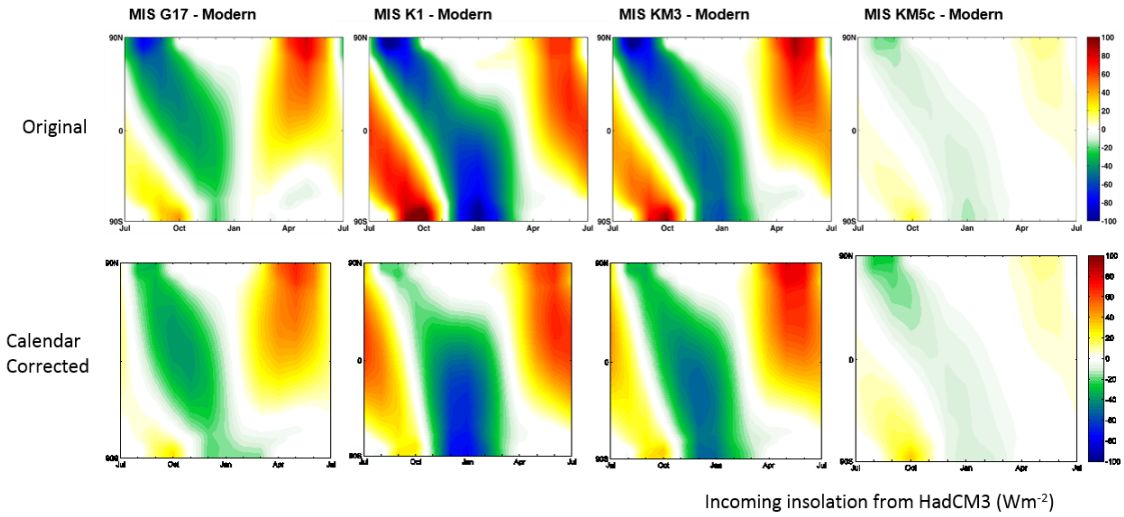

Figure C.1 Incoming insolation from HadCM3 for each interglacial (MIS G17, K1, KM3 and KM5c) minus a pre-industrial simulation (modern orbit), each plot showing changing incoming insolation by month and latitude. Top row showing the original results with no calendar correction applied and bottom row the calendar corrected incoming insolation.

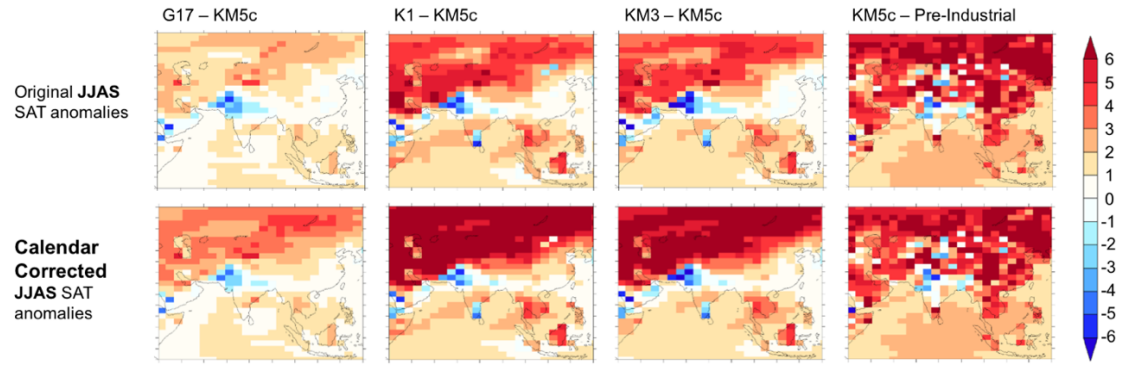

Figure C.2 HadCM3 SAT anomaly results for JJAS for three Piacenzian interglacials (MIS G17, K1 and KM3) minus the MIS KM5c and the far right column showing MIS KM5c minus a pre-industrial simulation. Top row indicates the original SAT results with no calendar correction applied and bottom row the calendar corrected SAT anomalies.

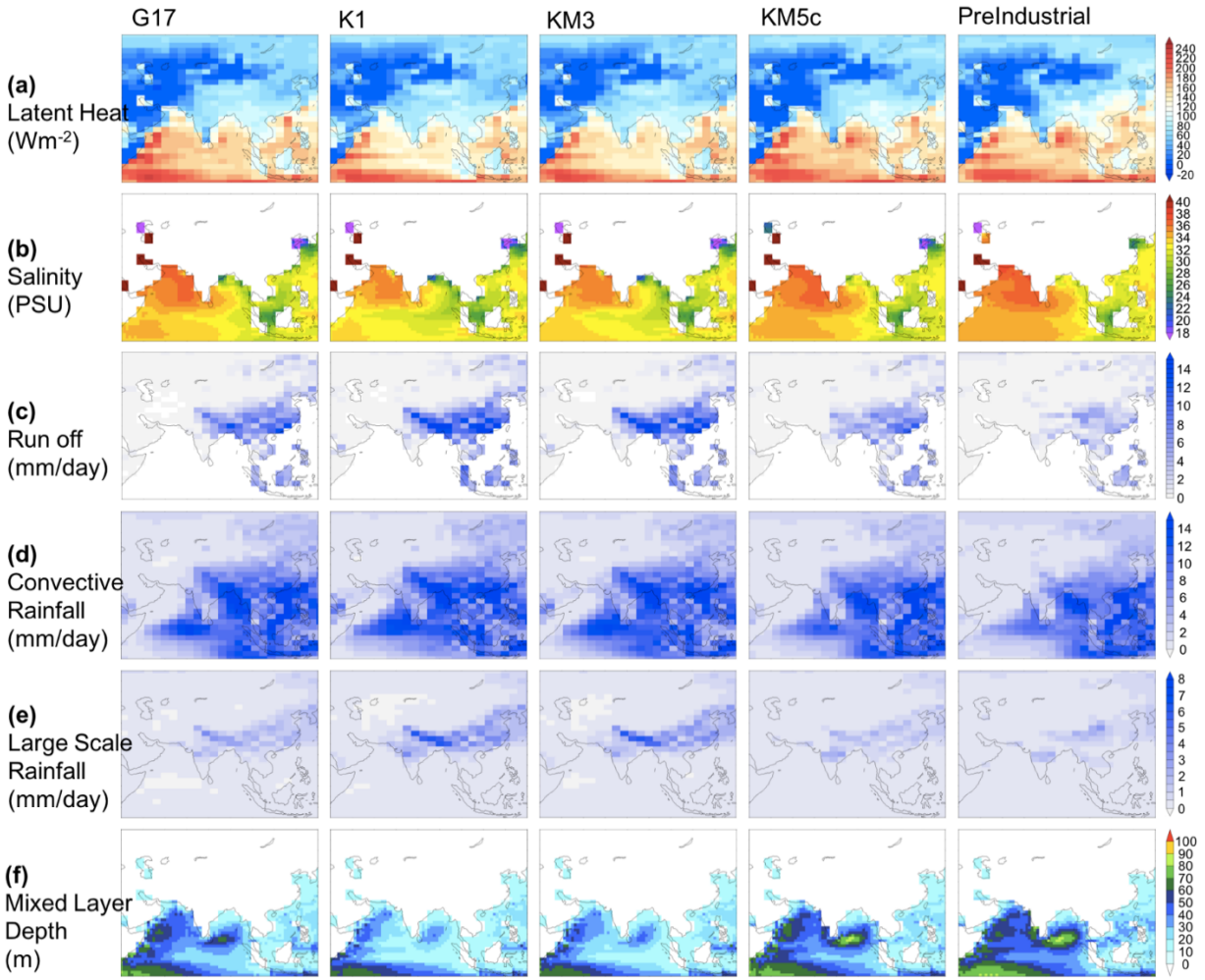

Figure C.3 HadCM3 absolute results for JJAS (June, July, August, September) for four Piacenzian interglacials (MIS G17, K1, KM3 and KM5c) and a pre-industrial simulation, showing (a) latent heat (Wm-2) (b) salinity (PSU) (c) run off (mm day-1) (d) convective rainfall (mm day-1) (e) large scale rainfall (mm day-1) and (f) mixed layer depth (m).

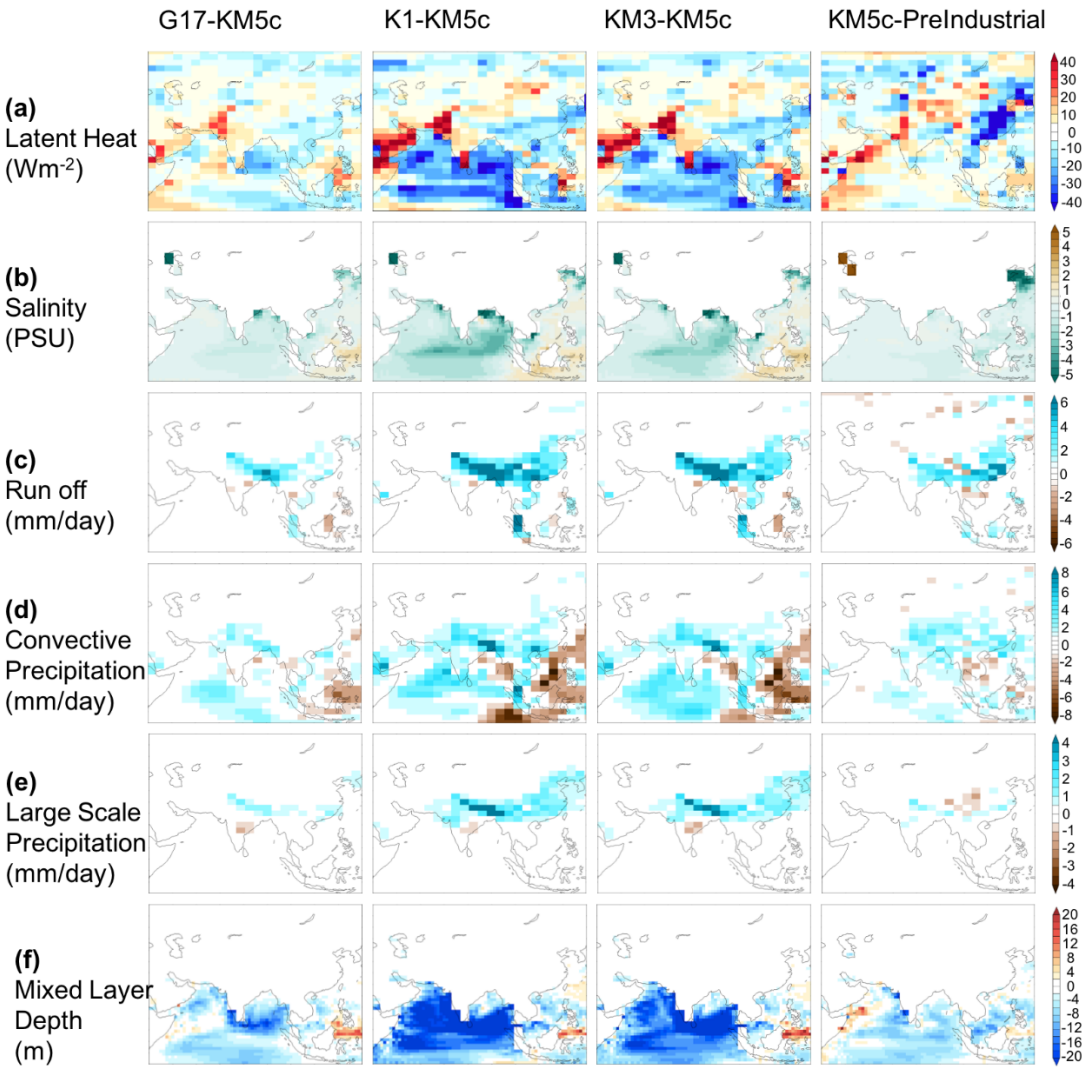

Figure C.4 HadCM3 anomaly results for JJAS (June, July, August, September) for three Piacenzian interglacials (MIS G17, K1, KM3) minus the MIS KM5c and MIS KM5c minus the pre-industrial simulation showing (a) latent heat (Wm-2) (b) salinity (PSU) (c) run off (mm day-1, (d) convective rainfall (mm day-1) (e) large scale rainfall (mm day-1) and (f) mixed layer depth (m).